

Reading and Problem Assignments for Physics 243A Surface Physics of Materials: Spectroscopy, Fall, 2016 (In order of coverage in lecture)

Reading:

• Woodruff and Delchar, "Modern Techniques of Surface Science", 2nd Edition--
Chapter 1
Chapter 2: Sections 2.1, pp.22 (bottom)-23(top) on Wood notation for surface structures,
2.4, and 2.5 (pp. 31-37), 2.9.6 on standing waves
Chapter 6: 6.9, 6.10, 6.11
Chapter 3: Sections 3.1, 3.2, 3.3, 3.5

• Zangwill, "Physics at Surfaces", downloadable Chapters 1-5 (see course website)--
Chapter 1: Everything except "The roughening transition"
Chapter 3: pp. 28-34, pp. 49-52 on STM
Pages 85-86, 192-196, 204-212
Chapter 2: All

Chapter 4: Introduction, with lighter reading of *The jellium model*, *One-dimensional band theory*, and *Three-dimensional band theory*, and detailed reading of *Photoelectron spectroscopy, Metals, and Alloys*

• Ibach, "Physics of Surfaces and Interfaces", downloadable book (see course website)--
Chapter 2: 2.1, 2.2
Chapter 8: 8.2

• Desjonqueres and Spanjaard, "Concepts of Surface Physics", excerpts downloadable from Course website: On STM current calculation, equilibrium shapes of surfaces, thermodynamics, kinetics and adsorption isotherms. No need to follow every step, but this fills in the line of arguments in Zangwill and lecture

• Fadley, "Basic Concepts of XPS", to be handed out, but also downloadable--
Sections I, II, and III. A-C, with remaining sections by the end of the course

• Attwood, Downloadable excerpt on synchrotron radiation from the book
"Soft X-Rays and Extreme Ultraviolet Radiation" (see course website)

Problem assignments:

Problem set 1-all. Due Thursday, October 13th

Problem set 2-all. Due Thursday, October 27th

Midterm exam: Tuesday, November 1st, open book and open notes. Computers OK, but no cell phones, or use of material from prior offerings of this course beyond that at the website.

Reading coverage for midterm

Next reading in blue:
Rest of "Basic Concepts"
+Molecular Orbital Basics & Tight-Binding Basics
(from website)

Office hours:

TA: Galina Malovichko- 2:00-3:00 PM, Mondays, Physics 416

**Instructor: Chuck Fadley, 2:30-3:30, Tuesdays and Thursdays,
Physics 241 (others by special appointment)**

**Class consultant: Shih-Chieh Lin- 4:20-5:20, Wednesdays, Physics
221**

Handing in problem sets:

Hand in problem sets in class, or in secure submission box with class number on it. The new homework submission boxes are located in the east wing at the first floor north entrance to the Physics Building – the same hallway where our student computer lab. is located (rm 106 Physics)

Table 1 Cohesive Energies* of the elements

Energy required to form separated neutral atoms from the solid at 0°K; the values in parentheses are at 298.15°K or at the melting point, whichever temperature is lower. To obtain the energy in J mol⁻¹, multiply the energy in kcal mol⁻¹ by 4.184 = 10³. To obtain the energy in ergs per atom, multiply the energy in eV per atom by 1.60219 × 10⁻¹².

H 4.48 103																	He				
Li 1.65 38.0	Be 3.33 76.9															B 5.81 134.	C 7.36 170.	N (114)	O (60)	F (20)	Ne 0.02 0.45
Na 1.13 26.0	Mg 1.53 35.3															Al 3.34 76.9	Si 4.64 107	P (79.2)	S 2.86 66.1	Cl (32.2)	Ar 0.080 1.85
\longleftrightarrow eV per atom \longleftrightarrow \longleftrightarrow kcal per mole \longleftrightarrow																					
K 0.941 21.7	Ca 1.825 42.1	Sc 3.93 90.6	Ti 4.855 112.0	V 5.30 122.	Cr 4.10 94.5	Mn 2.98 68.7	Fe 4.29 98.9	Co 4.387 101.2	Ni 4.435 102.3	Cu 3.50 80.8	Zn 1.35 31.1	Ga 2.78 64.2	Ge 3.87 89.3	As 3.0 69.	Se 2.13 49.2	Br 1.22 (28.2)	Kr 0.116 2.67				
Rb 0.858 19.8	Sr (39.1)	Y 4.387 101.2	Zr 6.316 145.7	Nb 7.47 172.	Mo 6.810 157.1	Tc	Ru 6.615 152.6	Rh 5.752 132.7	Pd 3.936 90.8	Ag 2.96 68.3	Cd 1.160 26.76	In 2.6 59	Sn 3.12 71.9	Sb 2.7 62.	Te 2.0 46	I (25.6)	Xe (3.57)				
Cs 0.827 19.1	Ba 1.86 (42.8)	La 4.491 103.6	Hf 6.35 146.	Ta 8.089 186.6	W 8.66 200.	Re 8.10 187.	Os (187)	Ir 6.93 160.	Pt 5.852 135.0	Au 3.78 87.3	Hg (0.694) (16.0)	Tl 1.87 43.2	Pb 2.04 47.0	Bi 2.15 49.6	Po (34.5)	At	Rn				
Fr	Ra	Ac																			
			Ce 4.77 110	Pr 3.9 89	Nd 3.35 77.2	Pm	Sm 2.11 48.6	Eu 1.80 41.5	Gd 4.14 95.4	Tb 4.1 94	Dy 3.1 71	Ho 3.0 70	Er 3.3 77	Tm 2.6 59	Yb 1.6 36	Lu (4.4) (102)					
			Th 5.926 136.7	Pa 5.46 126	U 5.405 124.7	Np 4.55 105	Pu 4.0 92	Am 2.6 60	Cm	Bk	Cf	Es	Fm	Md	No	Lw 3					

Cohesive energies and surface tension

<u>ELEMENT</u>	E_{COH} ($\frac{\text{kcal}}{\text{mol}}$)	ΔH_{FUS} ($\frac{\text{kcal}}{\text{mol}}$)	$\frac{\Delta H_{\text{FUS}}}{E_{\text{COH}}}$ (%)
Si	107	9.47	8.9%
Ca	42.1	2.23	5.3%
Sc	90.6	3.80	4.2%
Mn	68.7	3.45	5.0%
Fe	98.9	3.56	3.6%
Cu	80.8	3.11	3.8%
Zn	31.1	1.60	5.1%
Ge	89.3	8.30	9.3%

METALS
 ↓
 SEMICOND.
 ↓
 ~ 4-9%

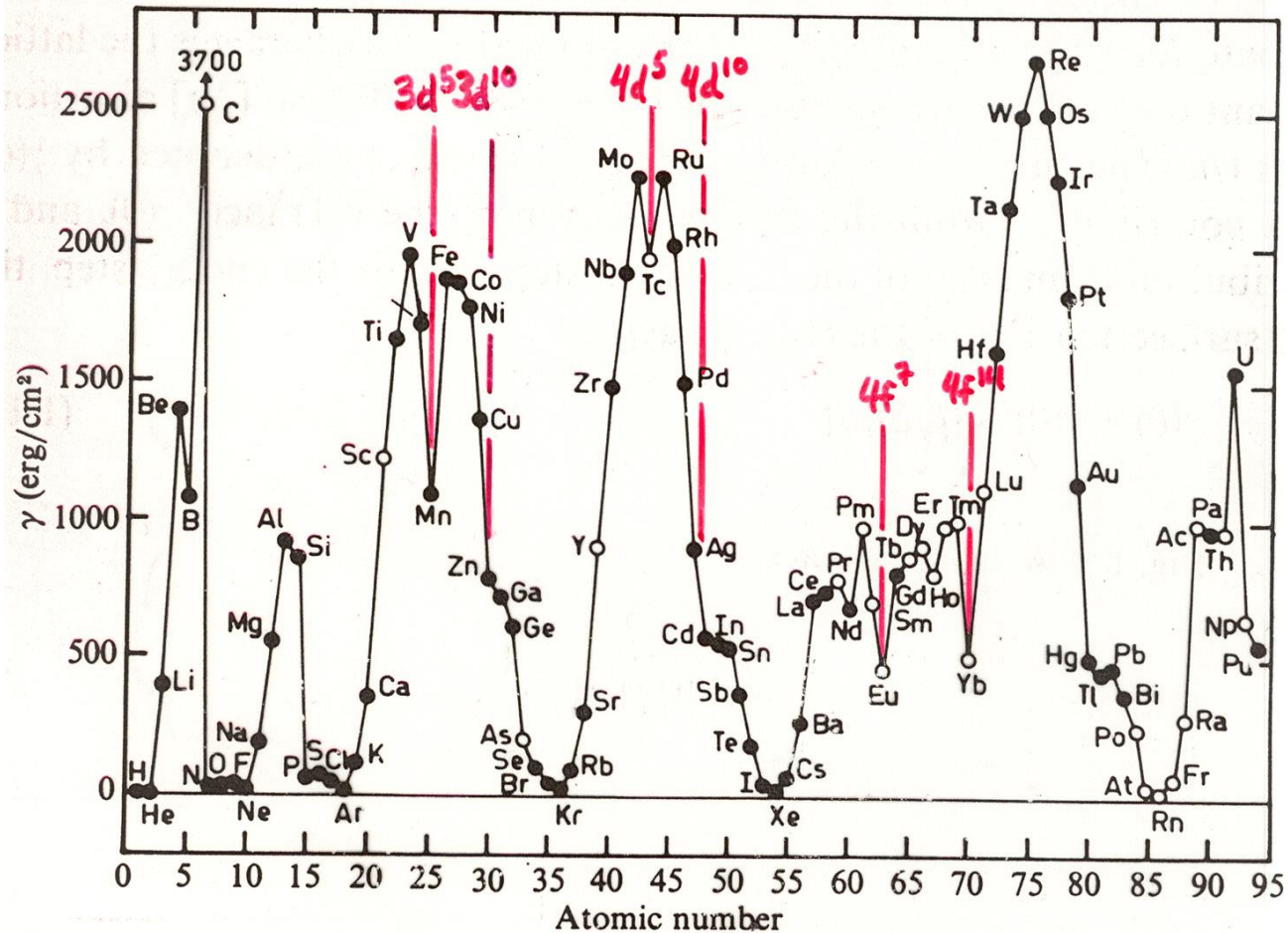
$$\Delta H_{\text{FUS}} \ll E_{\text{COH}}$$

$$\text{BOND STRENGTHS}_{\text{LIQ}} \approx \text{BOND STRENGTHS}_{\text{SOLID}}$$

$$\therefore \gamma_{\text{SOLID}} \approx \gamma_{\text{LIQUID}}$$

$$\gamma_{\text{SOLID}} > \gamma_{\text{LIQUID}}$$

Fig. 1.4. Surface tension of the elements in the liquid phase (Schmit, 1974).

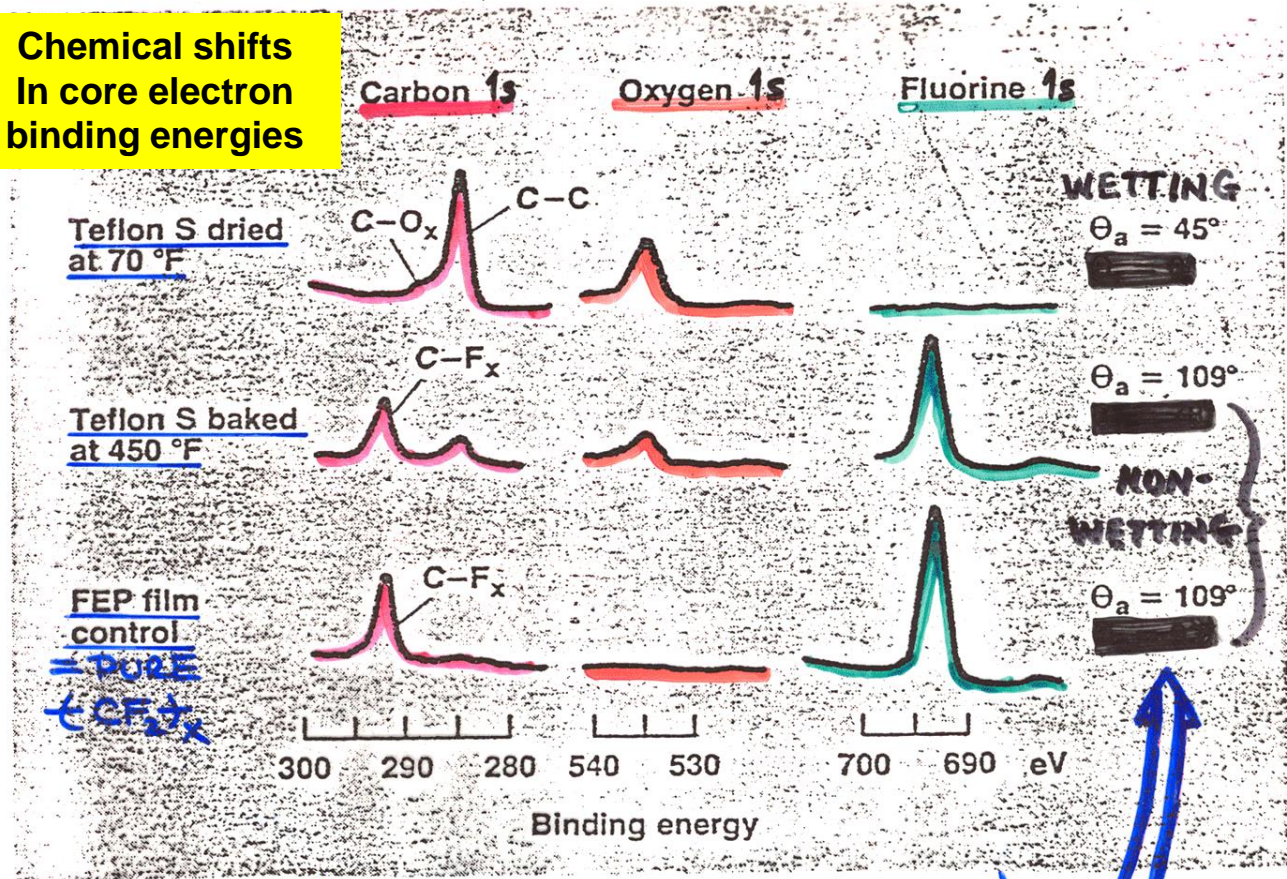


NOTE LOWER VALUES FOR HALF-FILLED HUND'S RULE STATES WITH REDUCED BONDING HYBRIDIZATION (d^5, f^7) AS WELL AS FOR FILLED-SHELL STATES

SURFACE TREATMENT OF A LOW-FRICTION POLYMERIC COATING FOR TOOLS

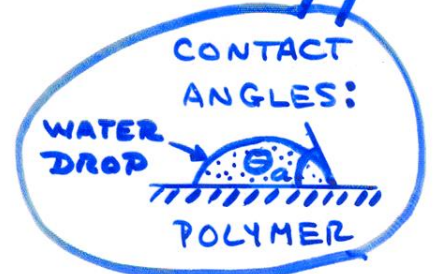
"TEFLON S" = A MIXTURE OF EPOXY AND $(CF_2)_x$

**Chemical shifts
in core electron
binding energies**



X-RAY PHOTOELECTRON SPECTRA

(D. DWIGHT, CHEMTECH, MARCH 1982)



The Wulff construction

$$\gamma(\theta) = \gamma(0) + (\beta/a)|\theta| + \text{ENERGY OF INT. BETWEEN STEPS}$$

ENERGY TO PRODUCE EACH STEP

Fig. 1.5. A vicinal surface.

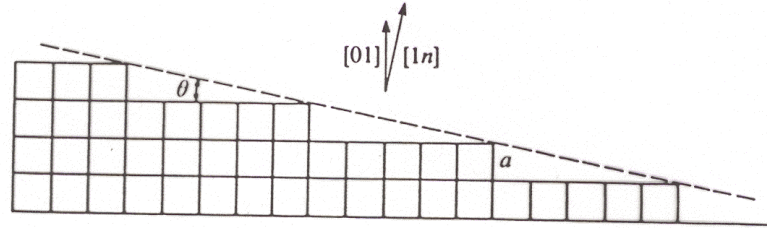
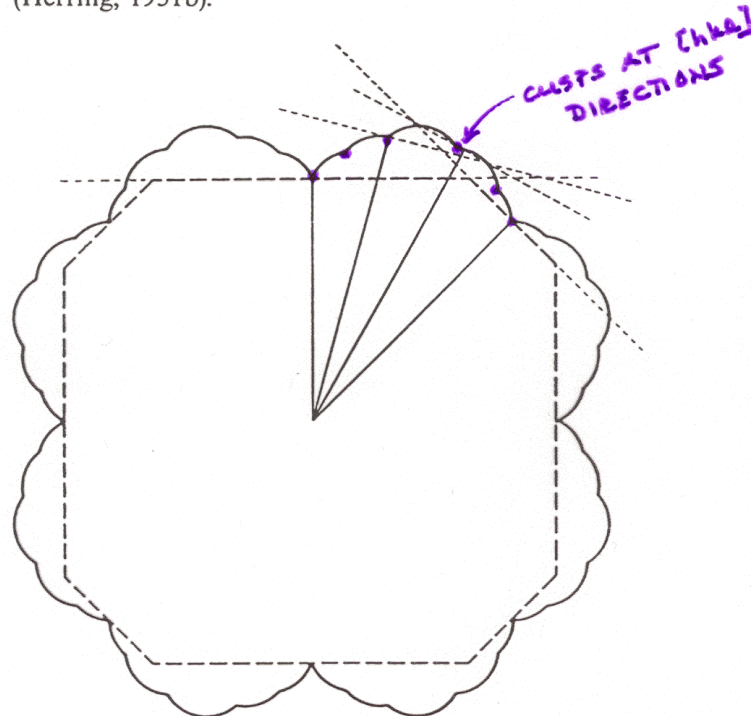
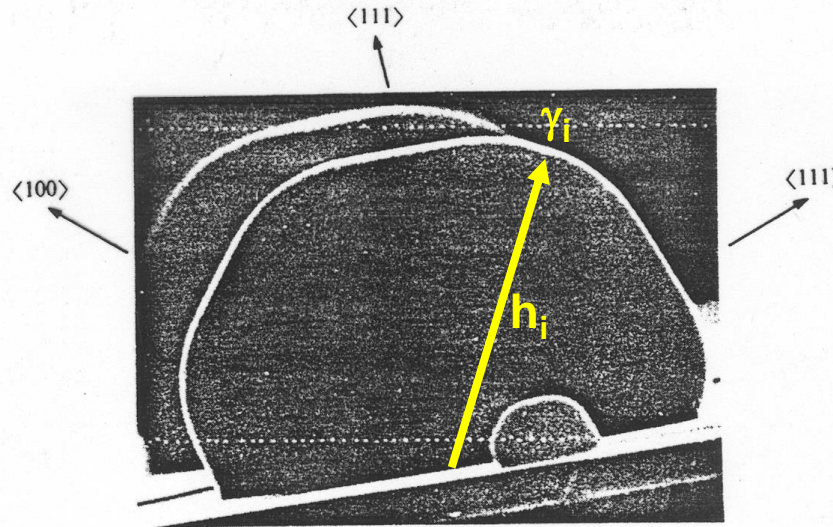


Fig. 1.6. Polar plot of the surface tension at $T = 0$ (solid curve) and the Wulff construction of the equilibrium crystal shape (dashed curve) (Herring, 1951b).



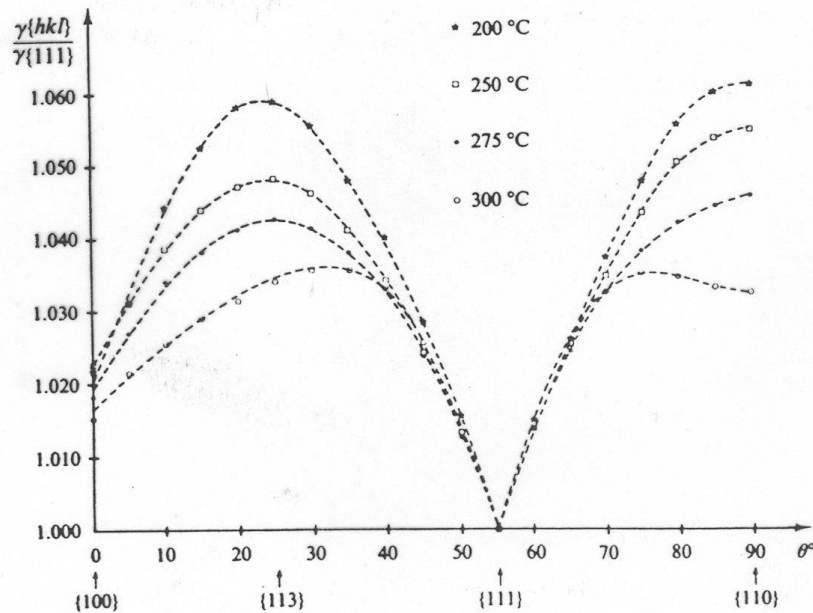
Scanning
electron
microscopy
Images of
Pb crystallites

Fig. 1.7. Electron micrograph of a lead crystal at 473 K (Heyraud & Metois, 1983).



Wulff theorem:
 $\gamma_i/h_i = \text{constant}$

Fig. 1.8. Anisotropy of γ relative to $\langle 111 \rangle$ for lead as a function of temperature (Heyraud & Metois, 1983).



Scanning tunneling microscopy Images of Pb crystallites

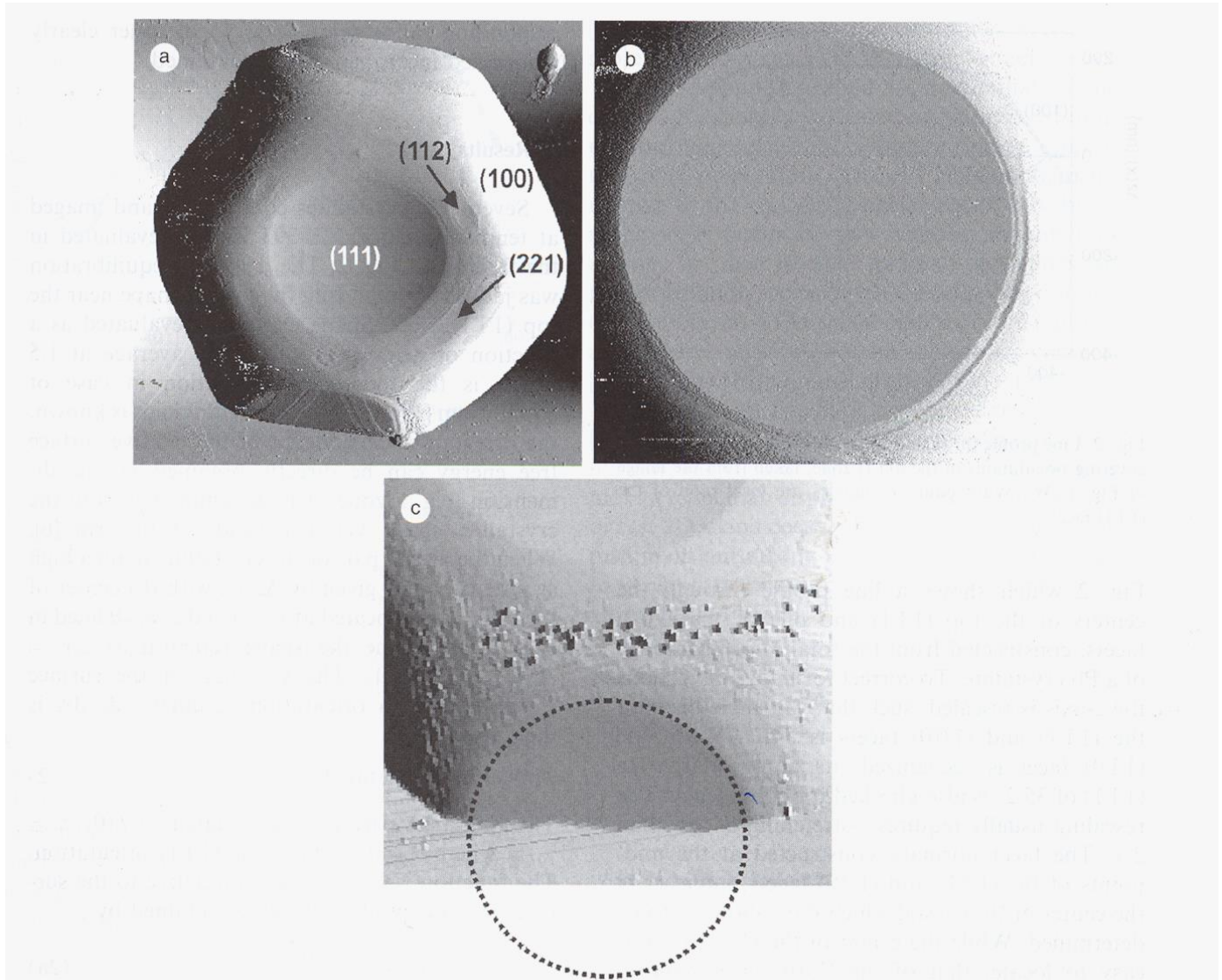


Fig. 1. STM images of equilibrated Pb crystallite. (a) Vertical projection of complete crystallite, with the (111) facet parallel to the substrate, $T = 323$ K. Note (112) and (221) facets near the periphery of the (111) facet. Large (100) facets are visible at the contact line. Image size: 1300×1300 nm². (b) Image of the (111) facet and vicinal range of same crystallite as in (a). A double tip effect is seen on the r.h.s. of the facet. Image size: 670×670 nm². (c) 3D image of crystallite at $T = 393$ K, with the (100) facet rotated into the paper plane; center of the (100) facet approximately at the contact line. Due to the higher temperature, some bumps have been generated by local surface-to-tip contacts. Lateral dimension: 600 nm.

C. Bombis et al.,
Surface Science 511
(2001) 83-96

Scanning tunneling microscopy images of Pb crystallites

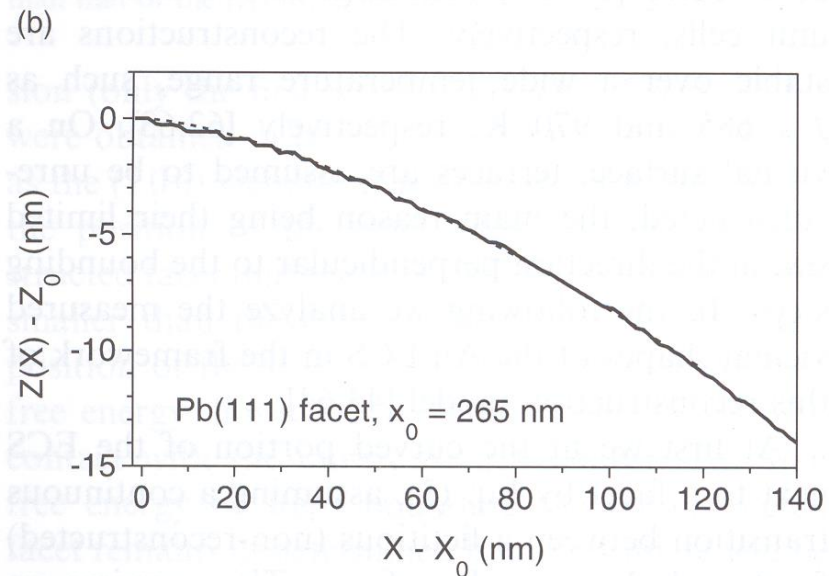
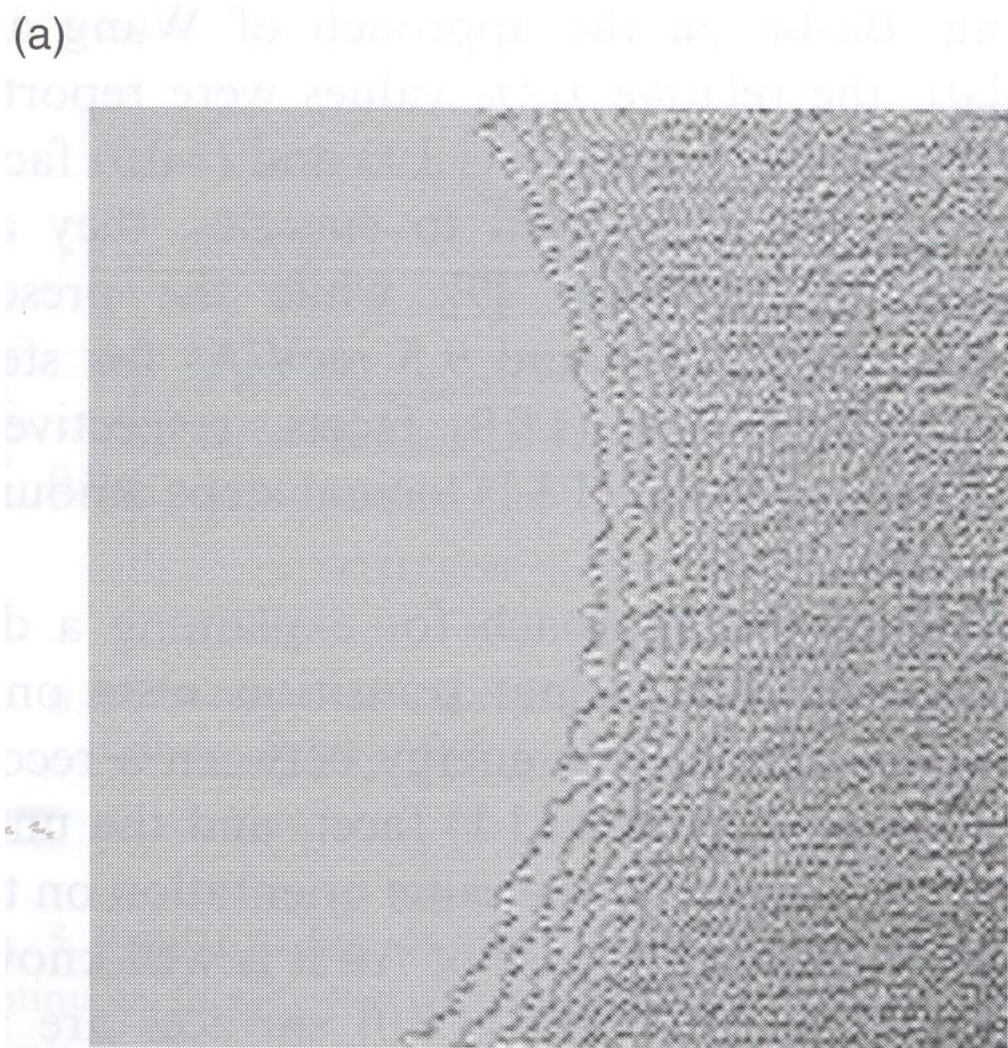
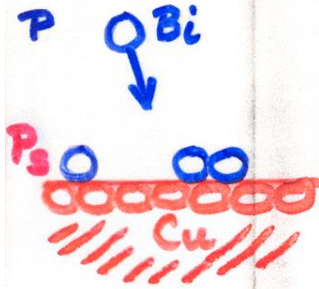
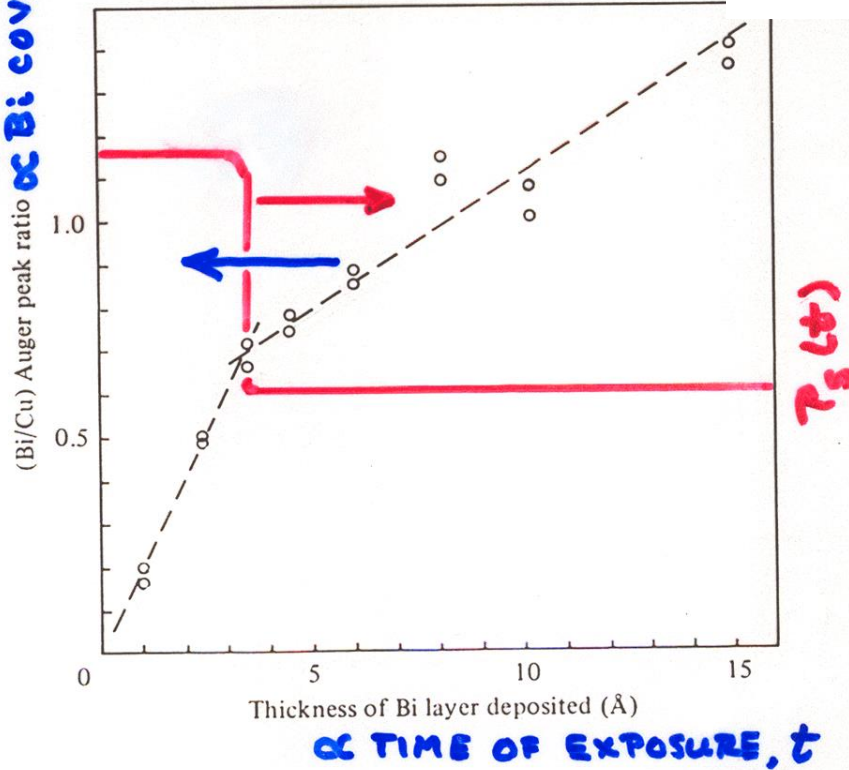


Fig. 2. (a) STM image of a section of the ECS of a Pb crystallite at 383 K. The image shows the facet to vicinal surface transition where the latter is characterized by a train of monoatomic steps. (b) Example of a line scan across the ECS in the area of facet to vicinal surface transition. The line scan, $z(x) - z_0$ versus $x - x_0$, normalized relative to the facet edge at z_0, x_0 , is fitted by Eq. (3) without the f_4 term.



∝ Bi COVERAGE

Fig. 3.44 Auger peak height ratio of 102 eV Bi peak to Cu 62 eV peak for Bi grown on an evaporated Cu substrate. Note the break or 'knee' corresponding to monolayer coverage (from Powell & Woodruff, 1976).

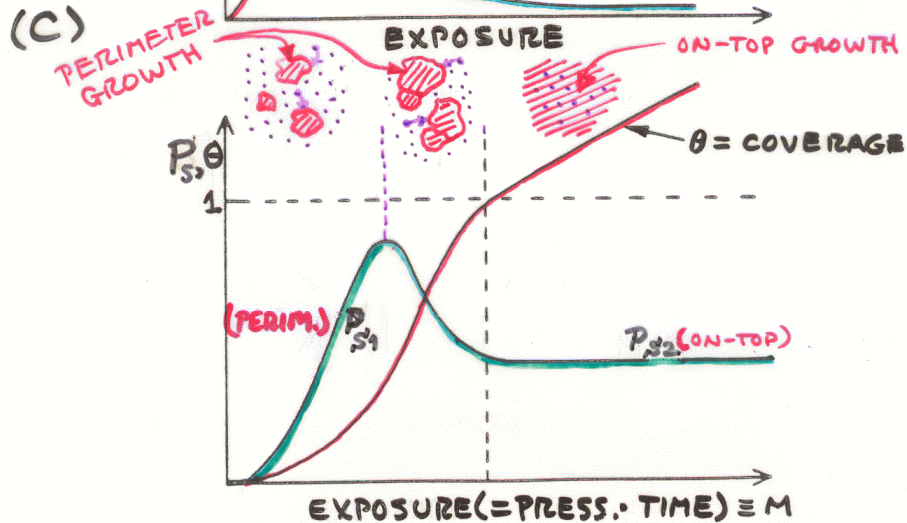
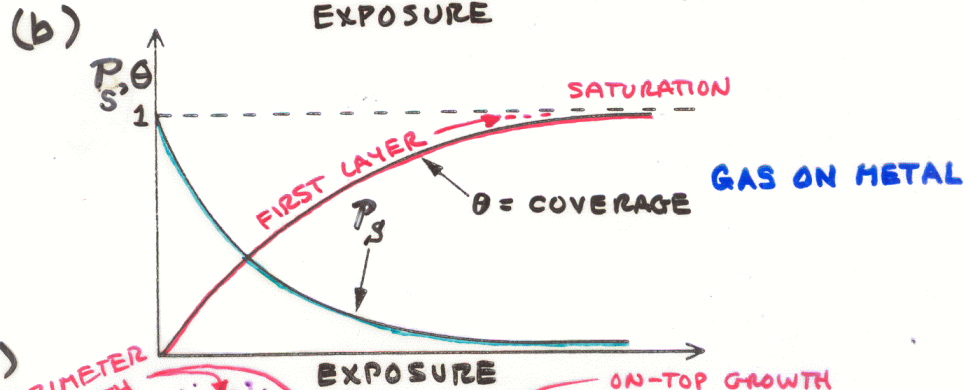
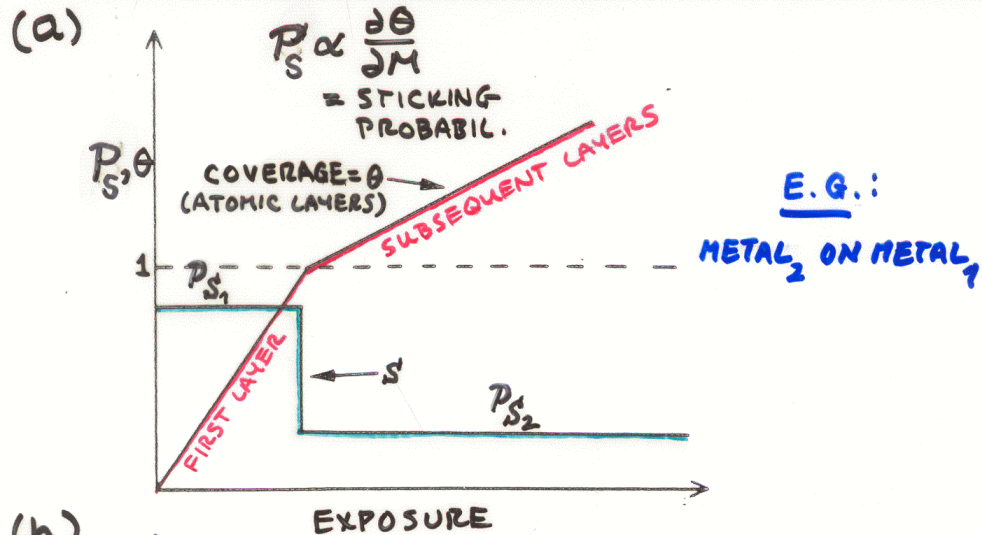


$$\left(\text{RATE OF OVERLAYER (Bi) GROWTH AT } t \right) = \frac{P_s(t)P(t)}{(2\pi k_B m T)^{1/2}}$$

$$\left(\text{OVERLAYER THICKNESS AT } t_0 \right) \propto \int_0^{t_0} \frac{P_s(t)P(t)}{(2\pi k_B m T)^{1/2}} dt$$

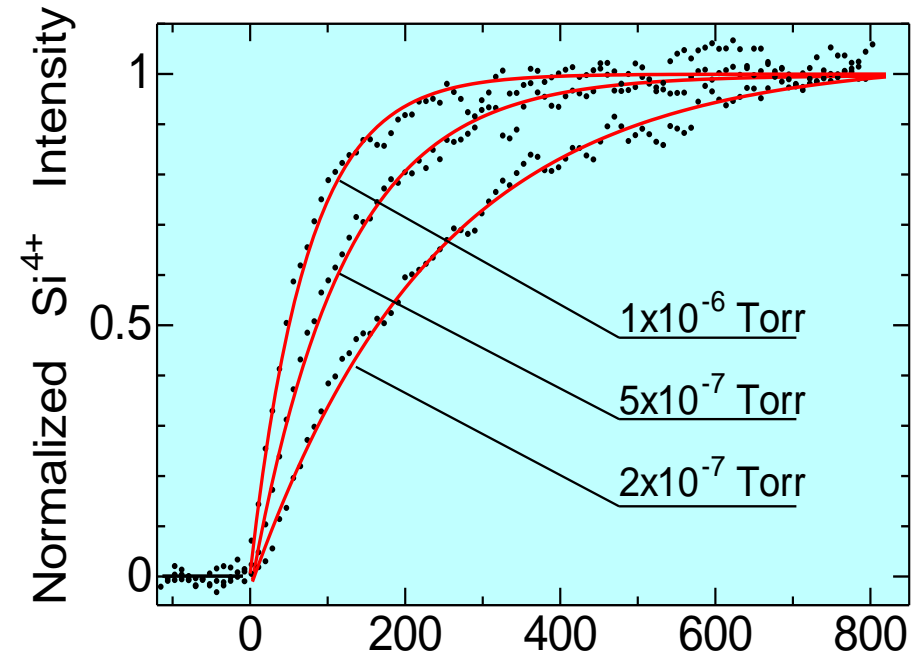
∴ $P_s(t) \propto$ SLOPE IF $P(t)$ CONSTANT

SOME TYPICAL COVERAGE / STICKING PROB. CURVES



From Prutton,
Surface Physics

Oxidation of Silicon: Time evolution at 580°C, Langmuir form



Langmuir-type adsorption:
Growth rate is proportional
to bare Si surface

$$\frac{d\theta}{dt} \propto P_S P (1 - \theta)^n$$

θ = oxide coverage

P_S = sticking probability

P = oxygen pressure

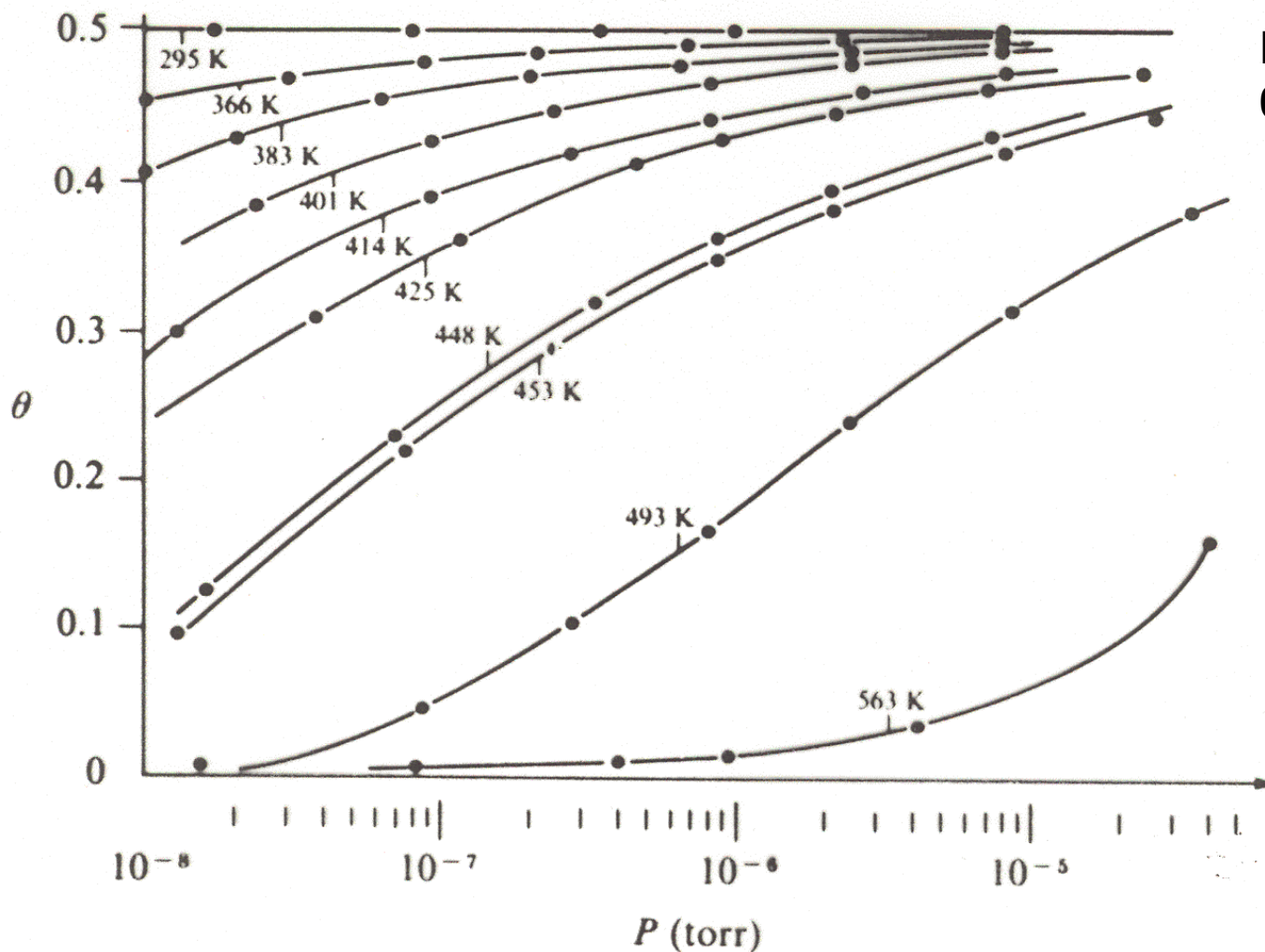
n = reaction order

The time evolution follows
 $n = 1 \rightarrow$ first-order Langmuirian

Sticking probability, $P_S = 0.016$ —constant if no interaction between adsorbed species

At Equilibrium!

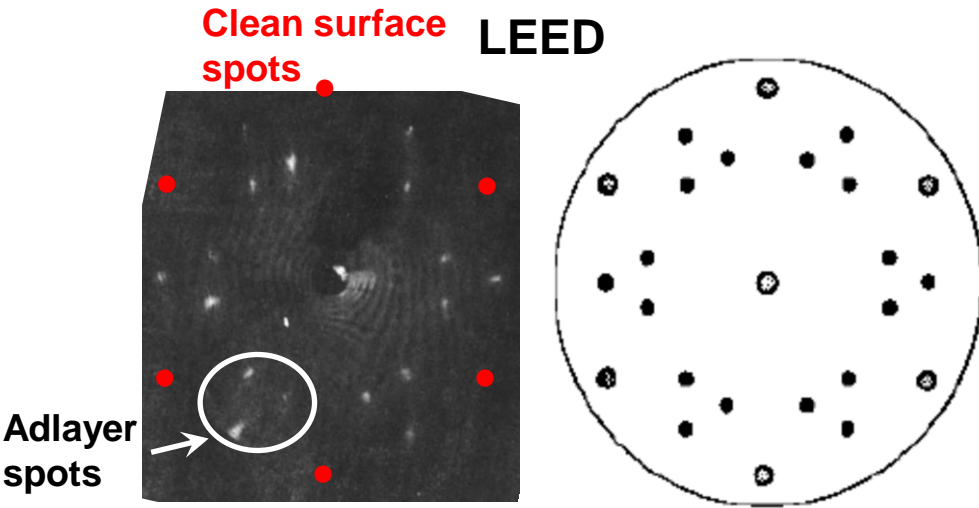
Fig. 9.2. Adsorption isotherms for CO/Pd(111) (Ertl & Koch, 1970).



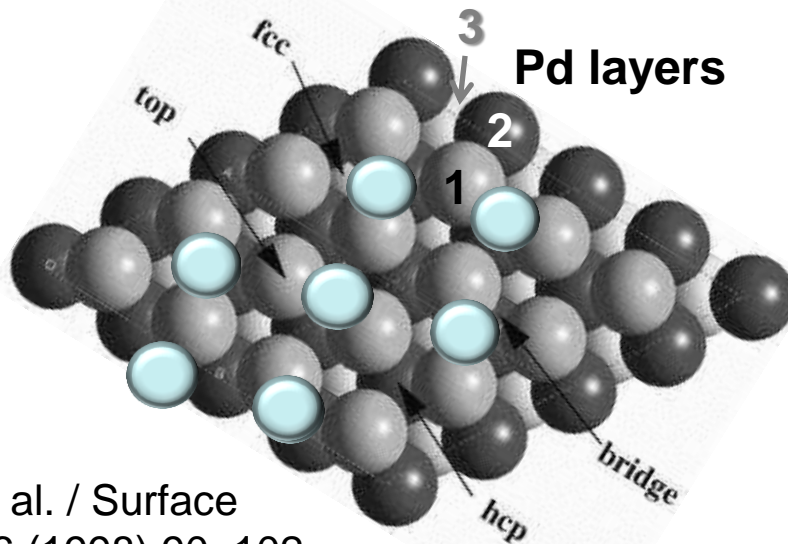
Final saturation for
0.5 coverage

FROM
ZANGWILL

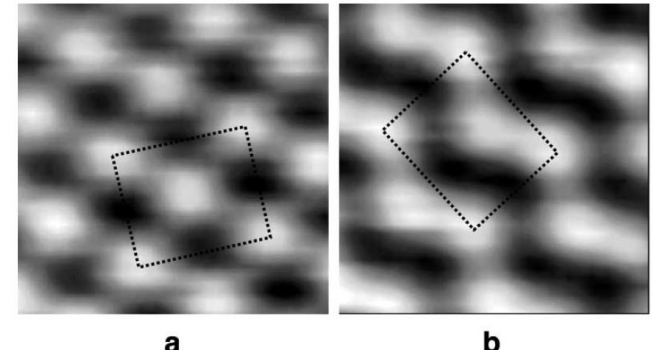
CO on Pd(111)- The 0.5 ML saturation structures-at equilibrium!



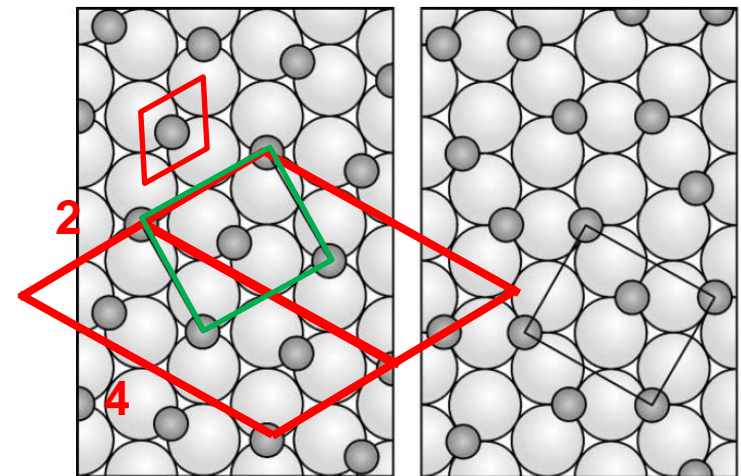
J. Electroanal. Chem., 353 (1993) 281–287
Pd(111)c(4×2)



STM



Coexistent- a slightly preferred at 120K



2 COs per rectangular cell, 4 COs per c(4x2)

Fig. 5. c(4×2)-2CO models. (a) CO molecules occupying bridge sites. (b) CO molecules in fcc and hcp threefold hollow sites. A primitive cell of each c(4×2) structure is indicated.

Diffusion of water on TiO_2 and dissociation at an oxygen vacancy defect on the surface

Topics in Catalysis (2010) 53:423–430
doi 10.1007/s11244-010-9454-3

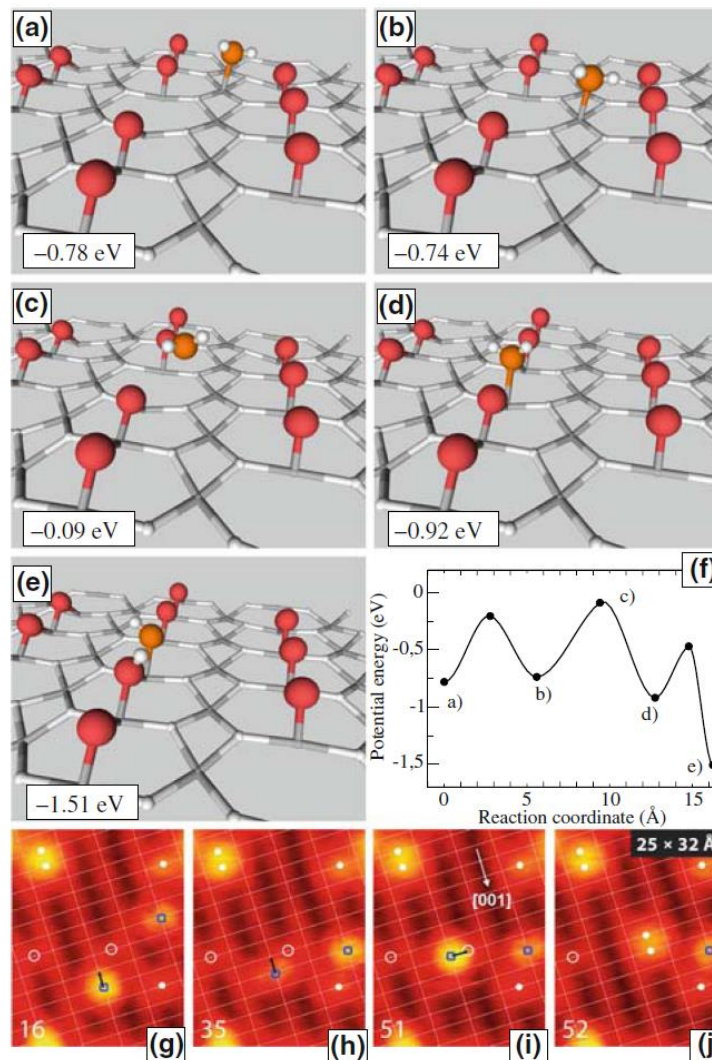
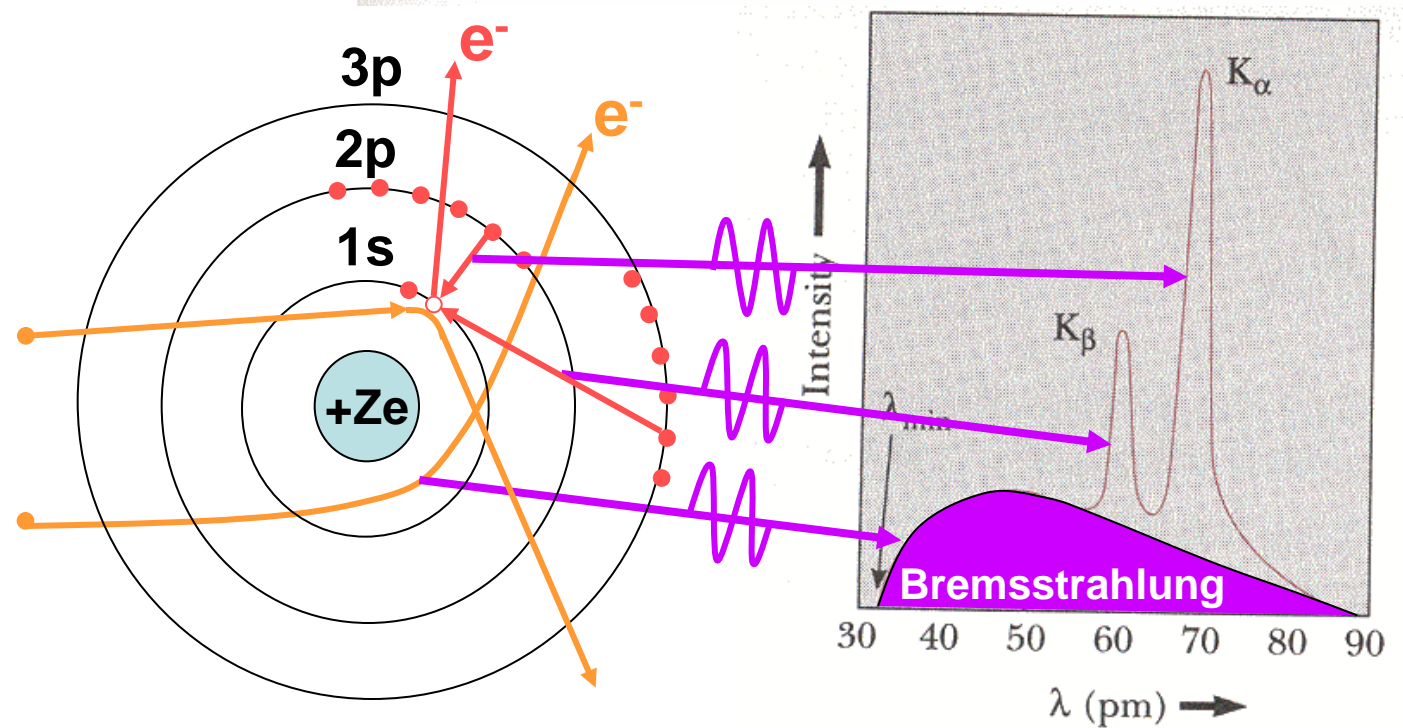
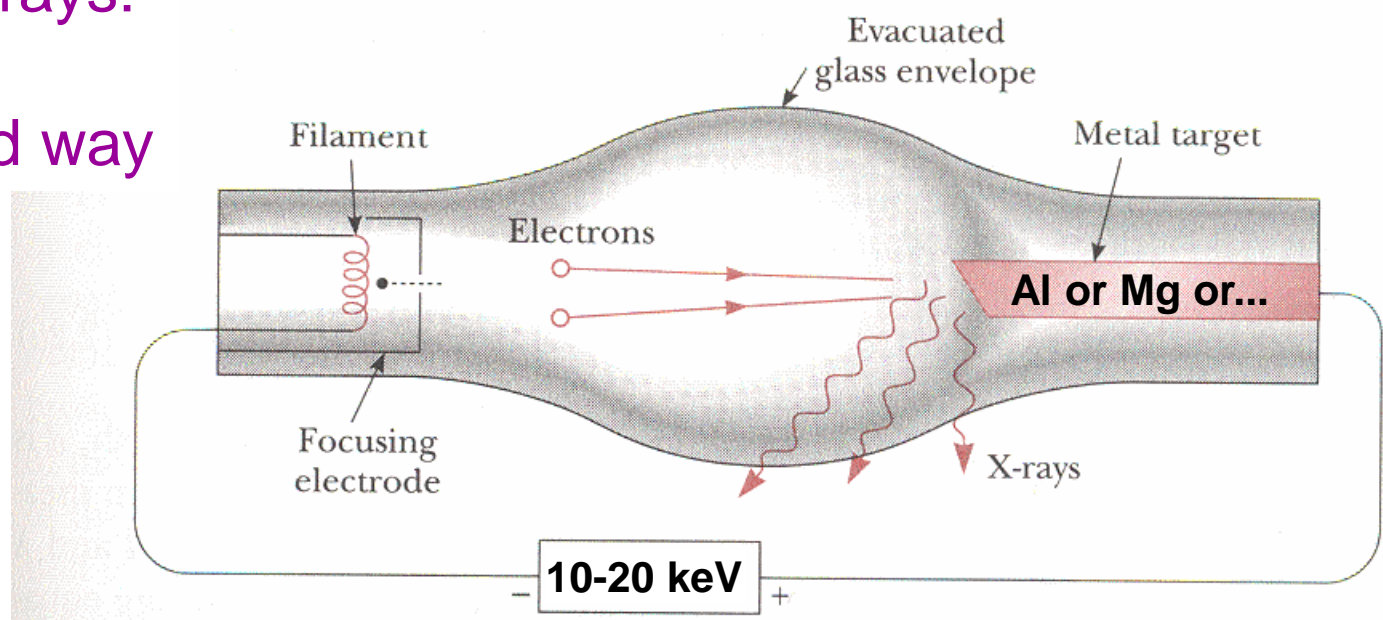


Fig. 4 a–b Configuration and adsorption potential energy (PW91) of adsorbed monomeric water at Ti_{5f} sites close to an O_{br} vacancy. c–d Transition and final state of an adsorbed water molecule that jumps into an O_{br} vacancy. e Configuration with a pair of H adatoms in the O_{br} row after the water has dissociated. f Potential energy diagram. g–j STM images showing the diffusion of an adsorbed water molecule (blue square) that dissociates in an O_{br} vacancy (white circle) forming a pair of H adatoms (two neighboring white dots). STM images are extracted from movie “dissociation” published with [22]

Other STM movies at:

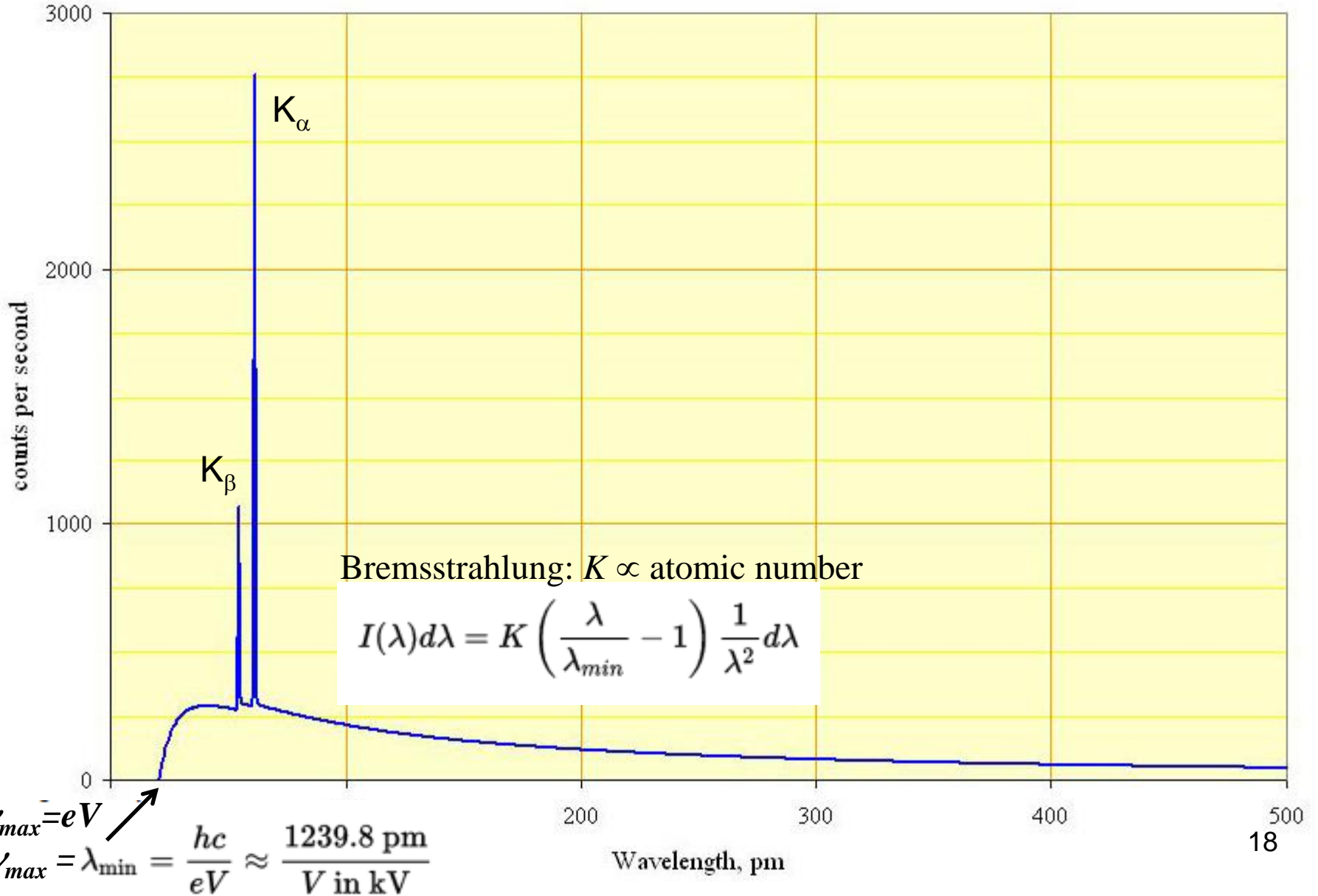
http://phys.au.dk/forskning/forskning_somraader/condensed-matter-physics/spm/stm-movies/

Producing x-rays:
the good
old-fashioned way



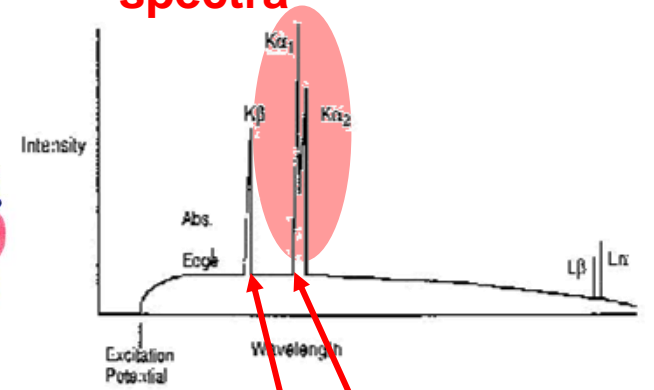
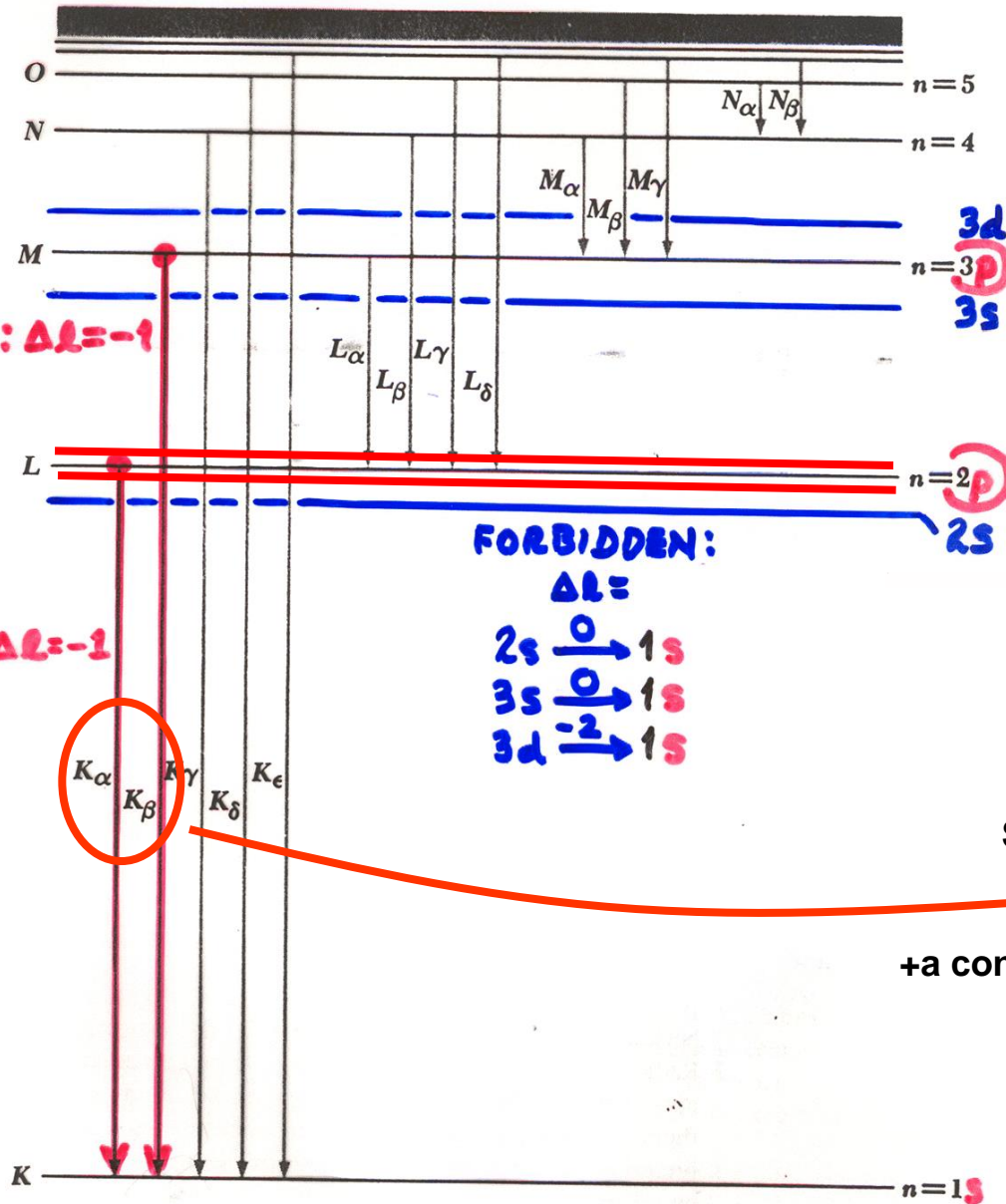
See Section 1.2 in "X-Ray Data Booklet"

X-ray spectrum from a rhodium target at 60 keV electron energy



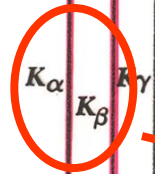
ALLOWED TRANSITIONS IN X-RAY EMISSION:

Spin-orbit splitting in high-resolution x-ray spectra



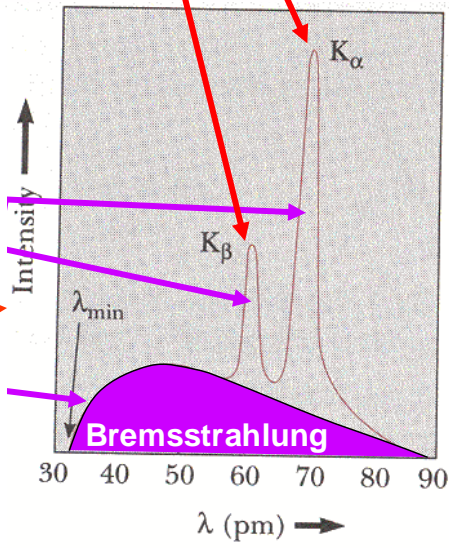
$2p, j = 3/2$
 $2p, j = 1/2$

$\Delta l = -1$



Line Spectra

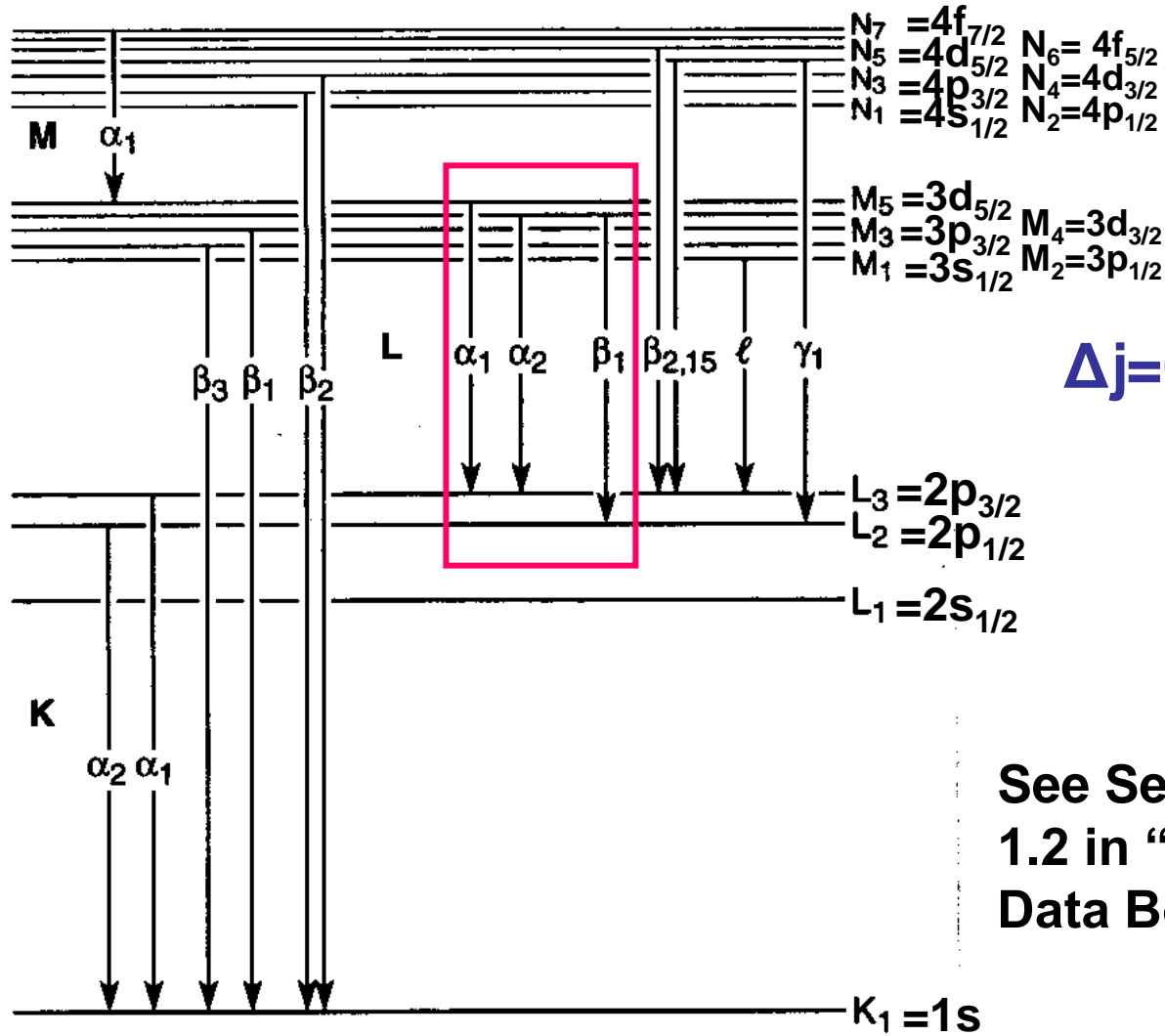
+ a continuum



X-Ray Nomenclature (from "X-Ray Data Booklet")

In general:

$$nl \rightarrow \begin{cases} \text{Spin-}nl_{j=l+1/2} \\ \text{orbit } nl_{j=l-1/2} \end{cases}$$



See Section 1.2 in "X-Ray Data Booklet"

Fig. 1-1. Transitions that give rise to the emission lines in Table 1-3.

X-Ray energies from the “X-Ray Data Booklet”

Table 1-2. Photon energies, in electron volts, of principal K-, L-, and M-shell emission lines.

Element	$K\alpha_1$	$K\alpha_2$	$K\beta_1$	$L\alpha_1$	$L\alpha_2$	$L\beta_1$	$L\beta_2$	$L\gamma_1$	$M\alpha_1$
3 Li	54.3								
4 Be	108.5								
5 B	183.3								
6 C	277								
7 N	392.4								
8 O	524.9								
9 F	676.8								
10 Ne	848.6	848.6							
11 Na	1,040.98	1,040.98	1,071.1						
12 Mg	1,253.60	1,253.60	1,302.2						
13 Al	1,486.70	1,486.27	1,557.45						
14 Si	1,739.98	1,739.38	1,835.94						
15 P	2,013.7	2,012.7	2,139.1						
16 S	2,307.84	2,306.64	2,464.04						
17 Cl	2,622.39	2,620.78	2,815.6						
18 Ar	2,957.70	2,955.63	3,190.5						
19 K	3,313.8	3,311.1	3,589.6						
20 Ca	3,691.68	3,688.09	4,012.7	341.3	341.3	344.9			
21 Sc	4,090.6	4,086.1	4,460.5	395.4	395.4	399.6			

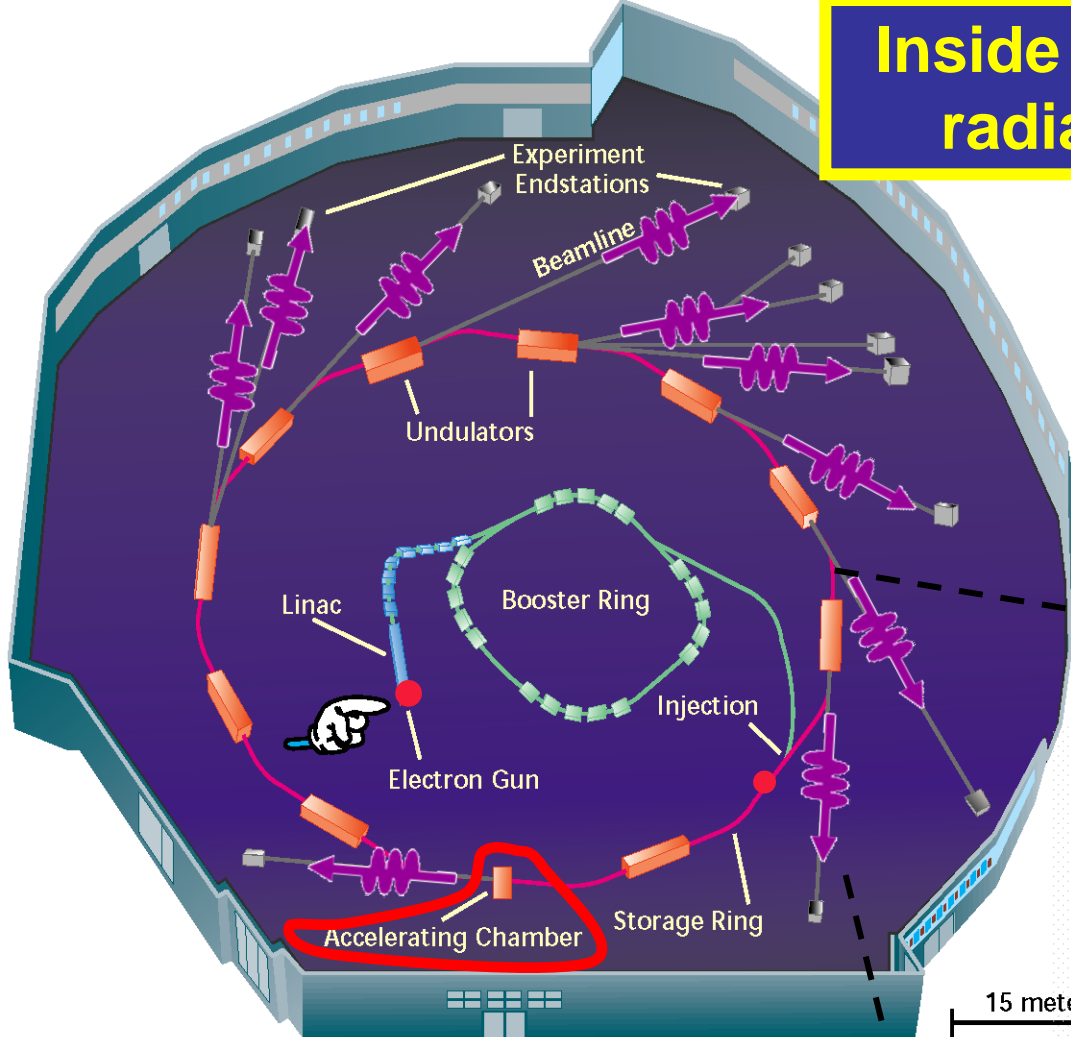
Popular laboratory sources
for photoelectron spectroscopy

X-Ray energies from the "X-Ray Data Booklet" (cont'd.)

Table 1-2. Energies of x-ray emission lines (continued).

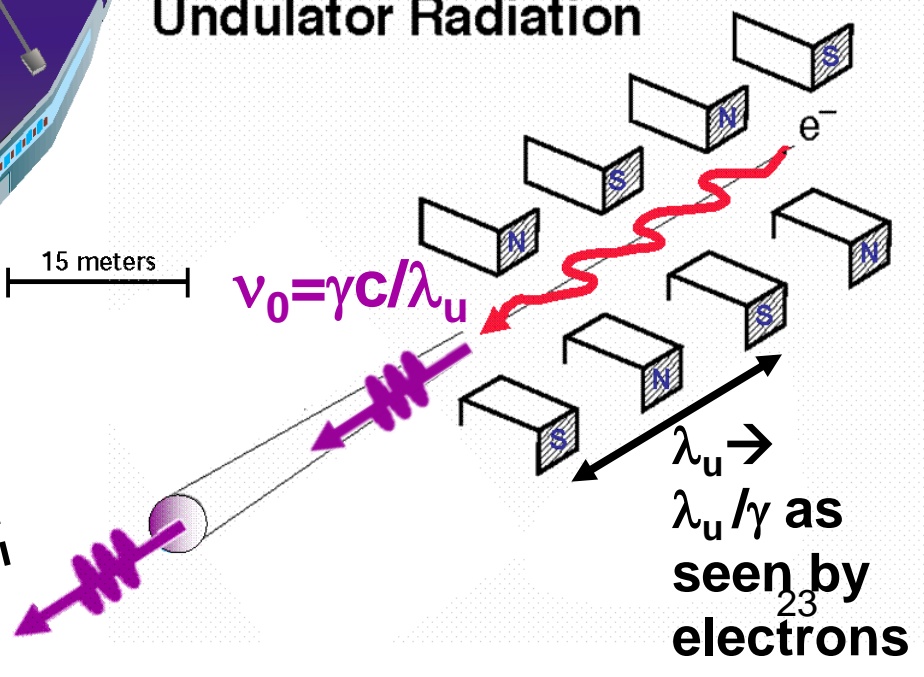
Element	$K\alpha_1$	$K\alpha_2$	$K\beta_1$	$L\alpha_1$	$L\alpha_2$	$L\beta_1$	$L\beta_2$	$L\gamma_1$	$M\alpha_1$
22 Ti	4,510.84	4,504.86	4,931.81	452.2	452.2	458.4			
23 V	4,952.20	4,944.64	5,427.29	511.3	511.3	519.2			
24 Cr	5,414.72	5,405.509	5,946.71	572.8	572.8	582.8			
25 Mn	5,898.75	5,887.65	6,490.45	637.4	637.4	648.8			
26 Fe	6,403.84	6,390.84	7,057.98	705.0	705.0	718.5			
27 Co	6,930.32	6,915.30	7,649.43	776.2	776.2	791.4			
28 Ni	7,478.15	7,460.89	8,264.66	851.5	851.5	868.8			
29 Cu	8,047.78	8,027.83	8,905.29	929.7	929.7	949.8			
30 Zn	8,638.86	8,615.78	9,572.0	1,011.7	1,011.7	1,034.7			
31 Ga	9,251.74	9,224.82	10,264.2	1,097.92	1,097.92	1,124.8			
32 Ge	9,886.42	9,855.32	10,982.1	1,188.00	1,188.00	1,218.5			
33 As	10,543.72	10,507.99	11,726.2	1,282.0	1,282.0	1,317.0			
34 Se	11,222.4	11,181.4	12,495.9	1,379.10	1,379.10	1,419.23			
35 Br	11,924.2	11,877.6	13,291.4	1,480.43	1,480.43	1,525.90			
36 Kr	12,649	12,598	14,112	1,586.0	1,586.0	1,636.6			
37 Rb	13,395.3	13,335.8	14,961.3	1,694.13	1,692.56	1,752.17			
38 Sr	14,165	14,097.9	15,835.7	1,806.56	1,804.74	1,871.72			
39 Y	14,958.4	14,882.9	16,737.8	1,922.56	1,920.47	1,995.84			
40 Zr	15,775.1	15,690.9	17,667.8	2,042.36	2,039.9	2,124.4	2,219.4	2,302.7	
41 Nb	16,615.1	16,521.0	18,622.5	2,165.89	2,163.0	2,257.4	2,367.0	2,461.8	
42 Mo	17,479.34	17,374.3	19,608.3	2,293.16	2,289.85	2,394.81	2,518.3	2,623.5	
43 Tc	18,367.1	18,250.8	20,619	2,424	2,420	2,538	2,674	2,792	
44 Ru	19,279.2	19,150.4	21,656.8	2,558.55	2,554.31	2,683.23	2,836.0	2,964.5	
45 Rh	20,216.1	20,073.7	22,723.6	2,696.74	2,692.05	2,834.41	3,001.3	3,143.8	
46 Pd	21,177.1	21,020.1	23,818.7	2,838.61	2,833.29	2,990.22	3,171.79	3,328.7	
47 Ag	22,162.92	21,990.3	24,942.4	2,984.31	2,978.21	3,150.94	3,347.81	3,519.59	
48 Cd	23,173.6	22,984.1	26,095.5	3,133.73	3,126.91	3,316.57	3,528.12	3,716.86	
49 In	24,209.7	24,002.0	27,275.9	3,286.94	3,279.29	3,487.21	3,713.81	3,920.81	
50 Sn	25,271.3	25,044.0	28,486.0	3,443.98	3,435.42	3,662.80	3,904.86	4,131.12	
51 Sb	26,359.1	26,110.8	29,725.6	3,604.72	3,595.32	3,843.57	4,100.78	4,347.79	
52 Te	27,472.3	27,201.7	30,995.7	3,769.33	3,758.8	4,029.58	4,301.7	4,570.9	
53 I	28,612.0	28,317.2	32,294.7	3,937.65	3,926.04	4,220.72	4,507.5	4,800.9	
54 Xe	29,779	29,458	33,624	4,109.9	—	—	—	—	
55 Cs	30,972.8	30,625.1	34,986.9	4,286.5	4,272.2	4,619.8	4,935.9	5,280.4	
56 Ba	32,193.6	31,817.1	36,378.2	4,466.26	4,450.90	4,827.53	5,156.5	5,531.1	
57 La	33,441.8	33,034.1	37,801.0	4,650.97	4,634.23	5,042.1	5,383.5	5,788.5	833
58 Ce	34,719.7	34,278.9	39,257.3	4,840.2	4,823.0	5,262.2	5,613.4	6,052	883
59 Pr	36,026.3	35,550.2	40,748.2	5,033.7	5,013.5	5,488.9	5,850	6,322.1	929
60 Nd	37,361.0	36,847.4	42,271.3	5,230.4	5,207.7	5,721.6	6,089.4	6,602.1	978
61 Pm	38,724.7	38,171.2	43,826	5,432.5	5,407.8	5,961	6,339	6,892	—
62 Sm	40,118.1	39,522.4	45,413	5,636.1	5,609.0	6,205.1	6,586	7,178	1,081

Inside a synchrotron radiation source



Electron speed near c :
 $0.999999994 c$, $\gamma = 3719$
 Einstein needed again—
Special Relativity

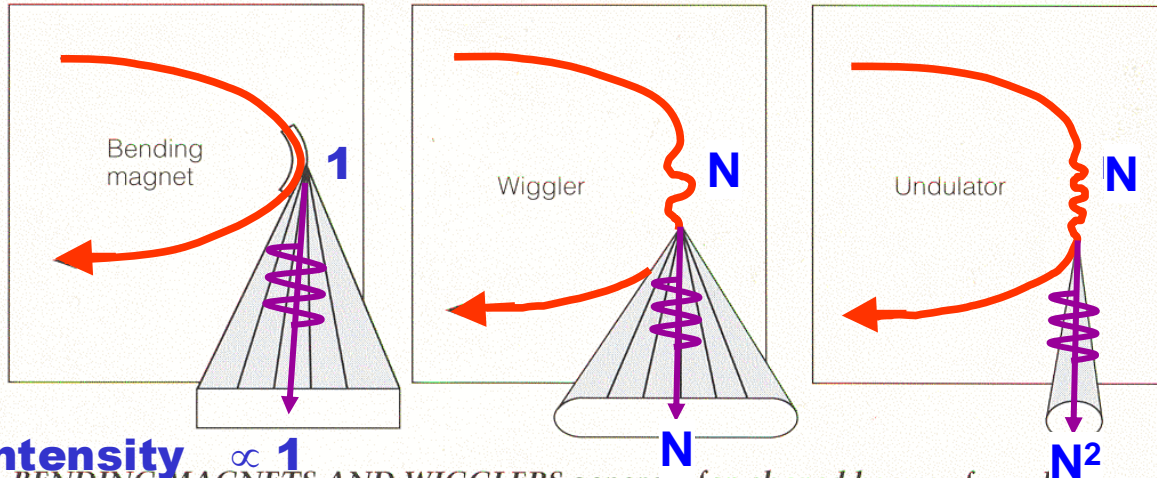
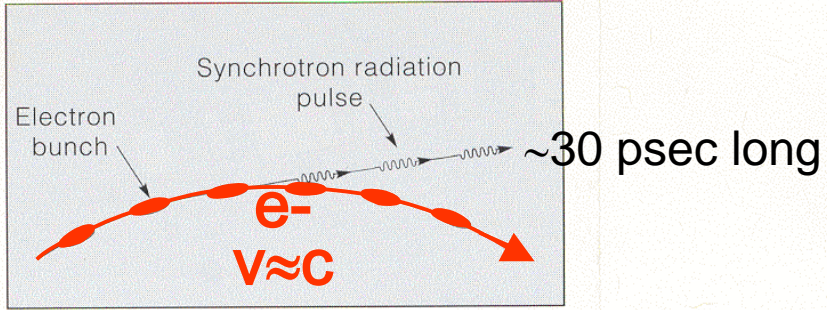
Undulator Radiation



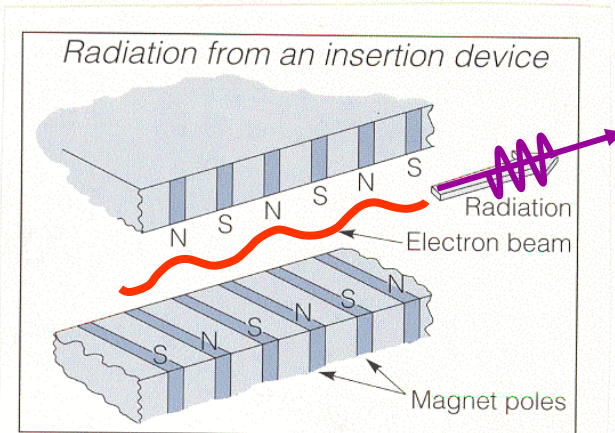
Radiofrequency Cavity

+Doppler
 $v = \gamma^2 c / \lambda_u$

Synchrotron Radiation Sources:



BENDING MAGNETS AND WIGGLERS generate fan-shaped beams of synchrotron radiation, whereas undulators emit pencil-thin beams.



Synchrotron Radiation Sources

$v = \beta c = 0.99999994 c \rightarrow \gamma \approx 2,900$

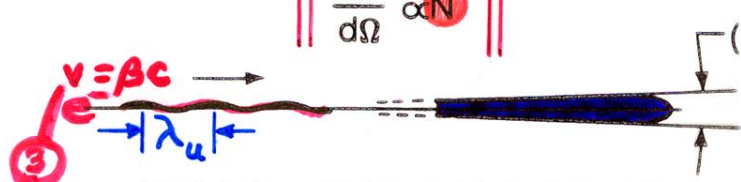


+DOPPLER SHIFT:



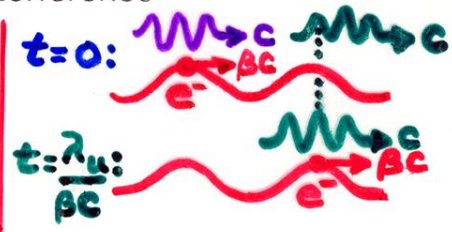
$\nu_0 = \nu \sqrt{\frac{1+\beta}{1-\beta}}$
 $\approx 5,700 \nu$!

$\frac{dP}{d\Omega} \propto N$



CHARACTERISTIC λ :
 $\frac{\lambda}{c} = \frac{\lambda_u}{\beta c} - \frac{\lambda_u}{c}$
 PLUS HARMONICS AT
 $\lambda/2, \lambda/3, \lambda/4, \dots$

$\frac{dP}{d\Omega} \propto N^2$
 $\Omega \propto \frac{1}{N}$
 $P \propto N$



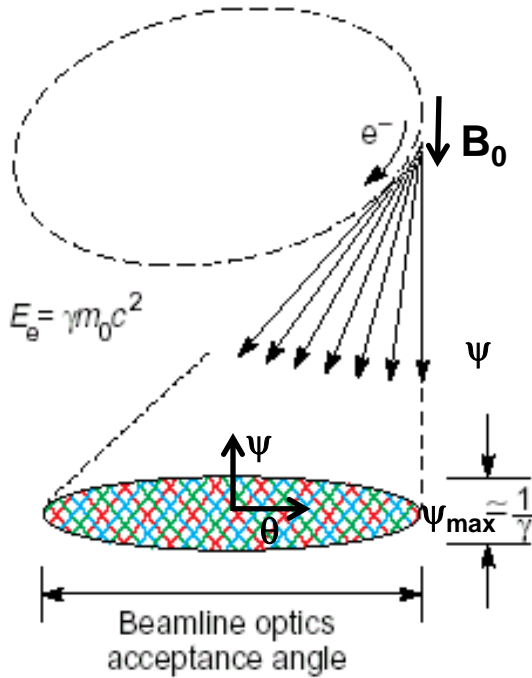
N = number of magnetic periods (~ 100)

IN GENERAL: $\gamma^{-1} = \frac{m_0 c^2}{E_e} = \frac{0.511}{E_e(\text{GeV})} \text{ mrad} = \theta_v = \text{VERTICAL ANGULAR WIDTH}$

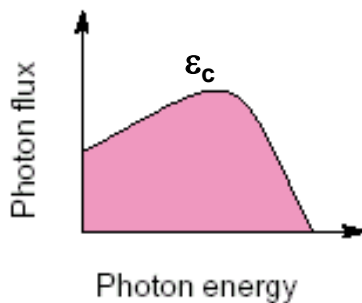
$\approx 0.34 \text{ mrad}$
 FOR ALS

Bend-Magnet Radiation

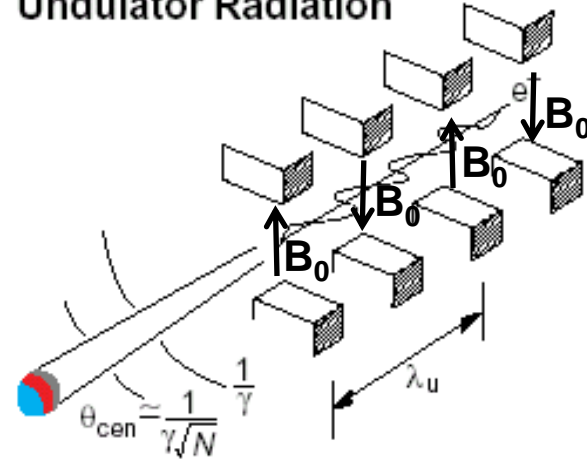
$$\gamma = \frac{1}{\sqrt{1 - \frac{v^2}{c^2}}}$$



$\epsilon_c =$ Critical energy [keV] = 0.665 E^2 [GeV]B[T]



Undulator Radiation



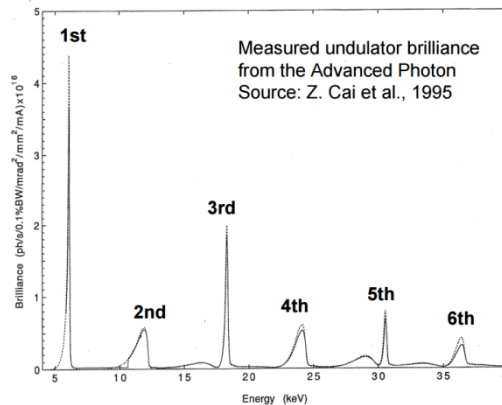
$$\lambda_x = \frac{\lambda_u}{2\gamma^2} (1 + \frac{K^2}{2} + \gamma^2\theta^2) \quad K = \frac{eB_0\lambda_u}{2\pi m_0 c}$$

In the central radiation cone:

$$\frac{\Delta\omega}{\omega} \approx \frac{1}{N}$$

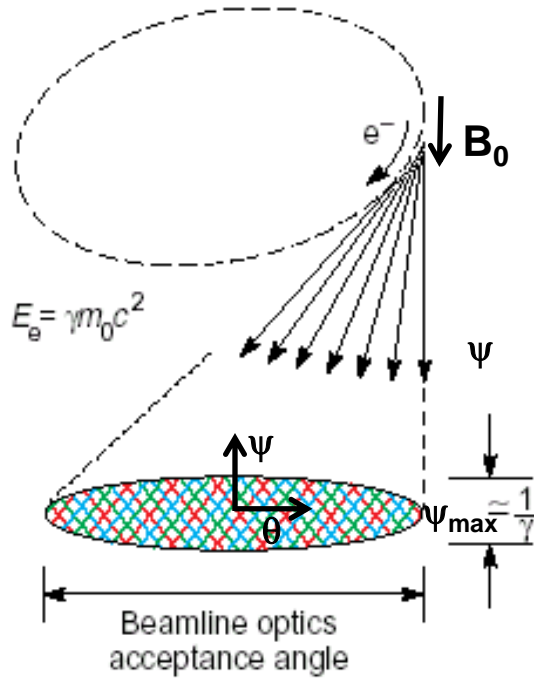
$$\theta_{cen} \approx \frac{1}{\gamma\sqrt{N}}$$

λ_x as observed will increase if the magnetic field B_0 is increased and/or the gap of the magnets is made smaller, or if viewed away from the axis by an angle θ
Odd harmonics are much stronger than even harmonics

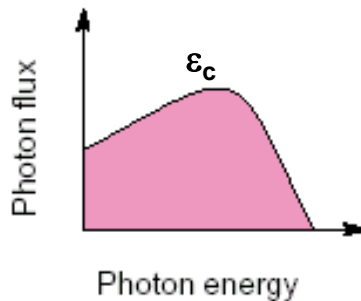


Bend-Magnet Radiation

$$\gamma = \frac{1}{\sqrt{1 - \frac{v^2}{c^2}}}$$



$\epsilon_c =$ Critical energy [keV] = 0.665 E^2 [GeV]B[T]



In practical units [photons · s⁻¹ · m^r · (0.1% bandwidth)⁻¹],

$$\left. \frac{d^2 \dot{S}_B}{d\theta d\psi} \right|_{\psi=0} = 1.327 \times 10^{13} E^2 [\text{GeV}] I [\text{A}] H_2(y)$$

1 mrad = 10⁻²(360/2π) = 0.0572°

The function $H_2(y)$ is shown in Fig. 2-1.

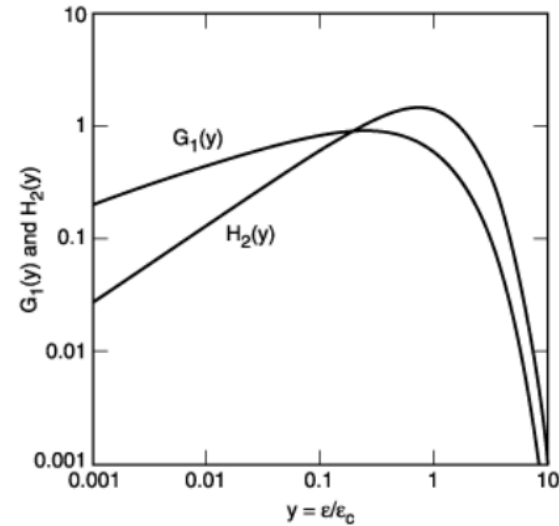


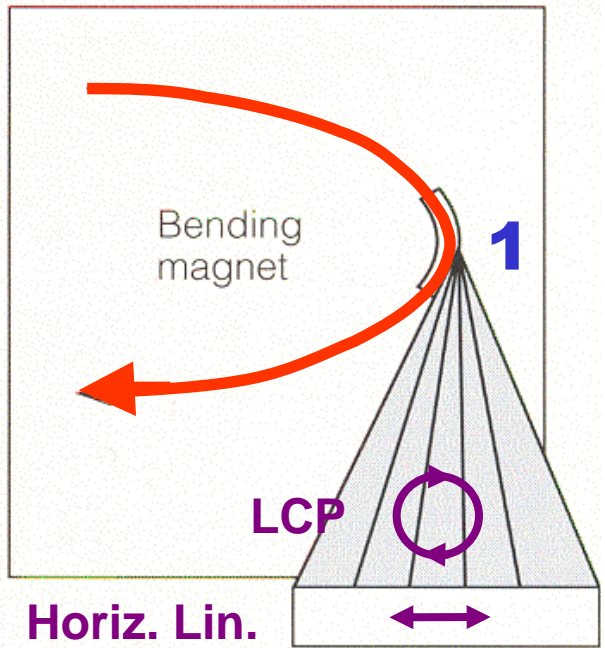
Fig. 2-1. The functions $G_1(y)$ and $H_2(y)$, where y is the ratio of photon energy to critical photon energy.

The distribution integrated over ψ is given by

In practical units [photons · s⁻¹ · m^r · (0.1% bandwidth)⁻¹],

$$\frac{dS_B}{d\theta} = 2.457 \times 10^{13} E [\text{GeV}] I [\text{A}] G_1(y)$$

Variable polarization with a bend magnet: above and below plane



Above plane



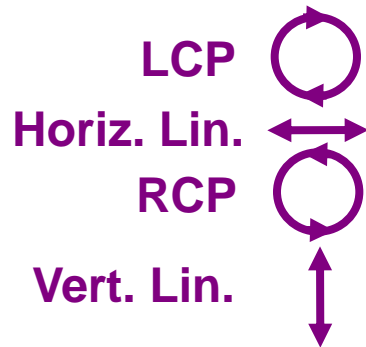
Horiz. Lin.



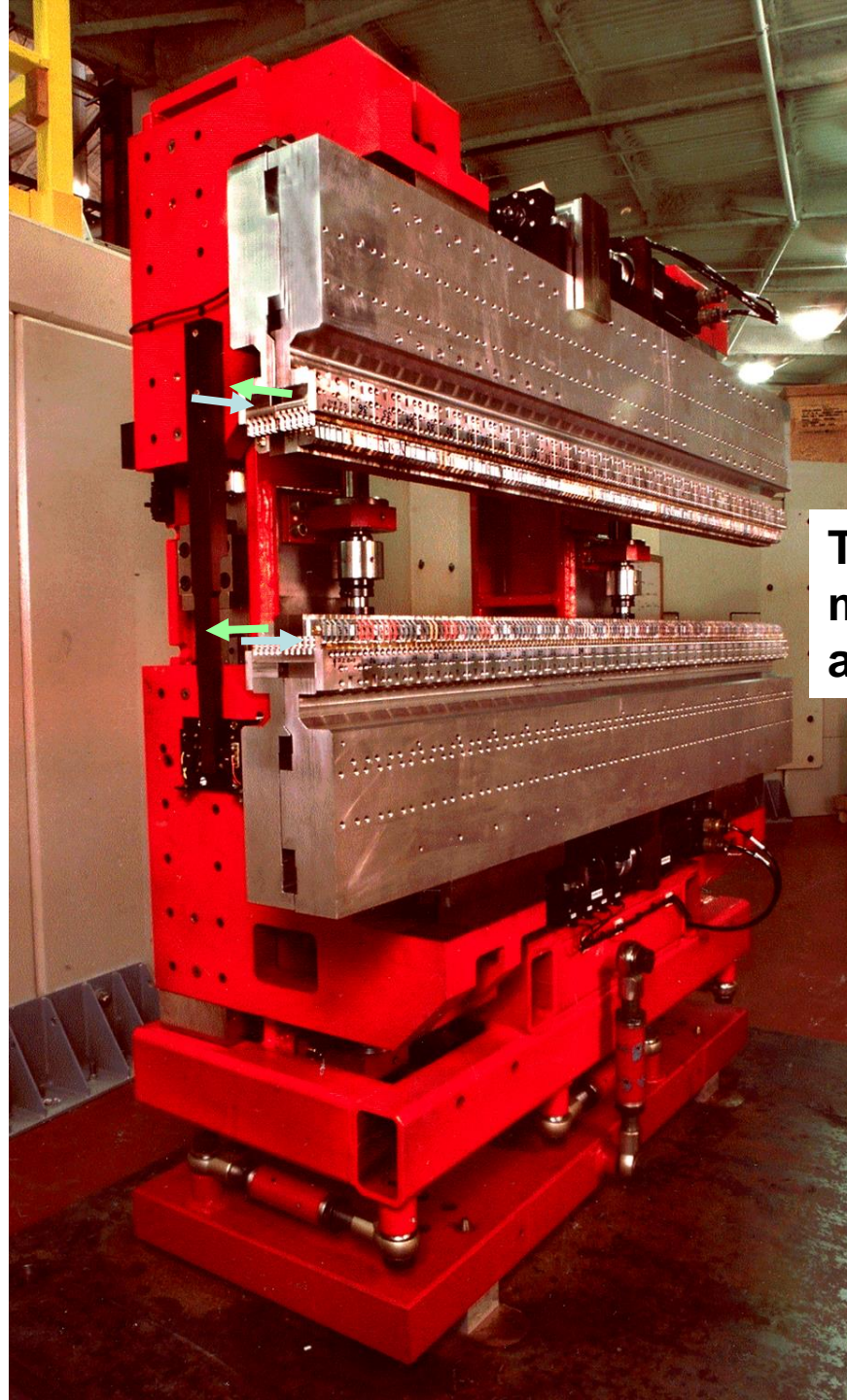
Below plane



Advanced
Light Source--
Sasaki-Carr
Elliptically-
Polarized
Undulator:
Variable light
polarization



[Can also vary polarization
to LCP, RCP by going
above and below the orbit
plane in a bend magnet]

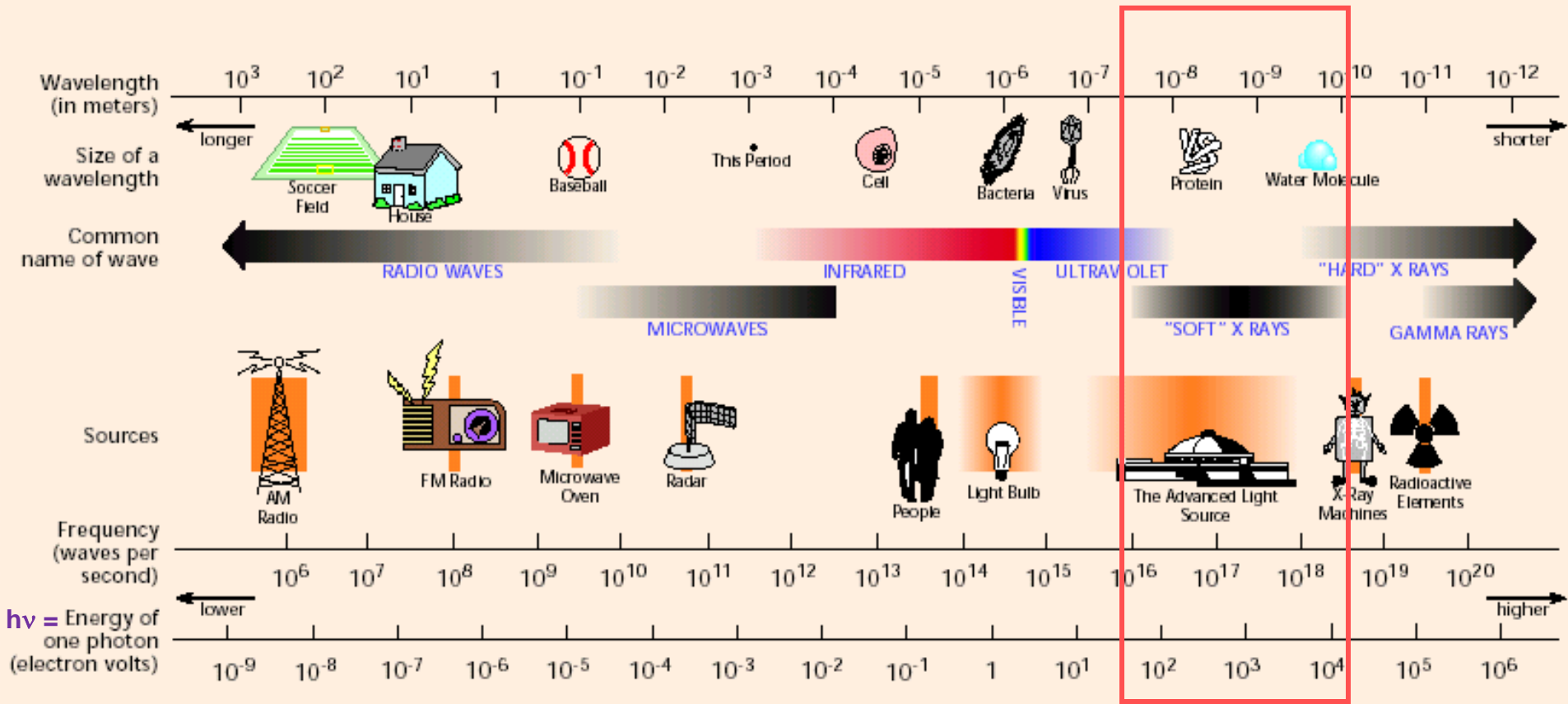


Translating
magnet
arrays

$$\lambda_x(\text{\AA}) = 12,398/[h\nu(\text{eV})]$$

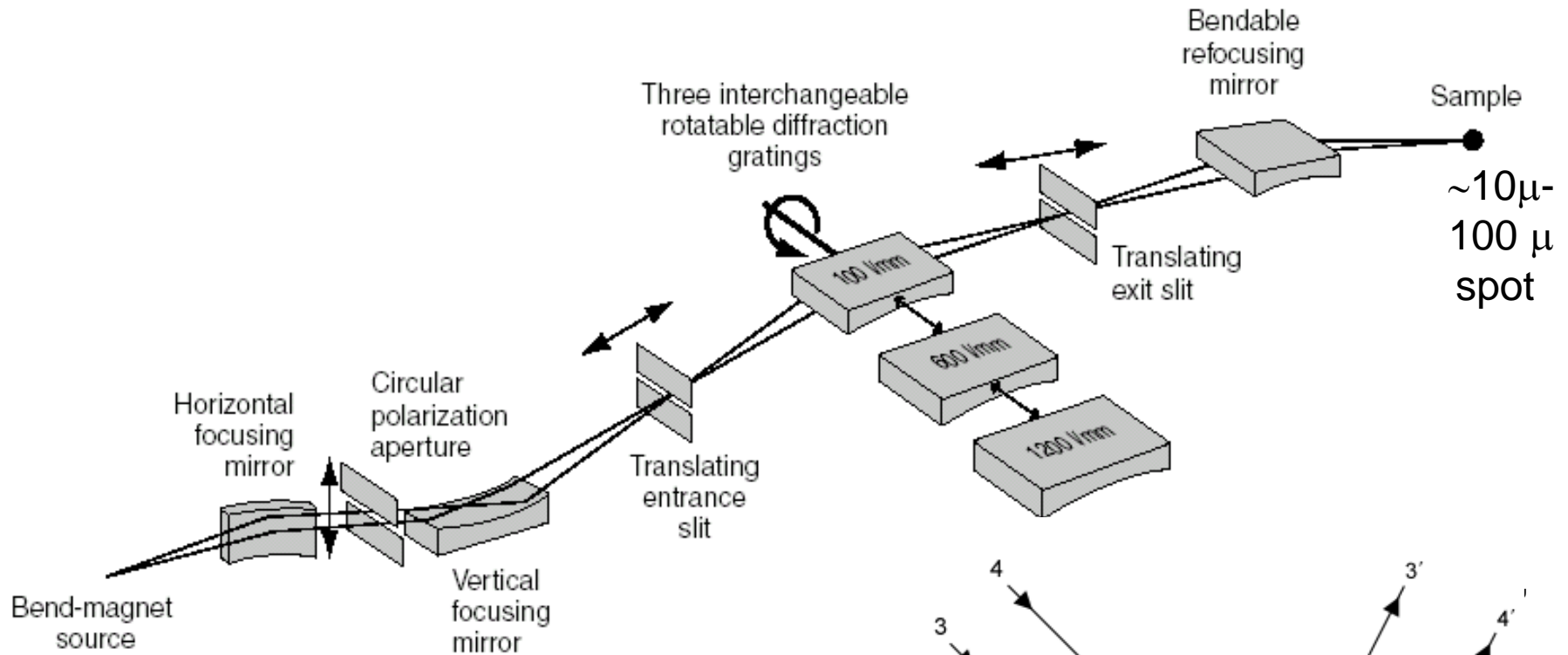
Vacuum Ultraviolet (VUV)- ~8-200 eV
 Soft x-rays ~200-2000 eV
 "Tender" x-rays ~2000-10000 eV

THE ELECTROMAGNETIC SPECTRUM

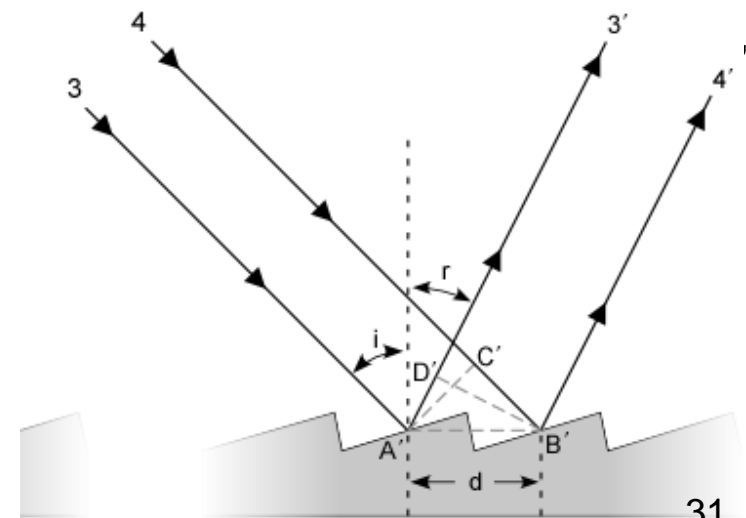


Typical surface/materials science expts.

Advanced Light Source-- Typical Soft X-Ray Spectroscopy Beamline Layout: to ca. 1500 eV

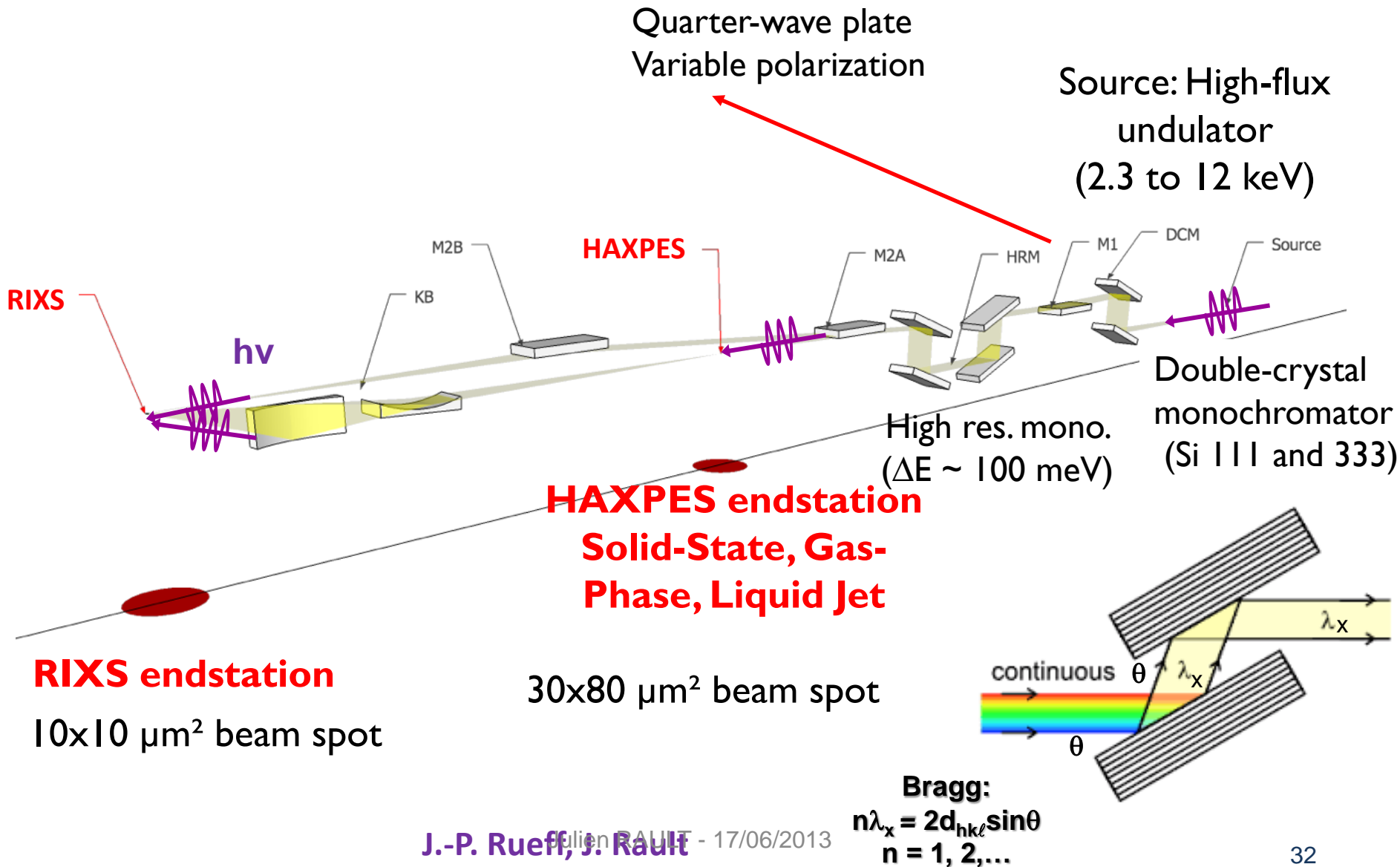


Schematic layout of Beamline 9.3.2.



$$n\lambda_x = d(\sin(i) - \sin(r))$$

Soleil (Paris)—Typical hard x-ray spectroscopy beamline



**MULTI-TECHNIQUE
SPECTROMETER/
DIFFRACTOMETER (MTSD)**

**5-axis
sample
manipulator**

**Scienta
electron
spectrometer
(hidden)**

**Sample prep.
chamber: LEED,
Knudsen cells,
electromagnet,...**

**ALS
BL 9.3.1
 $h\nu = 2-5 \text{ keV}$**

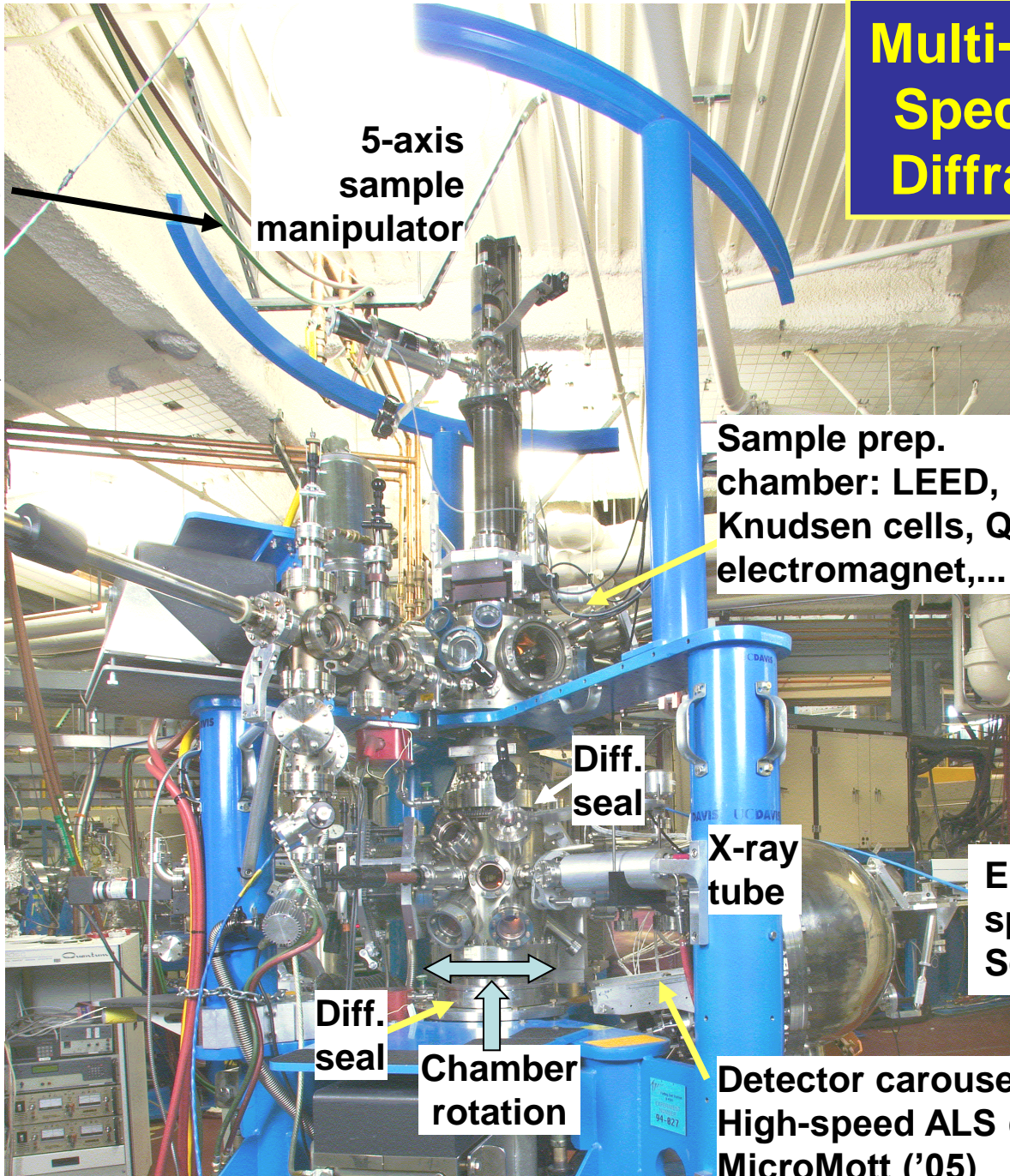


**Chamber
rotation**

**Scienta
soft x-ray
spectrometer**

Permits using all relevant soft and hard x-ray spectroscopies on a single sample:
PS, PD, PH; XAS (e^- or photon detection), XES/RIXS, with MCD, MLD

Multi-Technique Spectrometer/ Diffractometer



Sample manipulator:
to be upgraded, '05:
T down to ~6 K

Loadlock
for sample
introduction

Soft x-ray spectrometer:
Scienta
XES 300

5-axis
sample
manipulator

Sample prep.
chamber: LEED,
Knudsen cells, QCM,
electromagnet,...

Diff.
seal

X-ray
tube

Electron
spectrometer:
Scienta SES 200

Diff.
seal

Chamber
rotation

Detector carousel:
High-speed ALS detector ('05)
MicroMott ('05)

Synchrotron radiation sources of the world- about 41 and growing Free-electron laser (UV, X-ray)- about 5 and growing



Nature Photonics 9, 281 (2015)



San Francisco

Marin County

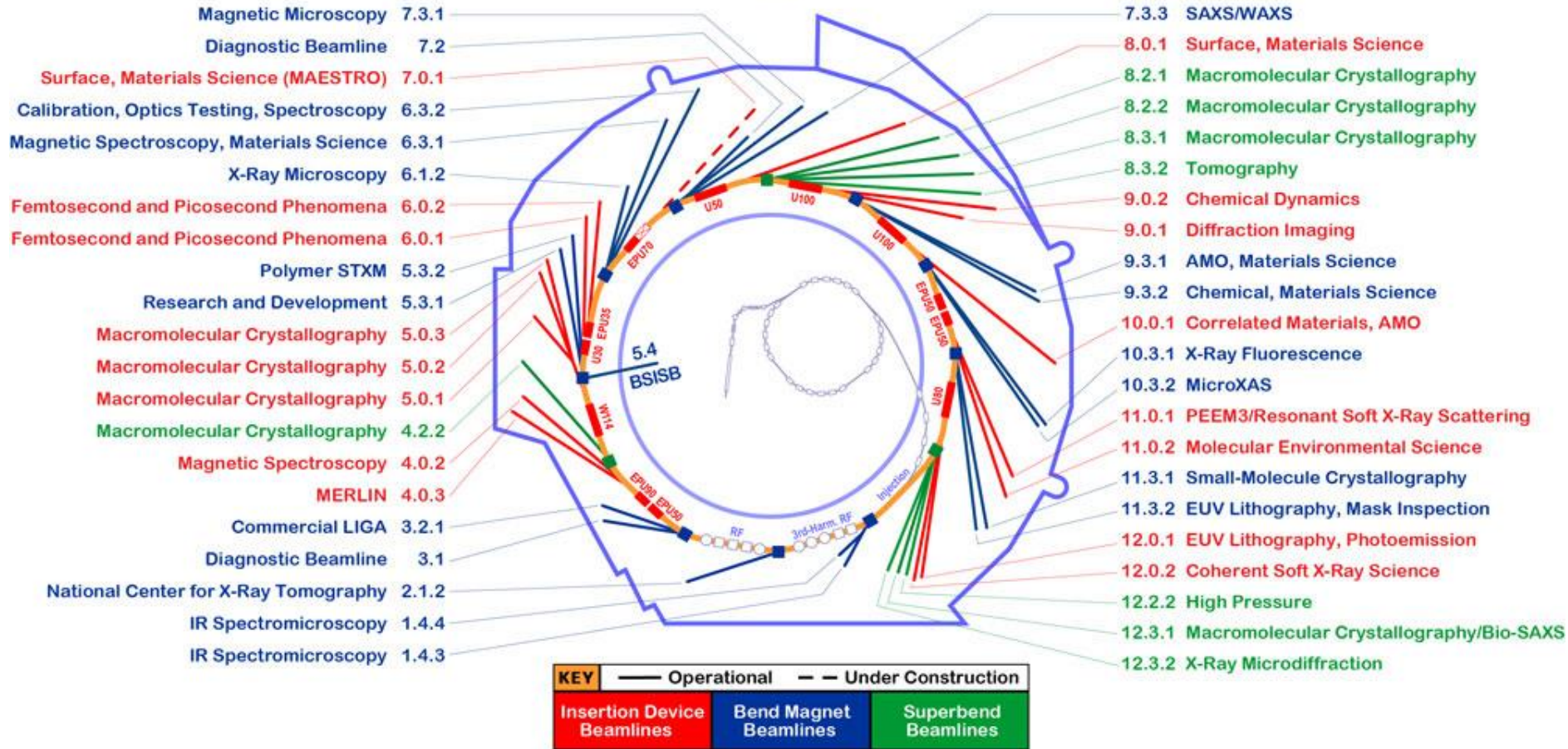
UC Berkeley

Advanced
Light Source

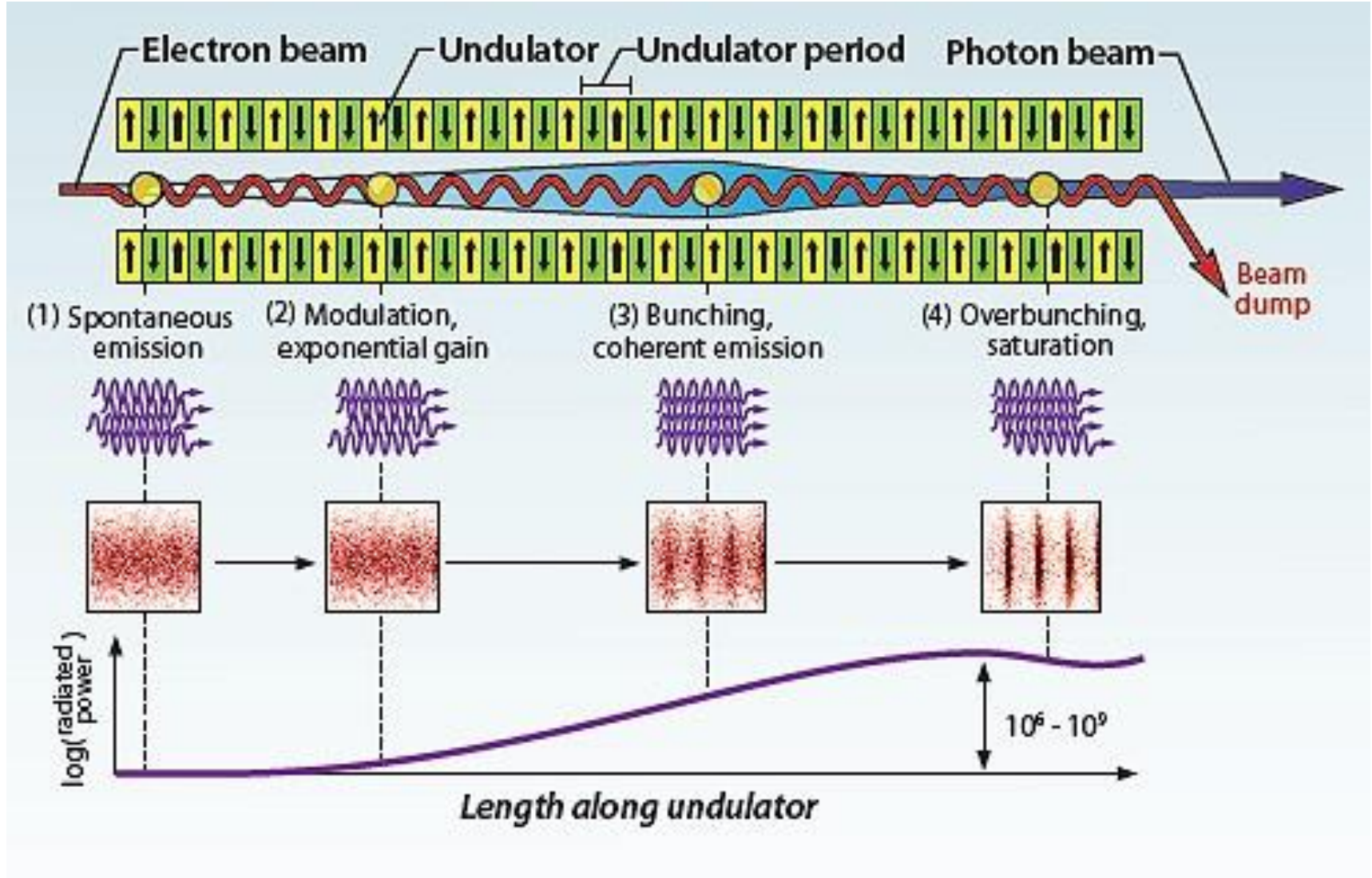
Group offices
& lab.

ALS Beamlines

January 2014



The Next Generation: The Free-Electron Laser

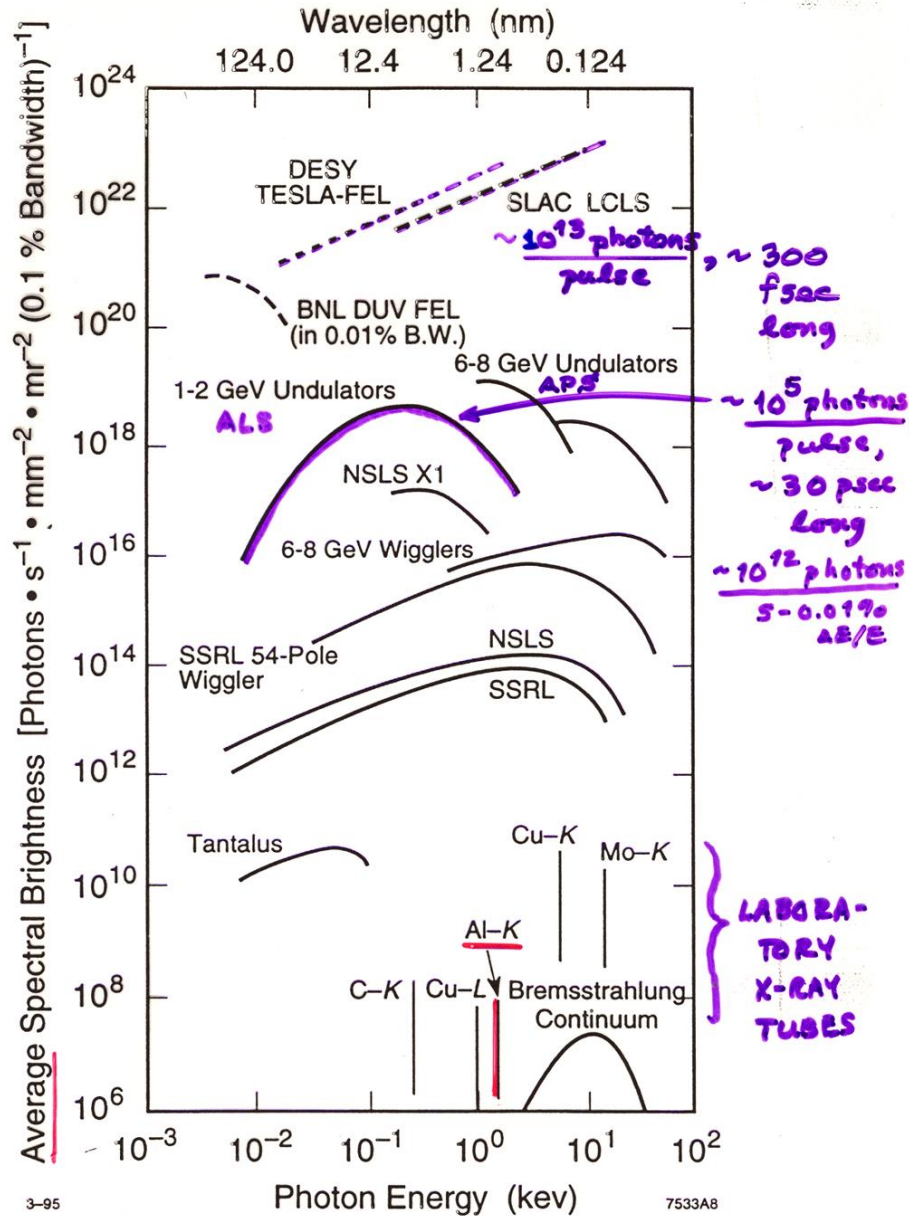


Average brightness

PRESENT
&
FUTURE

PRESENT

PAST



3-95

7533A8

Fig. 2. Average brightness comparisons of the LCLS and other light sources, including proposed FELs at Brookhaven [14] and DESY [15].

“X-Ray Data
Booklet”
39
See Fig. 2.10

Peak brightness

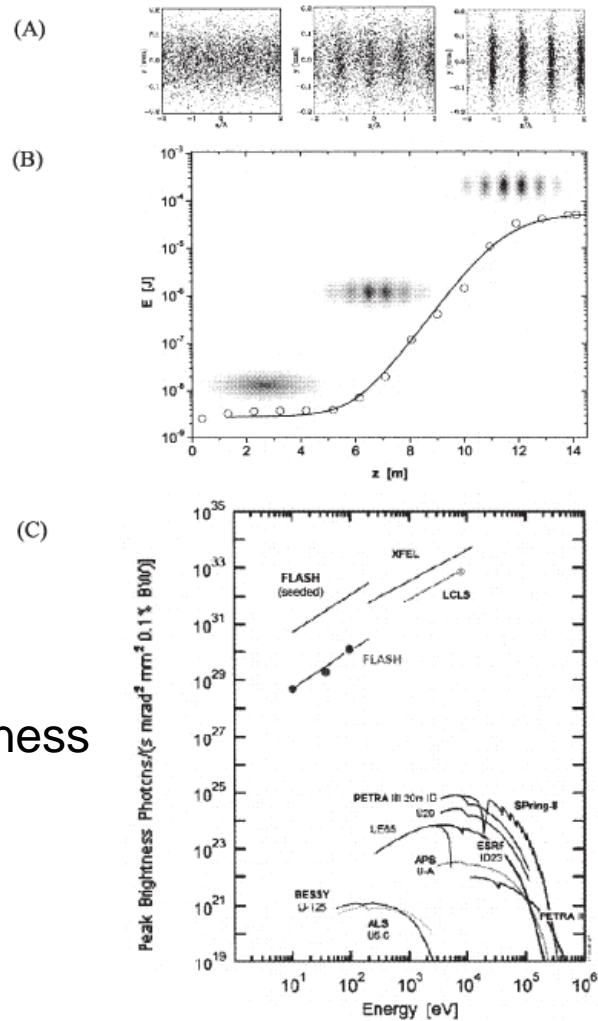
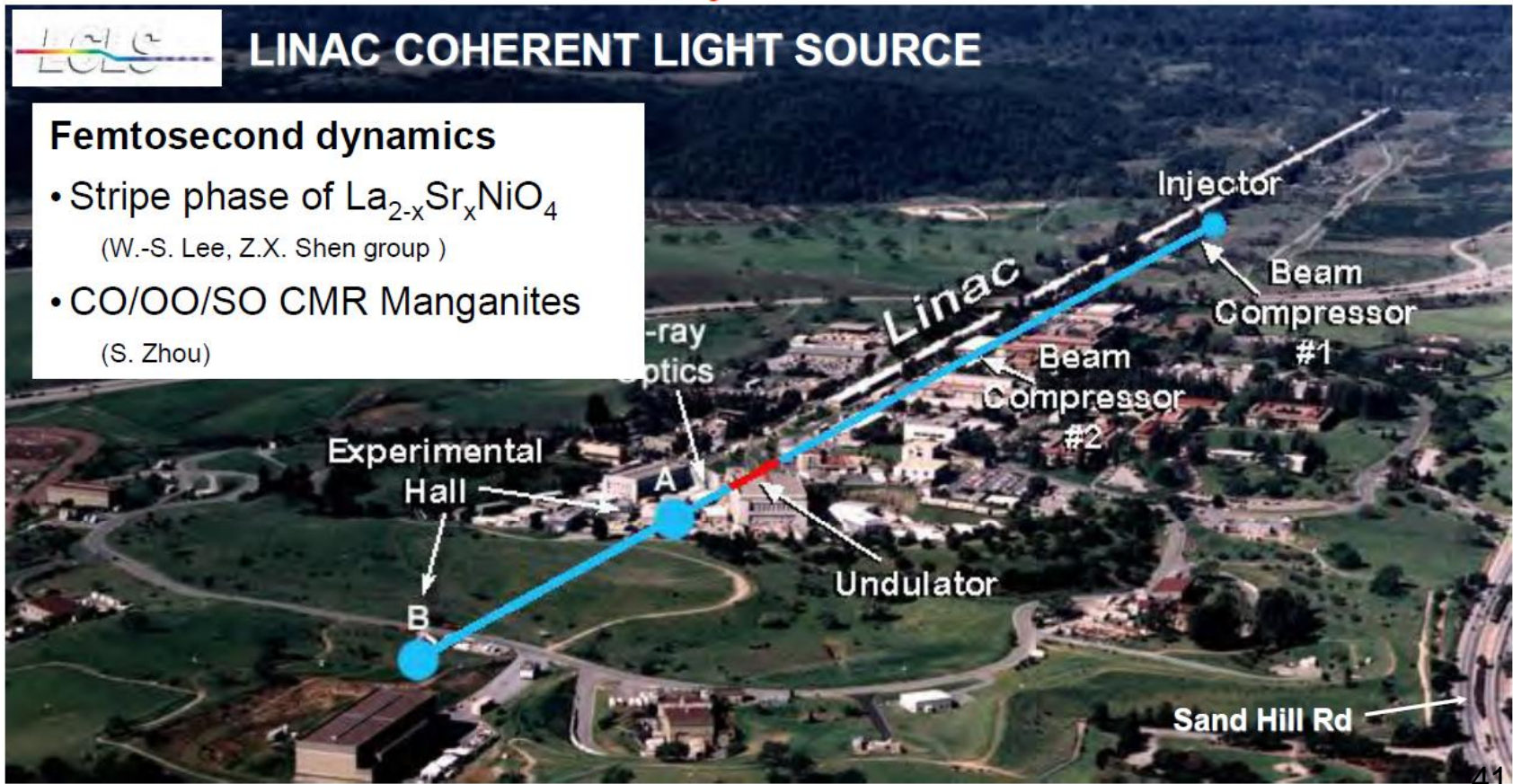


Figure 2-10. (A) Simulation of the electron microbunching process and (B) the exponential growth of FEL output energy due to microbunching (following S. Reiche and K.-J. Kim). (C) FEL beams have very short pulse duration and full spatial coherence, with peak brightness many orders of magnitude higher than 3rd generation synchrotron facilities [4, modified].

Future – Ultrafast X-ray Science X-ray Free-Electron Lasers!

SLAC National Accelerator Laboratory



The five ways in which x-rays interact with Matter:

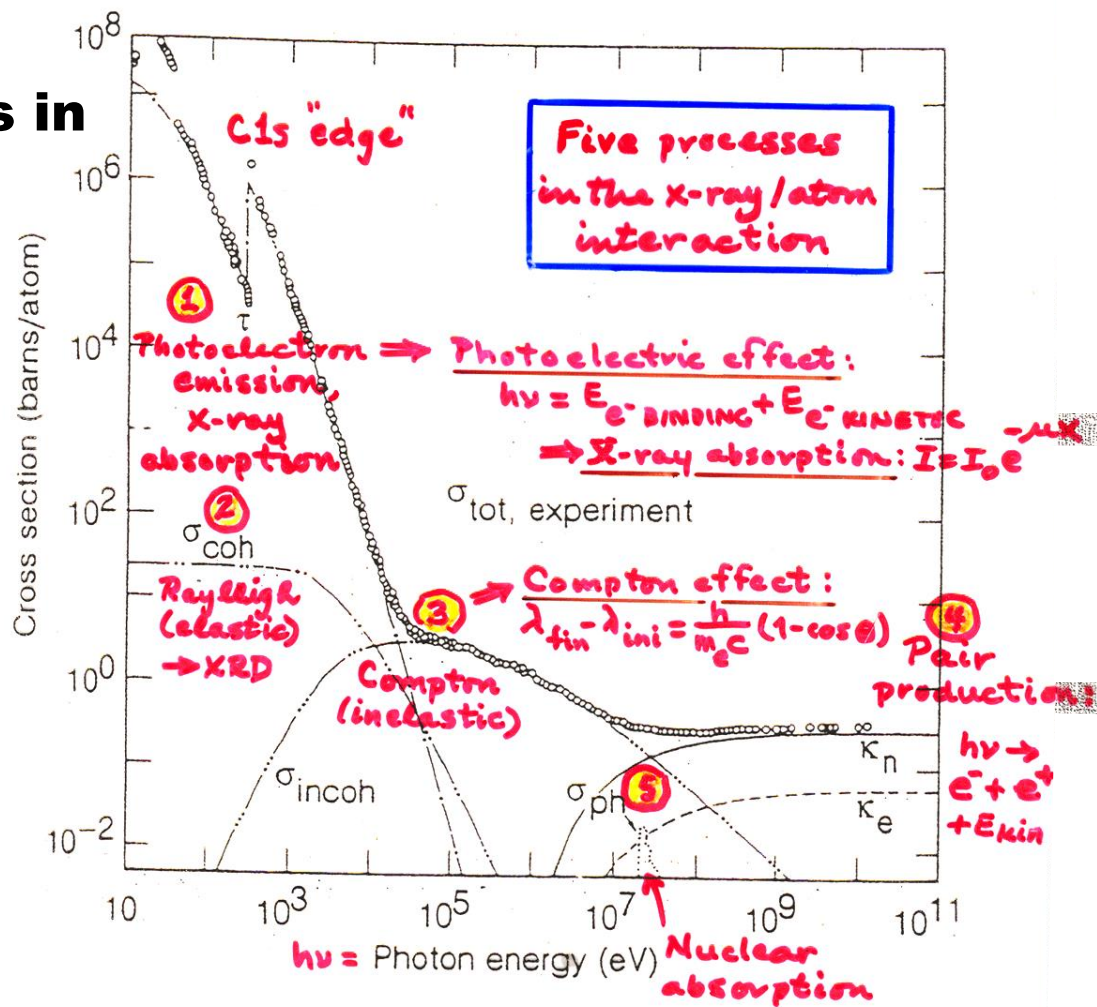
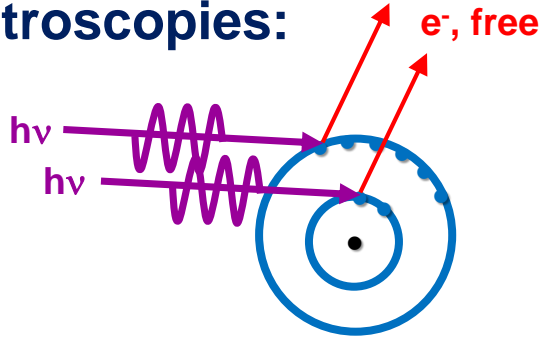


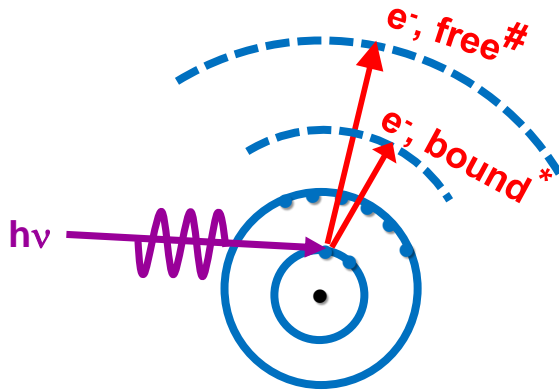
Fig. 3-1. Total photon cross section σ_{tot} in carbon, as a function of energy, showing the contributions of different processes: τ , atomic photo-effect (electron ejection, photon absorption); σ_{coh} , coherent scattering (Rayleigh scattering—atom neither ionized nor excited); σ_{incoh} , incoherent scattering (Compton scattering off an electron) κ_n , pair production, nuclear field; κ_e , pair production, electron field; σ_{ph} , photonuclear absorption (nuclear absorption usually followed by emission of a neutron or other particle). (From Ref. 3; figure courtesy of J. H. Hubbell.)

The vacuum ultraviolet, soft x-ray, hard x-ray measurements:

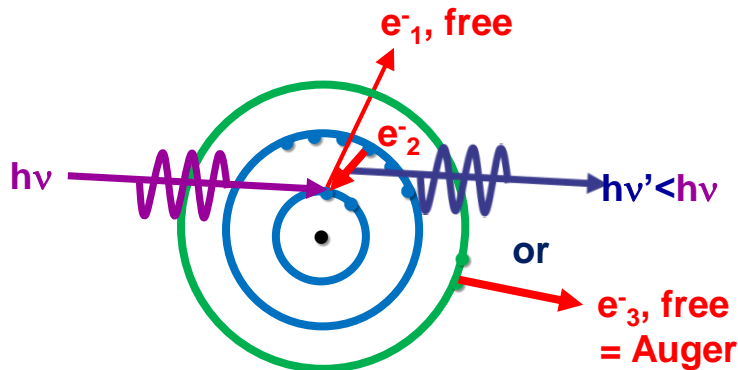
The spectroscopies:



PHOTOELECTRON SPECTROSCOPY=
PHOTOEMISSION – PS, PES, UPS, XPS
+ **DIFFRACTION-XPD, PhD**
+ HOLOGRAPHY-PH
+ MICROSCOPY-PEEM



X-RAY ABSORPTION SPECTROSCOPY- XAS
* NEAR-EDGE – NEXAFS, XANES
+ X-RAY MAGNETIC CIRCULAR/LINEAR
DICHROISM- XMCD, XMLD
EXTENDED- EXAFS, XAFS



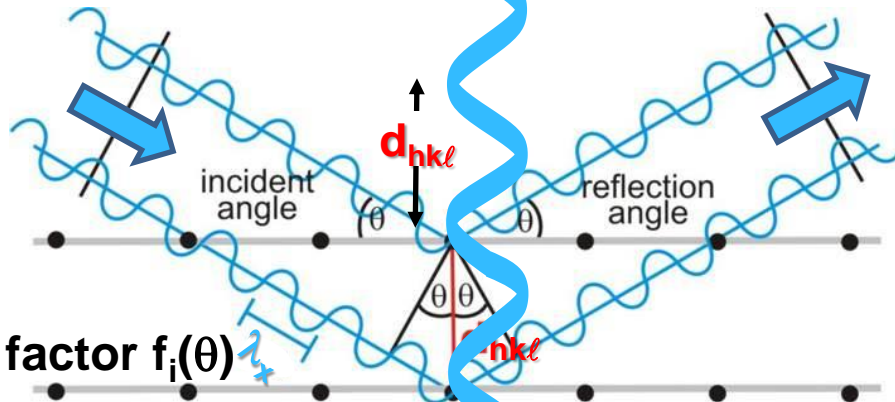
X-RAY EMISSION (FLUORESCENCE)
SPECTROSCOPY

+ AUGER ELECTRON SPECTROSCOPY
(Always accompanies photoelectron emission)

The ultraviolet, soft x-ray, hard x-ray measurements:

X-ray diffraction from crystals and multilayers, standing waves:

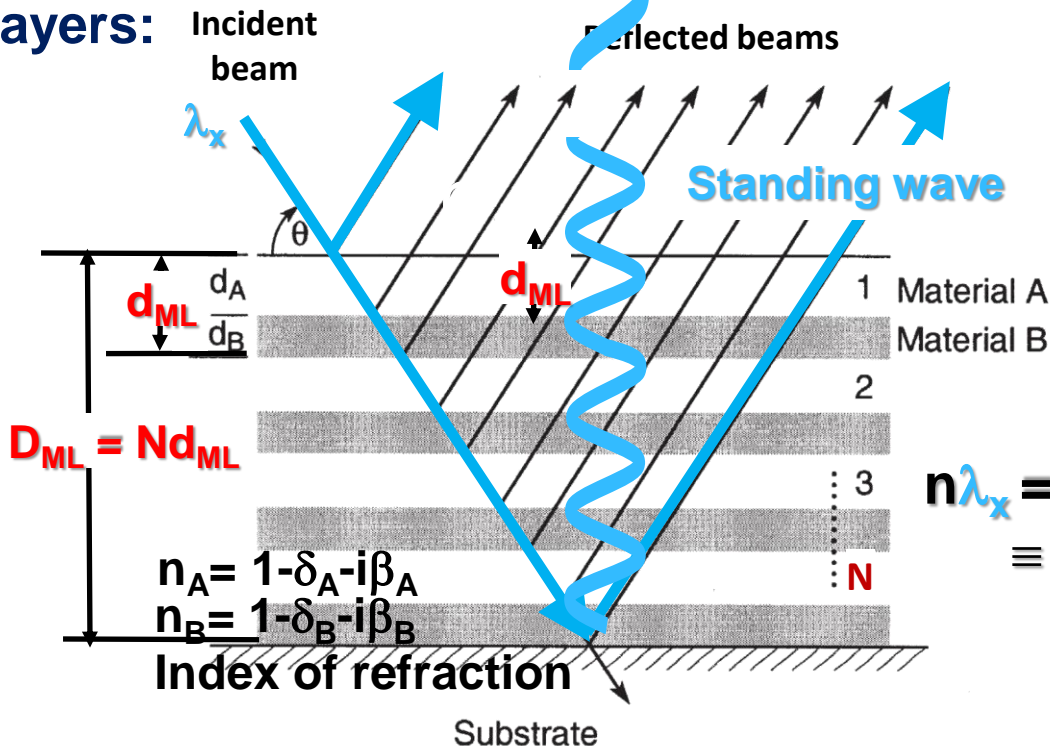
From crystals:



Bragg:
 $n\lambda_x = 2d_{hkl} \sin\theta$
 $n = 1, 2, \dots$

Atomic scattering factor $f_i(\theta)$

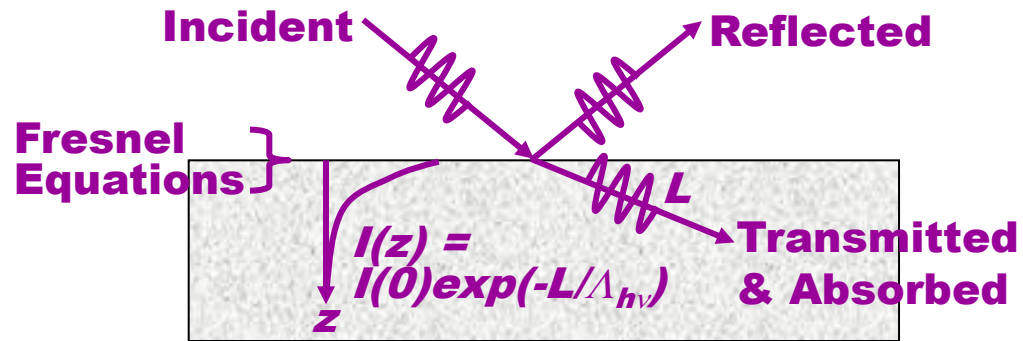
From multilayers:



+Kiessig fringes:
 $m\lambda_x = 2\sin\theta_m$
 $= 2D_{ML} \sin\theta_m$
 $m = \text{usually large (often unknown) number}$

Bragg:
 $n\lambda_x = 2(d_A + d_B) \sin\theta_n$
 $\equiv 2d_{ML} \sin\theta_n$
 $n = 1, 2, \dots$

A LITTLE X-RAY OPTICS



(E.G. See pp. 1-38, 1-44, 5-18-5-19 in X-Ray Data Booklet)

Index of refraction = $n = 1 - \delta - i\beta$

(Sometimes with + signs on δ and/or β)

$\delta = +$ no. = refractive decrement $\ll 1$

(Sometimes changes sign through absorption resonances)

$\beta = +$ no. = absorptive decrement $\ll 1$

δ and β linked by Kramers-Kronig transform

n also = $1 - (r_e/2\pi)\lambda_{hv}^2 \sum n_i f_i(0 = \text{fwd. scatt.})$

r_e = classical electron radius
 $= e^2/4\pi\epsilon_0 m_e e^2 = 2.817 \times 10^{-15} \text{ m}$
 $\lambda_{hv} = \text{x-ray wavelength}$

$n_i =$ no. i atoms per unit volume

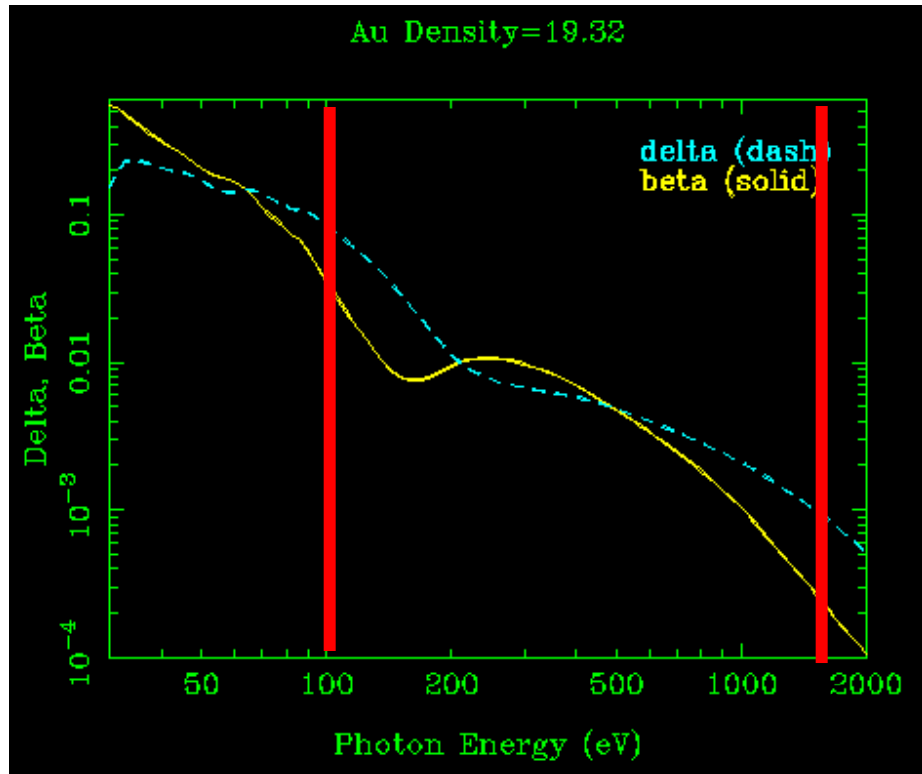
$f_i =$ x-ray scattering factor for i th type of atom, in forward direction

Exponential absorption length = $l_{\text{abs}} = \lambda_{hv}/(4\pi\beta) = \Lambda_{hv}$

$\theta_{\text{CRIT}} =$ critical grazing angle at which reflectivity begins ($R \approx 0.20$)
 $= [2\delta]^{0.5}$

Online data and calculations at:
http://henke.lbl.gov/optical_constants/getdb2.html

Sections 1.6 and 1.7 of X-Ray Data Booklet



coefficient μ (cm^2/g) is related to the transmitted intensity through a material of density ρ (g/cm^3) and thickness d by

$$I = I_0 e^{-\mu \rho d} \quad (1)$$

Thus, the linear absorption coefficient is μ_ℓ (cm^{-1}) = $\mu\rho$. For a pure material, the mass absorption coefficient is directly related to the total atomic absorption cross section σ_a (cm^2/atom) by

$$\mu = \frac{N_A}{A} \sigma_a \quad , \quad 4\pi\beta/\lambda_x = \mu_\ell = (N_A/A)\rho\sigma_a = 1/\Lambda_{\text{hv}} \quad (2)$$

where N_A is Avogadro's number and A is the atomic weight. For a compound material, the mass absorption coefficient is obtained from the sum of the absorption cross sections of the constituent atoms by

$$\mu = \frac{N_A}{MW} \sum_i x_i \sigma_{ai} \quad , \quad (3)$$

where the molecular weight of a compound containing x_i atoms of type i is $MW = \sum_i x_i A_i$. This approximation, which neglects interactions among the atoms in the material, is generally applicable for photon energies above about 30 eV and sufficiently far from absorption edges.

1.7 ATOMIC SCATTERING FACTORS

Eric M. Gullikson

The optical properties of materials in the photon energy range above about 30 eV can be described by the atomic scattering factors. The index of refraction of a material is related to the scattering factors of the individual atoms by

$$n = 1 - \delta - i\beta = 1 - \frac{r_e}{2\pi} \lambda^2 \sum_i n_i f_i(0) \quad , \quad (1)$$

where r_e is the classical electron radius, λ is the wavelength, and n_i is the number of atoms of type i per unit volume. The parameters δ and β are called the refractive index decrement and the absorption index, respectively. The complex atomic scattering factor for the forward scattering direction is

$$f(0) = f_1 + if_2 \quad . \quad (2)$$

The imaginary part is derived from the atomic photoabsorption cross section:

$$f_2 = \frac{\sigma_a}{2r_e\lambda} \quad . \quad (3)$$

The real part of the atomic scattering factor is related to the imaginary part by the Kramers-Kronig dispersion relation:

$$f_1 = Z^* + \frac{1}{\pi r_e h c} \int_0^\infty \frac{\varepsilon^2 \sigma_a(\varepsilon)}{E^2 - \varepsilon^2} d\varepsilon \quad . \quad (4)$$

In the high-photon-energy limit, f_1 approaches Z^* , which differs from the atomic number Z by a small relativistic correction:

$$Z^* = Z - (Z/82.5)^{2.37} \quad . \quad (5)$$

Sections 1.6 and 1.7 of X-Ray Data Booklet Plus the "Bible" of Soft X-Ray Optics: Henke, Gullikson, Davis, Atomic and Nuclear Data Tables 54, 181-342 (1993)

SOME X-RAY OPTICAL EFFECTS: REDUCED PENETRATION DEPTHS AND INCREASED REFLECTIVITY AT GRAZING INCIDENCE ANGLES

θ_{CRIT} = Grazing angle at which reflectivity begins ($R \approx 0.20$)
 $= [2\delta]^{0.5}$

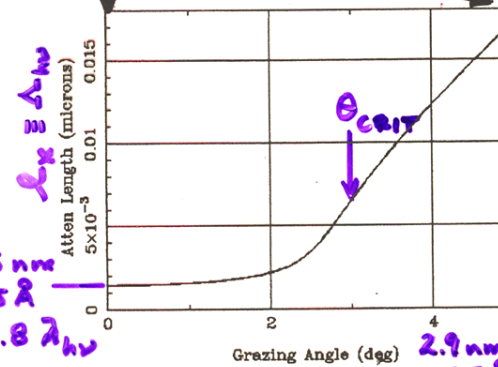
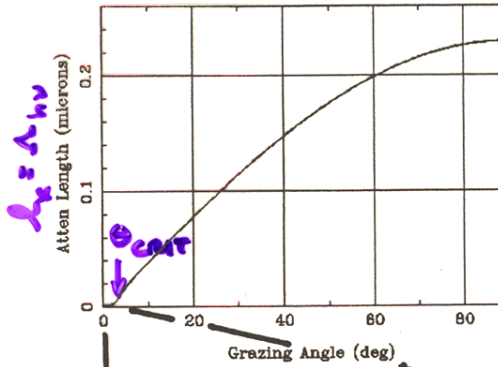
Calculated online from:
http://henke.lbl.gov/optical_constants/atten2.html

ENHANCED SURFACE SENSITIVITY @ GRAZING INCIDENCE



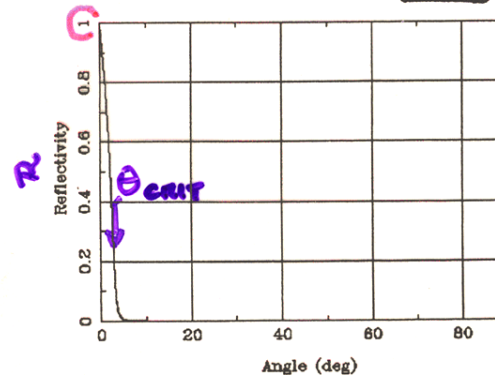
X-Ray Attenuation Length

Au Density=19.32, Energy=1487.eV



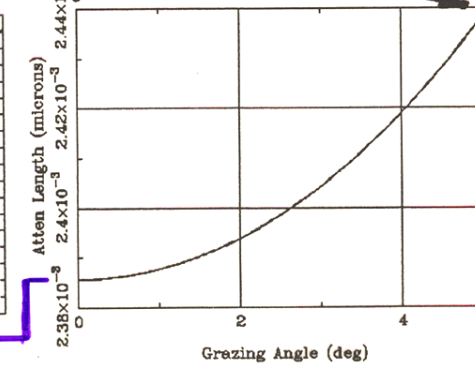
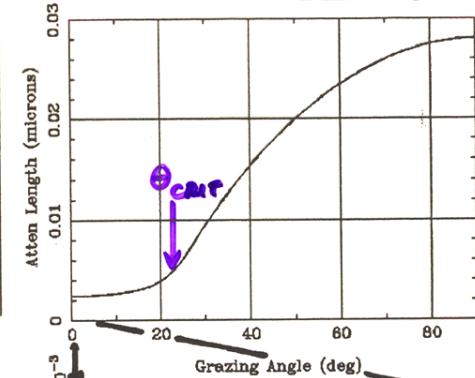
Mirror Reflectivity

Au Rho=19.32, Sig=0.nm, P=-1., E=1487.eV



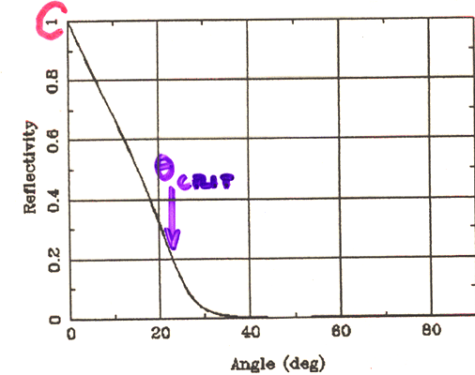
X-Ray Attenuation Length

Au Density=19.32, Energy=100.eV



Mirror Reflectivity

Au Rho=19.32, Sig=0.nm, P=-1., E=100.eV



Multilayer Reflectivity

- Top Material: Si . Density: -1 gm/cm³.
(enter negative value to use tabulated density.)
- Bottom Material: Mo . Density: -1 gm/cm³.
- Multilayer Period: 3.0 nm.
- Ratio of (Bottom layer thickness)/(Period): 0.5 .
- Interdiffusion thickness : 0 nm (Sigma).
- Number of periods: 20 (enter negative value for semi-infinite multilayer.)
- Substrate Material: SiO2 . Density: -1 gm/cm³.
- Polarization: -1 (-1 < pol < 1) where s=1, p=-1 and unpolarized=0.
- Scan Grazing Angle (deg) from 0 to 20 in 500 steps (< 500).
(NOTE: Energies must be in the range 30 eV < E < 30,000 eV, Wavelength between 0.041 nm < Wavelength < 41 nm, and Angles between 0 & 90 degrees.)
- At fixed Energy (eV) = 1000

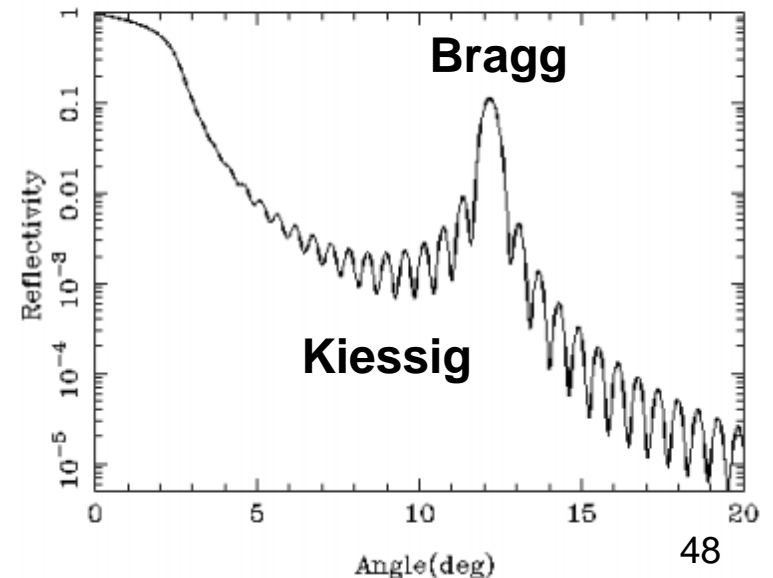
To request a press this button:

To reset to default values, press this button:

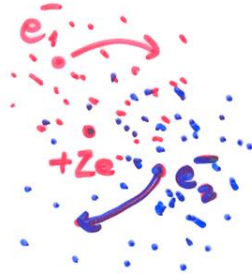
http://henke.lbl.gov/optical_constants/multi2.html

Multilayer Reflectivity

Si/Mo d=3.nm s=0.nm N=20 at 1000.eV, P=-1.



What properties do wave functions of overlapping (thus indistinguishable) particles have?—electrons as example:



$\psi = \psi(\vec{r}_1, \vec{s}_1; \vec{r}_2, \vec{s}_2)$, including spin of both electrons

But labels can't affect any measurable quantity.

E.g. – probability density :

$$|\psi(\vec{r}_1, \vec{s}_1; \vec{r}_2, \vec{s}_2)|^2 = |\psi(\vec{r}_2, \vec{s}_2; \vec{r}_1, \vec{s}_1)|^2$$

Therefore

$$\begin{aligned} \psi(\vec{r}_1, \vec{s}_1; \vec{r}_2, \vec{s}_2) &= \pm 1 \psi(\vec{r}_2, \vec{s}_2; \vec{r}_1, \vec{s}_1) \\ &\equiv \hat{P}_{12} \psi(\vec{r}_1, \vec{s}_1; \vec{r}_2, \vec{s}_2) \end{aligned}$$

with \hat{P}_{12} = permutation operator $\rightarrow \vec{r}_1, \vec{s}_1; \vec{r}_2, \vec{s}_2$ and eigenvalues of ± 1

Finally, all particles in two classes :

FERMIONS : (incl. e^- 's) : ψ antisymmetric

$$s = \frac{1}{2}, \frac{3}{2}, \frac{5}{2}, \dots$$

$$\hat{P}_{12} \psi = -1 \psi$$

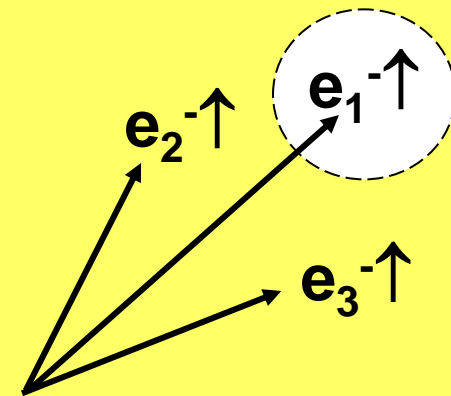
BOSONS : (incl. photons) : ψ symmetric

$$s = 0, 1, 2, \dots$$

$$\hat{P}_{12} \psi = +1 \psi$$

A brief review of electronic structure in atoms, molecules, and solids

Probability of finding two electrons at the same point in space with the same spin is zero: “the Fermi Hole”



→the Exchange Interaction
→Hund's 1st rule & magnetism

Antisymmetry and the Pauli Exclusion Principle:

Try Helium, 2 electrons in ground state 1s wave functions, "1s²"

Simple normalized antisymmetric trial wave function is

$$\psi(\vec{r}_1, \vec{s}_1; \vec{r}_2, \vec{s}_2) = \frac{1}{\sqrt{2}} \left[\varphi_{1s}(\vec{r}_1, \vec{s}_1 = \uparrow) \varphi_{1s}(\vec{r}_2, \vec{s}_2 = \downarrow) - \varphi_{1s}(\vec{r}_1, \vec{s}_1 = \downarrow) \varphi_{1s}(\vec{r}_2, \vec{s}_2 = \uparrow) \right]$$

interchanging labels gives

$$\begin{aligned} \psi(\vec{r}_2, \vec{s}_2; \vec{r}_1, \vec{s}_1) &= \frac{1}{\sqrt{2}} \left[\varphi_{1s}(\vec{r}_2, \vec{s}_2 = \uparrow) \varphi_{1s}(\vec{r}_1, \vec{s}_1 = \downarrow) - \varphi_{1s}(\vec{r}_2, \vec{s}_2 = \downarrow) \varphi_{1s}(\vec{r}_1, \vec{s}_1 = \uparrow) \right] \\ &= -\psi(\vec{r}_1, \vec{s}_1; \vec{r}_2, \vec{s}_2), \text{ as required} \end{aligned}$$

Can't tell which electron is spin up--indistinguishable

Also, if we try to put both electrons in 1s with spin-up (\uparrow), first term always cancels second term, and $\psi = 0!$ Therefore, we have the Pauli Exclusion Principle

A first try at many-electron wave functions:
The Hartree-Fock Method

Assume N-electron, P nucleus wave function to be:

$\Psi \approx \Phi = \text{Slater determinant}$

$$= \frac{1}{\sqrt{N!}} \begin{pmatrix} \phi_1(\vec{r}_1)\chi_1(\sigma_1) & \dots & \phi_N(\vec{r}_1)\chi_N(\sigma_1) \\ \vdots & \ddots & \vdots \\ \phi_1(\vec{r}_N)\chi_1(\sigma_N) & \dots & \phi_N(\vec{r}_N)\chi_N(\sigma_N) \end{pmatrix} \quad (35a)$$

↗ space: like 1s, 2s, ...
↘ spin: $\alpha(\uparrow)$ or $\beta(\downarrow)$

and also require orthonormality of one-electron orbitals

$$\int \phi_i^*(\vec{r})\phi_j(\vec{r})dV = \delta_{ij}$$

Minimize total energy → Hartree-Fock equations:

$$\hat{H}(\vec{r}_1)\phi_i(\vec{r}_1) = \epsilon_i\phi_i(\vec{r}_1); i = 1, 2, \dots, N \quad (42)$$

with:

$$\epsilon_i = \epsilon_i^0 + \sum_{j=1}^N [J_{ij} - \delta_{m_{s_i}, m_{s_j}} K_{ij}] \quad (47)$$

↑↑ or ↓↓

One-electron energies
or eigenvalues
≈ binding energy →
Koopmans' Theorem

One-electron integral:

$$\epsilon_i^0 = \left\langle \phi_i(\vec{r}_1) \left| -\frac{1}{2} \nabla_1^2 - \sum_{\ell=1}^P \frac{Z_\ell}{r_{1\ell}} \right| \phi_i(\vec{r}_1) \right\rangle \quad (48)$$

Note-- K_{ij} often
 J_{ij} in solid-state

Two-electron coulomb integral:

$$J_{ij} \equiv \left\langle \phi_i(\vec{r}_1) \left| \hat{J}_j \right| \phi_i(\vec{r}_1) \right\rangle = \iint \phi_i^*(\vec{r}_1)\phi_j^*(\vec{r}_2) \frac{1}{r_{12}} \phi_i(\vec{r}_1)\phi_j(\vec{r}_2) dV_1 dV_2 \quad (45)$$

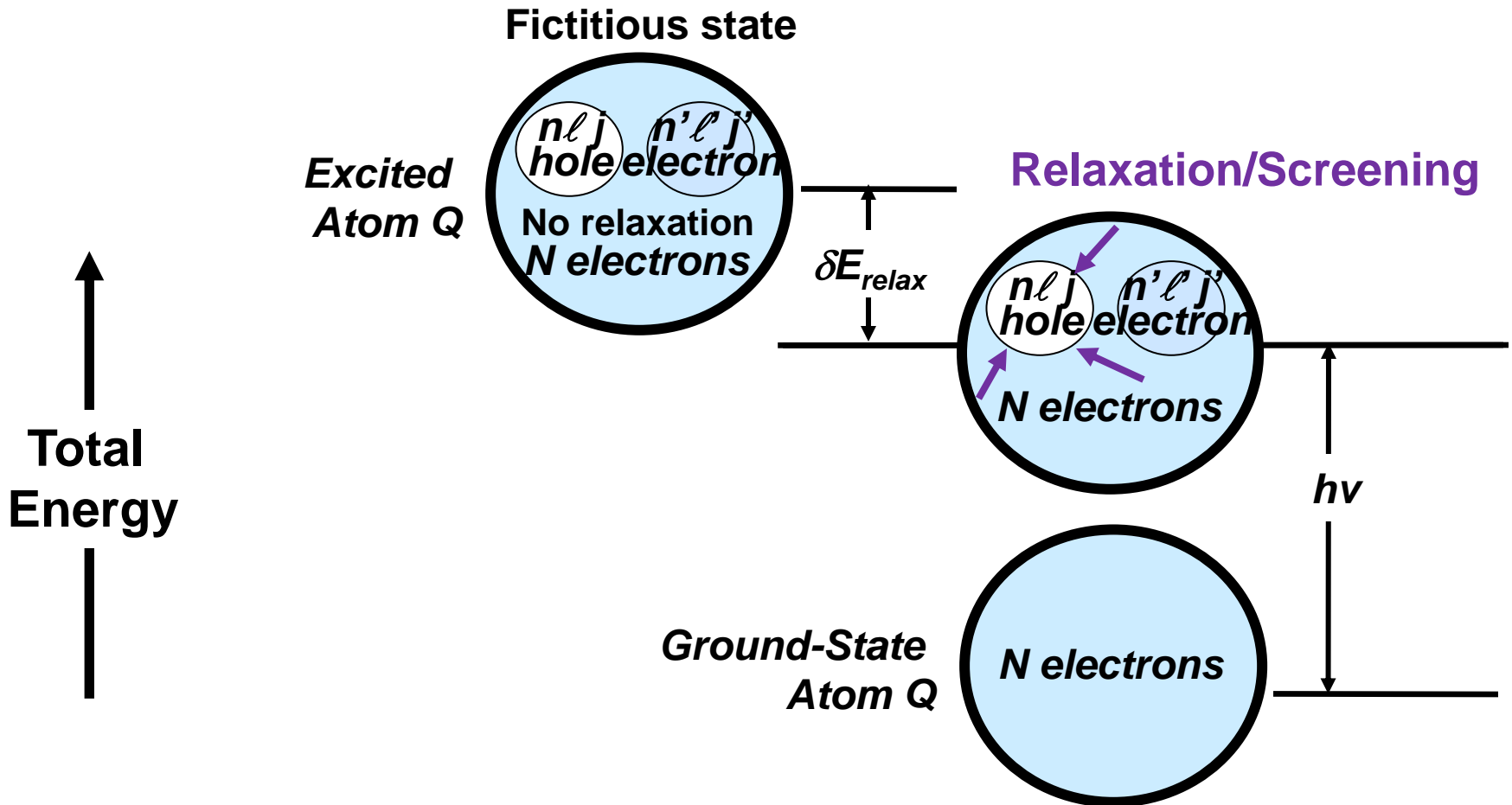
Two-electron exchange integral:

$$K_{ij} \equiv \left\langle \phi_i(\vec{r}_1) \left| \hat{K}_j \right| \phi_i(\vec{r}_1) \right\rangle = \iint \phi_i^*(\vec{r}_1)\phi_j^*(\vec{r}_2) \frac{1}{r_{12}} \phi_j(\vec{r}_1)\phi_i(\vec{r}_2) dV_1 dV_2 \quad (46)$$

Lowers energy—"attractive"

Basic energetics—Many e⁻ picture

X-ray absorption: $n\ell j \rightarrow n'\ell'j'$

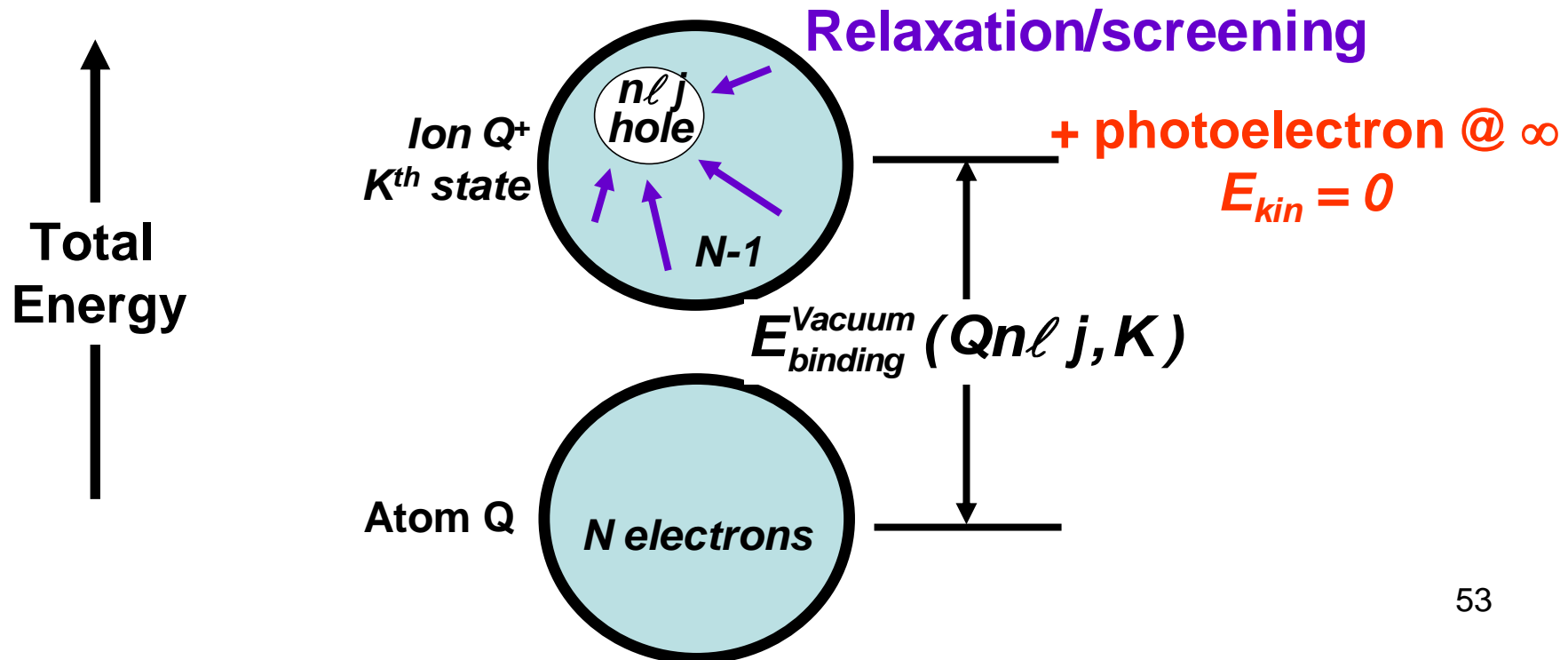


Basic energetics—Many e⁻ picture

Photoelectron emission: $n\ell j \rightarrow$ photoelectron at $E_{kinetic}$

$$h\nu = E_{binding}^{Vacuum} + E_{kinetic} = E_{binding}^{Fermi} + \varphi_{spectrometer} + E_{kinetic}$$

$$E_{binding}^{Vacuum}(Qn\ell j, K) = E_{final}(N-1, Qn\ell j \text{ hole}, K) - E_{initial}(N)$$



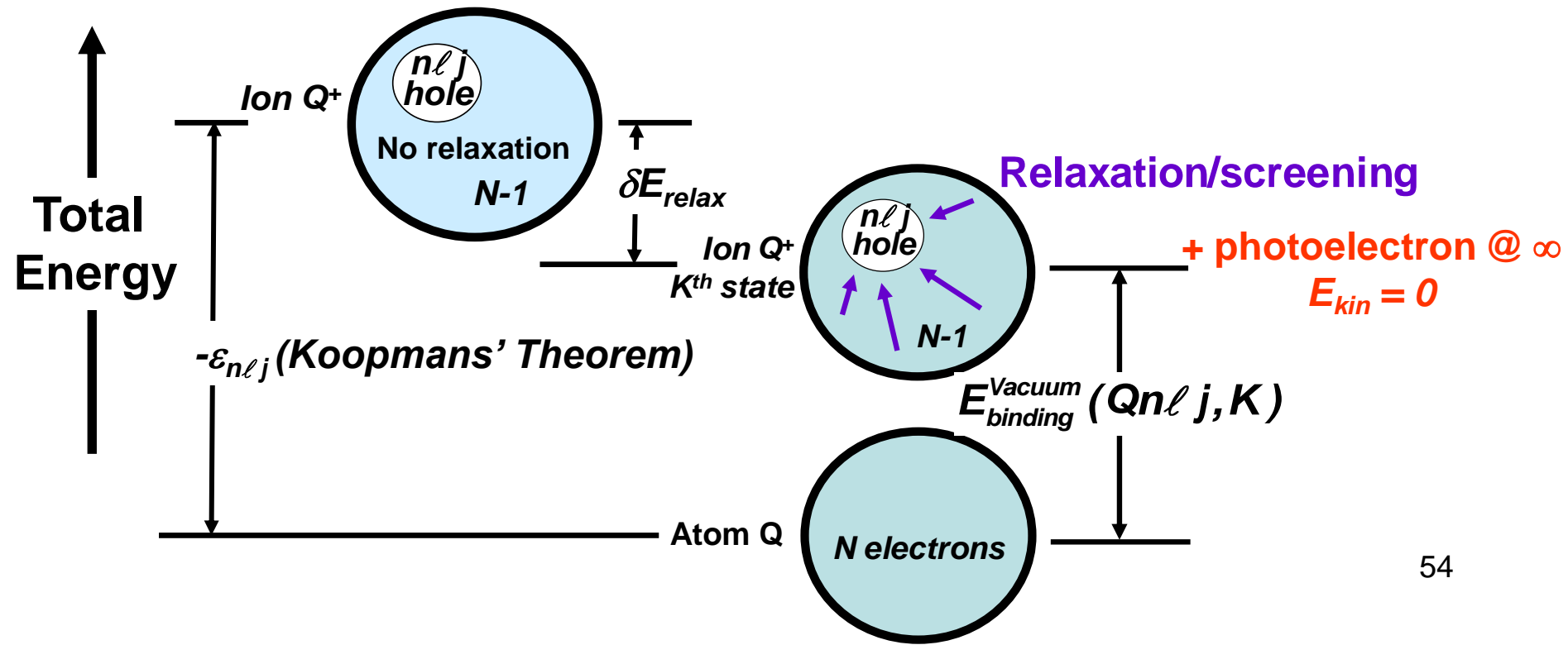
Basic energetics—Many e⁻ picture

Photoelectron emission: $n\ell j \rightarrow$ photoelectron at $E_{kinetic}$

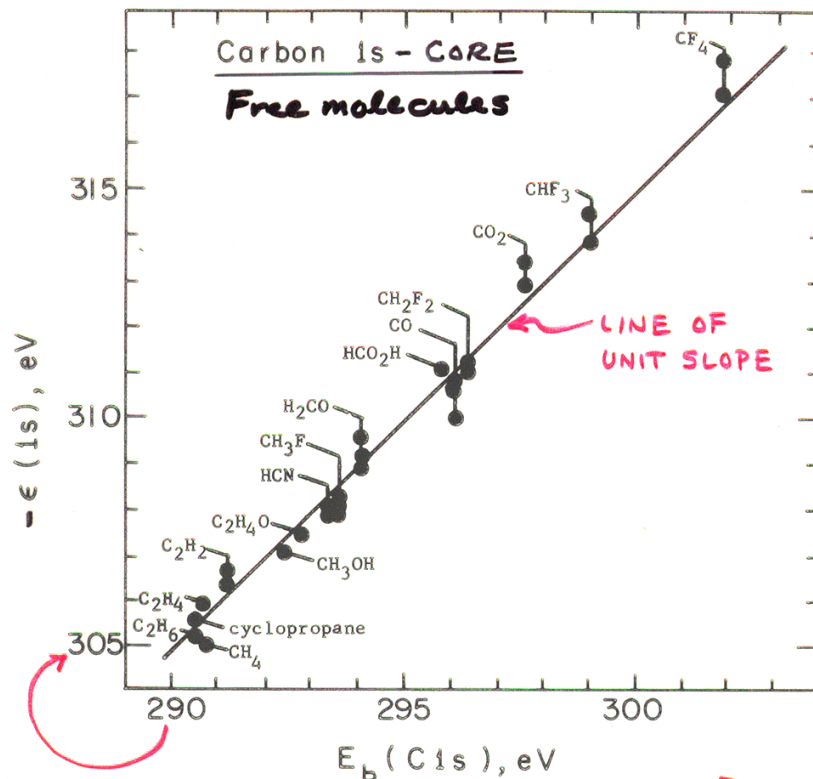
$$h\nu = E_{binding}^{Vacuum} + E_{kinetic} = E_{binding}^{Fermi} + \varphi_{spectrometer} + E_{kinetic}$$

$$E_{binding}^{Vacuum}(Qn\ell j, K) = E_{final}(N-1, Qn\ell j \text{ hole}, K) - E_{initial}(N)$$

Fictitious state



Koopmans' Theorem Calculation of C 1s Chemical Shifts in Small C-Containing Molecules



DIFF. = $\Delta E_{relax} \approx 15 \text{ eV} \approx \text{CONSTANT} \approx 5\% \text{ OF } E_b^V$

$\Delta E_b(\text{C } 1s, "1" - \text{CH}_4) = -\Delta E_{\text{C } 1s, "1" - \text{CH}_4}$

Figure 18 -- Plot of carbon 1s binding energies calculated via Koopmans' Theorem against experimental binding energies for several carbon-containing gaseous molecules. For some molecules, more than one calculated value is presented. The slope of the straight line is unity. The two scales are shifted with respect to one another by 15 eV, largely due to relaxation effects. All of the theoretical calculations were of roughly double-zeta accuracy or better. (From Shirley, reference 7.)

Correlation and screening effects beyond a single Slater determinant: configuration interaction:

For general N-electron state K:

$\Psi_K(N) = \text{weighted sum of Slater determinants } \Phi_j$

$$= \sum_j C_{jK} \Phi_j$$

with probability of each $|C_{jK}|^2$

For example, for Ne, a highly accurate CI calculation by Barr involving 1071 distinct configurations of spatial orbitals¹²³ yields the following absolute values for the coefficients multiplying the various members of a few more important configurations: $\Phi_1 = 1s^2 2s^2 2p^6 =$ Hartree-Fock configuration—0.984; $\Phi_2 = 1s^2 2s^1 2p^6 3s^1 = 0.005$; $\Phi_3 = 1s^2 2s^2 2p^5 3p = 0.009$; $\Phi_4 = 1s^2 2s^2 2p^4 4p^2 = 0.007-0.030$; and $\Phi_5 = 1s^2 2s^2 2p^4 3p 4p = 0.007-0.022$. Approximately 70 distinct configurations have coefficients larger than 0.010 in magnitude, but only that for Φ_1 is larger than 0.030.

In density-functional theory (DFT) → local-density approximation (LDA):

Effects of non-local exchange

$$K_{ij} \equiv \langle \phi_i(\vec{r}_1) | \hat{K}_j | \phi_i(\vec{r}_1) \rangle = \iint \phi_i^*(\vec{r}_1) \phi_j^*(\vec{r}_2) \frac{1}{r_{12}} \phi_j(\vec{r}_1) \phi_i(\vec{r}_2) dV_1 dV_2$$

and additional correlation effects are replaced in solving for ground-state one-electron orbitals by a local exchange-correlation potential:

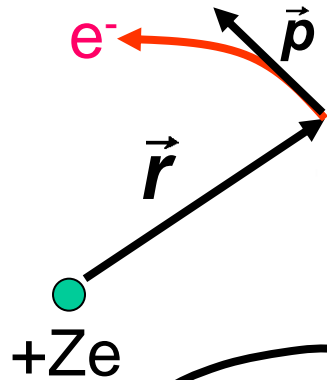
$$V_{ec, \uparrow(\downarrow)}(\vec{r}) \approx -\frac{3}{4} \left[\frac{3\rho_{\uparrow(\downarrow)}(\vec{r})}{\pi} \right]^{1/3} - \frac{0.056 \rho_{\uparrow(\downarrow)}^{1/3}(\vec{r})}{0.079 + \rho_{\uparrow(\downarrow)}^{1/3}(\vec{r})}$$

Where $\rho_{\uparrow(\downarrow)}(\vec{r}) = \sum_{i=1, \dots, N} \phi_{i, \uparrow(\downarrow)}^*(\vec{r}) \phi_{i, \uparrow(\downarrow)}(\vec{r}) = \sum_{i=1, \dots, N} |\phi_{i, \uparrow(\downarrow)}(\vec{r})|^2$

+ Various corrections/approximations going beyond this: generalized gradient approximation (GGA), GW and GW + cumulant expansions, dynamical mean field theory (DMFT), hybrid functionals mixing Hartree-Fock and LDA, quantum Monte Carlo, ...

The Hydrogenic Atom Schroedinger Equation: Spherical Polar Coordinates

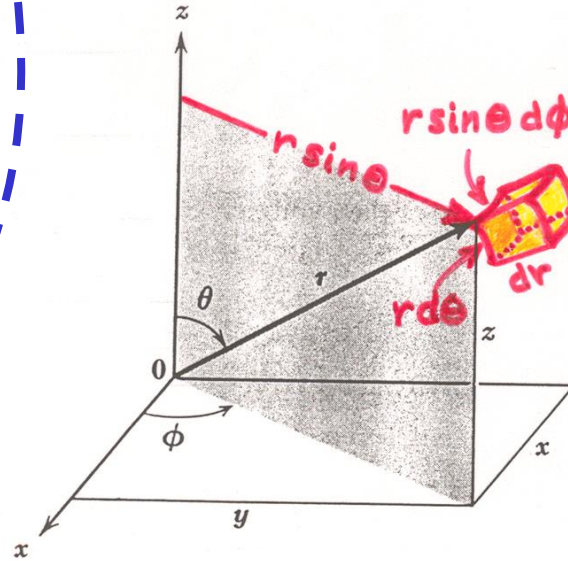
Classically:



$$V(r) = -Ze^2/4\pi\epsilon_0 r$$

$\vec{L} = \vec{r} \times \vec{p}$
is conserved

Quantum mechanically:



$$dV = r^2 dr \sin\theta d\theta d\phi$$

$$\int_0^\pi \sin\theta d\theta \int_0^{2\pi} d\phi = -\cos\theta \Big|_0^\pi \times 2\pi = 4\pi$$

$$x = r \sin\theta \cos\phi$$

$$y = r \sin\theta \sin\phi$$

$$z = r \cos\theta$$

Polar angle = $\theta = \arccos(z/r)$

Azimuthal angle = $\phi = \arctan(y/x)$

Converting to new coordinates

$$\hat{K} = -\frac{\hbar^2}{2\mu} \nabla^2 = -\frac{\hbar^2}{2\mu} \left[\frac{\partial^2}{\partial x^2} + \frac{\partial^2}{\partial y^2} + \frac{\partial^2}{\partial z^2} \right]$$

$$= -\frac{\hbar^2}{2\mu} \cdot \frac{1}{r^2 \sin\theta} \left[\sin\theta \frac{\partial}{\partial r} \left(r^2 \frac{\partial}{\partial r} \right) + \frac{\partial}{\partial \theta} \left(\sin\theta \frac{\partial}{\partial \theta} \right) + \frac{1}{\sin\theta} \frac{\partial^2}{\partial \phi^2} \right]$$

$$= -\frac{\hbar^2}{2\mu} \left[\frac{\partial^2}{\partial r^2} + \frac{2}{r} \frac{\partial}{\partial r} + \frac{1}{r^2} \frac{\partial^2}{\partial \theta^2} + \frac{1}{r^2} \cot\theta \frac{\partial}{\partial \theta} + \frac{1}{r^2 \sin^2\theta} \frac{\partial^2}{\partial \phi^2} \right]$$

∴ H-ATOM SCH. EQN. IS:

$$\hat{H}\Psi(r, \theta, \phi) = \hat{K}\Psi(r, \theta, \phi) - \frac{Ze^2}{4\pi\epsilon_0 r} \Psi = E\Psi$$

→ $Z_{\text{eff}}(r)$ IN MANY-E ATOM

- USE SEPARATION OF VARIABLES :

$$\Psi(r, \theta, \phi) = R(r) \Theta(\theta) \Phi(\phi)$$

- ASSUMED FORM -

- SUBSTITUTE, REARRANGE \rightarrow

$$\phi: \frac{d^2 \Phi}{d\phi^2} + C_\phi \Phi = 0 \Rightarrow \Phi(\phi) = A e^{\pm i C_\phi \phi} \quad (1)$$

$$\downarrow m_\ell = 0, \pm 1, \dots \quad \boxed{\Phi_{m_\ell}(\phi) = \frac{1}{\sqrt{2\pi}} e^{\pm i m_\ell \phi}} \quad \text{- COMPLEX}$$

$$\theta: \frac{1}{\sin \theta} \frac{d}{d\theta} \left(\sin \theta \frac{d\Theta}{d\theta} \right) + \left[C_\theta - \frac{m_\ell^2}{\sin^2 \theta} \right] \Theta = 0 \quad (2)$$

$$r: \left[-\frac{\hbar^2}{2\mu} \left(\frac{d^2}{dr^2} + \frac{2}{r} \frac{d}{dr} \right) + \frac{\ell(\ell+1)}{2\mu r^2} - \frac{Ze^2}{4\pi\epsilon_0 r} \right] R = ER \quad (3)$$

A "RADIAL SCHRÖDINGER EQN."

$$H_{op, radial} R = ER \Rightarrow$$

$$\boxed{E = E_n = -\frac{Ze^2}{8\pi\epsilon_0 a_0} \cdot \frac{1}{n^2}} \\ n = 1, 2, 3, \dots$$

- SOLVING FOR Θ WITH (2) \Rightarrow

$\Theta_{\ell m_\ell}(\theta) = \text{ASSOC. LEGENDRE POLYNOMIALS}$
IN $(\cos \theta)$ - REAL

$$\ell = 0, 1, 2, 3, \dots (n-1)$$

$$m_\ell = -\ell, -\ell+1, \dots, 0, \dots, +\ell-1, +\ell$$

$$2\ell+1$$

- SOLVING FOR R WITH (3) \Rightarrow

$R_{n\ell}(r) = \text{ASSOC. LAGUERRE FUNCTIONS ALSO}$
= (POLYNOMIAL IN r) $\cdot e^{-Zr/a_0}$ - REAL

Atomic orbitals:

COMPLEX, IF $m \neq 0$

TABLE 6.1

NORMALIZED WAVE FUNCTIONS OF THE HYDROGEN ATOM FOR $n = 1, 2,$ AND 3^* ($Z=1 = \text{HYDROGEN}$)

n	l	m_l	$\Phi_{m_l}(\phi)$	$\Theta_{lm_l}(\theta)$	$R_{nl}(r)$	$\Psi_{nlm_l}(r, \theta, \phi) = \Phi_{m_l} \Theta_{lm_l} R_{nl}$
1	0	0	$\frac{1}{\sqrt{2\pi}}$	$\frac{1}{\sqrt{2}}$	$\frac{2}{a_0^{3/2}} e^{-r/a_0}$	$\frac{1}{\sqrt{\pi} a_0^{3/2}} e^{-r/a_0}$
	0	0	$\frac{1}{\sqrt{2\pi}}$	$\frac{1}{\sqrt{2}}$	$\frac{1}{2\sqrt{2} a_0^{3/2}} \left(2 - \frac{r}{a_0}\right) e^{-r/2a_0}$	$\frac{1}{4\sqrt{2\pi} a_0^{3/2}} \left(2 - \frac{r}{a_0}\right) e^{-r/2a_0}$
2	1	0	$\frac{1}{\sqrt{2\pi}}$	$\frac{\sqrt{6}}{2} \cos \theta$	$\frac{1}{2\sqrt{6} a_0^{3/2}} \frac{r}{a_0} e^{-r/2a_0}$	$\frac{1}{4\sqrt{2\pi} a_0^{3/2}} \frac{r}{a_0} e^{-r/2a_0} \cos \theta$
2	1	± 1	$\frac{1}{\sqrt{2\pi}} e^{\pm i\phi}$	$\frac{\sqrt{3}}{2} \sin \theta$	$\frac{1}{2\sqrt{6} a_0^{3/2}} \frac{r}{a_0} e^{-r/2a_0}$	$\frac{1}{8\sqrt{\pi} a_0^{3/2}} \frac{r}{a_0} e^{-r/2a_0} \sin \theta e^{\pm i\phi}$
3	0	0	$\frac{1}{\sqrt{2\pi}}$	$\frac{1}{\sqrt{2}}$	$\frac{2}{81\sqrt{3} a_0^{3/2}} \left(27 - 18 \frac{r}{a_0} + 2 \frac{r^2}{a_0^2}\right) e^{-r/3a_0}$	$\frac{1}{81\sqrt{3\pi} a_0^{3/2}} \left(27 - 18 \frac{r}{a_0} + 2 \frac{r^2}{a_0^2}\right) e^{-r/3a_0}$
3	1	0	$\frac{1}{\sqrt{2\pi}}$	$\frac{\sqrt{6}}{2} \cos \theta$	$\frac{4}{81\sqrt{6} a_0^{3/2}} \left(6 - \frac{r}{a_0}\right) \frac{r}{a_0} e^{-r/3a_0}$	$\frac{\sqrt{2}}{81\sqrt{\pi} a_0^{3/2}} \left(6 - \frac{r}{a_0}\right) \frac{r}{a_0} e^{-r/3a_0} \cos \theta$
3	1	± 1	$\frac{1}{\sqrt{2\pi}} e^{\pm i\phi}$	$\frac{\sqrt{3}}{2} \sin \theta$	$\frac{4}{81\sqrt{6} a_0^{3/2}} \left(6 - \frac{r}{a_0}\right) \frac{r}{a_0} e^{-r/3a_0}$	$\frac{1}{81\sqrt{\pi} a_0^{3/2}} \left(6 - \frac{r}{a_0}\right) \frac{r}{a_0} e^{-r/3a_0} \sin \theta e^{\pm i\phi}$
3	2	0	$\frac{1}{\sqrt{2\pi}}$	$\frac{\sqrt{10}}{4} (3 \cos^2 \theta - 1)$	$\frac{4}{81\sqrt{30} a_0^{3/2}} \frac{r^2}{a_0^2} e^{-r/3a_0}$	$\frac{1}{81\sqrt{6\pi} a_0^{3/2}} \frac{r^2}{a_0^2} e^{-r/3a_0} (3 \cos^2 \theta - 1)$
3	2	± 1	$\frac{1}{\sqrt{2\pi}} e^{\pm i\phi}$	$\frac{\sqrt{15}}{2} \sin \theta \cos \theta$	$\frac{4}{81\sqrt{30} a_0^{3/2}} \frac{r^2}{a_0^2} e^{-r/3a_0}$	$\frac{1}{81\sqrt{\pi} a_0^{3/2}} \frac{r^2}{a_0^2} e^{-r/3a_0} \sin \theta \cos \theta e^{\pm i\phi}$
3	2	± 2	$\frac{1}{\sqrt{2\pi}} e^{\pm 2i\phi}$	$\frac{\sqrt{15}}{4} \sin^2 \theta$	$\frac{4}{81\sqrt{30} a_0^{3/2}} \frac{r^2}{a_0^2} e^{-r/3a_0}$	$\frac{1}{162\sqrt{\pi} a_0^{3/2}} \frac{r^2}{a_0^2} e^{-r/3a_0} \sin^2 \theta e^{\pm 2i\phi}$

*The quantity $a_0 = 4\pi\epsilon_0\hbar^2/me^2 = 5.3 \times 10^{-11}$ m is equal to the radius of the innermost Bohr orbit.

IS SAME FOR
MANY e^- ATOMS

CHANGES FOR
MANY e^- ATOMS

$$\Psi_{n\ell m_\ell m_s}(r, \theta, \phi, \text{spin}) = \Psi_{n\ell m_\ell}(r, \theta, \phi) \times [\alpha(\uparrow) \text{ or } \beta(\downarrow)]$$

$$Y_{\ell m_\ell}(\theta, \phi) =$$

The atomic orbitals:

With spin

"spherical harmonics"

COMPLEX, IF $m \neq 0$

But we can make them real for convenience

TABLE 6.1

NORMALIZED WAVE FUNCTIONS OF THE HYDROGEN ATOM FOR $n = 1, 2,$ AND 3^* ($Z=1 = \text{HYDROGEN}$)

n	ℓ	m_ℓ	$\Phi_{m_\ell}(\phi)$	$\Theta_{\ell m_\ell}(\theta)$	$R_{n\ell}(r)$	$\Psi_{n\ell m_\ell}(r, \theta, \phi) = \Phi_{m_\ell} \Theta_{\ell m_\ell} R_{n\ell}$
1	0	0	$\frac{1}{\sqrt{2\pi}}$	$\frac{1}{\sqrt{2}}$	$\frac{2}{a_0^{3/2}} e^{-r/a_0}$	$\frac{1}{\sqrt{\pi} a_0^{3/2}} e^{-r/a_0}$
2	0	0	$\frac{1}{\sqrt{2\pi}}$	$\frac{1}{\sqrt{2}}$	$\frac{1}{2\sqrt{2} a_0^{3/2}} \left(2 - \frac{r}{a_0}\right) e^{-r/2a_0}$	$\frac{1}{4\sqrt{2\pi} a_0^{3/2}} \left(2 - \frac{r}{a_0}\right) e^{-r/2a_0}$
2	1	0	$\frac{1}{\sqrt{2\pi}}$	$\frac{\sqrt{6}}{2} \cos \theta$	$\frac{1}{2\sqrt{6} a_0^{3/2}} \frac{r}{a_0} e^{-r/2a_0}$	$\frac{1}{4\sqrt{2\pi} a_0^{3/2}} \frac{r}{a_0} e^{-r/2a_0} \cos \theta \rightarrow \text{node for } \theta = 90^\circ$
2	1	± 1	$\frac{1}{\sqrt{2\pi}} e^{\pm i\phi}$	$\frac{\sqrt{3}}{2} \sin \theta$	$\frac{1}{2\sqrt{6} a_0^{3/2}} \frac{r}{a_0} e^{-r/2a_0}$	$\frac{1}{8\sqrt{\pi} a_0^{3/2}} \frac{r}{a_0} e^{-r/2a_0} \sin \theta e^{\pm i\phi}$
3	0	0	$\frac{1}{\sqrt{2\pi}}$	$\frac{1}{\sqrt{2}}$	$\frac{2}{81\sqrt{3} a_0^{3/2}} \left(27 - 18 \frac{r}{a_0} + 2 \frac{r^2}{a_0^2}\right) e^{-r/3a_0}$	$\frac{1}{81\sqrt{3\pi} a_0^{3/2}} \left(27 - 18 \frac{r}{a_0} + 2 \frac{r^2}{a_0^2}\right) e^{-r/3a_0}$
3	1	0	$\frac{1}{\sqrt{2\pi}}$	$\frac{\sqrt{6}}{2} \cos \theta$	$\frac{4}{81\sqrt{6} a_0^{3/2}} \left(6 - \frac{r}{a_0}\right) \frac{r}{a_0} e^{-r/3a_0}$	$\frac{\sqrt{2}}{81\sqrt{\pi} a_0^{3/2}} \left(6 - \frac{r}{a_0}\right) \frac{r}{a_0} e^{-r/3a_0} \cos \theta \rightarrow \text{node for } r = 6a_0$
3	1	± 1	$\frac{1}{\sqrt{2\pi}} e^{\pm i\phi}$	$\frac{\sqrt{3}}{2} \sin \theta$	$\frac{4}{81\sqrt{6} a_0^{3/2}} \left(6 - \frac{r}{a_0}\right) \frac{r}{a_0} e^{-r/3a_0}$	$\frac{1}{81\sqrt{\pi} a_0^{3/2}} \left(6 - \frac{r}{a_0}\right) \frac{r}{a_0} e^{-r/3a_0} \sin \theta e^{\pm i\phi}$
3	2	0	$\frac{1}{\sqrt{2\pi}}$	$\frac{\sqrt{10}}{4} (3 \cos^2 \theta - 1)$	$\frac{4}{81\sqrt{30} a_0^{3/2}} \frac{r^2}{a_0^2} e^{-r/3a_0}$	$\frac{1}{81\sqrt{6\pi} a_0^{3/2}} \frac{r^2}{a_0^2} e^{-r/3a_0} (3 \cos^2 \theta - 1) \rightarrow \text{nodes for } \cos^2 \theta = 1/3$
3	2	± 1	$\frac{1}{\sqrt{2\pi}} e^{\pm i\phi}$	$\frac{\sqrt{15}}{2} \sin \theta \cos \theta$	$\frac{4}{81\sqrt{30} a_0^{3/2}} \frac{r^2}{a_0^2} e^{-r/3a_0}$	$\frac{1}{81\sqrt{\pi} a_0^{3/2}} \frac{r^2}{a_0^2} e^{-r/3a_0} \sin \theta \cos \theta e^{\pm i\phi}$
3	2	± 2	$\frac{1}{\sqrt{2\pi}} e^{\pm 2i\phi}$	$\frac{\sqrt{15}}{4} \sin^2 \theta$	$\frac{4}{81\sqrt{30} a_0^{3/2}} \frac{r^2}{a_0^2} e^{-r/3a_0}$	$\frac{1}{162\sqrt{\pi} a_0^{3/2}} \frac{r^2}{a_0^2} e^{-r/3a_0} \sin^2 \theta e^{\pm 2i\phi}$

*The quantity $a_0 = 4\pi\epsilon_0\hbar^2/me^2 = 5.3 \times 10^{-11}$ m is equal to the radius of the innermost Bohr orbit.

IS SAME FOR MANY e^- ATOMS

CHANGES FOR MANY e^- ATOMS

$e^{-r/na_0} \rightarrow e^{-Zr/na_0}$ for hydrogenic
 $Z \rightarrow Z_{\text{eff}}(r)$ in many- e^- atoms

Overall, in a many-electron system:

- Anti-symmetry of total wave function implies:

Pauli Exclusion Principle:

No two electrons can have all the same quantum nos.

$$n, \ell, m_\ell, m_s$$

or, if spin-orbit split

$$n, \ell, j, m_j$$

- Electronic structure determined by filling n, ℓ (or n, ℓ, j) levels from lowest to highest energy ($E_{n\ell}$ or $E_{n\ell j}$ from radial Schrodinger Eqn. with Z_{eff})
- Partially filled subshells n, ℓ (or n, ℓ, j) have their lowest energy when a maximum no. of electrons have parallel spins = highest total spin angular momentum = \mathbf{S} (Hund's First Rule), and then they couple to yield highest total orbital angular momentum = \mathbf{L} (Hund's Second Rule)

MAKING THE ATOMIC ORBITALS REAL (E.G., FOR CHEMICAL BONDING):

$$\Psi_{nlm_l}(r, \theta, \phi) = R_{nl}(r) \underbrace{Y_{lm_l}(\theta, \phi)}_{\substack{\text{REAL} \\ 2\pi m_l}} \underbrace{\frac{1}{\sqrt{2\pi}} e^{im_l \phi}}_{\substack{\text{COMPLEX} \\ \text{IF } m_l \neq 0}}$$

SO JUST TAKE COMB. OF $\pm m_l$ AS:

$$\Psi_{nl(-)}(r, \theta, \phi) = \begin{cases} \frac{1}{2} [\Psi_{nlm_l} + \Psi_{nl-m_l}] \propto R_{nl} Y_{lm_l} \cos m_l \phi \\ \frac{1}{2i} [\Psi_{nlm_l} - \Psi_{nl-m_l}] \propto R_{nl} Y_{lm_l} \sin m_l \phi \end{cases}$$

REAL

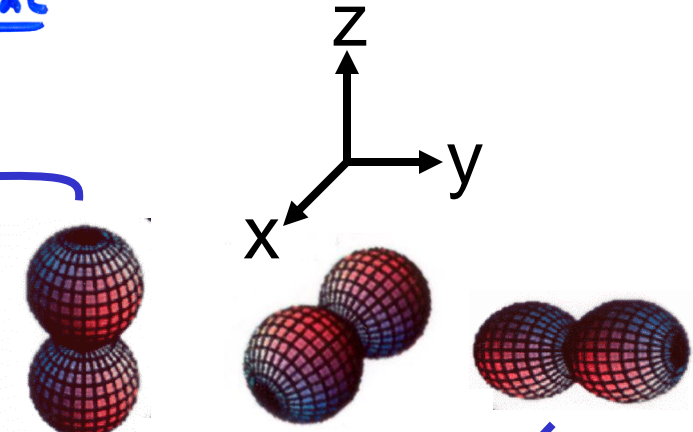
EXAMPLE: 2p ORBITALS

$\Psi_{210} = \Psi_{2p_0} = \Psi_{2p_z} \propto r \cos \theta = z$ (ALREADY REAL)

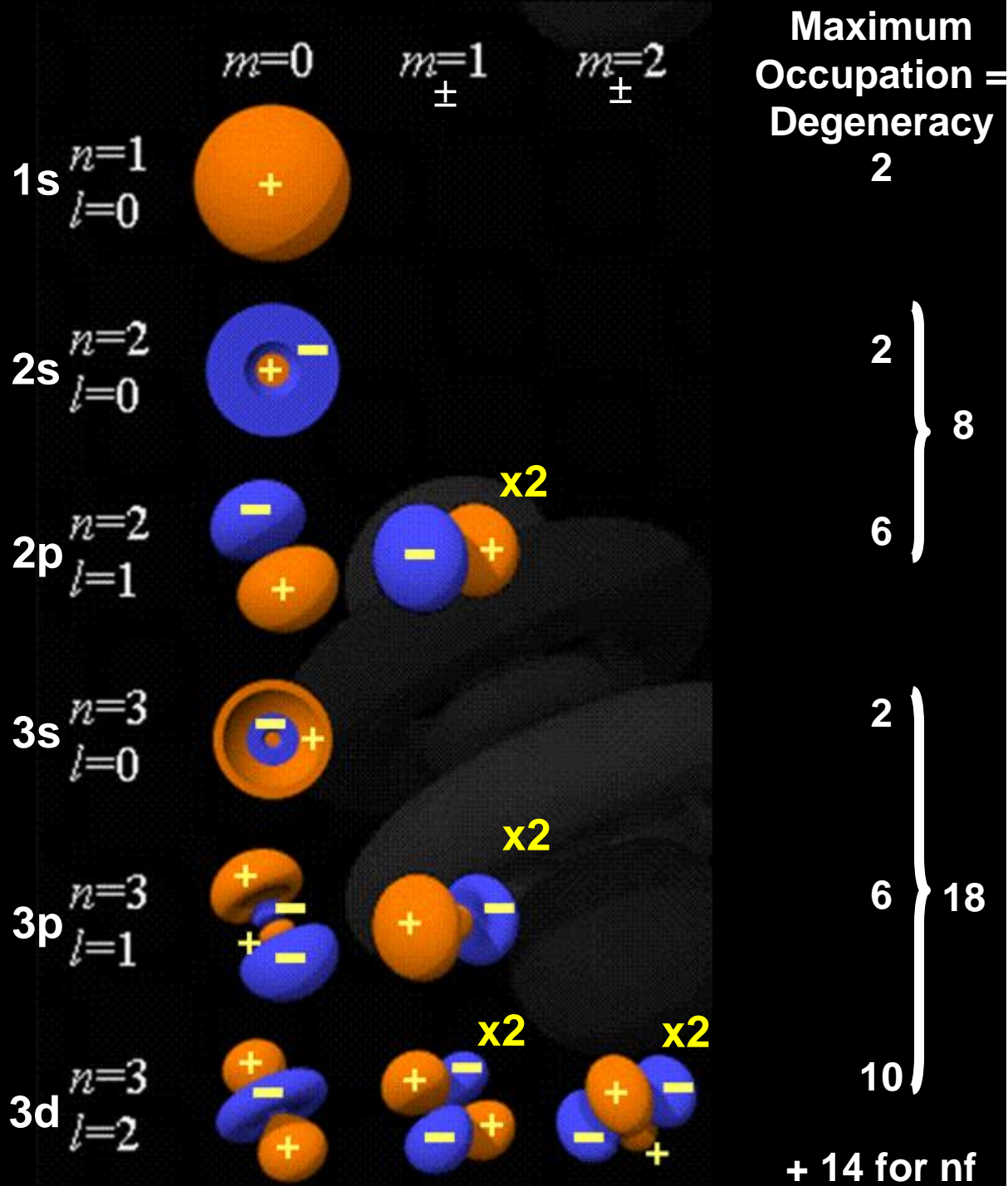
$\Psi_{211} = \Psi_{2p_{+1}} \propto r \sin \theta e^{i\phi} = r \sin \theta [\cos \phi + i \sin \phi]$
 $\Psi_{21-1} = \Psi_{2p_{-1}} \propto r \sin \theta e^{-i\phi} = r \sin \theta [\cos \phi - i \sin \phi]$

$\frac{1}{2} [\Psi_{2p_{+1}} + \Psi_{2p_{-1}}] = \Psi_{2p_x} \propto r \sin \theta \cos \phi = x$

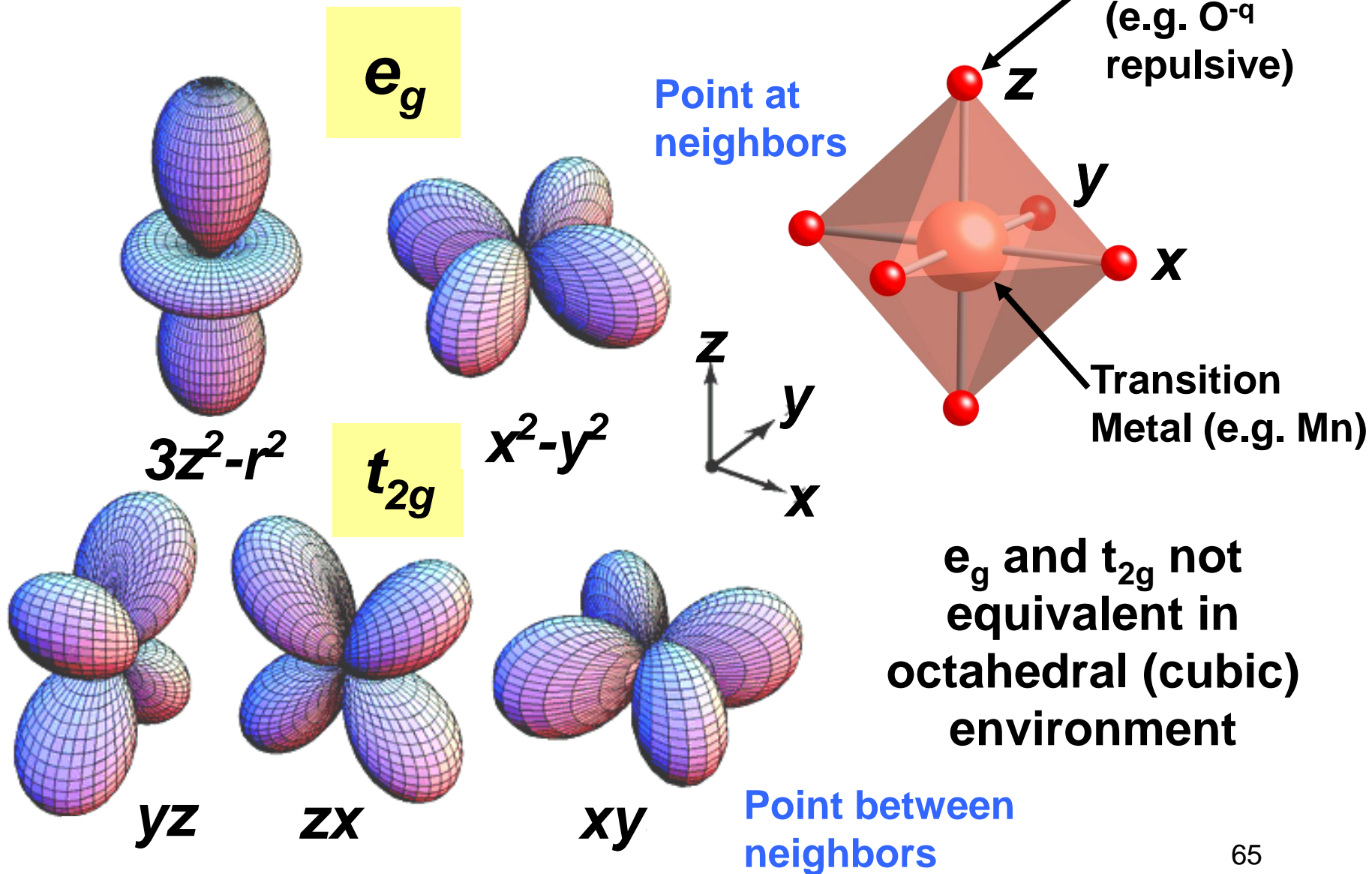
$\frac{1}{2i} [\Psi_{2p_{+1}} - \Psi_{2p_{-1}}] = \Psi_{2p_y} \propto r \sin \theta \sin \phi = y$



Filling the Atomic Orbitals:

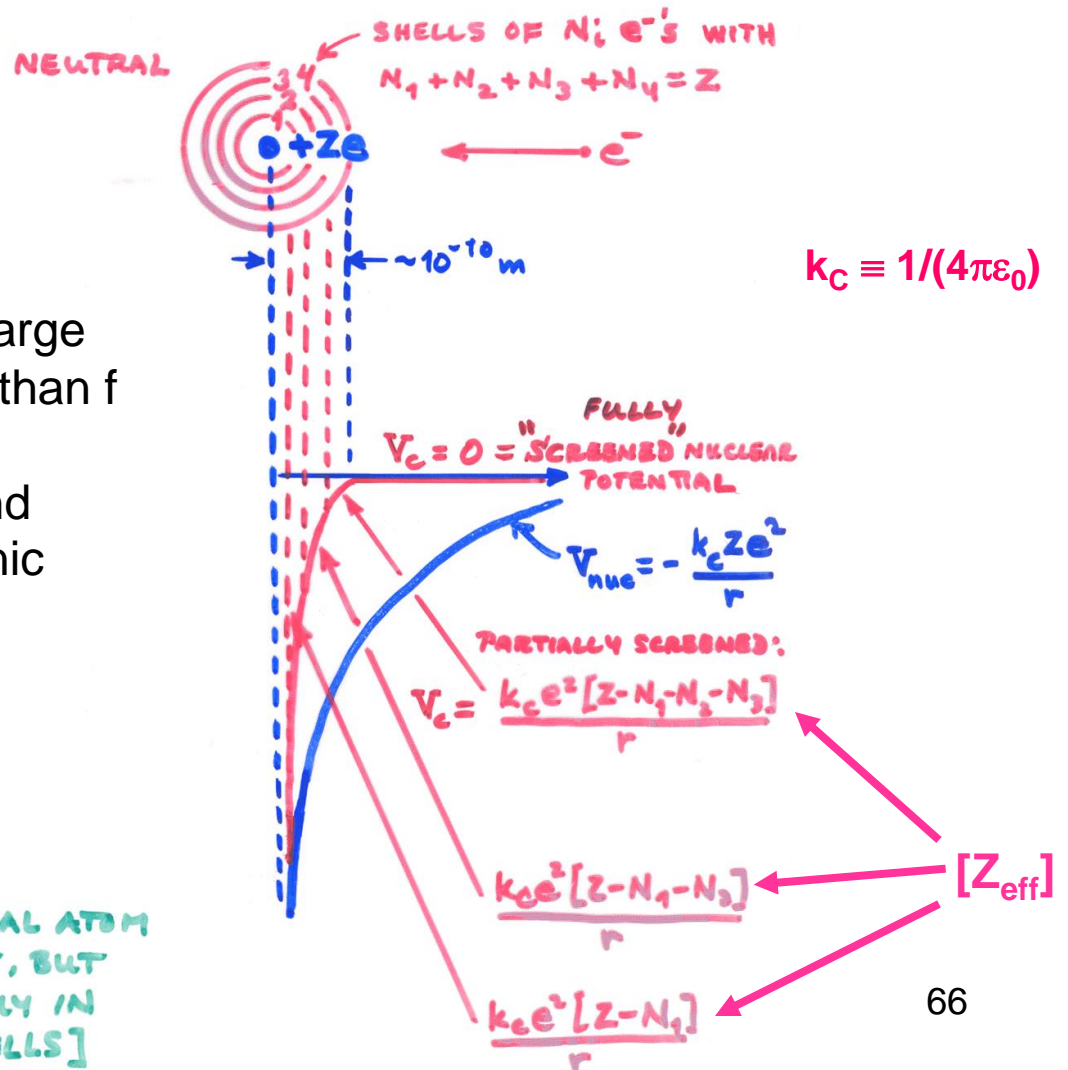


And the same thing for the d orbitals:



Intraatomic electron screening in many-electron atoms--a simple model

POINT CHARGE ($\sim e^-$) + SPHERICAL SHELLS
OF e^- CHARGE (\sim ORBITS) AROUND POINT-
CHARGE NUCLEUS $\Rightarrow \sim$ ATOM :



In many-electron atoms:
For a given n, s feels nuclear charge
more than p, more than d, more than f

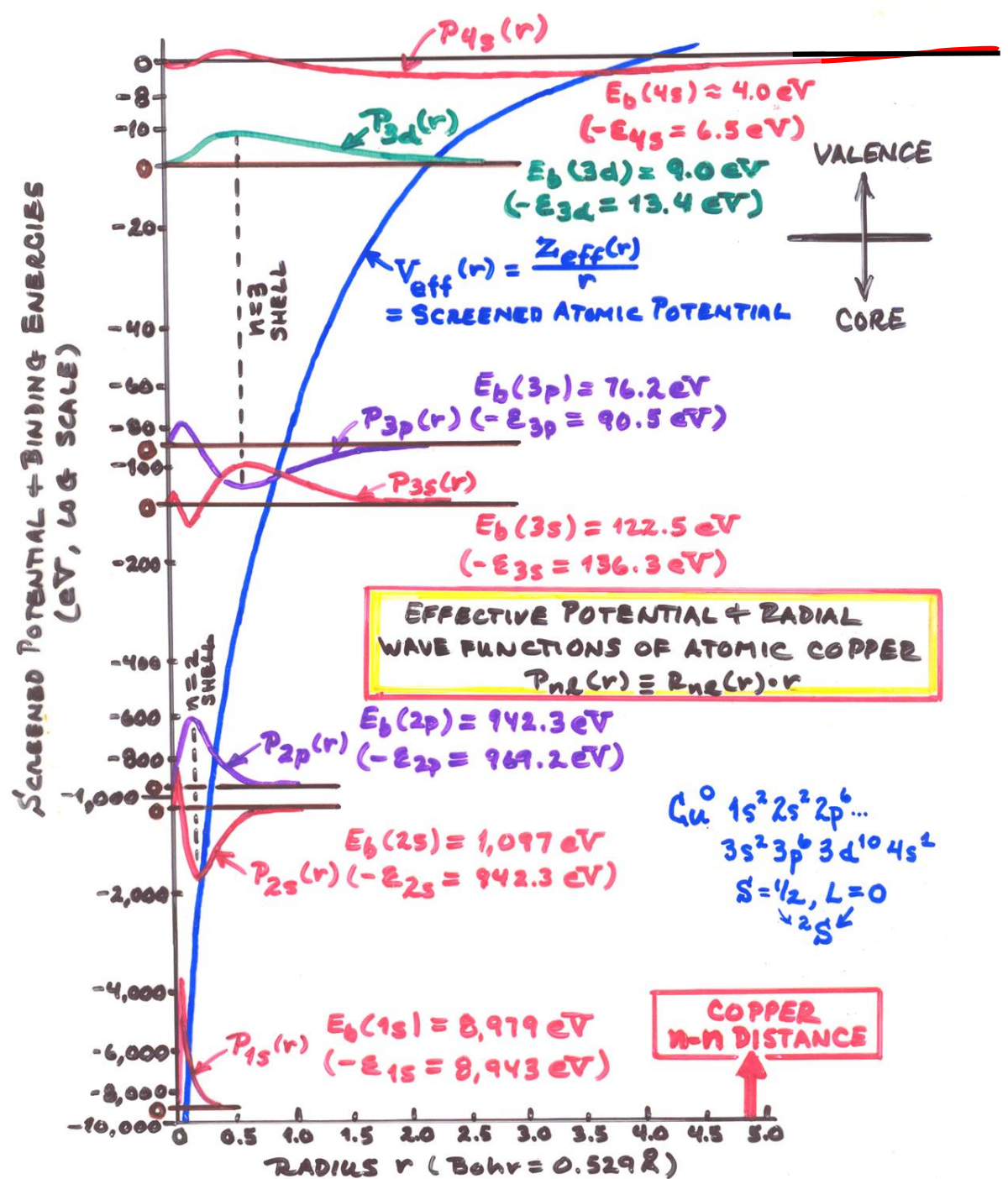
Yields $Z_{eff}(r)$ in simple picture, and
lifts degeneracy on ℓ in hydrogenic
atom

[CHARGE IN REAL ATOM
SMEARED OUT, BUT
STILL ROUGHLY IN
RADIAL SHELLS]

Intraatomic electron screening in many-electron atoms--a self-consistent Q.M. calculation

Plus radial one-electron functions:
 $P_{nl}(r) \equiv rR_{nl}(r)$

General useful rule:
 $(n-l)$ maxima in radial probability density $P_{nl}(r)^2 \equiv r^2 R_{nl}(r)^2$



OBSERVED (+ CALCULATED) ORDER OF FILLING ATOMIC LEVELS:

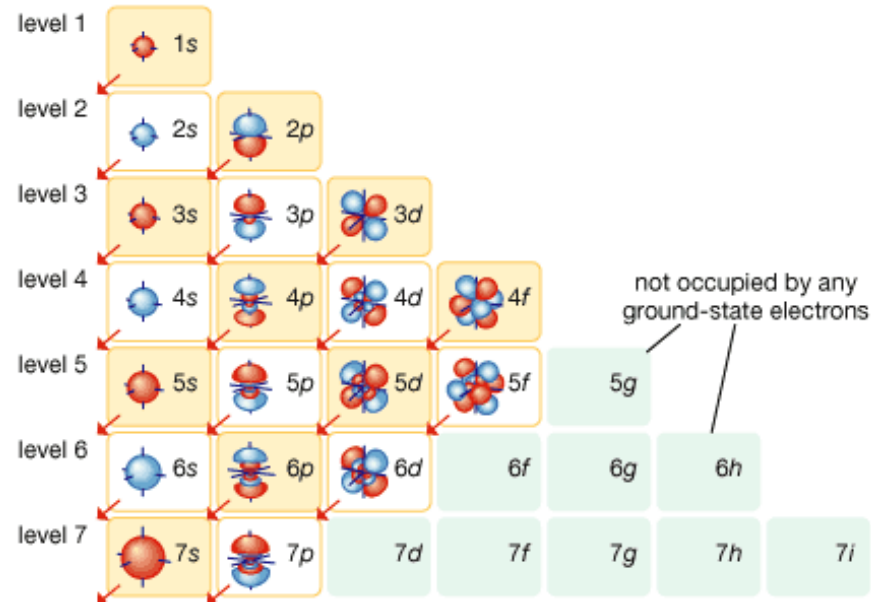
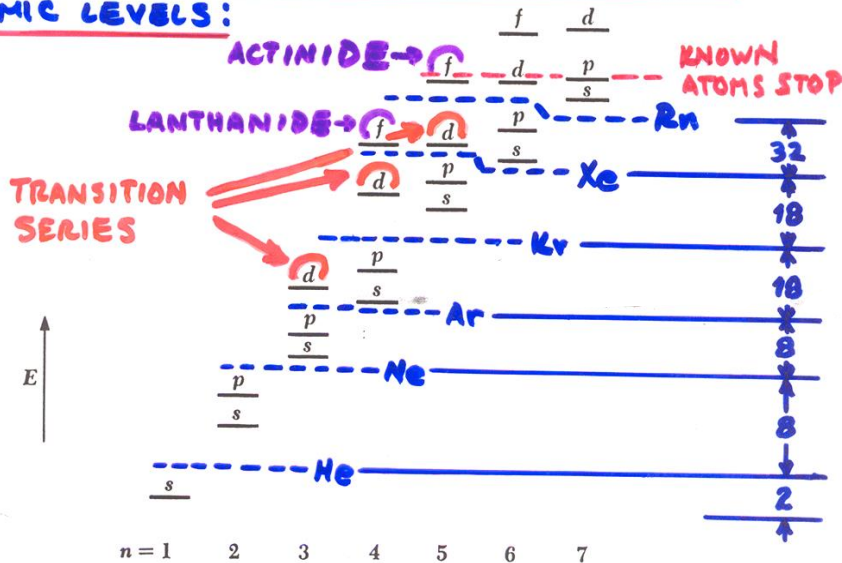


FIGURE 7.13 The sequence of quantum states in an atom. Not to scale.

EXAMPLE CONFIGURATIONS:

Z	ATOM	CONFIG.	GROUND-STATE OPEN SHELL COUPLING?
8	O	$1s^2 2s^2 2p^4$	$\uparrow\downarrow$ \uparrow \uparrow $2p_{-1}$ $2p_0$ $2p_{+1}$
26	Fe	$1s^2 2s^2 2p^6 3s^2 3p^6 3d^6 4s^2$	$\uparrow\downarrow$ \uparrow \uparrow \uparrow \uparrow $3d_{-2}$ $3d_{-1}$ $3d_0$ $3d_{+1}$ $3d_{+2}$ \Rightarrow LARGE μ_{3d} + MAGNETISM
63	Eu	$1s^2 2s^2 2p^6 3s^2 3p^6 3d^{10} 4s^2 4p^6 4d^{10} 4f^7 6s^2$	\uparrow \uparrow \uparrow \uparrow \uparrow \uparrow \uparrow $4f_{-3}$ $4f_{-2}$ $4f_{-1}$ $4f_0$ $4f_{+1}$ $4f_{+2}$ $4f_{+3}$ ALSO MAGNETIC!

Exchange interaction.
Hund's First Rule:
highest total spin angular momentum

s²

TRANSITION METALS

Periodic Table, with the Outer Electron Configurations of Neutral Atoms in Their Ground States

p¹ p² p³ p⁴ p⁵ p⁶

The notation used to describe the electronic configuration of atoms and ions is discussed in all textbooks of introductory atomic physics. The letters *s*, *p*, *d*, ... signify electrons having orbital angular momentum 0, 1, 2, ... in units \hbar ; the number to the left of the letter denotes the principal quantum number of one orbit, and the superscript to the right denotes the number of electrons in the orbit.

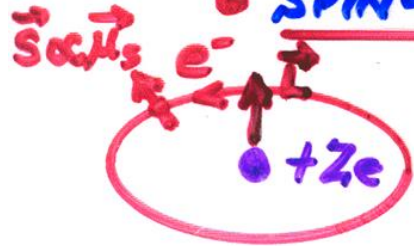
H ¹																	He ²				
1s																	1s ²				
Li ³	Be ⁴															B ⁵	C ⁶	N ⁷	O ⁸	F ⁹	Ne ¹⁰
2s	2s ²															2s ² 2p	2s ² 2p ²	2s ² 2p ³	2s ² 2p ⁴	2s ² 2p ⁵	2s ² 2p ⁶
Na ¹¹	Mg ¹²															Al ¹³	Si ¹⁴	P ¹⁵	S ¹⁶	Cl ¹⁷	Ar ¹⁸
3s	3s ²															3s ² 3p	3s ² 3p ²	3s ² 3p ³	3s ² 3p ⁴	3s ² 3p ⁵	3s ² 3p ⁶
K ¹⁹	Ca ²⁰	Sc ²¹	Ti ²²	V ²³	Cr ²⁴	Mn ²⁵	Fe ²⁶	Co ²⁷	Ni ²⁸	Cu ²⁹	Zn ³⁰	Ga ³¹	Ge ³²	As ³³	Se ³⁴	Br ³⁵	Kr ³⁶				
4s	4s ²	3d	3d ²	3d ³	3d ⁵	3d ⁵	3d ⁶	3d ⁷	3d ⁸	3d ¹⁰	3d ¹⁰	4s ² 4p	4s ² 4p ²	4s ² 4p ³	4s ² 4p ⁴	4s ² 4p ⁵	4s ² 4p ⁶				
Rb ³⁷	Sr ³⁸	Y ³⁹	Zr ⁴⁰	Nb ⁴¹	Mo ⁴²	Tc ⁴³	Ru ⁴⁴	Rh ⁴⁵	Pd ⁴⁶	Ag ⁴⁷	Cd ⁴⁸	In ⁴⁹	Sn ⁵⁰	Sb ⁵¹	Te ⁵²	I ⁵³	Xe ⁵⁴				
5s	5s ²	4d	4d ²	4d ⁴	4d ⁵	4d ⁶	4d ⁷	4d ⁸	4d ¹⁰	4d ¹⁰	4d ¹⁰	5s ² 5p	5s ² 5p ²	5s ² 5p ³	5s ² 5p ⁴	5s ² 5p ⁵	5s ² 5p ⁶				
Cs ⁵⁵	Ba ⁵⁶	La ⁵⁷	Hf ⁷²	Ta ⁷³	W ⁷⁴	Re ⁷⁵	Os ⁷⁶	Ir ⁷⁷	Pt ⁷⁸	Au ⁷⁹	Hg ⁸⁰	Tl ⁸¹	Pb ⁸²	Bi ⁸³	Po ⁸⁴	At ⁸⁵	Rn ⁸⁶				
6s	6s ²	5d	4f ¹⁴	5d ²	5d ³	5d ⁴	5d ⁵	5d ⁶	5d ⁹	5d ⁹	5d ¹⁰	5d ¹⁰	6s ² 6p	6s ² 6p ²	6s ² 6p ³	6s ² 6p ⁴	6s ² 6p ⁵	6s ² 6p ⁶			
Fr ⁸⁷	Ra ⁸⁸	Ac ⁸⁹	<p>4f¹⁴ ... 4f(5d) FILLING ... 4f¹⁴</p>																		
7s	7s ²	6d	Ce ⁵⁸	Pr ⁵⁹	Nd ⁶⁰	Pm ⁶¹	Sm ⁶²	Eu ⁶³	Gd ⁶⁴	Tb ⁶⁵	Dy ⁶⁶	Ho ⁶⁷	Er ⁶⁸	Tm ⁶⁹	Yb ⁷⁰	Lu ⁷¹	<p>RARE EARTHS</p>				
			4f ²	4f ³	4f ⁴	4f ⁵	4f ⁶	4f ⁷	4f ⁷	4f ⁸	4f ¹⁰	4f ¹¹	4f ¹²	4f ¹³	4f ¹⁴	4f ¹⁴					
			6s ²	6s ²	6s ²	6s ²	6s ²	6s ²	6s ²	6s ²	6s ²	6s ²	6s ²	6s ²	6s ²	6s ²					
			5d	5d	5d	5d	5d	5d	5d	5d	5d	5d	5d	5d	5d	5d					
			7s ²	7s ²	7s ²	7s ²	7s ²	7s ²	7s ²	7s ²	7s ²	7s ²	7s ²	7s ²	7s ²	7s ²					
			Th ⁹⁰	Pa ⁹¹	U ⁹²	Np ⁹³	Pu ⁹⁴	Am ⁹⁵	Cm ⁹⁶	Bk ⁹⁷	Cf ⁹⁸	Es ⁹⁹	Fm ¹⁰⁰	Md ¹⁰¹	No ¹⁰²	Lr ¹⁰³	<p>ACTINIDES</p>				
			6d ²	5f ²	5f ³	5f ⁵	5f ⁶	5f ⁷	5f ⁷	5f ⁷	5f ⁷	5f ⁷	5f ⁷	5f ⁷	5f ⁷	5f ⁷					
			7s ²	7s ²	7s ²	7s ²	7s ²	7s ²	7s ²	7s ²	7s ²	7s ²	7s ²	7s ²	7s ²	7s ²					

□ = EXCEPTIONS

◻ = EXCEPTIONS

→ d⁵ + d¹⁰ : 1/2 FILLED / FILLED MORE STABLE

• SPIN-ORBIT SPLITTING OF LEVELS:



⇒ EFFECTIVE \vec{B} (NUCLEUS AROUND e^-) $\propto \vec{L}$

$$\hat{H}_{s.o} = \xi(r) \vec{L} \cdot \vec{S}$$

- SPLITS ALL nl LEVELS $2(2l+1)$
 - $nl_j = l + 1/2 \rightarrow 2l+2$
 - $nl_j = l - 1/2 \rightarrow 2l$
- MIXES SPIN + ORBITAL ANGULAR MOM.:

$$\psi_{nljm_j} = C_1 \psi_{nl, m_j - 1/2} \begin{pmatrix} 1 \\ 0 \end{pmatrix} + C_2 \psi_{nl, m_j + 1/2} \begin{pmatrix} 0 \\ 1 \end{pmatrix}$$

\parallel
 $m_s = +1/2$
 \parallel
 \uparrow

\parallel
 $m_s = -1/2$
 \parallel
 \downarrow

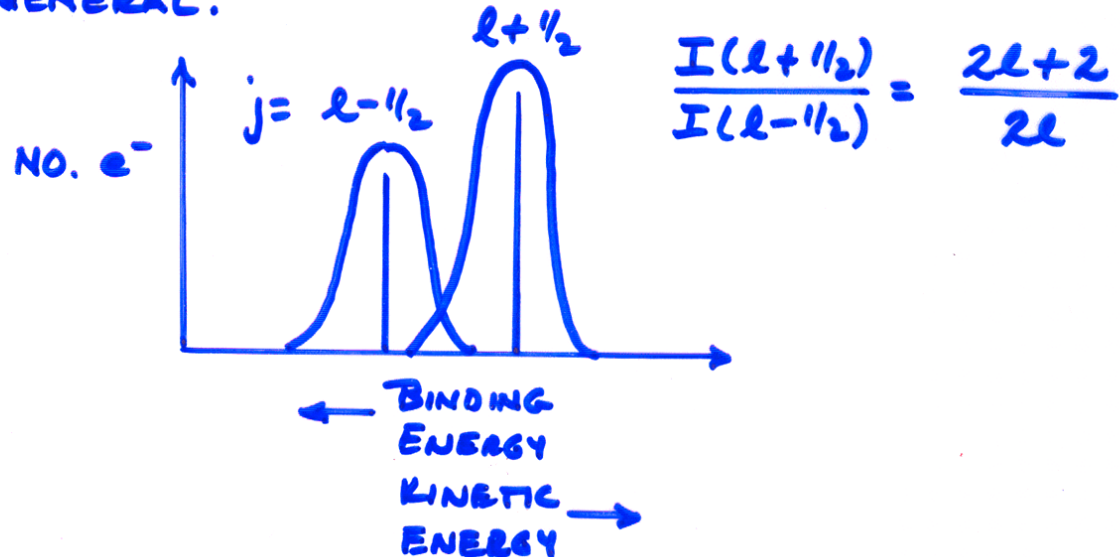
WITH C1 AND C2 TABULATED CLEBSCH-GORDAN OR WIGNER 3j SYMBOLS

SOME SPIN-ORBIT SPLITTINGS: (IN eV)

$2p^6$ \swarrow \searrow $2p_{1/2}^2$ $2p_{3/2}^4$	$Z = 13$ (Al) 0.4	28 (Ni) 17.8	46 (Pd) 157.0
$3d^{10}$ \swarrow \searrow $3d_{3/2}^4$ $3d_{5/2}^6$	$Z = 30$ (Zn) 0.1	48 (Cd) 6.7	64 (Gd) 32.3
$4f^{14}$ \swarrow \searrow $4f_{5/2}^6$ $4f_{7/2}^8$	$Z = 74$ (W) 2.2	84 (Pb) 7.0	92 (U) 64

INCREASE WITH Z FOR A GIVEN LEVEL.

IN GENERAL:



X-Ray Data Booklet--Section 1.1 ELECTRON BINDING ENERGIES

The energies are given in eV relative to the vacuum level for the rare gases and for H₂, N₂, O₂, F₂, and Cl₂; relative to the Fermi level for the metals; and relative to the top of the valence bands for semiconductors (and insulators).

Electronic configuration	Element	K 1s	L ₁ 2s	L ₂ 2p _{1/2}	L ₃ 2p _{3/2}	M ₁ 3s	M ₂ 3p _{1/2}	M ₃ 3p _{3/2}
1s	1 H	13.6						
1s²	2 He	24.6*						
1s² 2s	3 Li	54.7*						
1s² 2s²	4 Be	111.5*						
1s² 2s² 2p	5 B	188*						
1s² 2s² 2p²	6 C	284.2*						
1s² 2s² 2p³	7 N	409.9*	37.3*	~ 9	~ 9			
1s² 2s² 2p⁴	8 O	543.1*	41.6*	~ 13	~ 13			
1s² 2s² 2p⁵	9 F	696.7*	~ 45	~ 17	~ 17			
1s² 2s² 2p⁶	10 Ne	870.2*	48.5*	21.7*	21.6*			
[Ne] 3s	11 Na	1070.8†	63.5†	30.65	30.81			
[Ne] 3s²	12 Mg	1303.0†	88.7	49.78	49.50			
[Ne] 3s² 3p	13 Al	1559.6	117.8	72.95	72.55			
[Ne] 3s² 3p²	14 Si	1839	149.7*b	99.82	99.42			
[Ne] 3s² 3p³	15 P	2145.5	189*	136*	135*			
[Ne] 3s² 3p⁴	16 S	2472	230.9	163.6*	162.5*			
[Ne] 3s² 3p⁵	17 Cl	2822.4	270*	202*	200*			
[Ne] 3s² 3p⁶	18 Ar	3205.9*	326.3*	250.6†	248.4*	29.3*	15.9*	15.7*
[Ar] 4s	19 K	3608.4*	378.6*	297.3*	294.6*	34.8*	18.3*	18.3*
[Ar] 4s²	20 Ca	4038.5*	438.4†	349.7†	346.2†	44.3 †	25.4†	25.4†
	21 Sc	4492	498.0*	403.6*	398.7*	51.1*	28.3*	28.3*
	22 Ti	4966	560.9†	460.2†	453.8†	58.7†	32.6†	32.6†

Valence levels

Interpolated, extrapolated

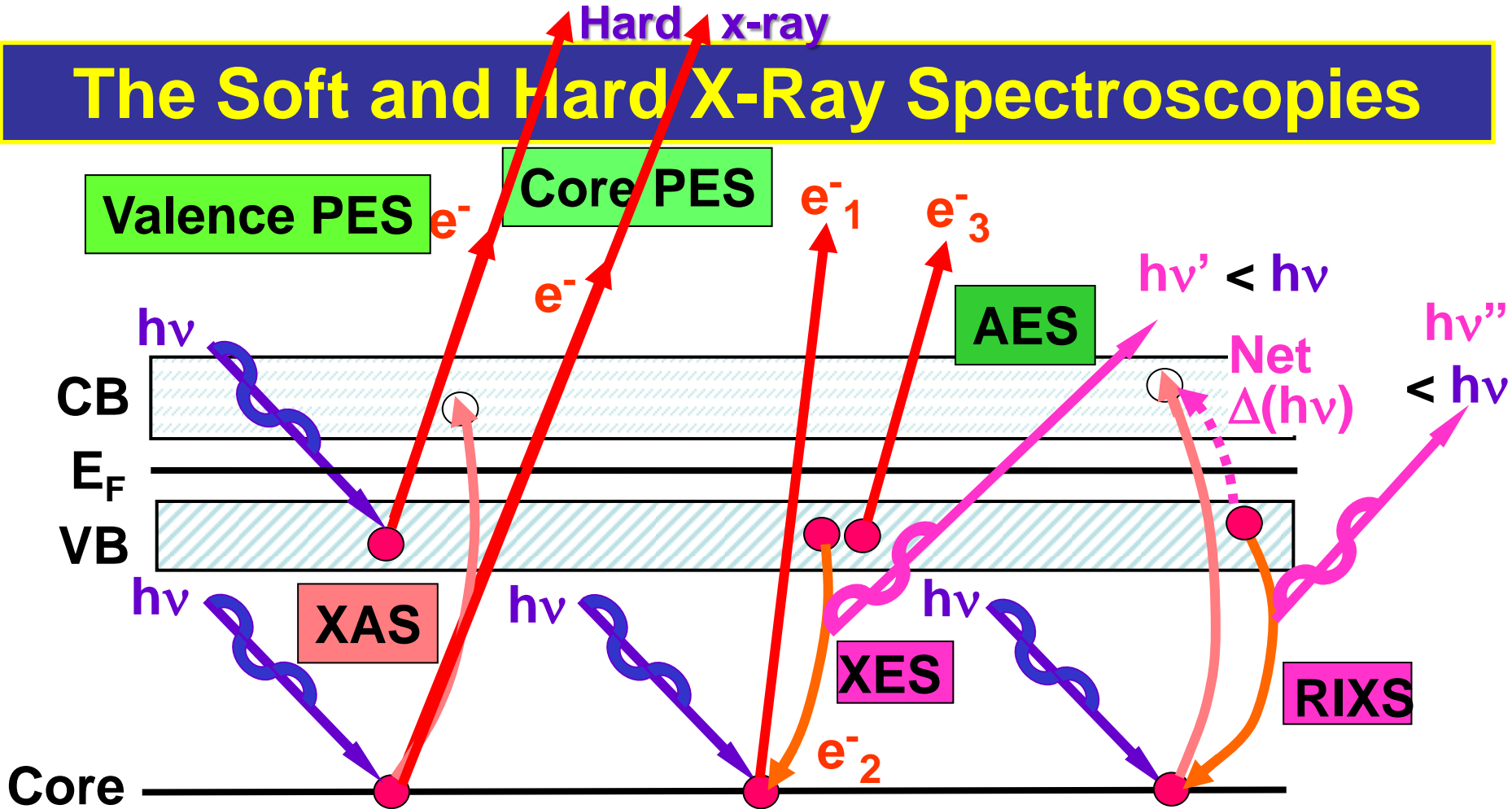
Missing valence B.E.s

Valence levels

X-Ray Data Booklet--Section 1.1 ELECTRON BINDING ENERGIES

Element	K 1s	L ₁ 2s	L ₂ 2p _{1/2}	L ₃ 2p _{3/2}	M ₁ 3s	M ₂ 3p _{1/2}	M ₃ 3p _{3/2}	M ₄ 3d _{3/2}	M ₅ 3d _{5/2}	N ₁ 4s	N ₂ 4p _{1/2}	N ₃ 4p _{3/2}
23 V	5465	626.7†	519.8†	512.1†	66.3†	37.2†	37.2†	Valence levels				
24 Cr	5989	696.0†	583.8†	574.1†	74.1†	42.2†	42.2†					
25 Mn	6539	769.1†	649.9†	638.7†	82.3†	47.2†	47.2†					
26 Fe	7112	844.6†	719.9†	706.8†	91.3†	52.7†	52.7†					
27 Co	7709	925.1†	793.2†	778.1†	101.0†	58.9†	59.9†					
28 Ni	8333	1008.6†	870.0†	852.7†	110.8†	68.0†	66.2†					
29 Cu	8979	1096.7†	952.3†	932.7	122.5†	77.3†	75.1†					
30 Zn	9659	1196.2*	1044.9*	1021.8*	139.8*	91.4*	88.6*	10.2*	10.1*	Valence levels		
31 Ga	10367	1299.0*b	1143.2†	1116.4†	159.5†	103.5†	100.0†	18.7†	18.7†			
32 Ge	11103	1414.6*b	1248.1*b	1217.0*b	180.1*	124.9*	120.8*	29.8	29.2			
33 As	11867	1527.0*b	1359.1*b	1323.6*b	204.7*	146.2*	141.2*	41.7*	41.7*			
34 Se	12658	1652.0*b	1474.3*b	1433.9*b	229.6*	166.5*	160.7*	55.5*	54.6*			
35 Br	13474	1782*	1596*	1550*	257*	189*	182*	70*	69*			
36 Kr	14326	1921	1730.9*	1678.4*	292.8*	222.2*	214.4	95.0*	93.8*			
37 Rb	15200	2065	1864	1804	326.7*	248.7*	239.1*	113.0*	112*	30.5*	16.3*	15.3*
38 Sr	16105	2216	2007	1940	358.7†	280.3†	270.0†	136.0†	134.2†	38.9†	21.3	20.1†
39 Y	17038	2373	2156	2080	392.0*b	310.6*	298.8*	157.7†	155.8†	43.8*	24.4*	23.1*
40 Zr	17998	2532	2307	2223	430.3†	343.5†	329.8†	181.1†	178.8†	50.6†	28.5†	27.1†
41 Nb	18986	2698	2465	2371	466.6†	376.1†	360.6†	205.0†	202.3†	56.4†	32.6†	30.8†
42 Mo	20000	2866	2625	2520	506.3†	411.6†	394.0†	231.1†	227.9†	63.2†	37.6†	35.5†
43 Tc	21044	3043	2793	2677	544*	447.6	417.7	257.6	253.9*	69.5*	42.3*	39.9*
44 Ru	22117	3224	2967	2838	586.1*	483.5†	461.4†	284.2†	280.0†	75.0†	46.3†	43.2†
45 Rh	23220	3412	3146	3004	628.1†	521.3†	496.5†	311.9†	307.2†	81.4*b	50.5†	47.3†
46 Pd	24350	3604	3330	3173	671.6†	559.9†	532.3†	340.5†	335.2†	87.1*b	55.7†a	50.9†
47 Ag	25514	3806	3524	3351	719.0†	603.8†	573.0†	374.0†	368.3	97.0†	63.7†	58.3†

The Soft and Hard X-Ray Spectroscopies



PES = photoemission = photoelectron spectroscopy

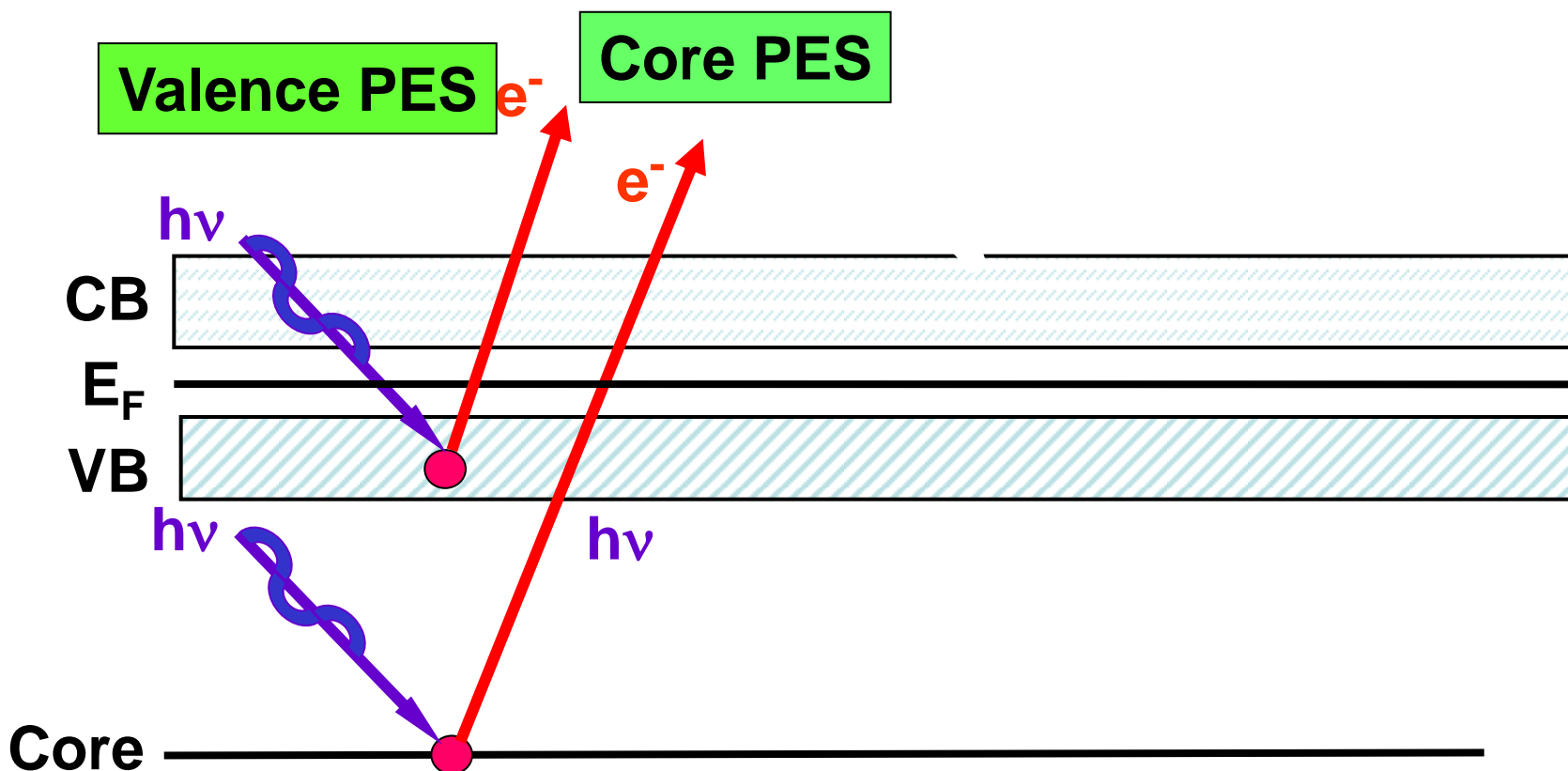
XAS = x-ray absorption spectroscopy

AES = Auger electron spectroscopy

XES = x-ray emission spectroscopy

RIXS = resonant inelastic x-ray scattering / x-ray Raman scatt.

The Soft and Hard X-Ray Spectroscopies



PES = photoemission = photoelectron spectroscopy

XAS = x-ray absorption spectroscopy

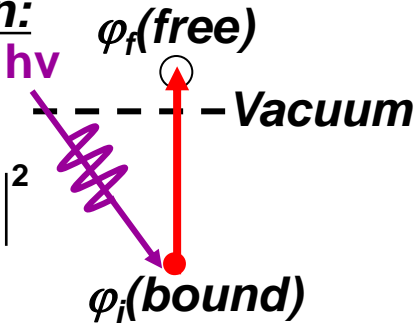
AES = Auger electron spectroscopy

XES = x-ray emission spectroscopy

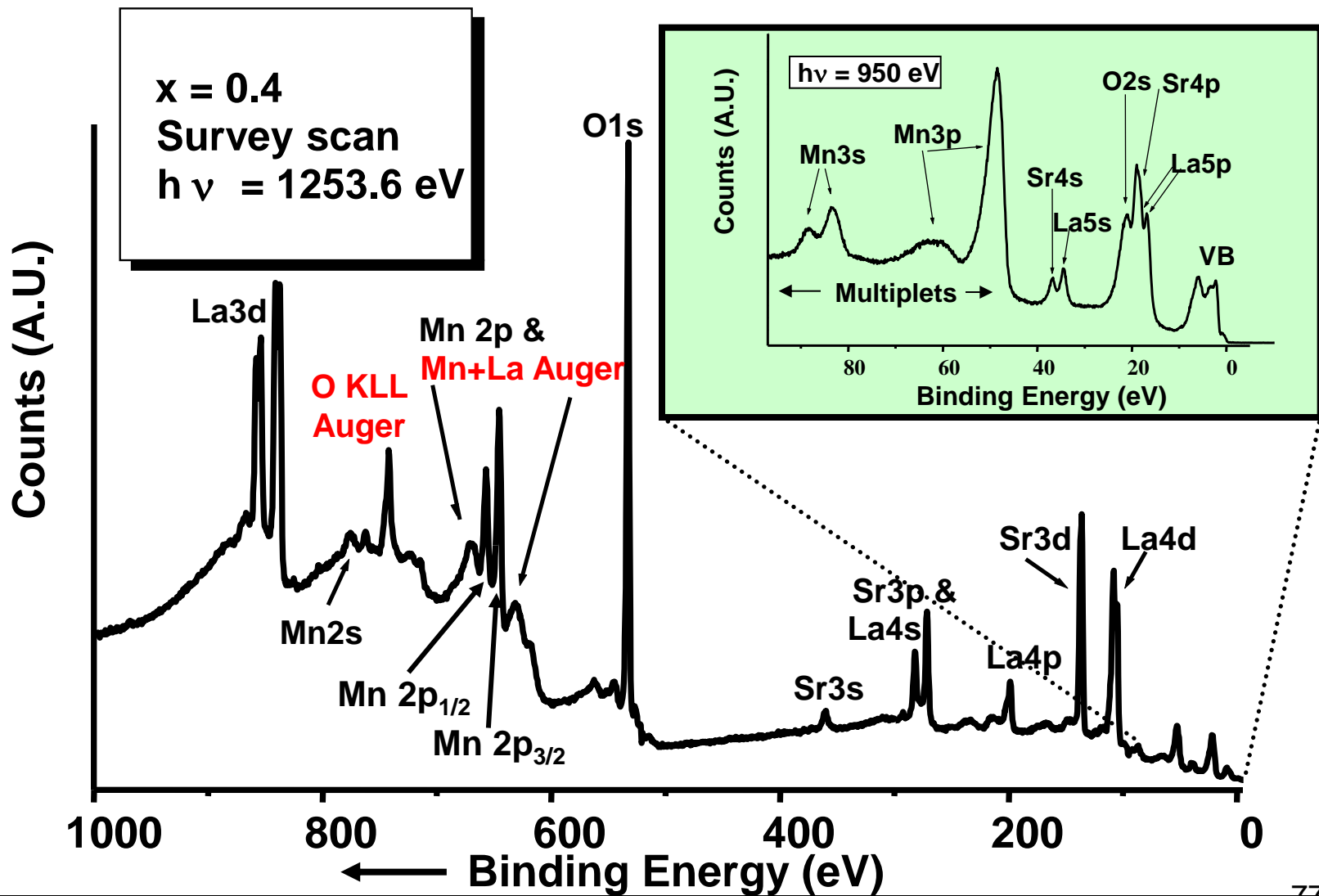
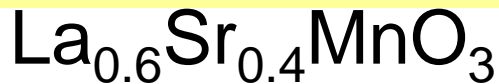
REXS/RIXS = resonant elastic/inelastic x-ray scattering

MATRIX ELEMENTS IN The Soft and Hard X-Ray Spectroscopies: DIPOLE LIMIT

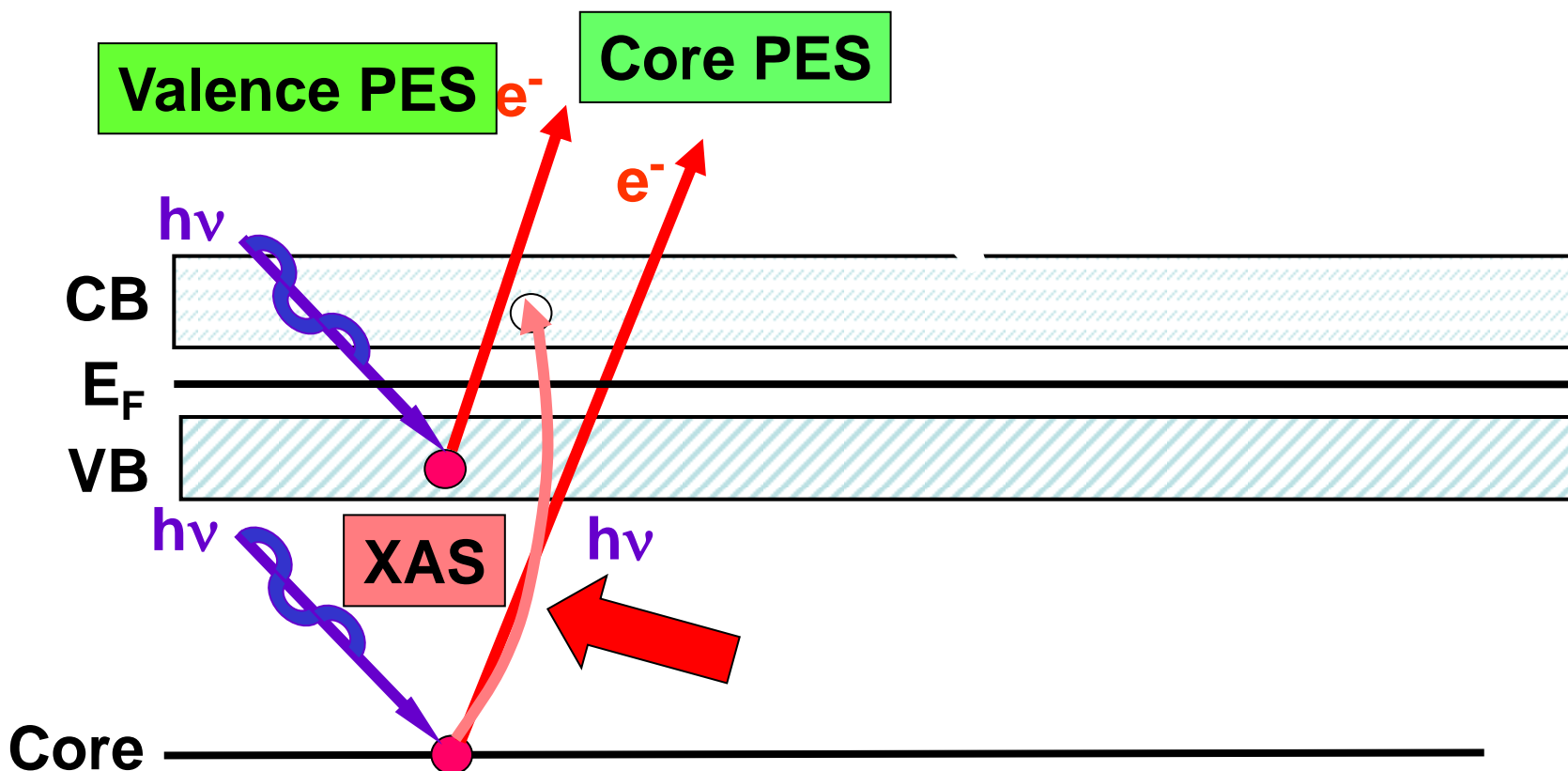
- Photoelectron spectroscopy/photoemission:

$$I \propto |\hat{\mathbf{e}} \cdot \langle \varphi_f(\mathbf{1}) | \vec{r} | \varphi_i(\mathbf{1}) \rangle|^2$$


Core and valence photoemission



The Soft and Hard X-Ray Spectroscopies



PES = photoemission = photoelectron spectroscopy

XAS = x-ray absorption spectroscopy

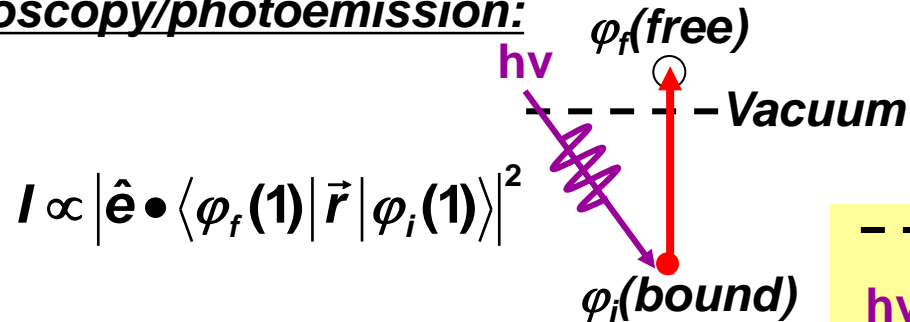
AES = Auger electron spectroscopy

XES = x-ray emission spectroscopy

REXS/RIXS = resonant elastic/inelastic x-ray scattering

MATRIX ELEMENTS IN The Soft and Hard X-Ray Spectroscopies: DIPOLE LIMIT

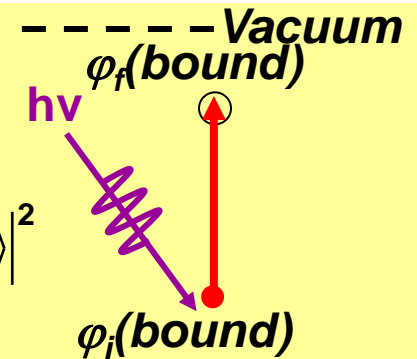
- Photoelectron spectroscopy/photoemission:



$$I \propto |\hat{\mathbf{e}} \cdot \langle \varphi_f(\mathbf{1}) | \vec{r} | \varphi_i(\mathbf{1}) \rangle|^2$$

- Near-edge x-ray absorption:

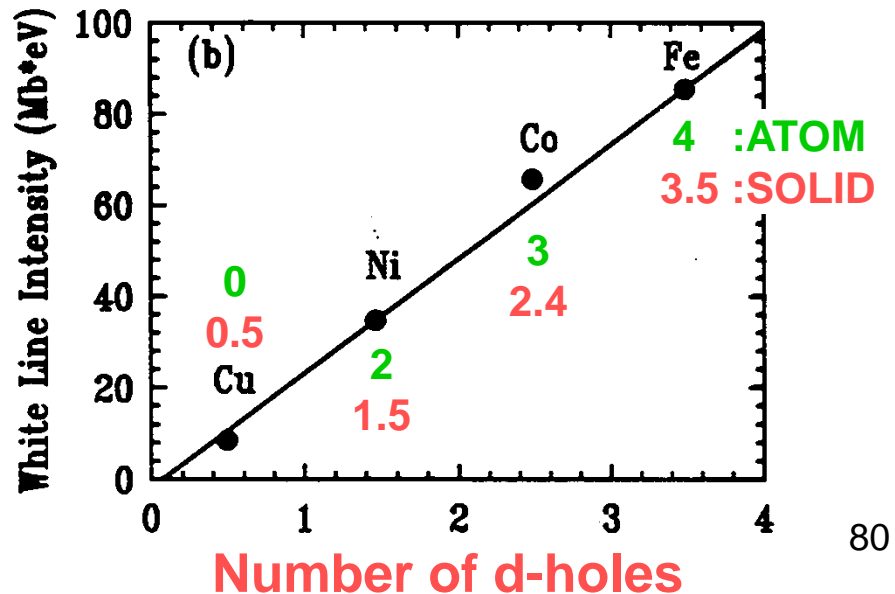
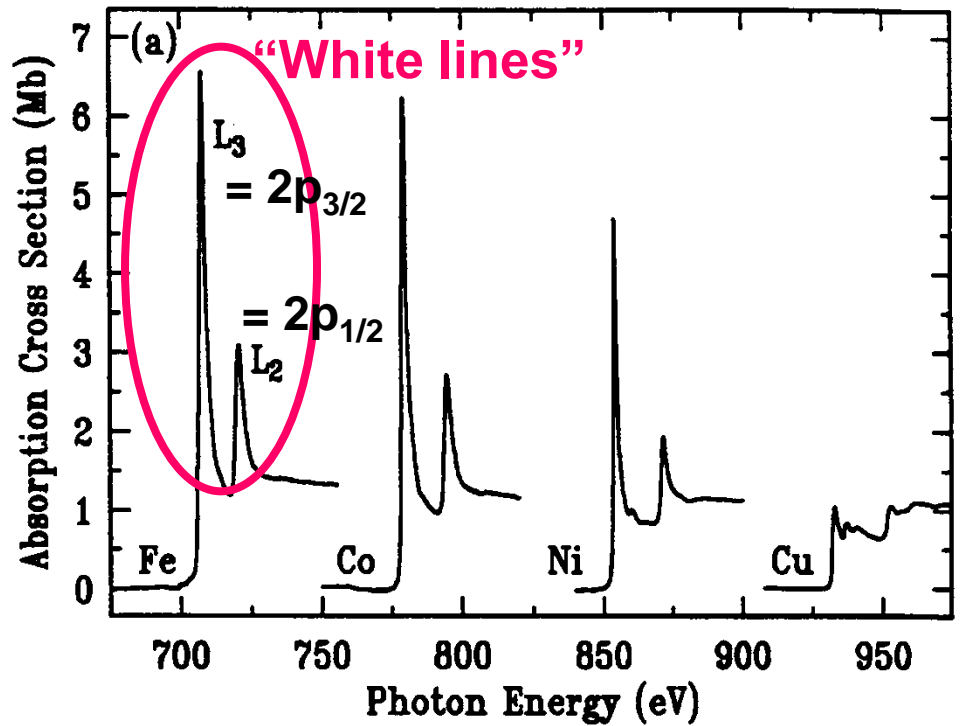
$$I \propto |\hat{\mathbf{e}} \cdot \langle \varphi_f(\mathbf{1}) | \vec{r} | \varphi_i(\mathbf{1}) \rangle|^2$$



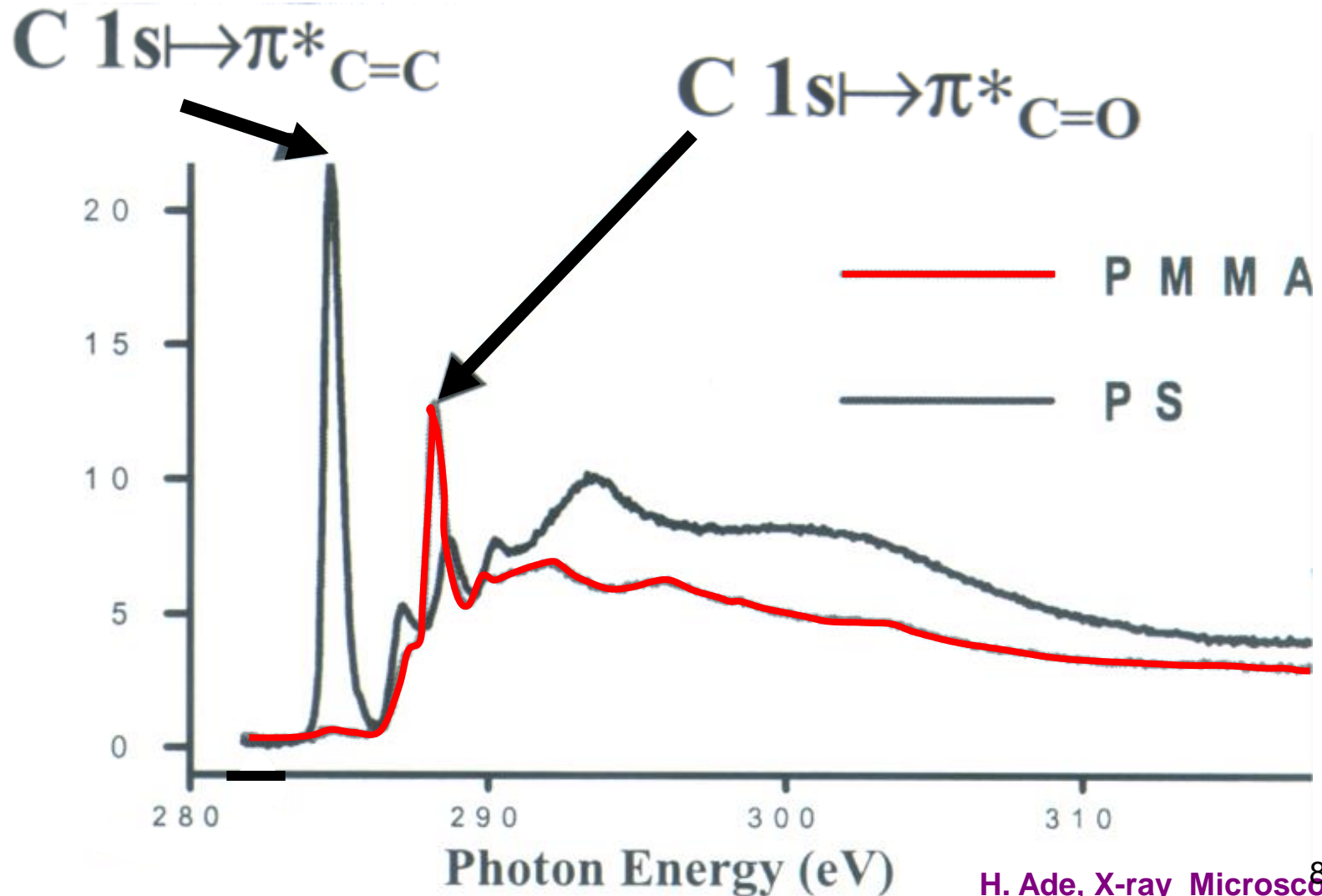
Variation of Near-Edge X-Ray Absorption Fine Structure (NEXAFS) with Atomic No. for Some 3d Transition Metals

J. Stohr, "NEXAFS Spectroscopy" (Spring, 1992),
 Stohr and Siegmann, "Magnetism: From Fundamentals to Nanoscale Dynamics" (Springer Series in Solid-State Sciences, 2006),
 Chapter 9
 Download from 243A website:

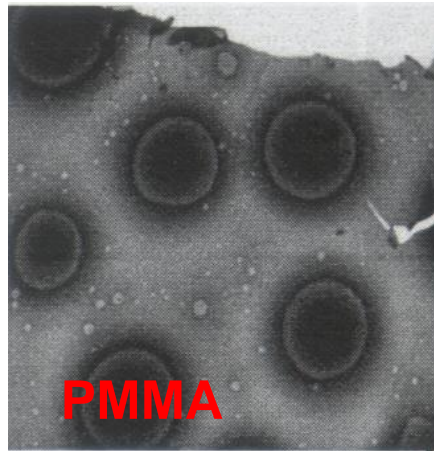
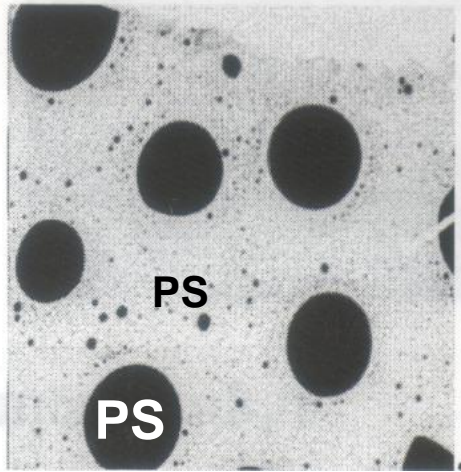
<http://physics.ucdavis.edu/Classes/Physics243A/XMCD.stohr.siegmann.abridged-for-emailing.pdf>



Variation of Near-Edge X-Ray Absorption Fine Structure (NEXAFS) for Different Polymers

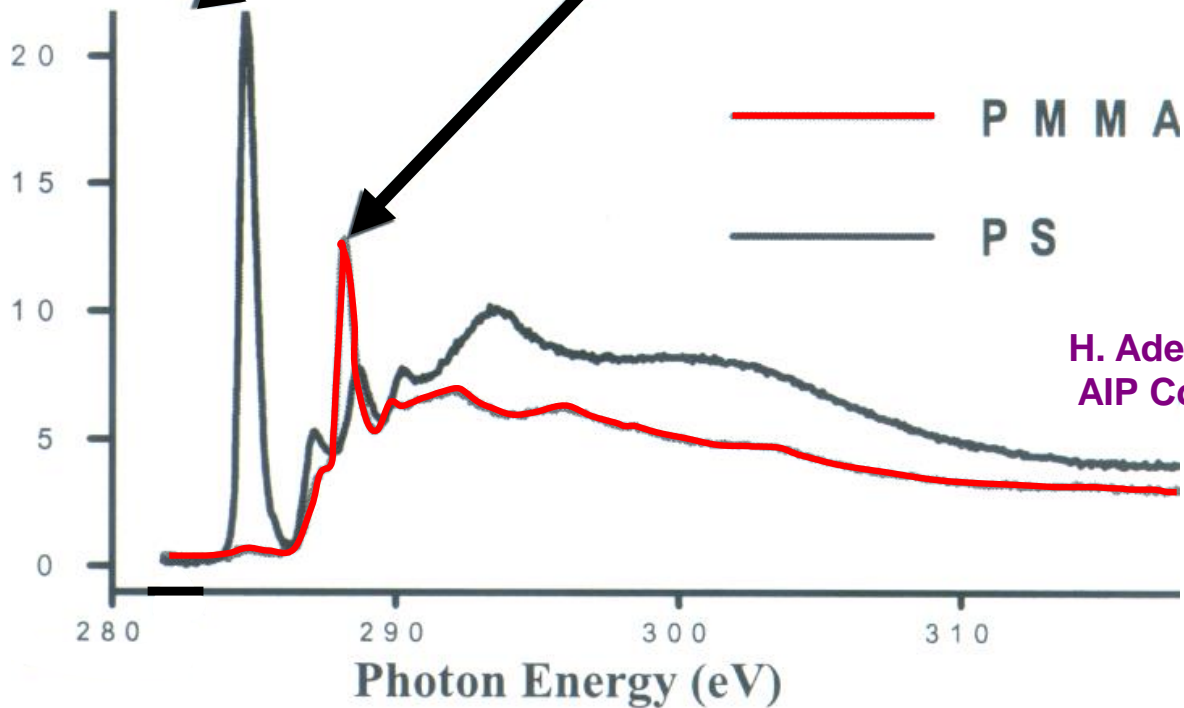


SCANNING TRANSMISSION X-RAY MICROSCOPY OF POLYMER BLEND



$C\ 1s \rightarrow \pi^*_{C=C}$

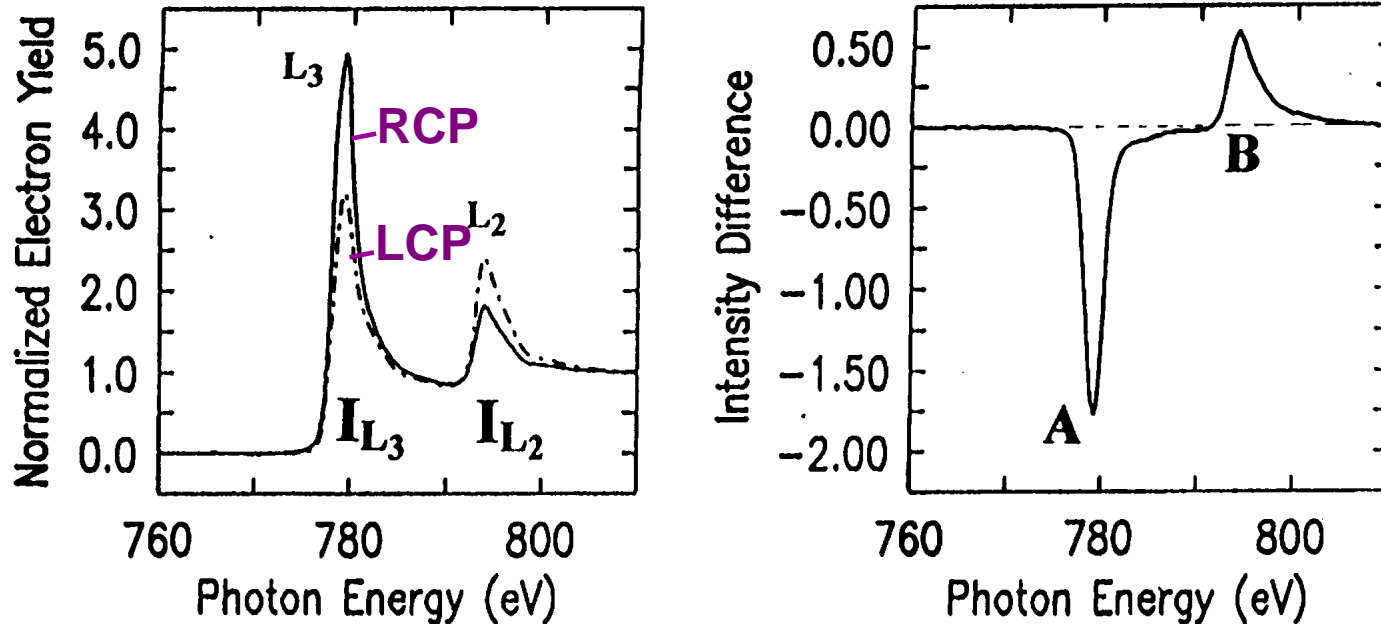
$C\ 1s \rightarrow \pi^*_{C=O}$



H. Ade, *X-ray Microscopy 99*,
AIP Conf. Proc. 507, p.197

Magnetic Circular Dichroism in X-Ray Absorption (XMCD)

Ferromagnetic cobalt with magnetization along incident light direction



Very useful sum rules:

Spin magnetic moment — $[A - 2B]_{\alpha} = -\frac{C}{\mu_B} (m_{spin})$

Orbital magnetic moment — $[A + B]_{\alpha} = -\frac{3C}{2\mu_B} m_{orbital}^{\alpha}$

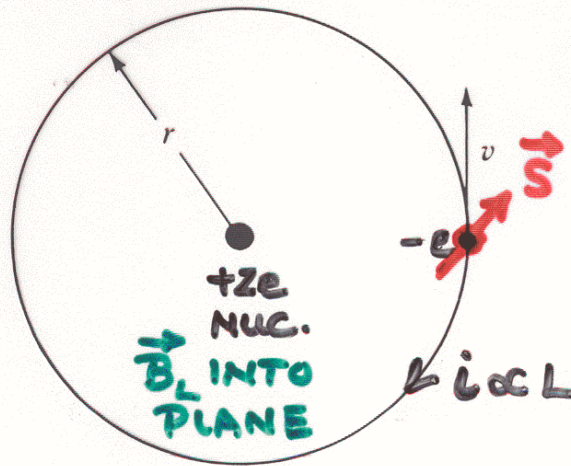
83

$C = (\text{constant}) \times (\text{radial matrix element squared}) \frac{L_{Final}}{3[2L_{Final} + 1]}$

$\alpha \rightarrow$ component along magnetic field

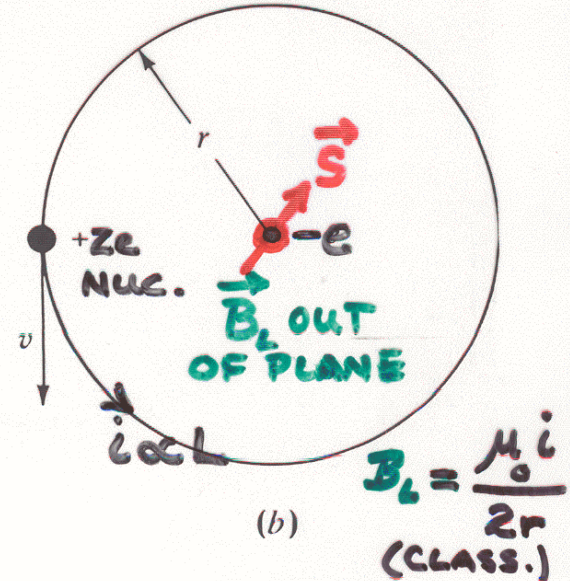
A FINAL (RELATIVISTIC) ATOMIC INTERACTION: SPIN-ORBIT COUPLING

(a) An electron circles an atomic nucleus, as viewed from the frame of reference of the nucleus. (b) From the electron's frame of reference, the nucleus is circling it. The magnetic field the electron experiences as a result is directed upward from the plane of the paper. The interaction between the electron's spin magnetic moment and this magnetic field leads to the phenomenon of spin-orbit coupling.



(a)

**NUCLEAR
REST FRAME**



(b)

**ELECTRON
REST FRAME**

$$E_{S-O} = -\vec{\mu}_S \cdot \vec{B}_L$$

$$E_{S-O} \propto +\vec{S} \cdot \vec{L}$$

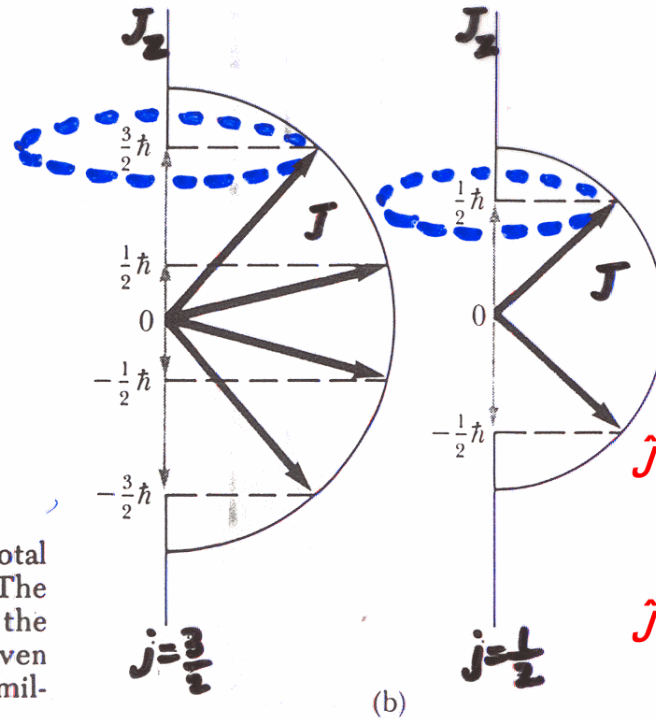
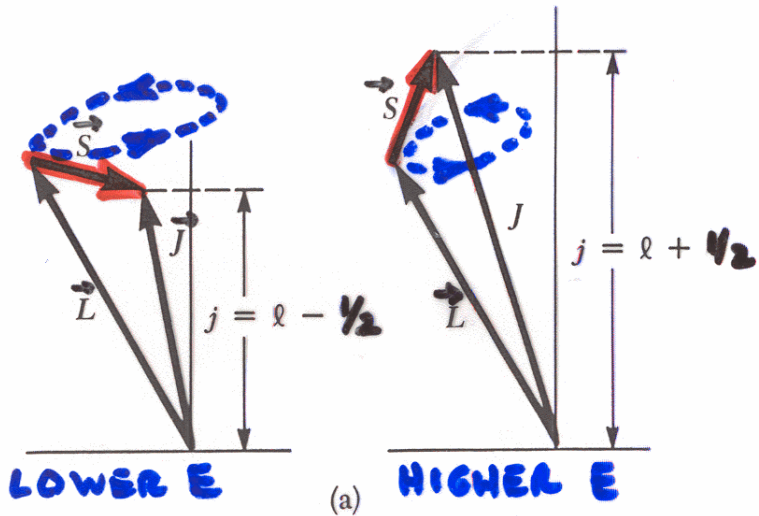
ADDS TO \hat{H} IN
SCHRÖD. EQN.

$$\hat{H}\psi = \hat{K}\psi + V\psi + \hat{H}_{S-O}\psi = E\psi$$

Spin-orbit coupling and a new angular momentum J

\hat{H}_{S-O}
 E_{S-O}

COUPLES \vec{S} AND \vec{L} TO NEW "CONSERVED" \vec{J} :



AGAIN
 PRECESSING
 VECTOR
 MODEL

Eigenfunctions:

$$\hat{J}^2 \Psi_{n,l,s=1/2,j,m_j} = \hbar^2 j(j+1) \Psi_{n,l,s=1/2,j,m_j}$$

$$\hat{J}_z \Psi_{n,l,s=1/2,j,m_j} = \hbar m_j \Psi_{n,l,s=1/2,j,m_j}$$

Figure 8.12 (a) A vector model for determining the total angular momentum $J = L + S$ of a single electron. (b) The allowed orientations of the total angular momentum J for the states $j = \frac{3}{2}$ and $j = \frac{1}{2}$. Notice that there are now an even number of orientations possible, not the odd number familiar from the space quantization of L alone.

$|\vec{J}| = \hbar \sqrt{j(j+1)}$

WITH: $j = \begin{cases} l - 1/2 \\ l + 1/2 \end{cases}$

$J_z = \hbar m_j$

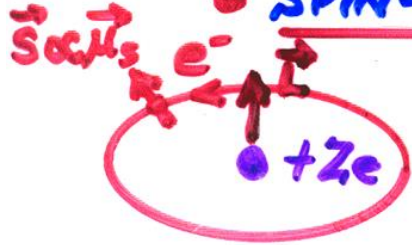
WITH: $m_j = -j, -j+1, \dots, +j$

$2j+1$ DEGENERACY
 $\Psi_{n,l,s=1/2,j,m_j} \Rightarrow$ NOTATION "nLj"

GOOD QUANTUM NOS. IF E_{S-O} STRING

Magnetic Circular Dichroism in X-Ray Absorption (XMCD): Only happens because of the spin-orbit effect

• SPIN-ORBIT SPLITTING OF LEVELS:



⇒ EFFECTIVE \vec{B} (NUCLEUS AROUND e^-) $\propto \vec{L}$

$$\hat{H}_{s.o.} = \xi(r) \vec{L} \cdot \vec{S}$$

- SPLITS ALL nl LEVELS $2(2l+1)$
 - $nl_j = l + 1/2 \rightarrow 2l+2$
 - $nl_j = l - 1/2 \rightarrow 2l$

• MIXES SPIN + ORBITAL ANGULAR MOM.::

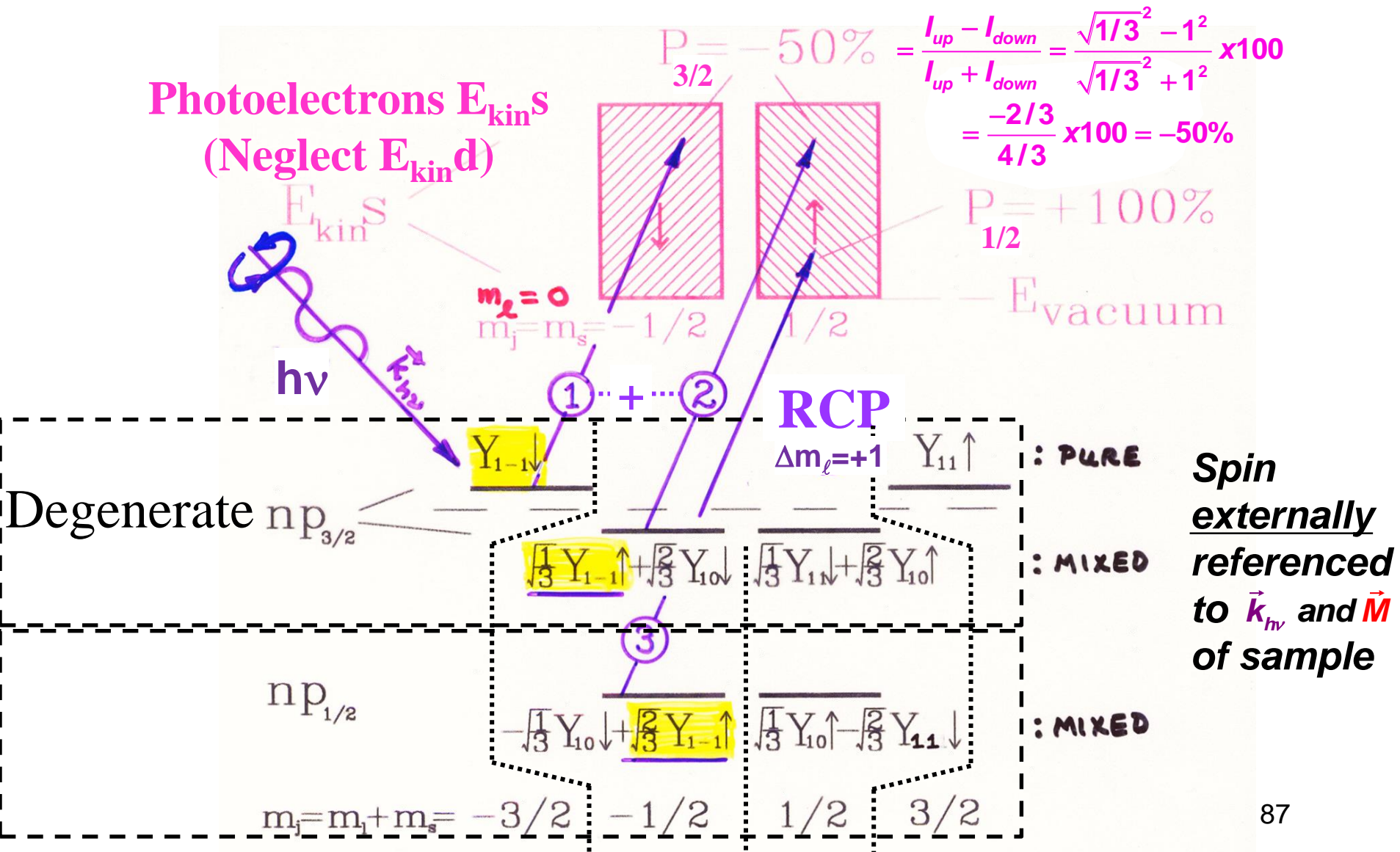
$$\psi_{nljm_j} = C_1 \psi_{nl, m_j - 1/2} \begin{pmatrix} 1 \\ 0 \end{pmatrix} + C_2 \psi_{nl, m_j + 1/2} \begin{pmatrix} 0 \\ 1 \end{pmatrix}$$

\parallel
 $m_s = +1/2$
 \parallel
 \uparrow

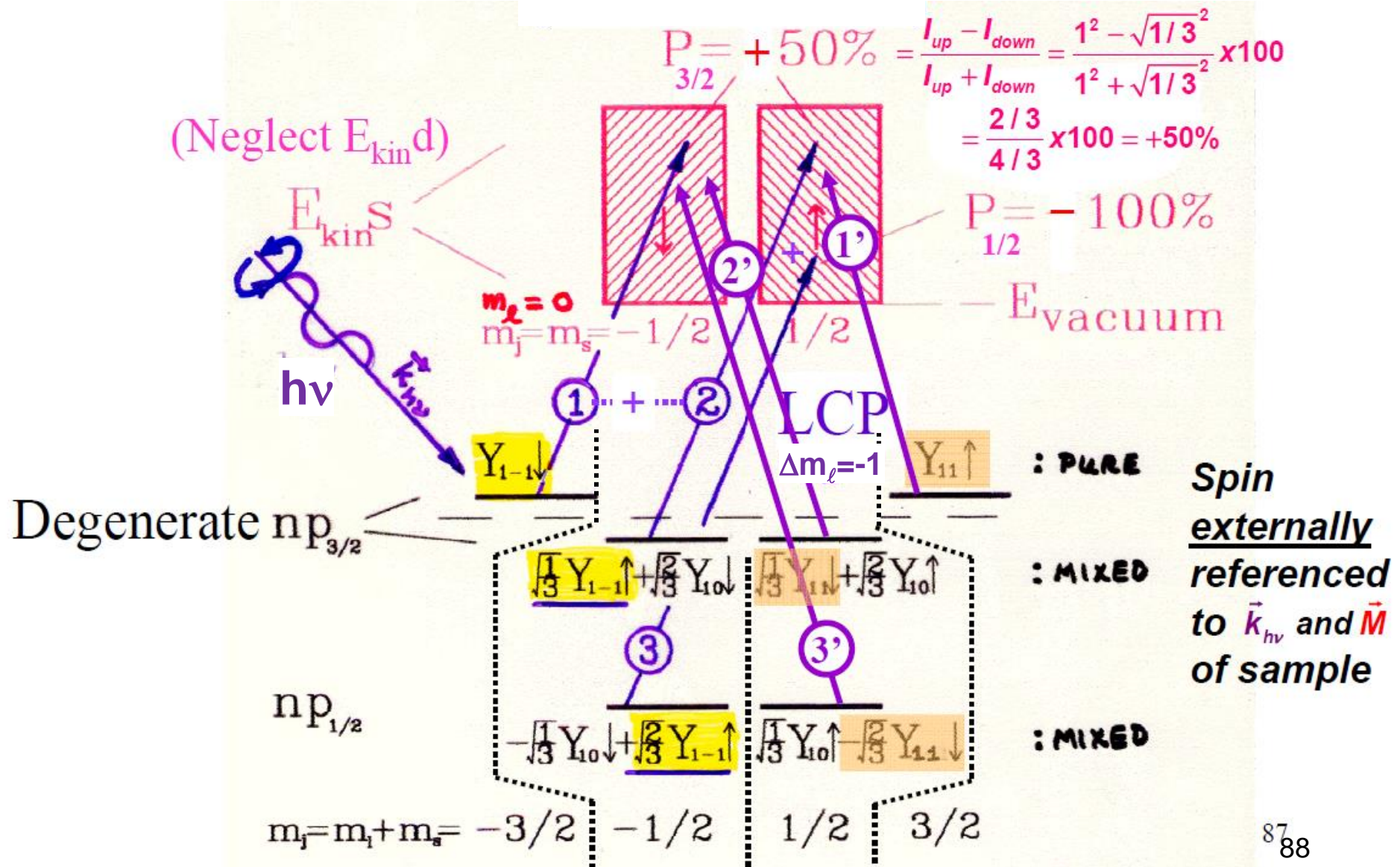
\parallel
 $m_s = -1/2$
 \parallel
 \downarrow

WITH C1 AND C2 TABULATED CLEBSCH-GORDAN
OR WIGNER 3j SYMBOLS

Example: Photoelectron spin polarization from spin-orbit coupling and circularly-polarized radiation—The Fano Effect



Photoelectron spin polarization from spin-orbit coupling and circularly-polarized radiation—The Fano Effect

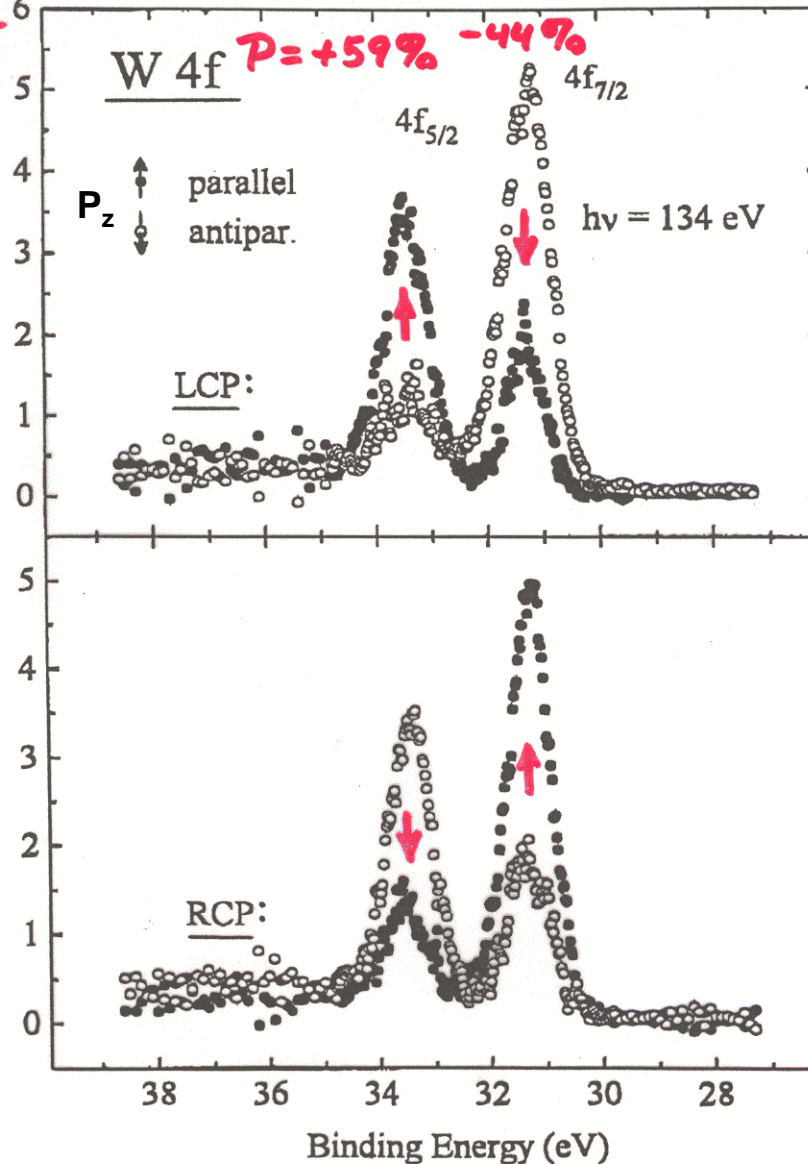
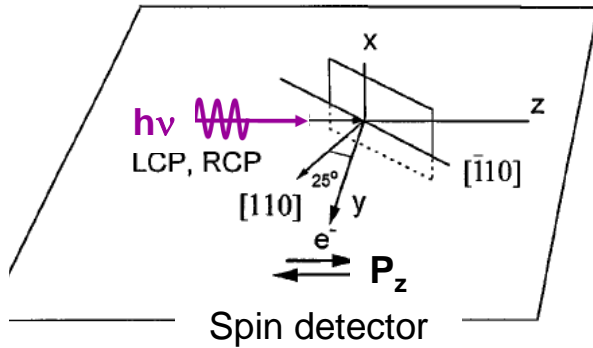


Fano effect and spin polarization (SP) in core photoelectron spectra—expt.

SPIN-ORBIT SPLIT

LEVEL (b)
EXCITED
WITH
CIRCULAR
POLARIZATION
(FANO EFFECT)

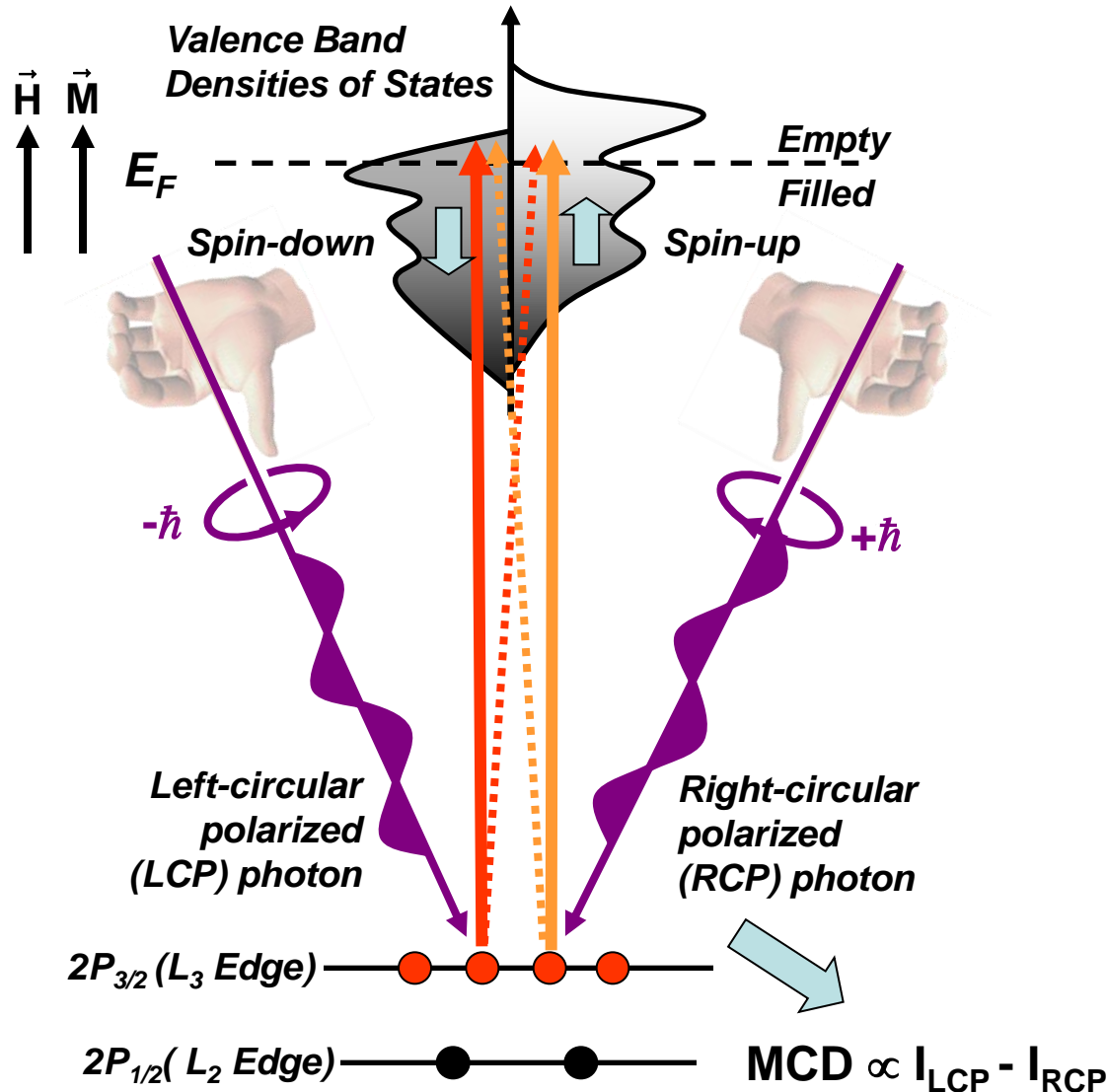
Intensity (arb. units)



EXPT. - STARKE ET AL.
 PRB 53, 210544
 (1996)

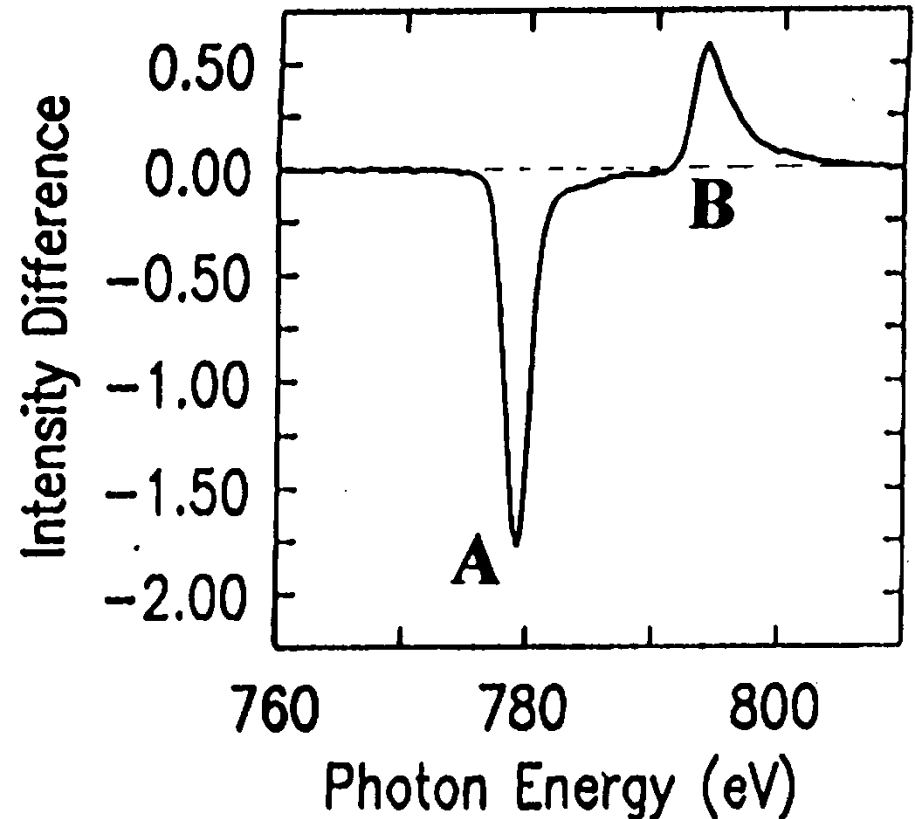
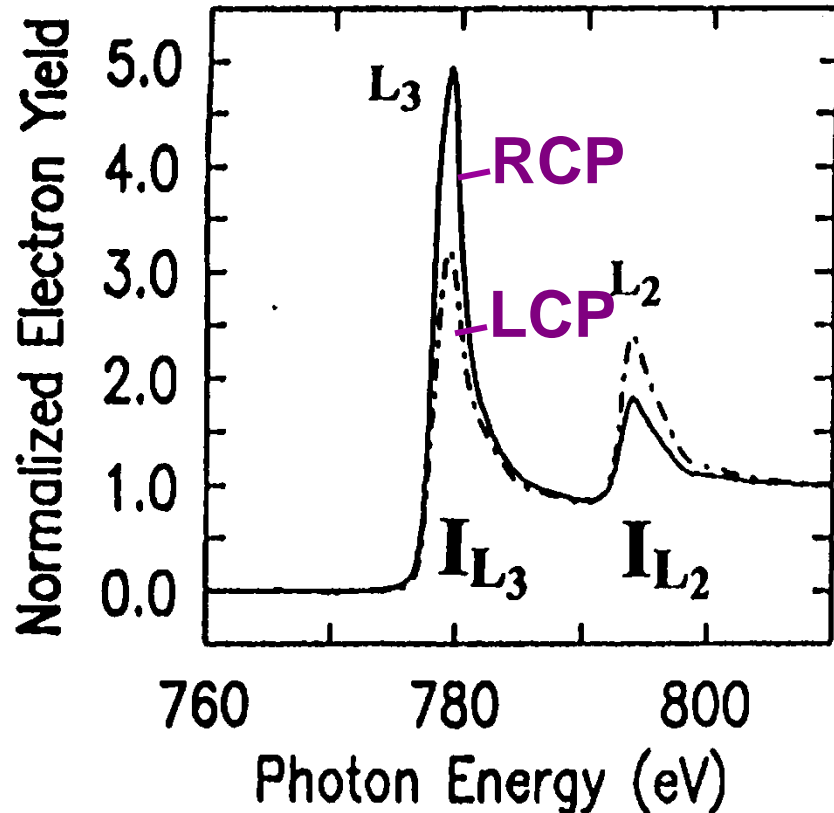
Magnetic Circular Dichroism in X-Ray Absorption (XMCD)

J. Stohr, *Journal of Magnetism and Magnetic Materials* 200 (1999) 470–497



Magnetic Circular Dichroism in X-Ray Absorption (XMCD)

Ferromagnetic cobalt with magnetization along incident light direction



Very useful sum rules: Spin magnetic moment—

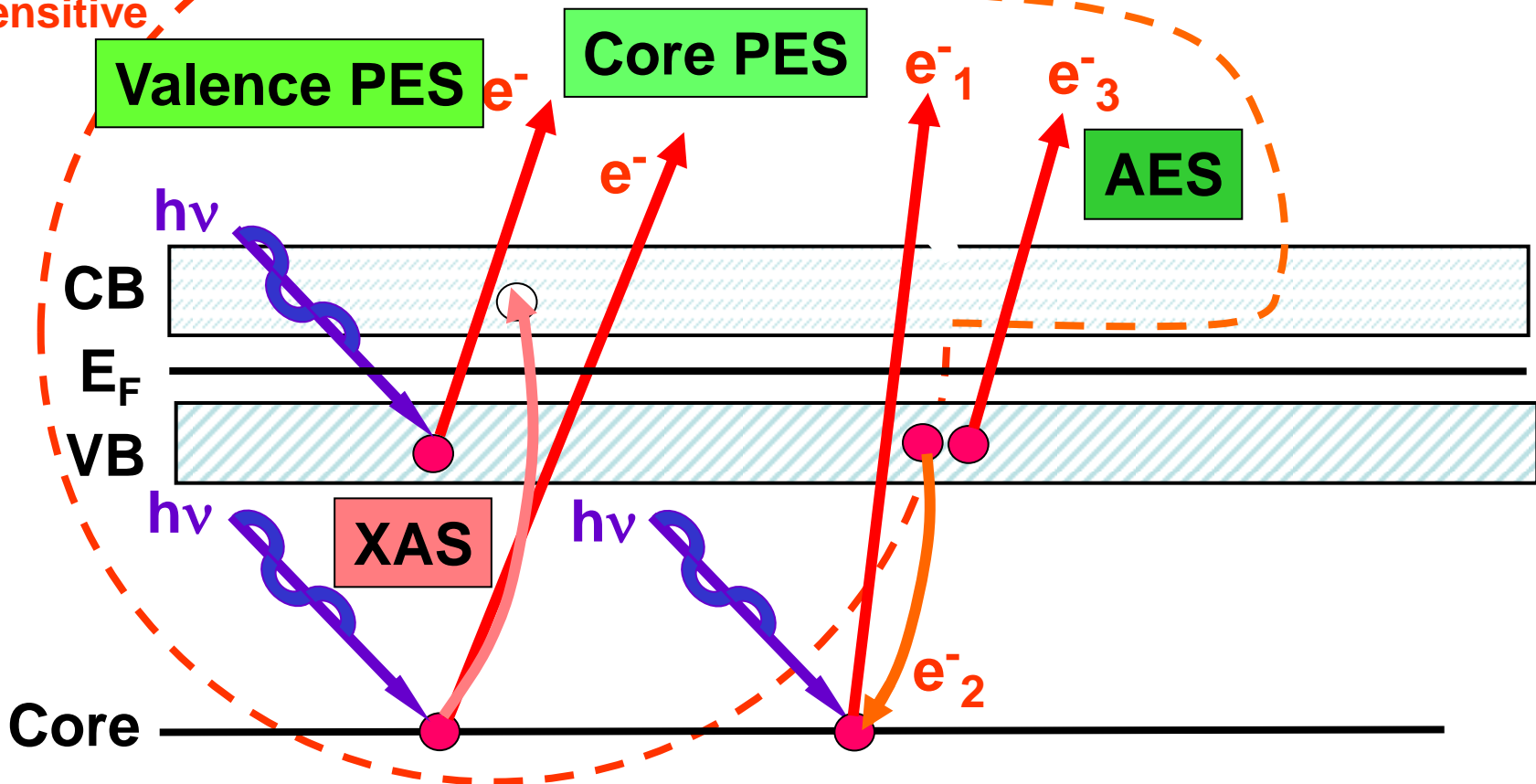
$$[A - 2B]_{\alpha} = -\frac{C}{\mu_B} (m_{spin})$$

Orbital magnetic moment—
($\alpha \rightarrow$ component along magnetic field)

$$[A + B]_{\alpha} = -\frac{3C}{2\mu_B} m_{orbital}^{\alpha}$$

The Soft and Hard X-Ray Spectroscopies

Electron-out:
surface
sensitive



PES = photoemission = photoelectron spectroscopy

XAS = x-ray absorption spectroscopy

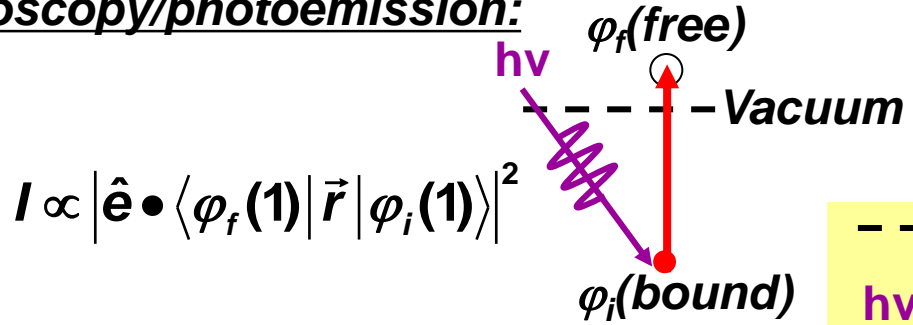
AES = Auger electron spectroscopy

XES = x-ray emission spectroscopy

REXS/RIXS = resonant elastic/inelastic x-ray scattering

MATRIX ELEMENTS IN The Soft and Hard X-Ray Spectroscopies: DIPOLE LIMIT

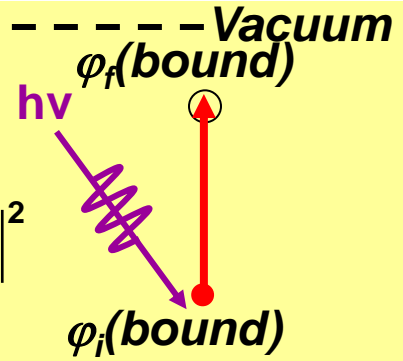
• Photoelectron spectroscopy/photoemission:



$$I \propto \left| \hat{e} \cdot \langle \varphi_f(\mathbf{1}) | \vec{r} | \varphi_i(\mathbf{1}) \rangle \right|^2$$

• Near-edge x-ray absorption:

$$I \propto \left| \hat{e} \cdot \langle \varphi_f(\mathbf{1}) | \vec{r} | \varphi_i(\mathbf{1}) \rangle \right|^2$$



• Auger electron emission:

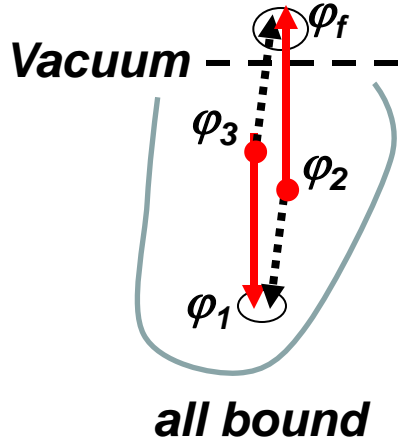
$$I \propto \left| \langle \varphi_f(\mathbf{1}) \varphi_1(\mathbf{2}) \left| \frac{e^2}{r_{12}} \right| \varphi_3(\mathbf{1}) \varphi_2(\mathbf{2}) \rangle - \langle \varphi_1(\mathbf{1}) \varphi_f(\mathbf{2}) \left| \frac{e^2}{r_{12}} \right| \varphi_3(\mathbf{1}) \varphi_2(\mathbf{2}) \rangle \right|^2$$

Exchange

with $r_{12} = |\vec{r}_1 - \vec{r}_2|$, and

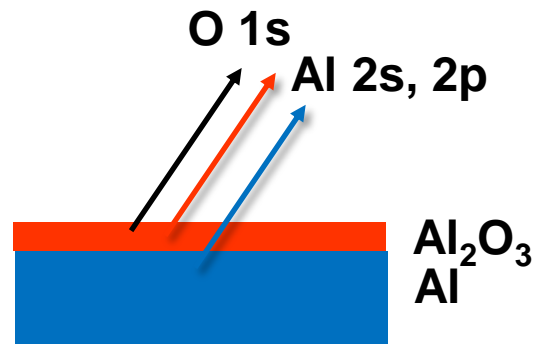
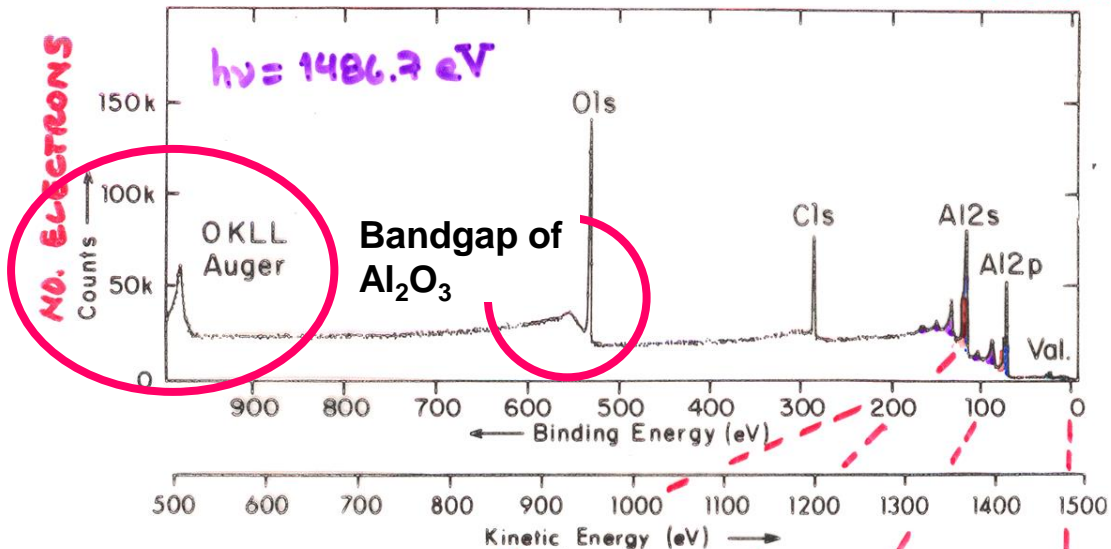
$$\frac{e^2}{|\vec{r}_1 - \vec{r}_2|} = 4\pi e^2 \sum_{l=0}^{\infty} \sum_{m_l=-l}^l \frac{1}{2l+1} \frac{r_{<}^l}{r_{>}^{l+1}} Y_l^{m_l}(\theta_1, \phi_1) [Y_l^{m_l}(\theta_2, \phi_2)]^*$$

a complex operator, no simple selection rules



all bound

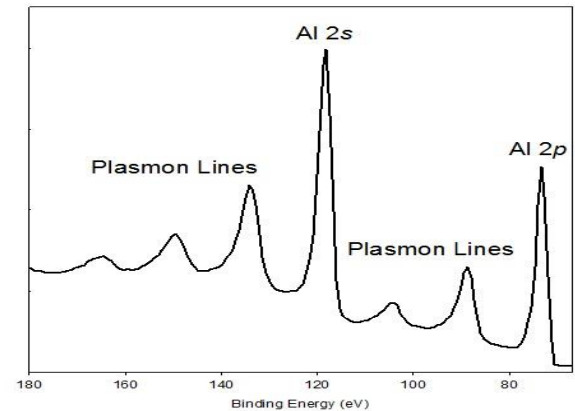
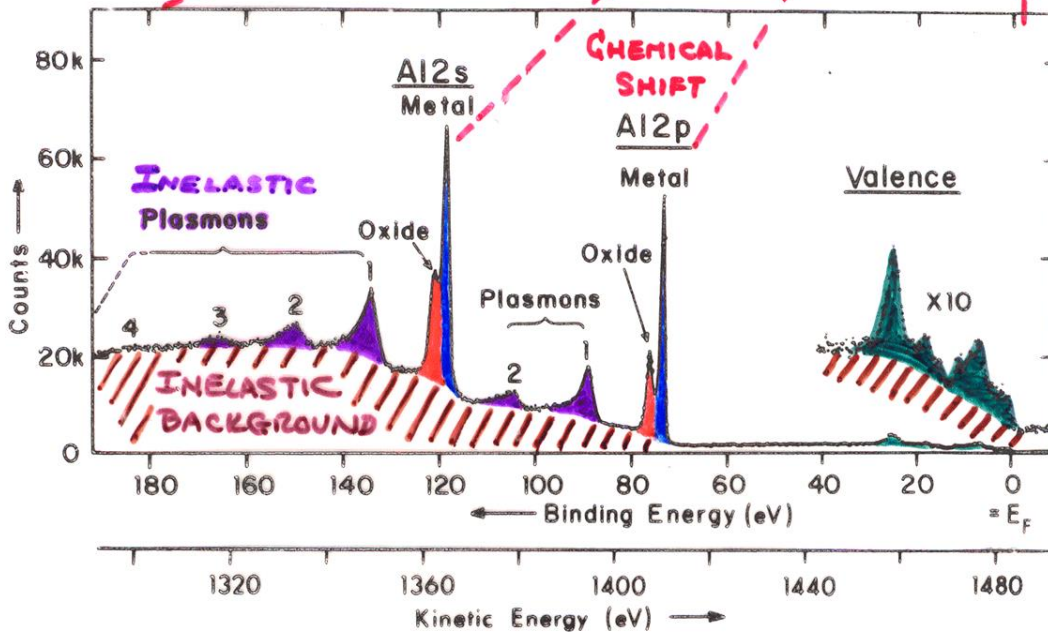
TYPICAL PHOTOELECTRON SPECTRA: OXIDIZED ALUMINUM



Plasmons:

$$E_{\text{plasmon}} = \hbar\omega_p = \hbar(n_{\text{valence}} e^2 / m_e \epsilon_0)^{1/2}$$

CLEAN ALUMINUM



“Basic Concepts of XPS”
Figure 1

THE AUGER PROCESS

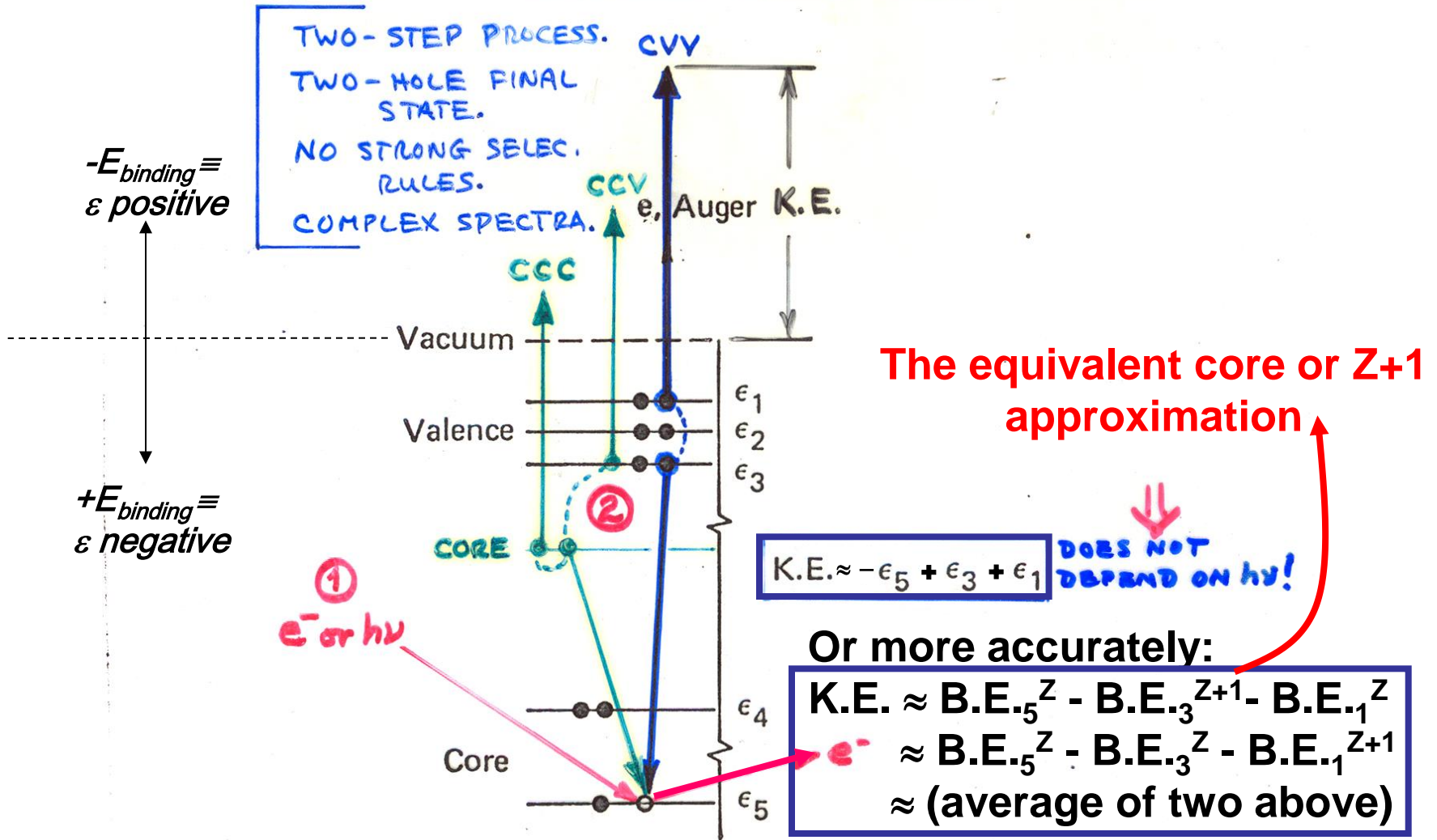
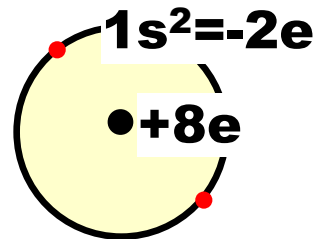


Figure 2. Scheme of the Auger process. A valence-level involved Auger emission is illustrated here, but the two electrons involved also could have come from core level, ε_4 , provided $\varepsilon_5 - 2\varepsilon_4 > 0$.

The equivalent core or Z+1 approximation

O: Z = 8

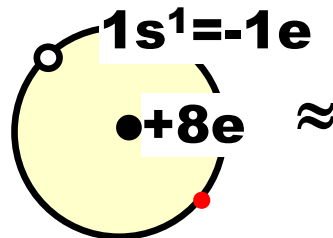
O core = O 1s² = O⁶⁺



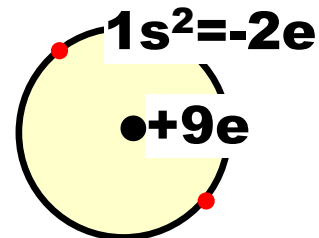
Assume:

O⁶⁺ core with

1s hole = O⁷⁺ =



≈

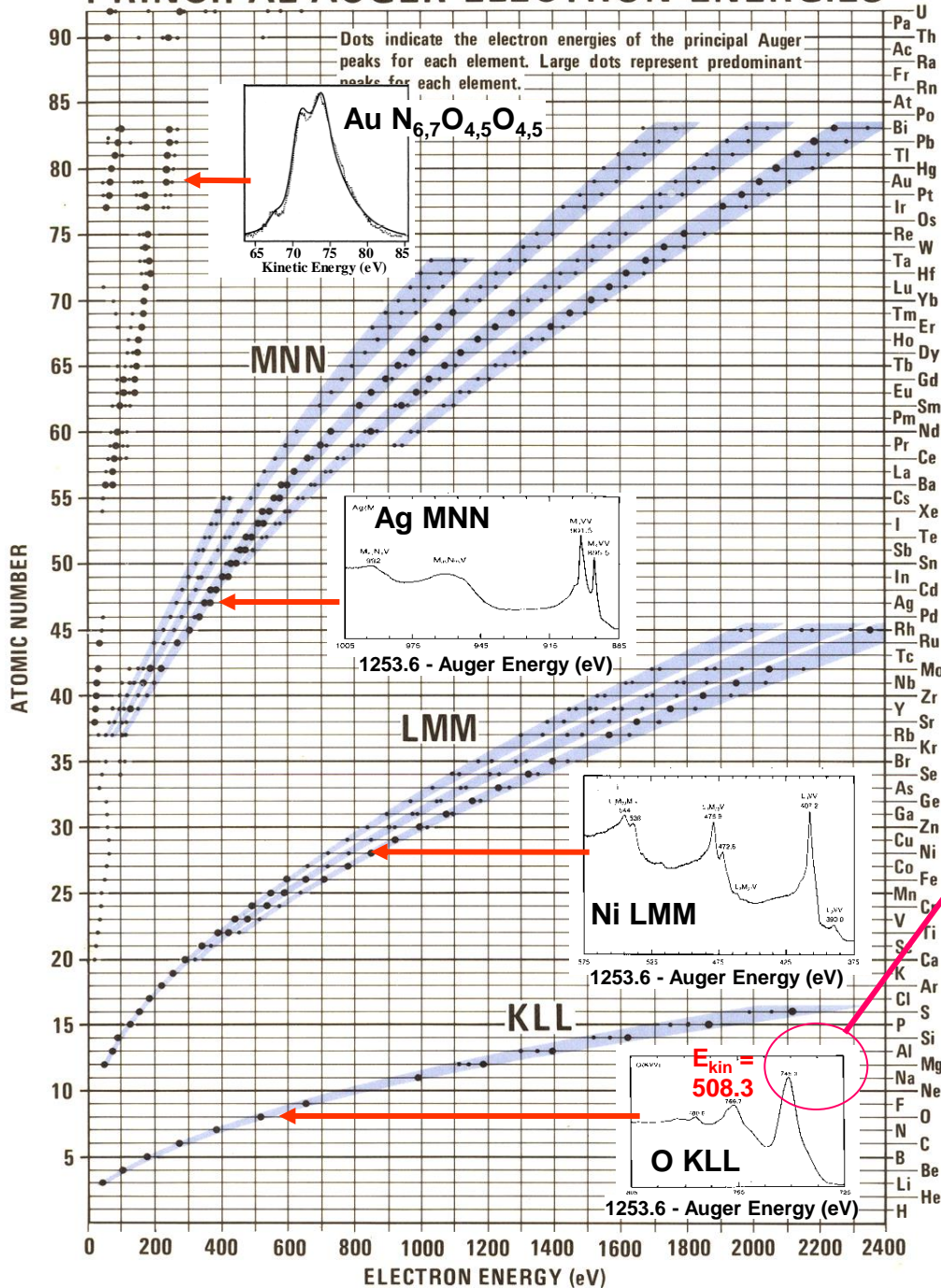


= F⁷⁺ core

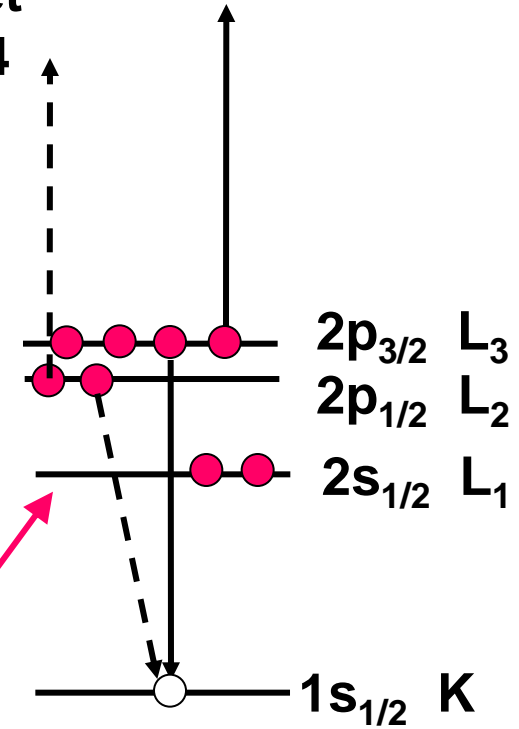
F: Z = 9

Plus see pp. 92-93 in
"Basic Concepts of XPS"

PRINCIPAL AUGER ELECTRON ENERGIES



X-Ray Data Booklet Fig. 1.4



$$\begin{aligned}
 \text{K.E.} &\approx \text{B.E.}_{1s}^{Z=8} - \text{B.E.}_{2p}^9 - \text{B.E.}_{2p}^8 \\
 &\approx \text{B.E.}_{1s}^8 + \text{B.E.}_{2p}^8 - \text{B.E.}_{2p}^9 \\
 &\approx 543.1 - 17 - 13 \approx \mathbf{513 \text{ eV}}
 \end{aligned}$$

X-Ray Data Booklet--Section 1.1 ELECTRON BINDING ENERGIES

The energies are given in eV relative to the vacuum level for the rare gases and for H₂, N₂, O₂, F₂, and Cl₂; relative to the Fermi level for the metals; and relative to the top of the valence bands for semiconductors (and insulators).

	Electronic Element configuration	K 1s	L ₁ 2s	L ₂ 2p _{1/2}	L ₃ 2p _{3/2}	M ₁ 3s	M ₂ 3p _{1/2}	M ₃ 3p _{3/2}
1s	1 H	13.6						
1s ²	2 He	24.6*						
1s ² 2s	3 Li	54.7*						
1s ² 2s ²	4 Be	111.5*						
1s ² 2s ² 2p	5 B	188*						
1s ² 2s ² 2p ²	6 C	284.2*						
1s ² 2s ² 2p ³	7 N	409.9*	37.3*	~ 9	~ 9			
1s ² 2s ² 2p ⁴	8 O	543.1*	41.6*	~ 13	~ 13			
1s ² 2s ² 2p ⁵	9 F	696.7*	~ 45	~ 17	~ 17			
1s ² 2s ² 2p ⁶	10 Ne	870.2*	48.5*	21.7*	21.6*			
[Ne] 3s	11 Na	1070.8†	63.5†	30.65	30.81			
[Ne] 3s ²	12 Mg	1303.0†	88.7	49.78	49.50			
[Ne] 3s ² 3p	13 Al	1559.6	117.8	72.95	72.55			
[Ne] 3s ² 3p ²	14 Si	1839	149.7*b	99.82	99.42			
[Ne] 3s ² 3p ³	15 P	2145.5	189*	136*	135*			
[Ne] 3s ² 3p ⁴	16 S	2472	230.9	163.6*	162.5*			
[Ne] 3s ² 3p ⁵	17 Cl	2822.4	270*	202*	200*			
[Ne] 3s ² 3p ⁶	18 Ar	3205.9*	326.3*	250.6†	248.4*	29.3*	15.9*	15.7*
[Ar] 4s	19 K	3608.4*	378.6*	297.3*	294.6*	34.8*	18.3*	18.3*
[Ar] 4s ²	20 Ca	4038.5*	438.4†	349.7†	346.2†	44.3 †	25.4†	25.4†
	21 Sc	4492	498.0*	403.6*	398.7*	51.1*	28.3*	28.3*
	22 Ti	4966	560.9†	460.2†	453.8†	58.7†	32.6†	32.6†

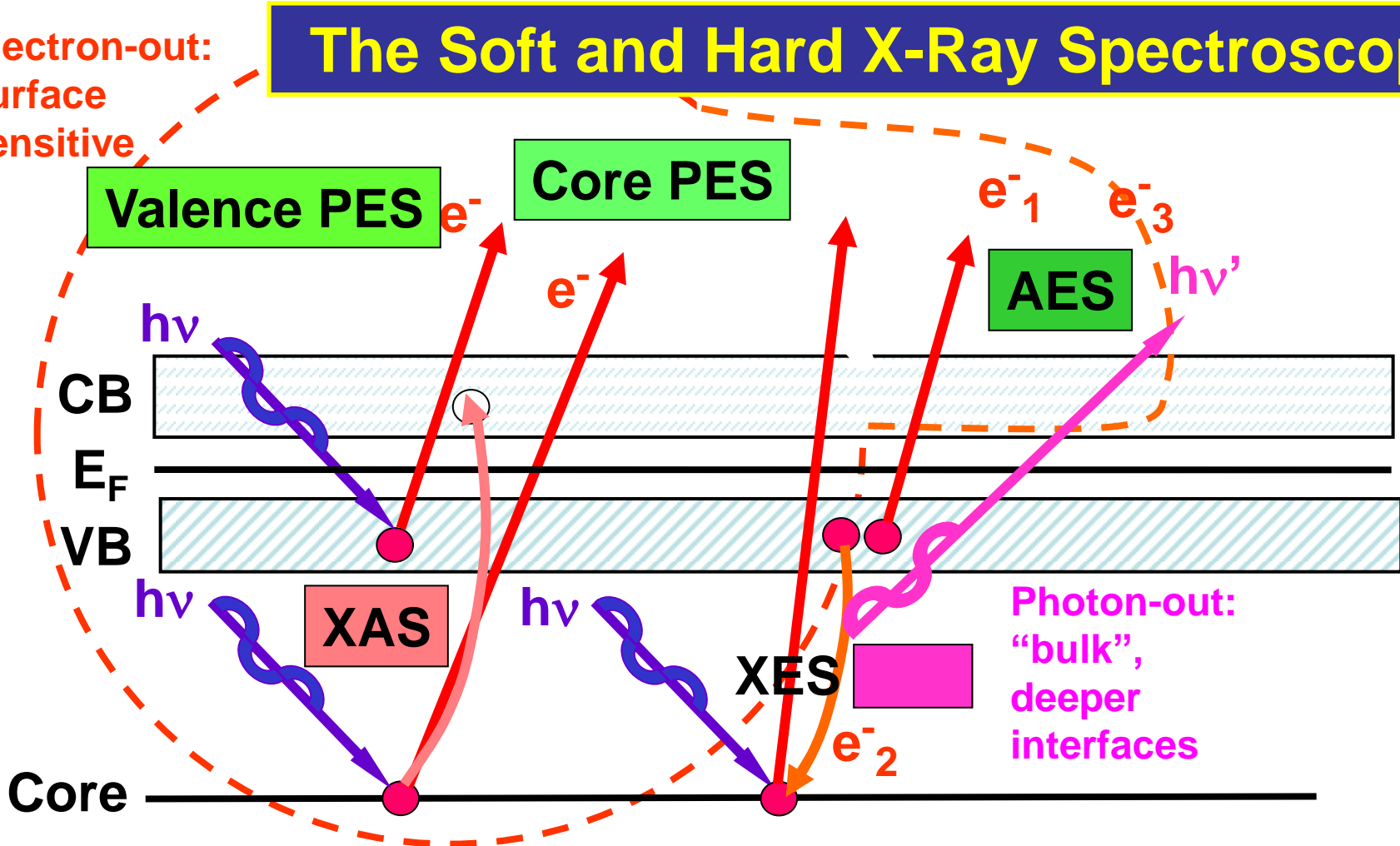
Valence levels

Interpolated,
extrapolated

Missing
valence
B.E.s

Valence levels

The Soft and Hard X-Ray Spectroscopies



PES = photoemission = photoelectron spectroscopy

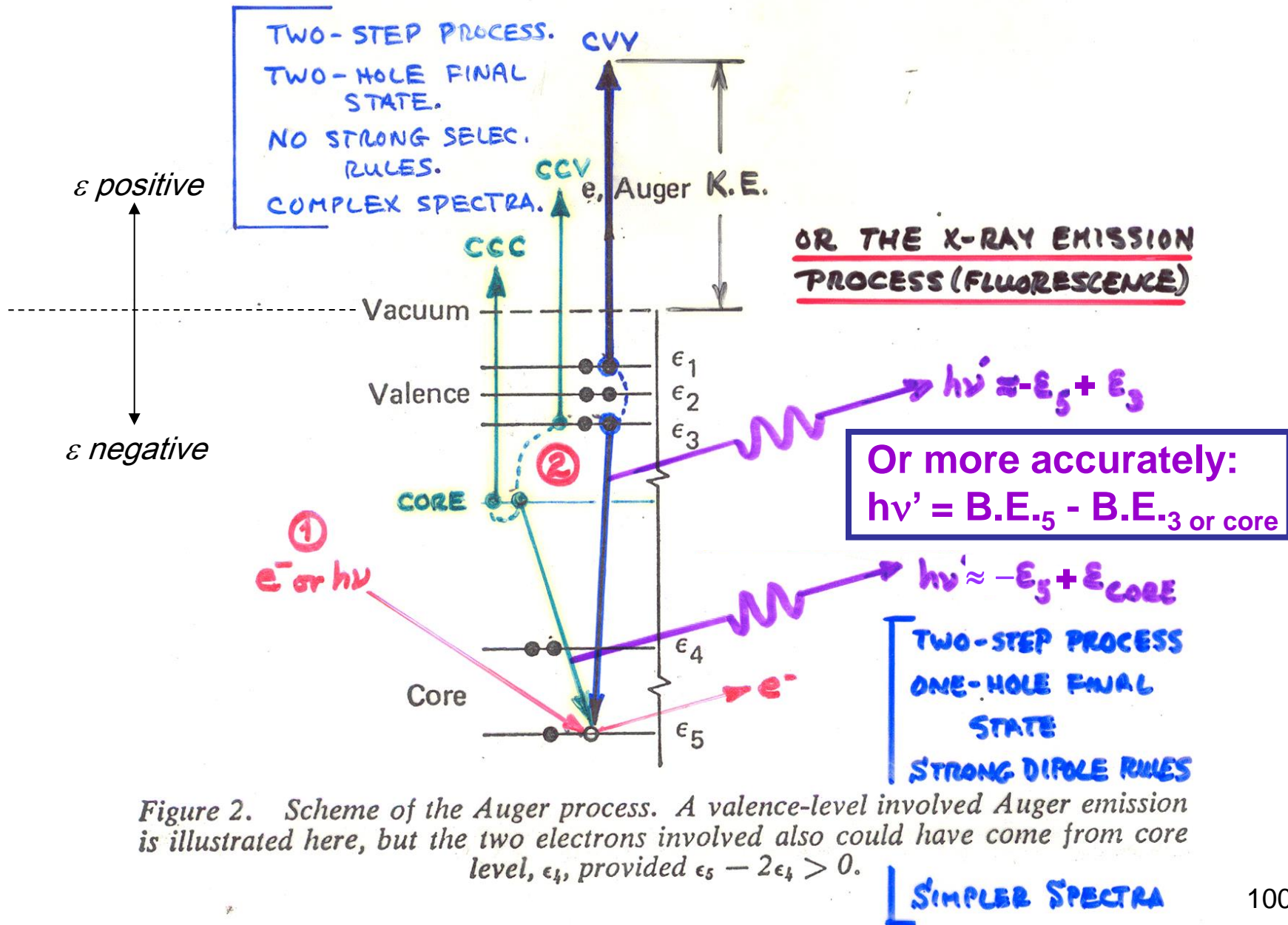
XAS = x-ray absorption spectroscopy

AES = Auger electron spectroscopy

XES = x-ray emission spectroscopy

REXS/RIXS = resonant elastic/inelastic x-ray scattering

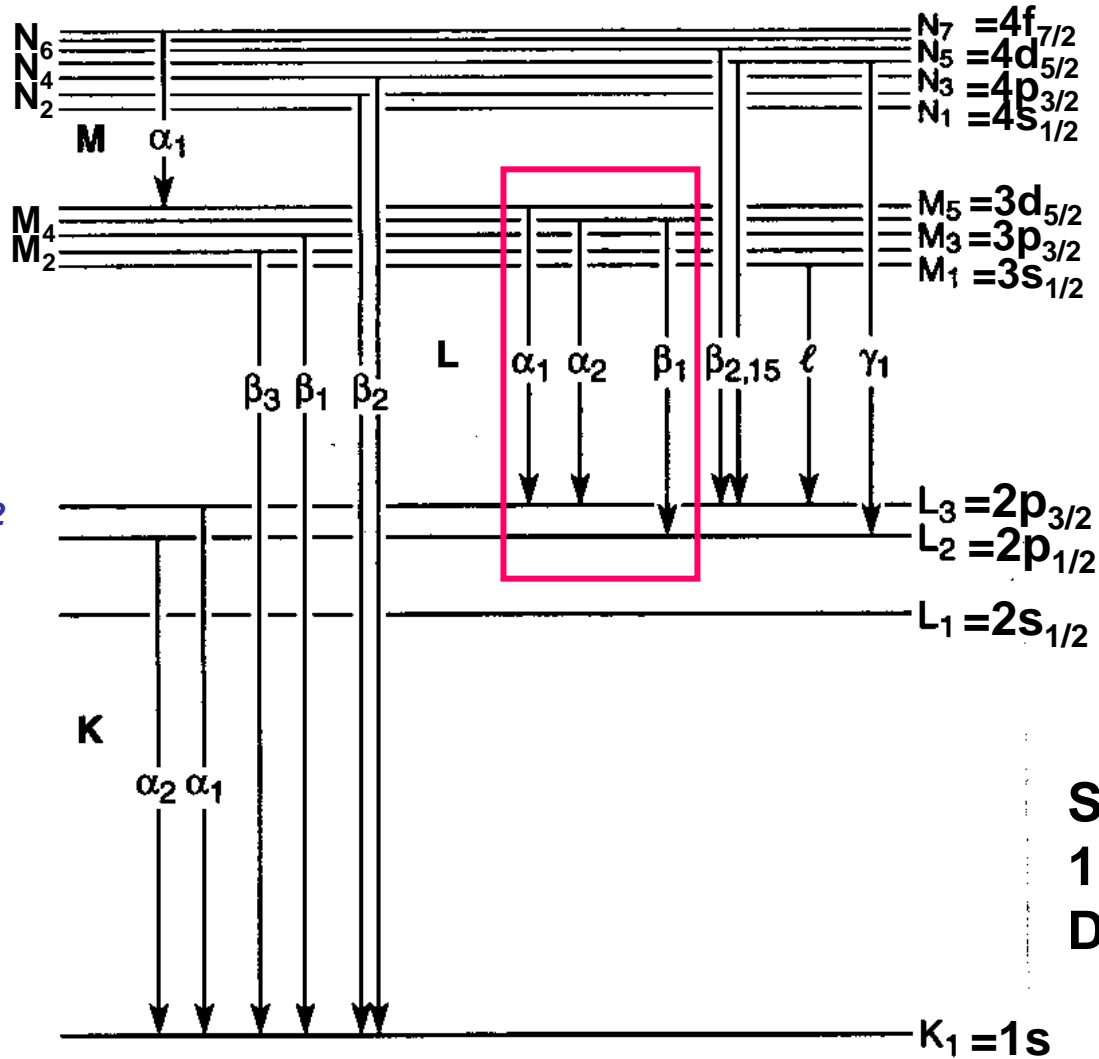
THE AUGER PROCESS



**X-Ray
Nomenclature
(from "X-Ray
Data Booklet")**

In general:

$$nl \begin{cases} \text{Spin-}nl_{j=l+1/2} \\ \text{orbit } nl_{j=l-1/2} \end{cases}$$



$\Delta j = 0, \pm 1$

**See Section
1.2 in "X-Ray
Data Booklet"**

Fig. 1-1. Transitions that give rise to the emission lines in Table 1-3.

Electron binding energies

Element	K 1s	L ₁ 2s	L ₂ 2p _{1/2}	L ₃ 2p _{3/2}	M ₁ 3s	M ₂ 3p _{1/2}	M ₃ 3p _{3/2}	M ₄ 3d _{3/2}	M ₅ 3d _{5/2}
23 V	5465	626.7†	519.8†	512.1†	66.3†	37.2†	37.2†		
24 Cr	5989	696.0†	583.8†	574.1†	74.1†	42.2†	42.2†		
25 Mn	6539	769.1†	649.9†	638.7†	82.3†	47.2†	47.2†		
26 Fe	7112	844.6†	719.9†	706.8†	91.3†	52.7†	52.7†		
27 Co	7709	925.1†	793.2†	778.1†	101.0†	58.9†	59.9†		
28 Ni	8333	1008.6†	870.0†	852.7†	110.8†	68.0†	66.2†		
29 Cu	8979	1096.7†	952.3†	932.7	122.5†	77.3†	75.1†		
30 Zn	9659	1196.2*	1044.9*	1021.8*	139.8*	91.4*	88.6*	10.2*	10.1*

Diff. = 11.2

Table 1-2. Energies of x-ray emission lines (continued).

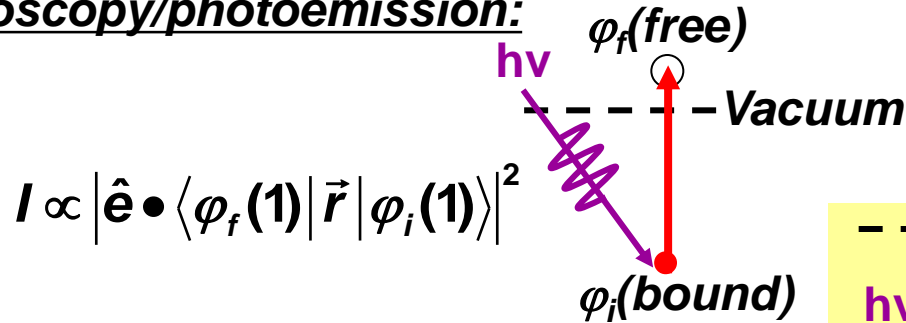
Element	Kα ₁	Kα ₂	Kβ ₁	Lα ₁	Lα ₂	Lβ ₁	Lβ ₂	Lγ ₁	Mα ₁
22 Ti	4,510.84	4,504.86	4,931.81	452.2	452.2	458.4			
23 V	4,952.20	4,944.64	5,427.29	511.3	511.3	519.2			
24 Cr	5,414.72	5,405.509	5,946.71	572.8	572.8	582.8			
25 Mn	5,898.75	5,887.65	6,490.45	637.4	637.4	648.8			
26 Fe	6,403.84	6,390.84	7,057.98	705.0	705.0	718.5			
27 Co	6,930.32	6,915.30	7,649.43	776.2	776.2	791.4			
28 Ni	7,478.15	7,460.89	8,264.66	851.5	851.5	868.8			
29 Cu	8,047.78	8,027.83	8,905.29	929.7	929.7	949.8			
30 Zn	8,638.86	8,615.78	9,572.0	1,011.7	1,011.7	1,034.7			

Diff. = 11.4

**See Tables 1.1
and 1.2 in X-Ray
Data Booklet**

MATRIX ELEMENTS IN The Soft and Hard X-Ray Spectroscopies: DIPOLE LIMIT

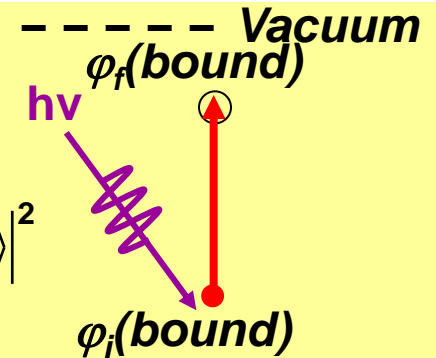
- Photoelectron spectroscopy/photoemission:



$$I \propto |\hat{\mathbf{e}} \cdot \langle \varphi_f(\mathbf{1}) | \vec{r} | \varphi_i(\mathbf{1}) \rangle|^2$$

- Near-edge x-ray absorption:

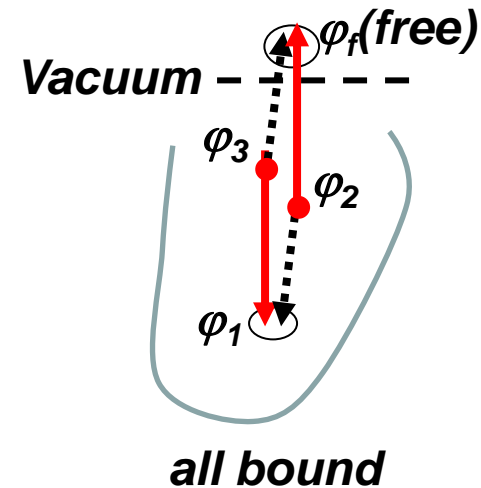
$$I \propto |\hat{\mathbf{e}} \cdot \langle \varphi_f(\mathbf{1}) | \vec{r} | \varphi_i(\mathbf{1}) \rangle|^2$$



- Auger electron emission:

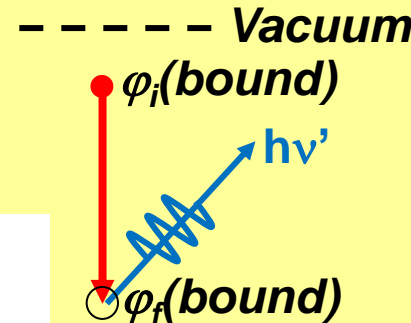
$$I \propto \left| \langle \varphi_f(\mathbf{1})\varphi_1(\mathbf{2}) | \frac{e^2}{r_{12}} | \varphi_3(\mathbf{1})\varphi_2(\mathbf{2}) \rangle - \langle \varphi_1(\mathbf{1})\varphi_f(\mathbf{2}) | \frac{e^2}{r_{12}} | \varphi_3(\mathbf{1})\varphi_2(\mathbf{2}) \rangle \right|^2$$

Direct Exchange



- X-ray emission:

$$I \propto |\hat{\mathbf{e}} \cdot \langle \varphi_f(\mathbf{1}) | \vec{r} | \varphi_i(\mathbf{1}) \rangle|^2$$



1.3 FLUORESCENCE YIELDS FOR K AND L SHELLS

Jeffrey B. Kortright

Fluorescence yields for the *K* and *L* shells for the elements $5 \leq Z \leq 110$ are plotted in Fig. 1-2; the data are based on Ref. 1. These yields represent the probability of a core hole in the *K* or *L* shells being filled by a radiative process, in competition with nonradiative processes. Auger processes are the only nonradiative processes competing with fluorescence for the *K* shell and

Fluorescence yield \equiv FY

FY = probability of radiative decay \rightarrow x-ray emission)

$1 - \text{FY} =$ probability of non-radiative decay \rightarrow Auger electron emission

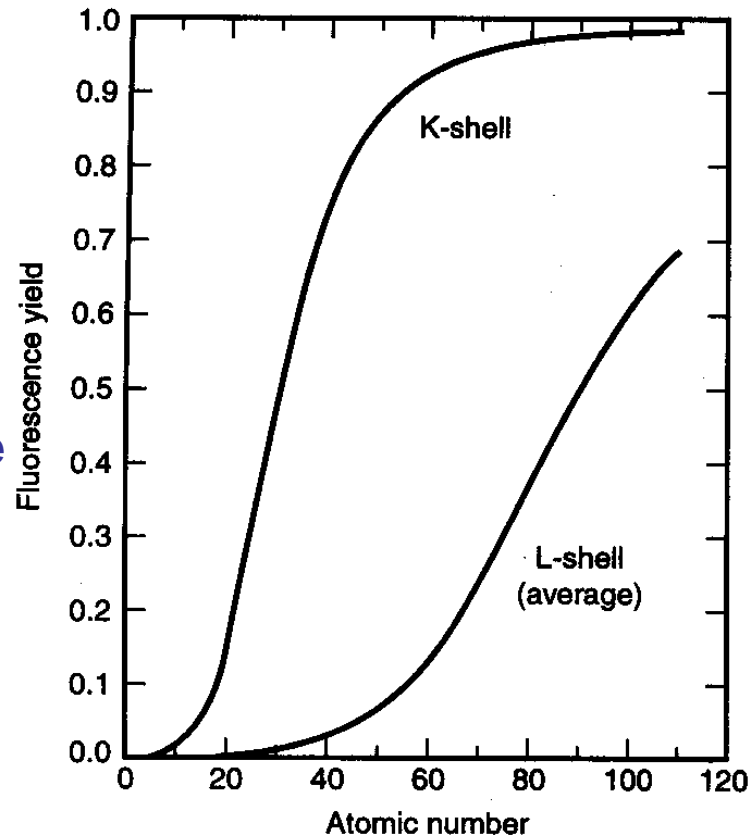
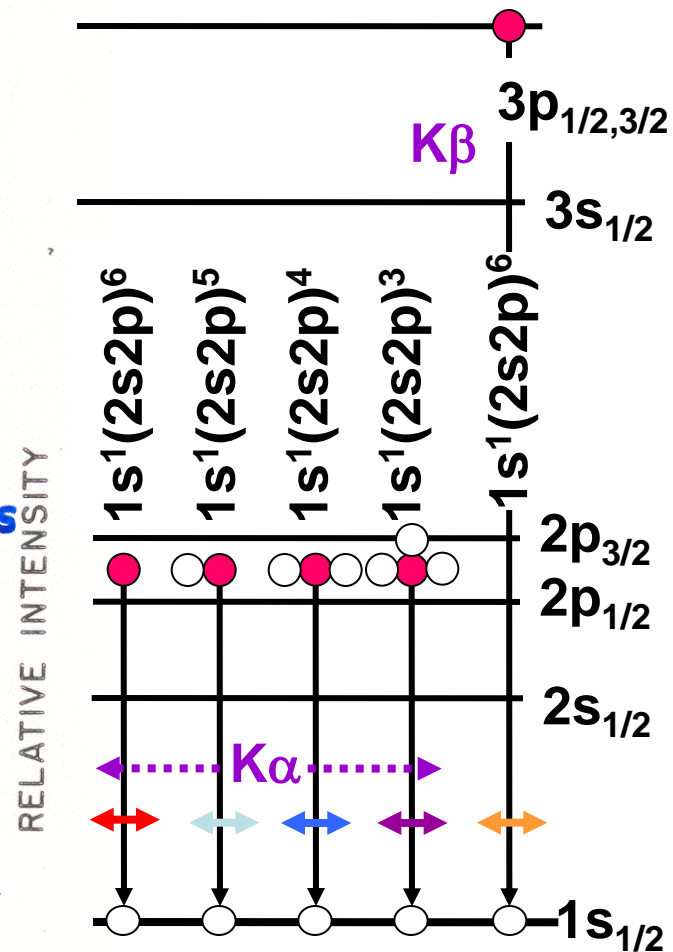
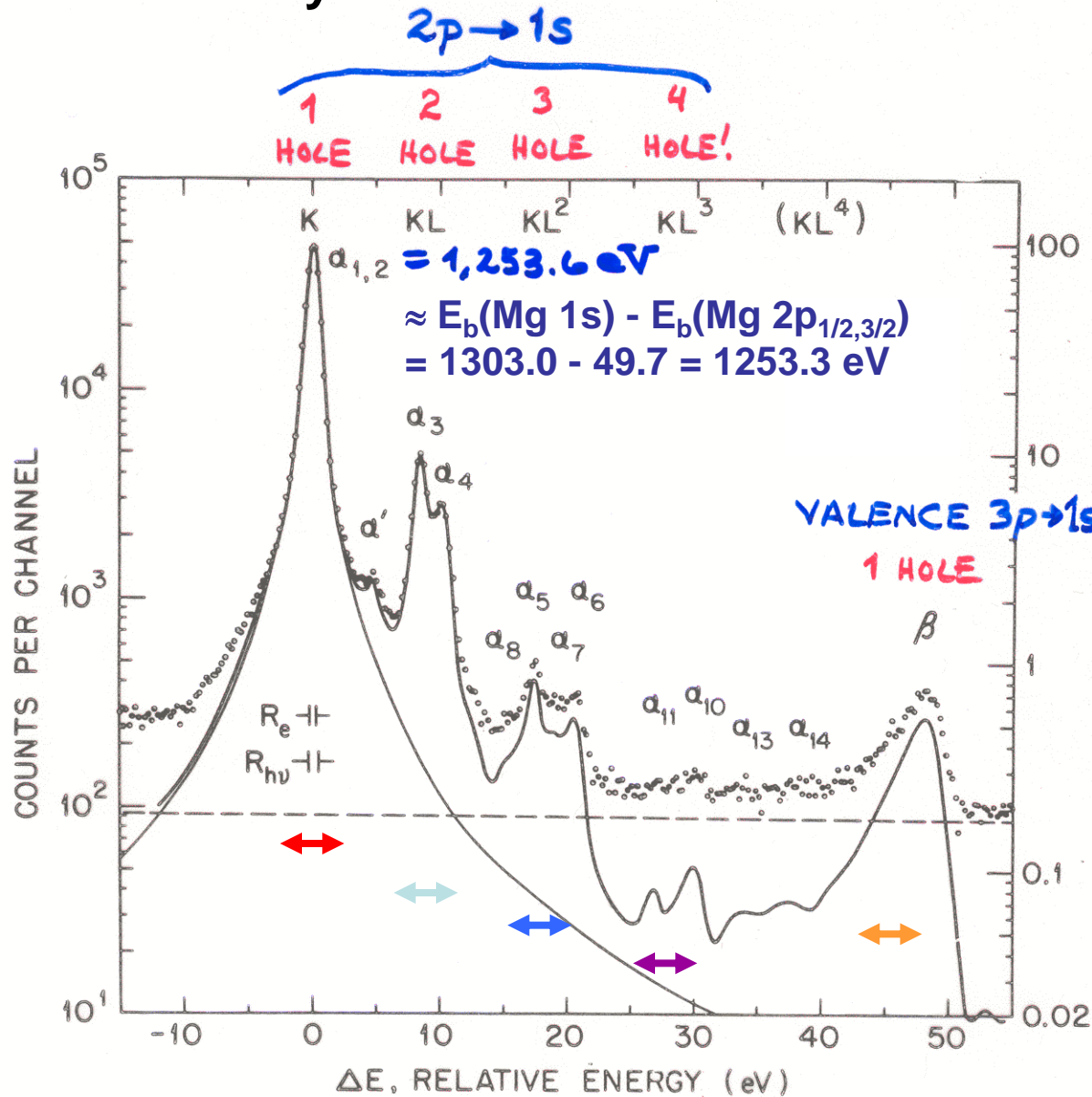


Fig. 1-2. Fluorescence yields for *K* and *L* shells for elements 5 to 110. The plotted curve for the *L* shell represents the average of *L*₁, *L*₂, and *L*₃ effective yields.

Many electron effects and satellites in x-ray emission



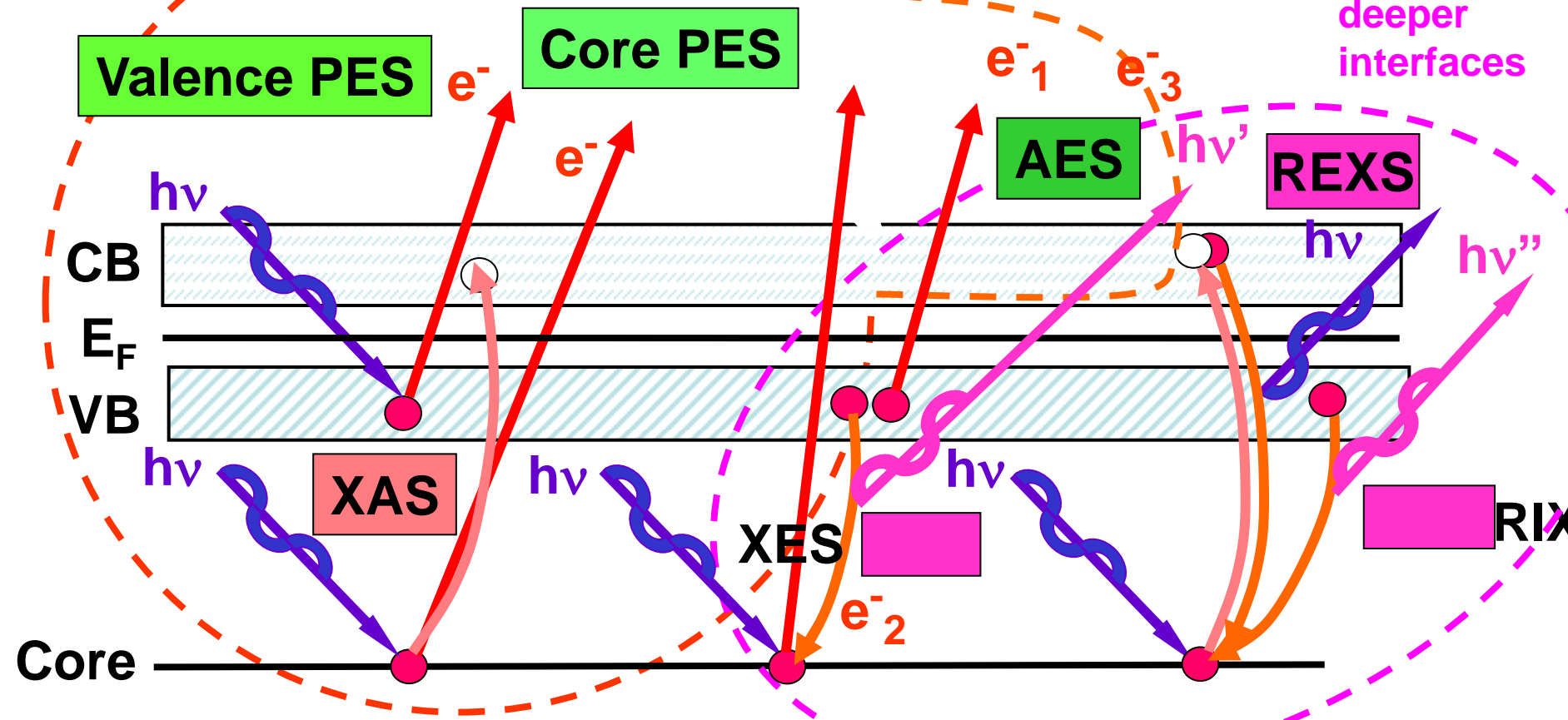
Mg K series of x-rays:
 atomic no. = 12
 Fluorescence Yield ≈ 0.03

A STANDARD LABORATORY X-RAY SOURCE

Electron-out:
surface
sensitive

The Soft and Hard X-Ray Spectroscopies

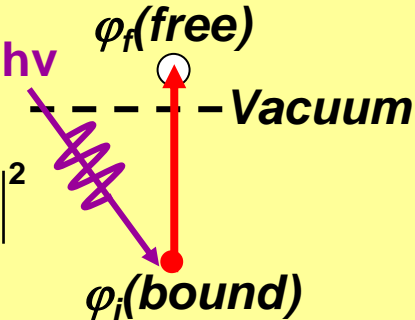
Photon-out:
"bulk",
deeper
interfaces



PES = photoemission = photoelectron spectroscopy
XAS = x-ray absorption spectroscopy
AES = Auger electron spectroscopy
XES = x-ray emission spectroscopy
REXS/RIXS = resonant elastic/inelastic x-ray scattering

MATRIX ELEMENTS IN The Soft and Hard X-Ray Spectroscopies: RESONANT EFFECTS

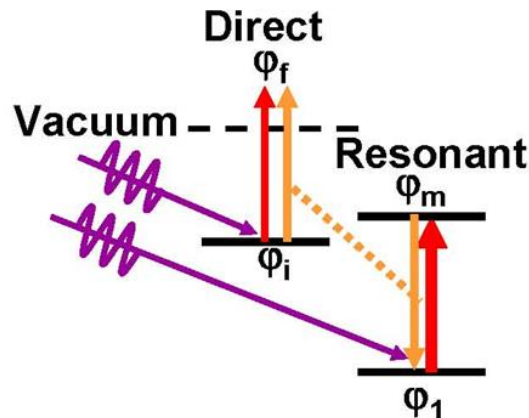
- **Non-resonant photoemission:**

$$I \propto \left| \hat{\mathbf{e}} \cdot \langle \varphi_f(\mathbf{1}) | \vec{r} | \varphi_i(\mathbf{1}) \rangle \right|^2$$


- **Resonant photoemission:**

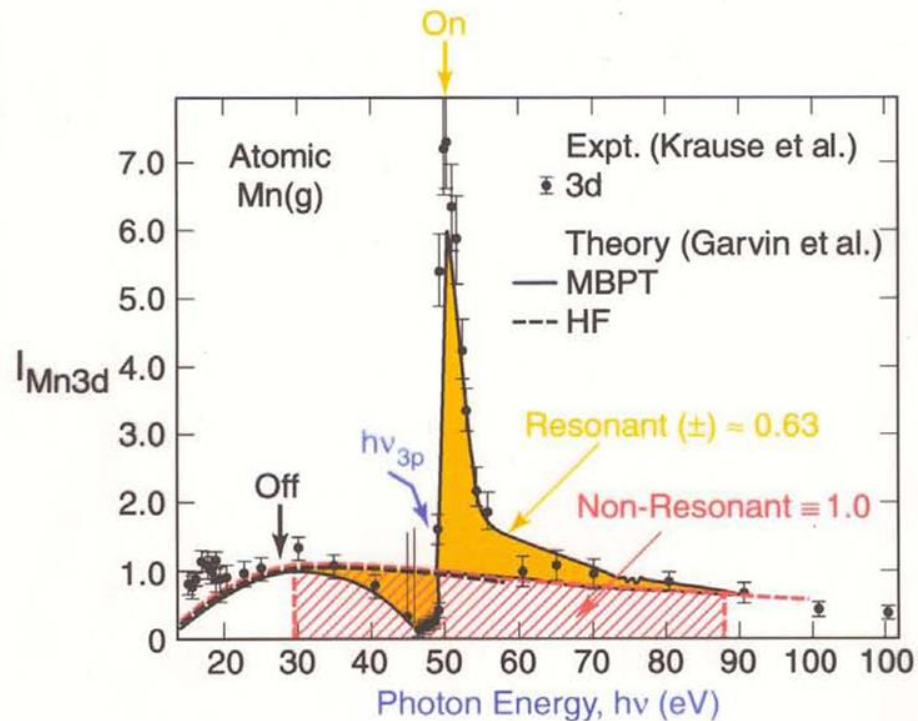
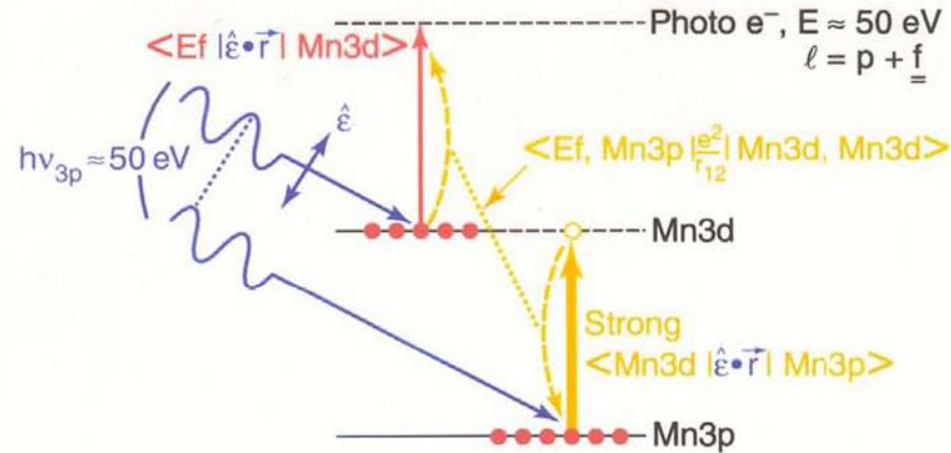
$$I \propto \left| \langle \varphi_f(\mathbf{1}) | \hat{\mathbf{e}} \cdot \vec{r} | \varphi_i(\mathbf{1}) \rangle + \sum_m \langle \varphi_f(\mathbf{1}) \varphi_1(\mathbf{2}) | \frac{e^2}{r_{12}} | \varphi_i(\mathbf{1}) \varphi_m(\mathbf{2}) \rangle \langle \varphi_m(\mathbf{1}) | \hat{\mathbf{e}} \cdot \vec{r} | \varphi_1(\mathbf{1}) \rangle \right|^2$$

$$\times \delta(h\nu - (E_m - E_1))$$



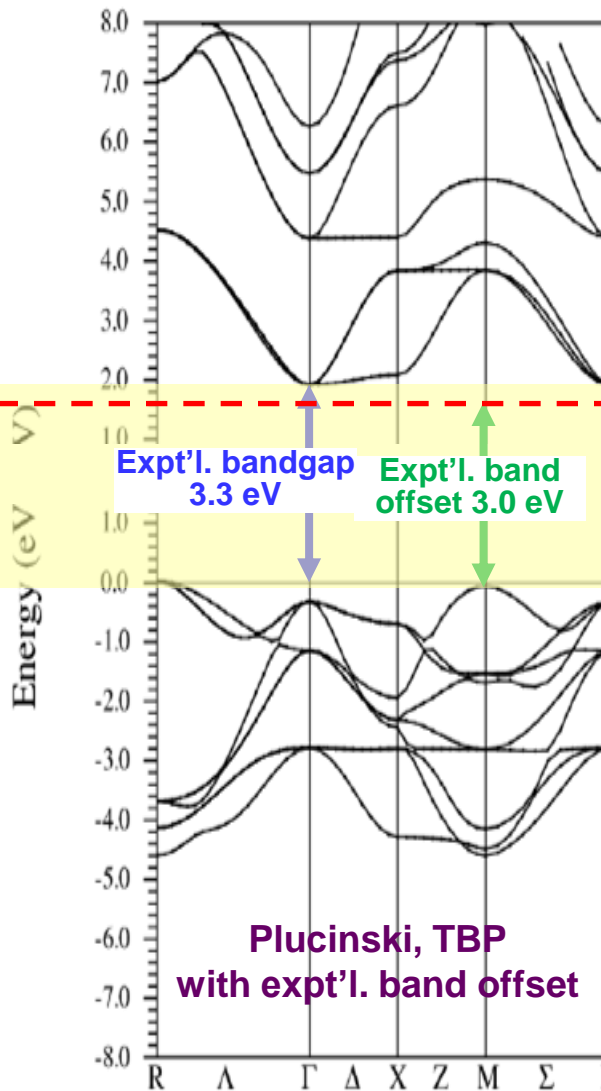
Single-atom resonant photoemission:

Ex. – Mn atom: Mn3d emission, resonance with Mn3p

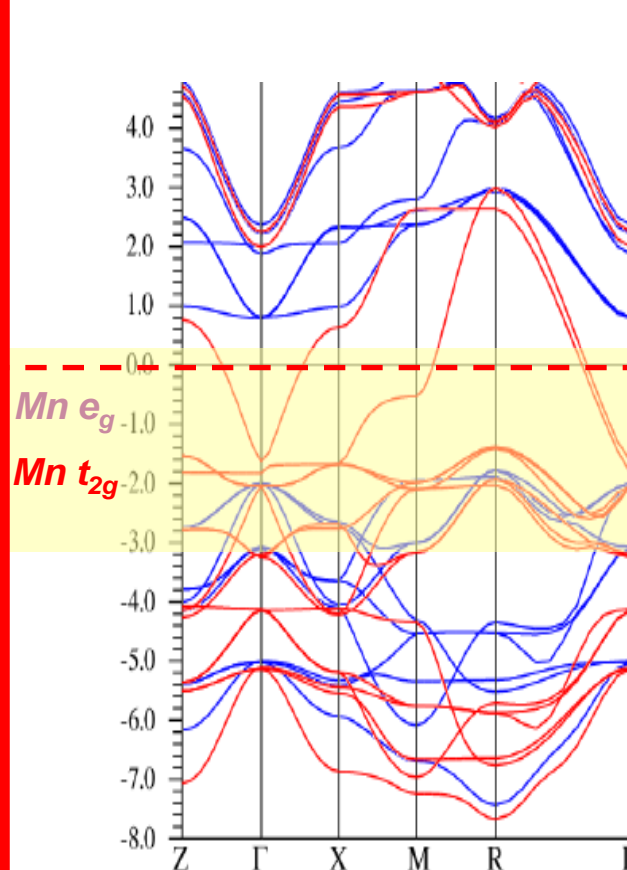


SrTiO₃ and La_{0.67}Sr_{0.33}MnO₃ band structures and DOS

SrTiO₃-band insulator



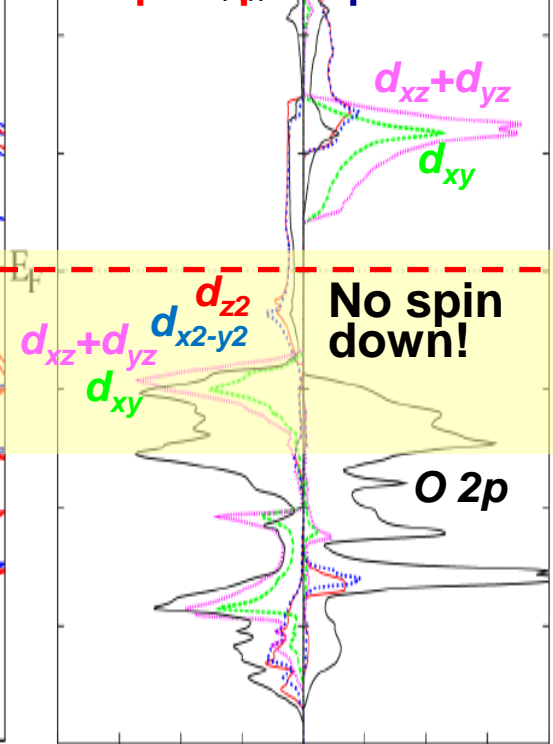
La_{0.67}Sr_{0.33}MnO₃- Half-Metallic Ferromagnet



Chikamatsu et al.,
PRB **73**, 195105 (2006);
Plucinski, TBP

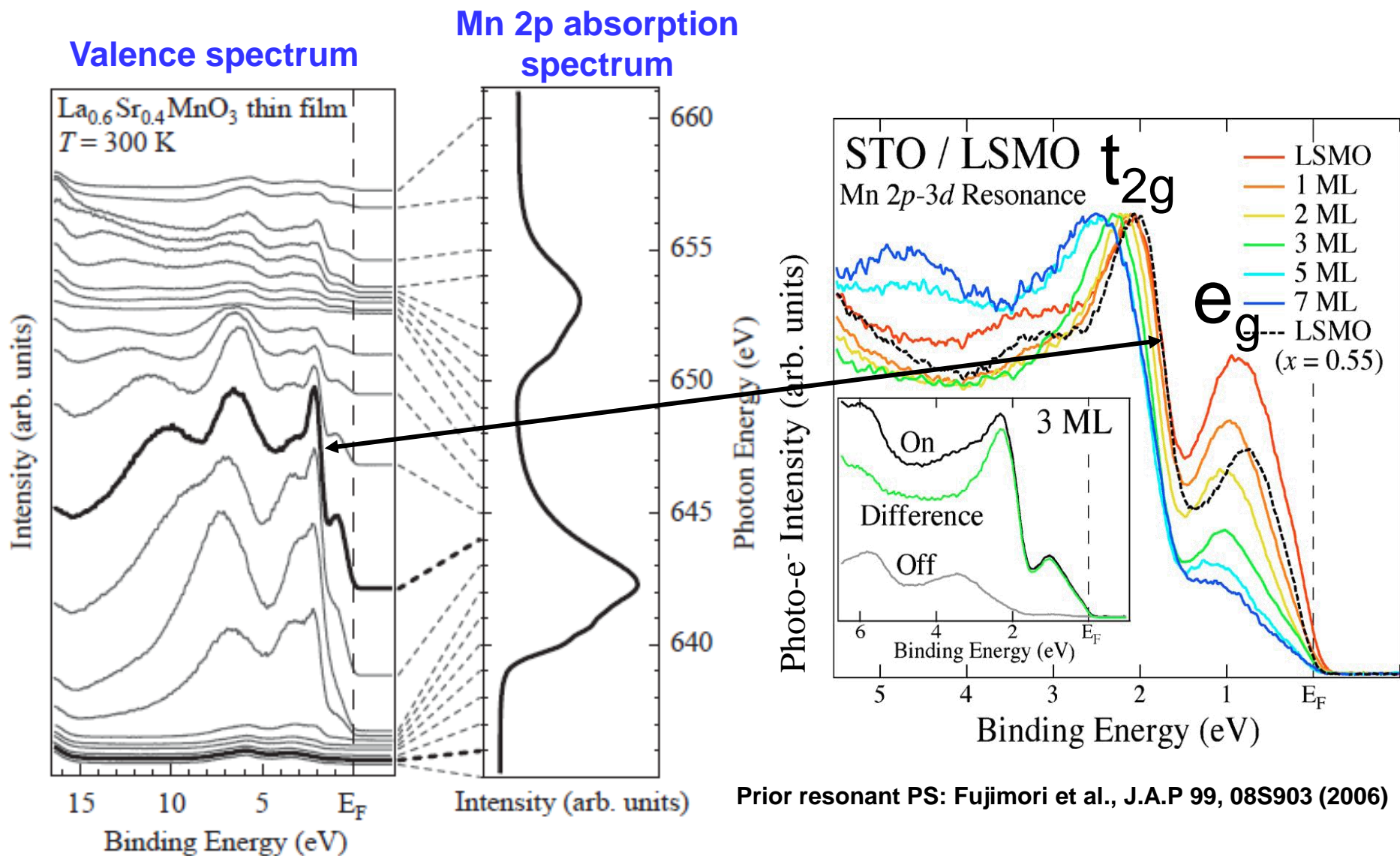
Projected DOSs

Spin-up Spin-down



Zheng, Binggeli, J. Phys. Cond. Matt. **21**, 115602 (2009)
Plucinski, TBP

Resonant Photoemission— $\text{La}_{0.6}\text{Sr}_{0.4}\text{MnO}_3$, Mn 3d with Mn 2p

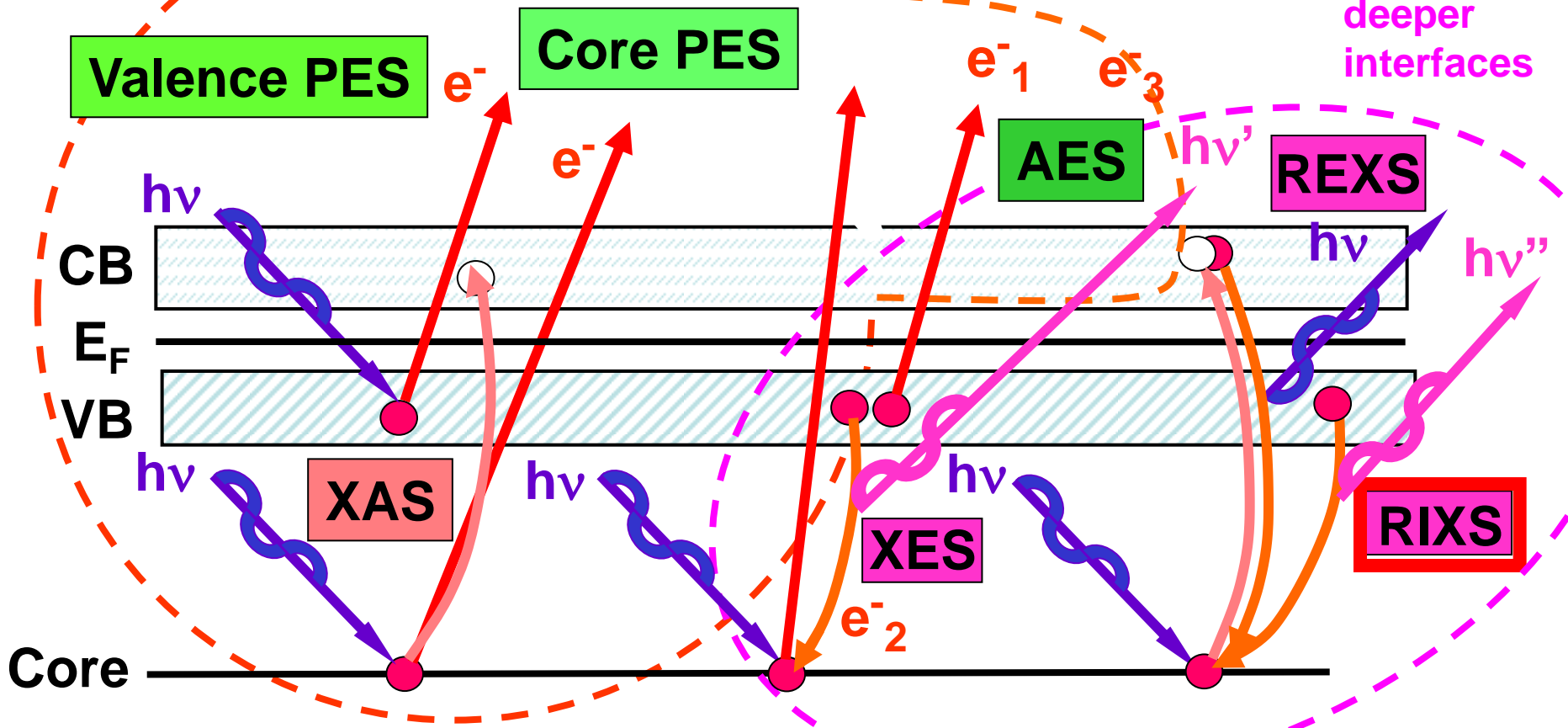


K. Horiba et al. / Journal of Magnetism and Magnetic Materials 272–276 (2004) 436–437

Electron-out:
surface
sensitive

The Soft and Hard X-Ray Spectroscopies

Photon-out:
"bulk",
deeper
interfaces

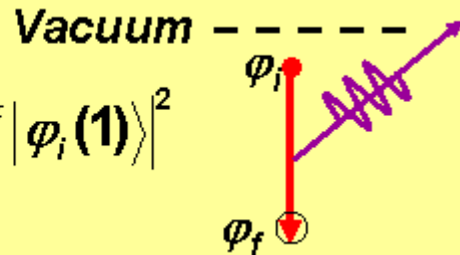


PES = photoemission = photoelectron spectroscopy
XAS = x-ray absorption spectroscopy
AES = Auger electron spectroscopy
XES = x-ray emission spectroscopy
REXS/RIXS = resonant elastic/inelastic x-ray scattering

MATRIX ELEMENTS IN The Soft and Hard X-Ray Spectroscopies: RESONANT EFFECTS

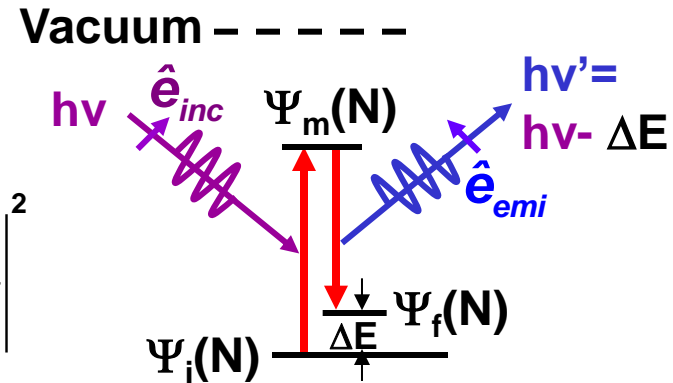
- X-ray emission:

$$I \propto |\hat{\mathbf{e}} \cdot \langle \varphi_f(\mathbf{1}) | \vec{r} | \varphi_i(\mathbf{1}) \rangle|^2$$



- Resonant inelastic x-ray scattering--The Kramers-Heisenberg Equation:

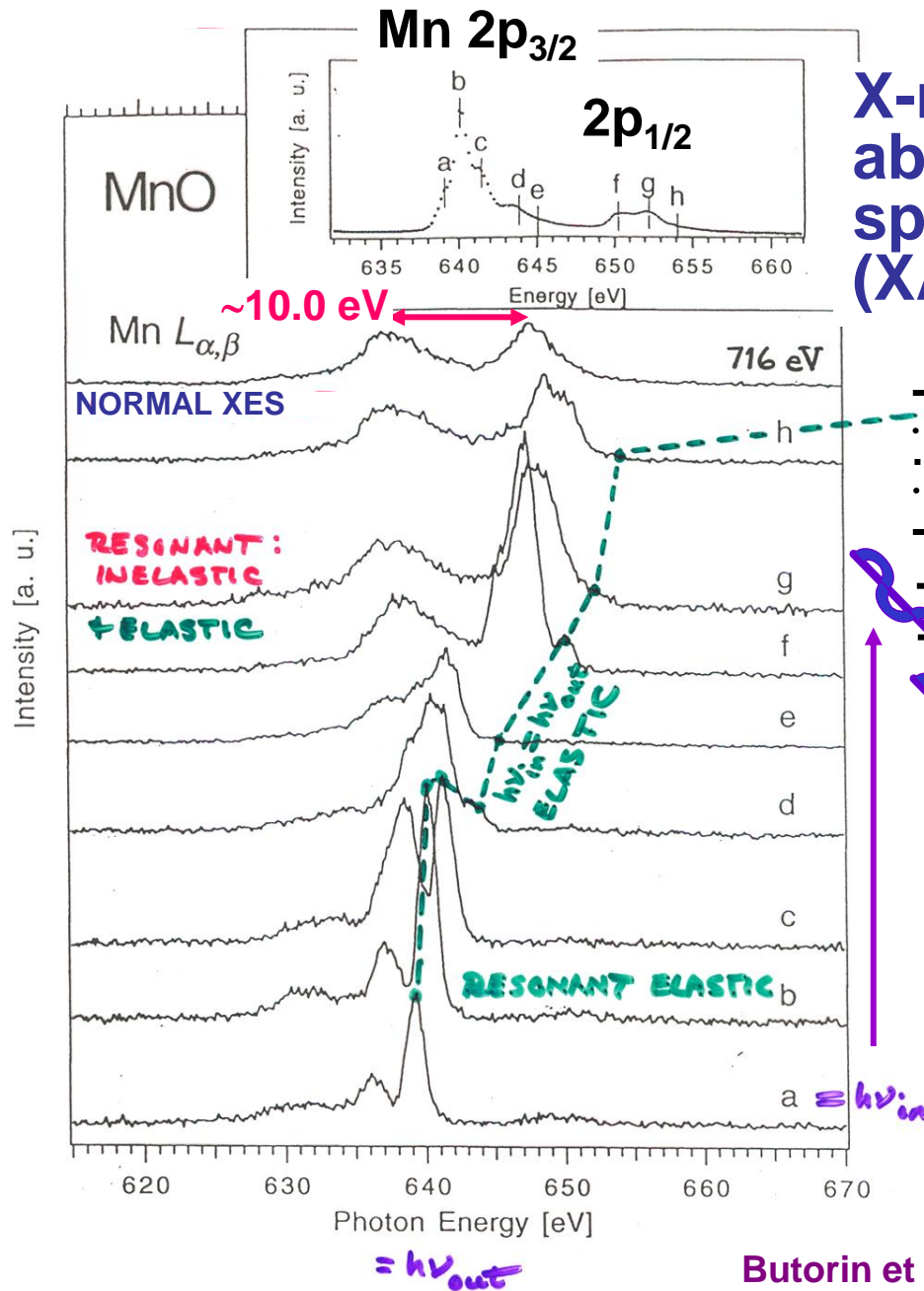
$$I \propto \sum_f \left| \sum_m \frac{\langle \Psi_f(N) | \hat{\mathbf{e}}_{emi} \cdot \vec{r} | \Psi_m(N) \rangle \langle \Psi_m(N) | \hat{\mathbf{e}}_{inc} \cdot \vec{r} | \Psi_i(N) \rangle}{h\nu + E_i(N) - E_m(N) - i\Gamma_m} \right|^2 \times \delta(h\nu - (E_m(N) - E_i(N)))$$



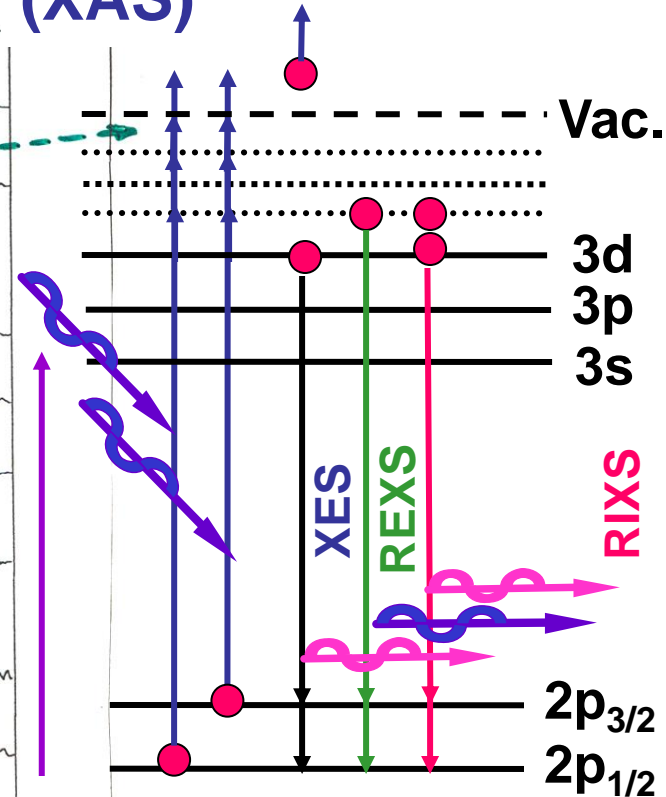
$$N_m(t) = N_m(0) e^{-\frac{2\Gamma_m t}{\hbar}} = N_m(0) e^{-\frac{t}{T_{lifetime}}}$$

X-ray fluorescence spectroscopy
 = X-ray emission spectroscopy (XES)
 and Resonant inelastic x-ray scattering (RIXS)

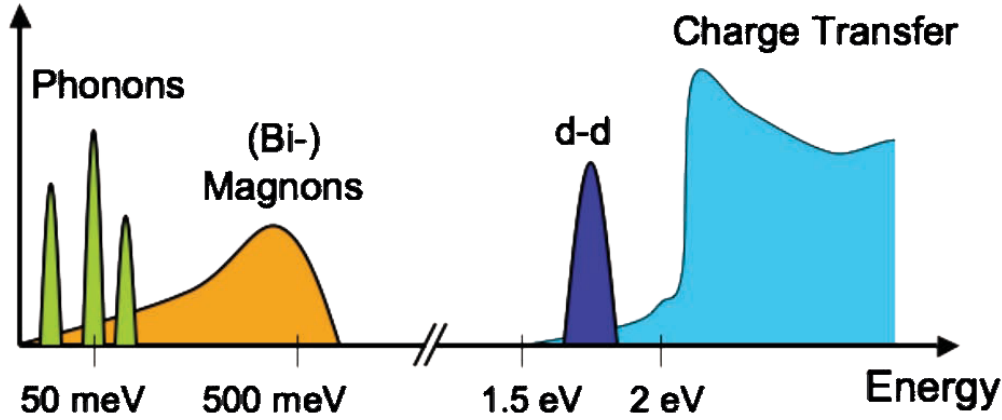
inelastic x-ray scattering (RIXS)
 and Resonant elastic x-ray scattering (REXS)



X-ray absorption spectroscopy (XAS)

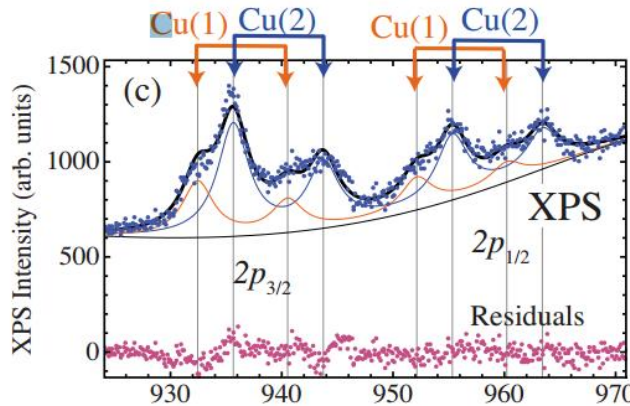
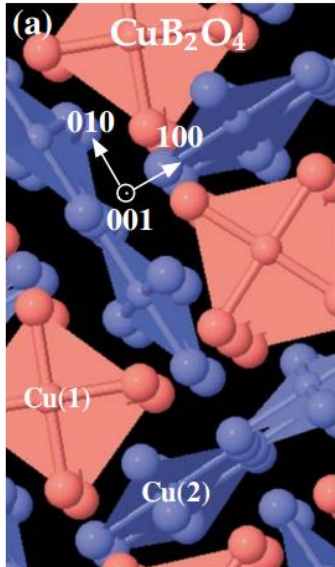


Excitations probed by RIXS

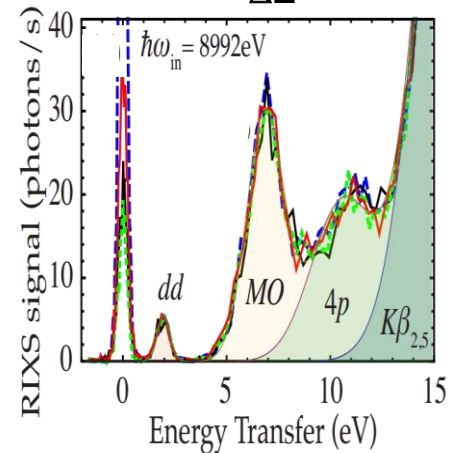
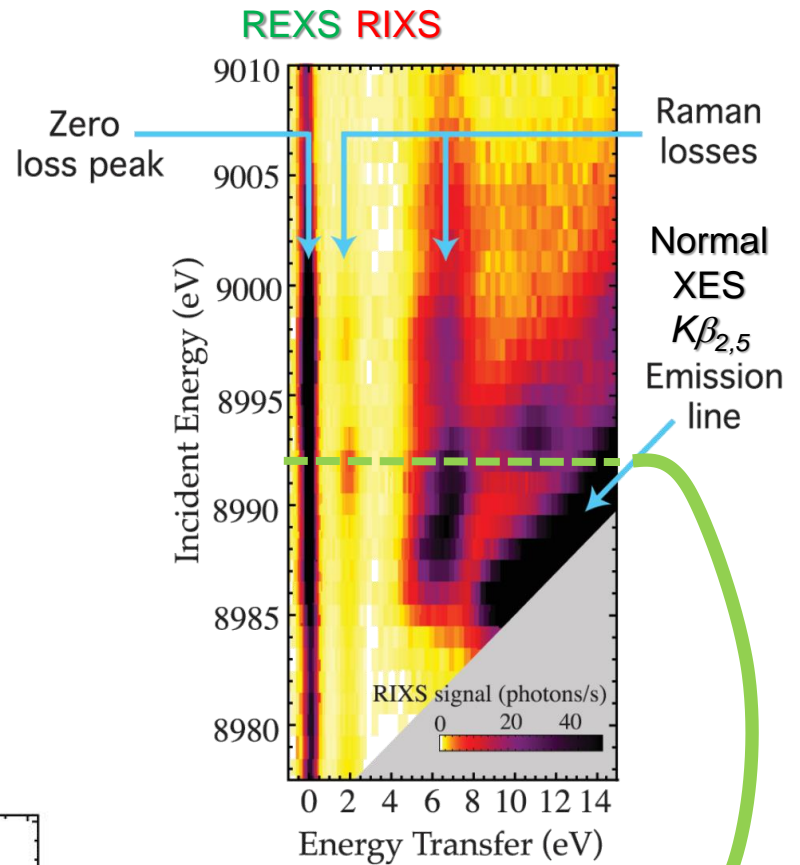


Aments et al., Rev. Mod. Phys.
83, 705 (2011)

Example: CuB_2O_4 plaquettes



Hancock et al., Phys. Rev. B 80,
092509 (2009)



The Soft and Hard X-Ray Spectroscopies

EXAFS
Atomic structure

XAS
unoccupied DOS
(2° e- and hν Detection)

Valence PES -
band struct.,
quasipart. exc.,
DOS, spin pol.

Core PES -
stoichiometry
BE shifts
splittings, MCD
spin polarization
diffraction

XES, RIXS -
band structure,
partial DOS,
d-d/other
excitations

Deeper

"Bulk"

Surface/near surface

XES → "Bulk"

Valence PES

Core PE

CB

E_F

VB

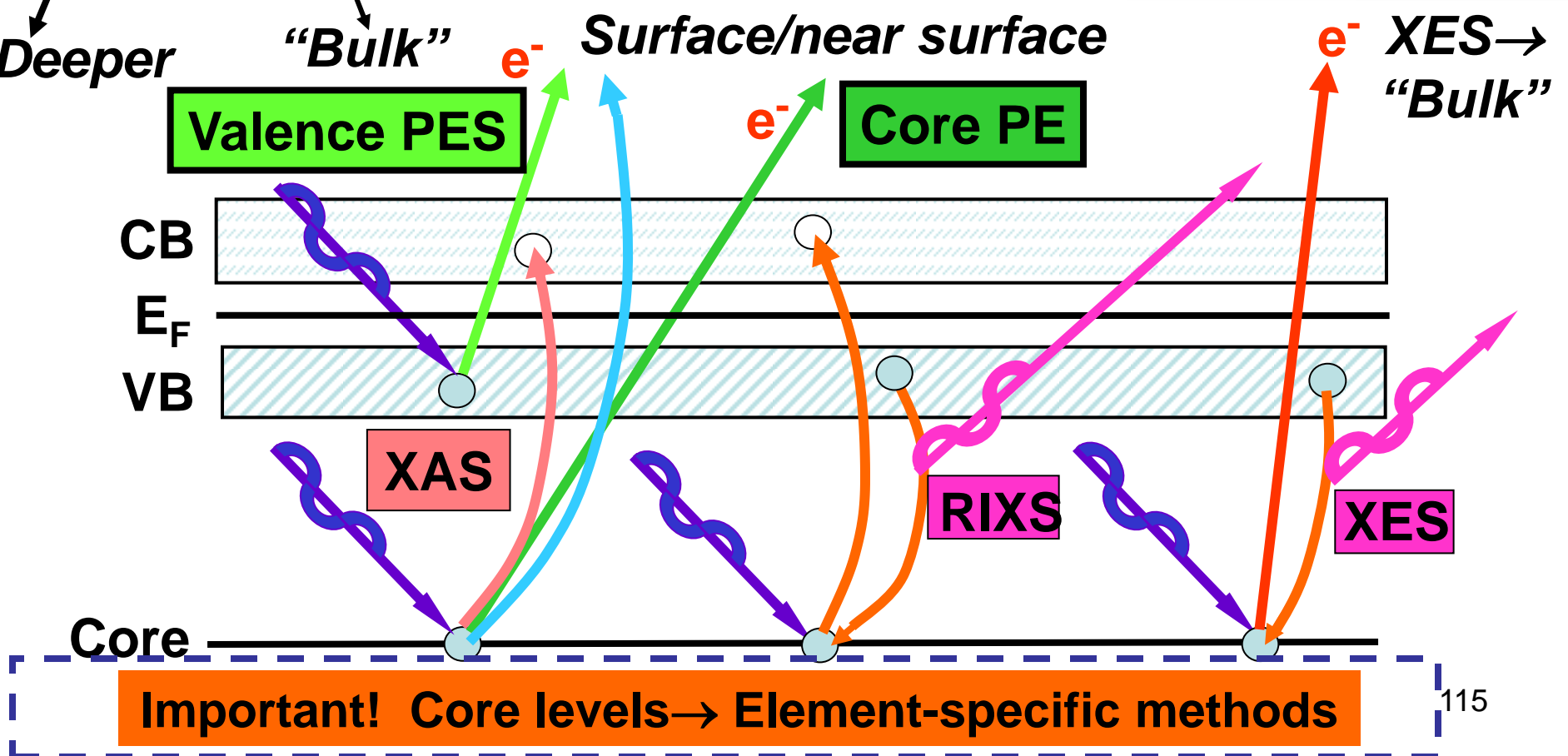
XAS

RIXS

XES

Core

Important! Core levels → Element-specific methods



INTENSITIES IN PHOTOELECTRON SPECTRA:

- GENERAL: FINAL STATE κ (κ -SUBSHELL + ALL OTHER DESIG.)

$$\text{INT.}_{\kappa} \propto |\hat{\epsilon} \cdot \langle \Psi_{\text{tot}}^{\kappa}(N, \kappa) | \sum_{i=1}^N \vec{r}_i | \Psi_{\text{tot}}^i(N) \rangle|^2 \quad (\text{DIPOLE APPROX.})$$

INTENSITIES IN PHOTOELECTRON SPECTRA:

- GENERAL: FINAL STATE K (k -SUBSHELL + ALL OTHER DESIG.)

$$\text{INT.}_K \propto |\hat{e} \cdot \langle \Psi_{\text{tot}}^f(N, K) | \sum_{i=1}^N \vec{r}_i | \Psi_{\text{tot}}^i(N) \rangle|^2 \quad (\text{DIPOLE APPROX.})$$

- BORN-OPPENHEIMER: e^- 's FAST, VIBRATIONS SLOW

$$\text{INT.}_K \propto \underbrace{|\langle \Psi_{\text{vib}, \nu}^f | \Psi_{\text{vib}, \nu}^i \rangle|^2}_{\text{FRANCK-CONDON FACTOR}} |\hat{e} \cdot \langle \Psi_{e^-}^f(N, K) | \sum_{i=1}^N \vec{r}_i | \Psi_{e^-}^i(N) \rangle|^2$$

INTENSITIES IN PHOTOELECTRON SPECTRA:

- GENERAL: FINAL STATE k (k -SUBSHELL + ALL OTHER DESIG.)

$$\text{INT.}_k \propto |\hat{e} \cdot \langle \Psi_{\text{tot}}^f(N, k) | \sum_{i=1}^N \vec{r}_i | \Psi_{\text{tot}}^i(N) \rangle|^2 \quad (\text{DIPOLE APPROX.})$$

- BORN-OPENHEIMER: e^- 's FAST, VIBRATIONS SLOW

$$\text{INT.}_k \propto \underbrace{|\langle \Psi_{\text{vib}, \nu}^f | \Psi_{\text{vib}, \nu}^i \rangle|^2}_{\text{FRANCK-CONDON FACTOR}} |\hat{e} \cdot \langle \Psi_e^f(N, k) | \sum_{i=1}^N \vec{r}_i | \Psi_e^i(N) \rangle|^2$$

- SUDDEN APPROXIMATION: $\Psi_k \rightarrow \Psi_f \approx \text{PHOTO}^-$ (FAST)



$$\text{INT.}_k \propto |\langle \Psi_{\text{vib}, \nu}^f | \Psi_{\text{vib}, \nu}^i \rangle|^2 \underbrace{|\langle \Psi_e^f(N-1, k) | \Psi_e^i(N-1, k) \rangle|^2}_{k \text{ MISSING}}$$

$$|\hat{e} \cdot \langle \varphi_f | \vec{r} | \varphi_k \rangle|^2 \quad \text{SAME SUBSHELL COUPLING + TOTAL L, S} \rightarrow \text{"MONOPOLE"}$$

$\hookrightarrow \text{NORMAL } \frac{dG_k}{d\Omega}$

INTENSITIES IN PHOTOELECTRON SPECTRA:

- GENERAL: FINAL STATE κ (κ -SUBSHELL + ALL OTHER DESIG.)

$$\text{INT. } \kappa \propto |\hat{e} \cdot \langle \Psi_{\text{tot}}^f(N, \kappa) | \sum_{i=1}^N \vec{r}_i | \Psi_{\text{tot}}^i(N) \rangle|^2 \quad (\text{DIPOLE APPROX.})$$

- BORN-OPPENHEIMER: e^- 'S FAST, VIBRATIONS SLOW

$$\text{INT. } \kappa \propto \underbrace{|\langle \Psi_{\text{vib}, \nu}^f | \Psi_{\text{vib}, \nu}^i \rangle|^2}_{\text{FRANCK-CONDON FACTOR}} |\hat{e} \cdot \langle \Psi_e^f(N, \kappa) | \sum_{i=1}^N \vec{r}_i | \Psi_e^i(N) \rangle|^2$$

- SUDDEN APPROXIMATION: $\Psi_{\kappa} \rightarrow \Psi_f \approx \text{PHOTO}e^-$ (FAST)



$$\text{INT. } \kappa \propto |\langle \Psi_{\text{vib}, \nu}^f | \Psi_{\text{vib}, \nu}^i \rangle|^2 \underbrace{|\langle \Psi_e^f(N-1, \kappa) | \Psi_e^i(N-1, \kappa) \rangle|^2}_{k \text{ MISSING}}$$

$$|\hat{e} \cdot \langle \varphi_f | \vec{r} | \varphi_{\kappa} \rangle|^2 \quad \text{SAME SUBSHELL COUPLING + TOTAL L, S} \rightarrow \text{"MONOPOLE"}$$

$\hookrightarrow \text{NORMAL } \frac{d\sigma_{\kappa}}{d\Omega}$

- SLATER DETS. FOR $\Psi_e^f = \det(\varphi_1', \varphi_2', \dots, \varphi_{k-1}', \varphi_{k+1}', \dots, \varphi_N')$

$$\Psi_e^i = \det(\varphi_1, \varphi_2, \dots, \varphi_{k-1}, \varphi_{k+1}, \dots, \varphi_N)$$

$$\text{INT. } \kappa \propto |\langle \Psi_{\text{vib}, \nu}^f | \Psi_{\text{vib}, \nu}^i \rangle|^2 \underbrace{|\langle \varphi_1' | \varphi_1 \rangle|^2 |\langle \varphi_2' | \varphi_2 \rangle|^2 \dots}_{\text{SHAKE-UP/SHAKE-OFF}} \dots$$

$$|\langle \varphi_{k-1}' | \varphi_{k-1} \rangle|^2 |\langle \varphi_{k+1}' | \varphi_{k+1} \rangle|^2 \dots |\langle \varphi_N' | \varphi_N \rangle|^2$$

$$|\hat{e} \cdot \langle \varphi_f | \vec{r} | \varphi_{\kappa} \rangle|^2$$

1e- DIPOLE $\rightarrow d\sigma/d\Omega$

(N-1)e- SHAKE-UP/
SHAKE-OFF \rightarrow
"MONOPOLE"

INTENSITIES IN PHOTOELECTRON SPECTRA:

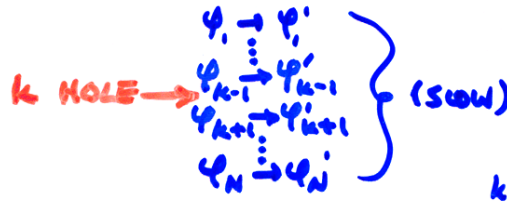
- GENERAL: FINAL STATE κ (κ -SUBSHELL + ALL OTHER DESIG.)

$$\text{INT.}_{\kappa} \propto |\hat{e} \cdot \langle \Psi_{\text{tot}}^f(N, \kappa) | \sum_{i=1}^N \vec{r}_i | \Psi_{\text{tot}}^i(N) \rangle|^2 \quad (\text{DIPOLE APPROX.})$$

- BORN-OPPENHEIMER: e^- 's FAST, VIBRATIONS SLOW

$$\text{INT.}_{\kappa} \propto \underbrace{|\langle \Psi_{\text{vib}, \nu}^f | \Psi_{\text{vib}, \nu}^i \rangle|^2}_{\text{FRANCK-CONDON FACTOR}} |\hat{e} \cdot \langle \Psi_e^f(N, \kappa) | \sum_{i=1}^N \vec{r}_i | \Psi_e^i(N) \rangle|^2$$

- SUDDEN APPROXIMATION: $\Psi_{\kappa} \rightarrow \Psi_f \approx \text{PHOTO}e^-$ (FAST)



$$\text{INT.}_{\kappa} \propto |\langle \Psi_{\text{vib}, \nu}^f | \Psi_{\text{vib}, \nu}^i \rangle|^2 |\langle \Psi_e^f(N-1, \kappa) | \Psi_e^i(N-1, \kappa) \rangle|^2$$

$$|\hat{e} \cdot \langle \varphi_f | \vec{r} | \varphi_{\kappa} \rangle|^2 \quad \text{SAME SUBSHELL COUPLING + TOTAL L, S} \rightarrow \text{"MONOPOLE"}$$

\hookrightarrow NORMAL $\frac{d\sigma_{\kappa}}{d\Omega}$

- SLATER DETS. FOR $\Psi_e^f = \det(\varphi'_1, \varphi'_2, \dots, \varphi'_{k-1}, \varphi'_{k+1}, \dots, \varphi'_N)$

$$\Psi_e^i = \det(\varphi_1, \varphi_2, \dots, \varphi_{k-1}, \varphi_{k+1}, \dots, \varphi_N)$$

$$\text{INT.}_{\kappa} \propto |\langle \Psi_{\text{vib}, \nu}^f | \Psi_{\text{vib}, \nu}^i \rangle|^2 |\langle \varphi'_1 | \varphi_1 \rangle|^2 |\langle \varphi'_2 | \varphi_2 \rangle|^2 \dots$$

$$|\langle \varphi'_{k-1} | \varphi_{k-1} \rangle|^2 |\langle \varphi'_{k+1} | \varphi_{k+1} \rangle|^2 \dots |\langle \varphi'_N | \varphi_N \rangle|^2$$

$$|\hat{e} \cdot \langle \varphi_f | \vec{r} | \varphi_{\kappa} \rangle|^2$$

1e- DIPOLE $\rightarrow d\sigma/d\Omega$

**(N-1)e- SHAKE-UP/
SHAKE-OFF \rightarrow
"MONOPOLE"**

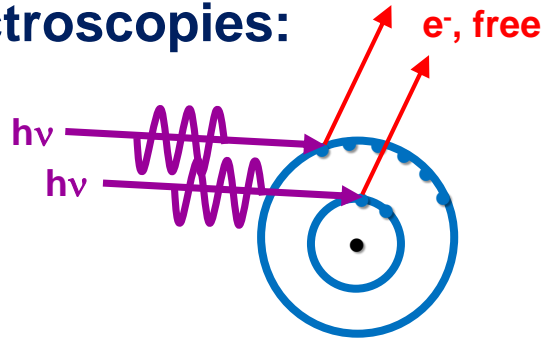
"Basic Concepts of XPS"
Section 3.D.

- PLUS DIFFRACTION EFFECTS IN φ_f ESCAPE: PD or EXAFS

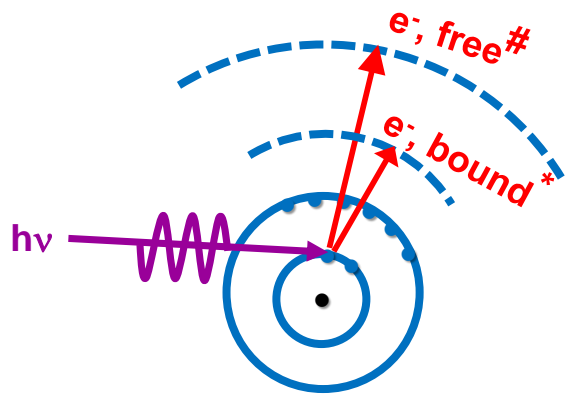
Section 6.D.

The vacuum ultraviolet, soft x-ray, hard x-ray measurements:

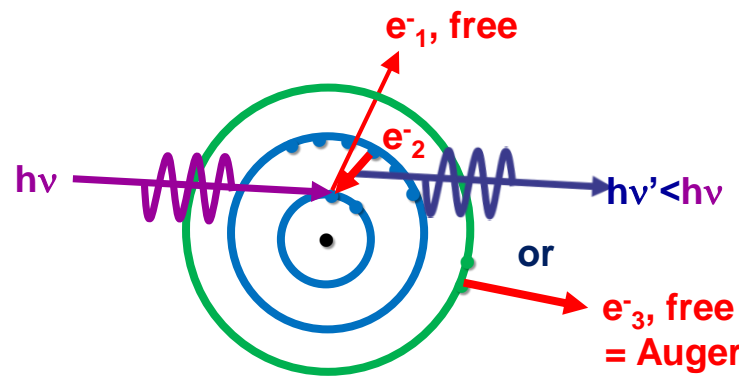
The spectroscopies:



PHOTOELECTRON SPECTROSCOPY=
PHOTOEMISSION – PS, PES, UPS, XPS
+ **DIFFRACTION-XPD, PhD**
+ HOLOGRAPHY-PH
+ MICROSCOPY-PEEM



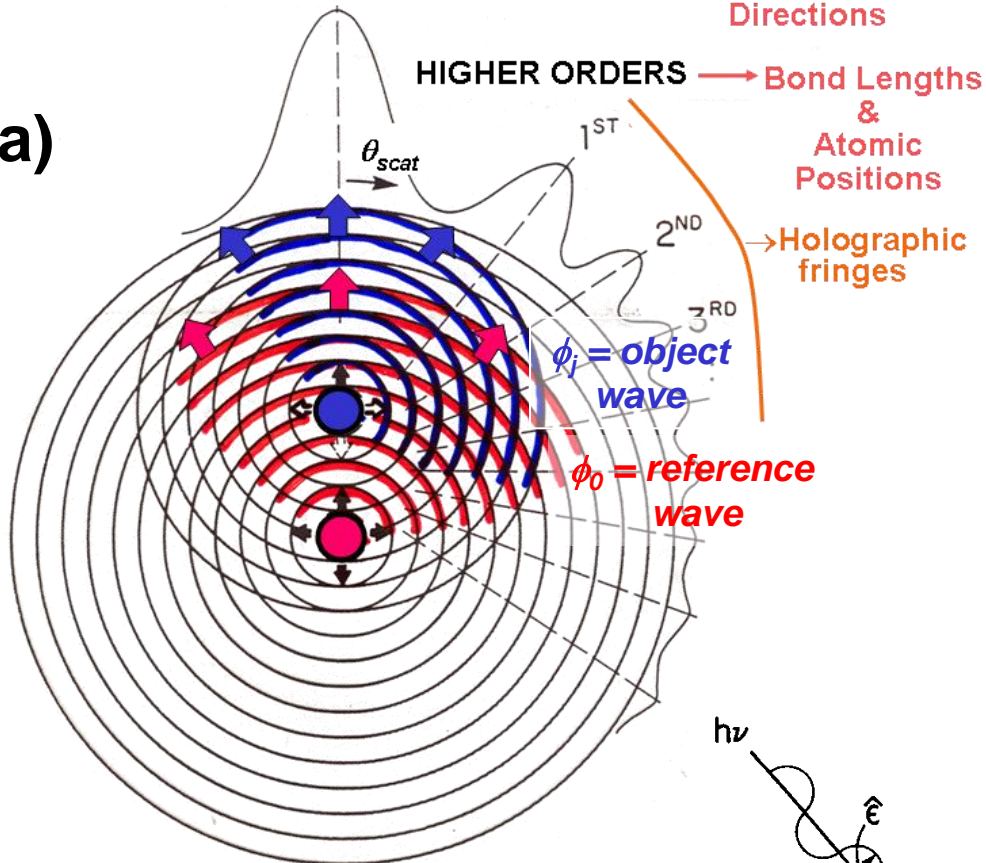
X-RAY ABSORPTION SPECTROSCOPY- XAS
* NEAR-EDGE – NEXAFS, XANES
+ X-RAY MAGNETIC CIRCULAR/LINEAR
DICHROISM- XMCD, XMLD
EXTENDED- EXAFS, XAFS



X-RAY EMISSION (FLUORESCENCE)
SPECTROSCOPY
+ AUGER ELECTRON SPECTROSCOPY
(Always accompanies photoelectron emission)

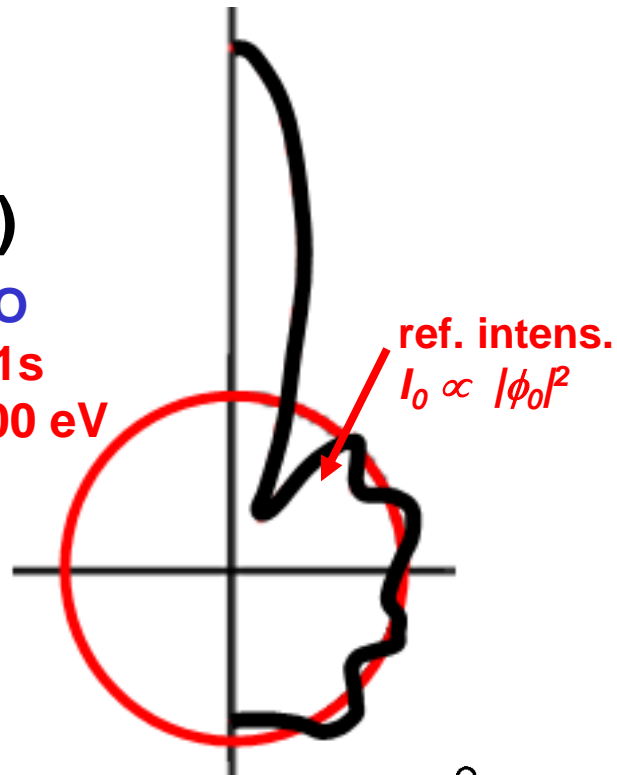
FORWARD SCATT. = "0TH ORDER" → Bond & Low-index Directions

(a)

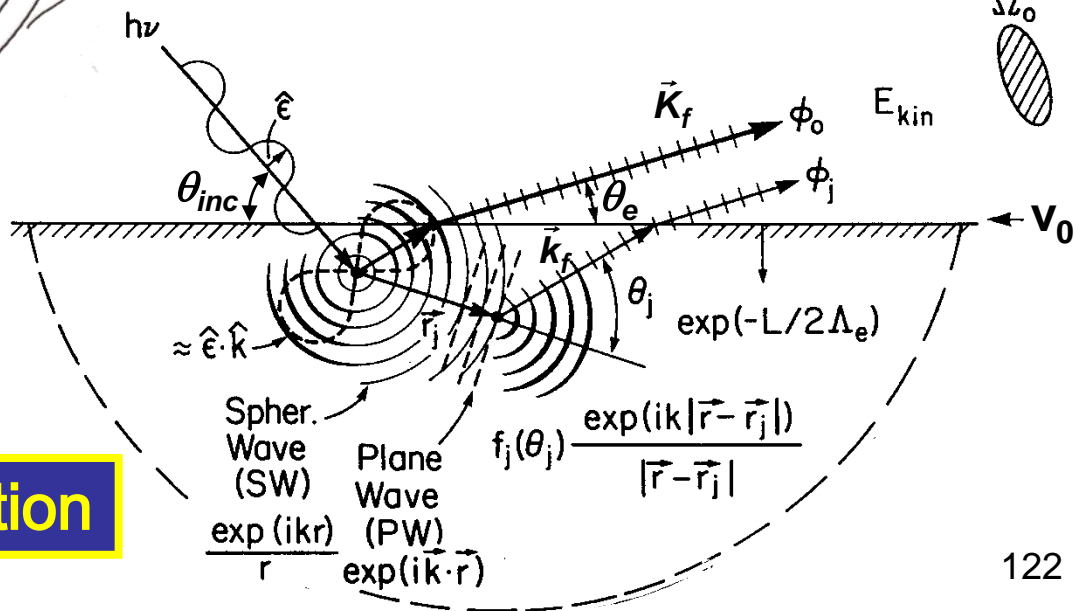


(b)

CO
C1s
500 eV



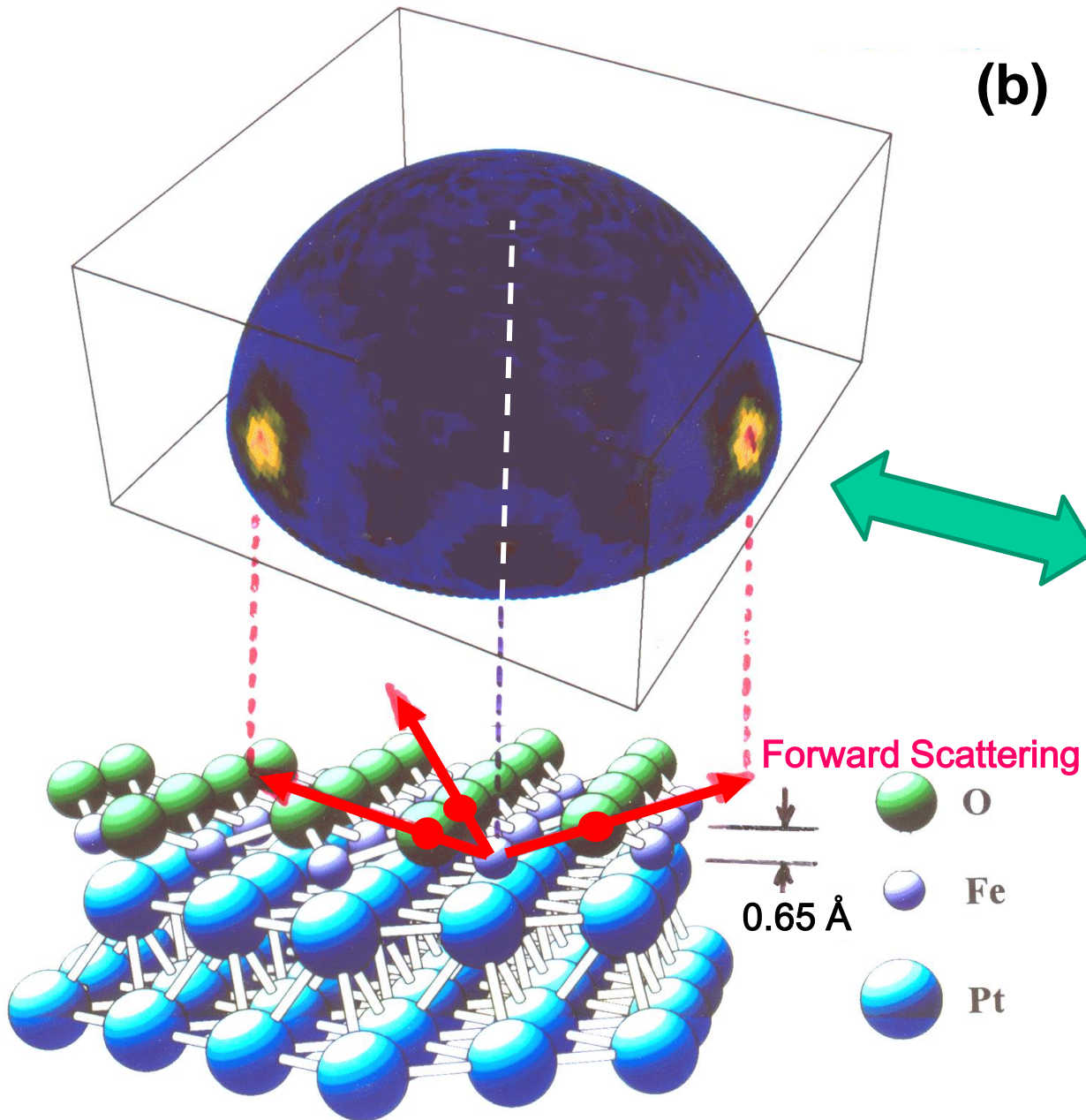
(c)



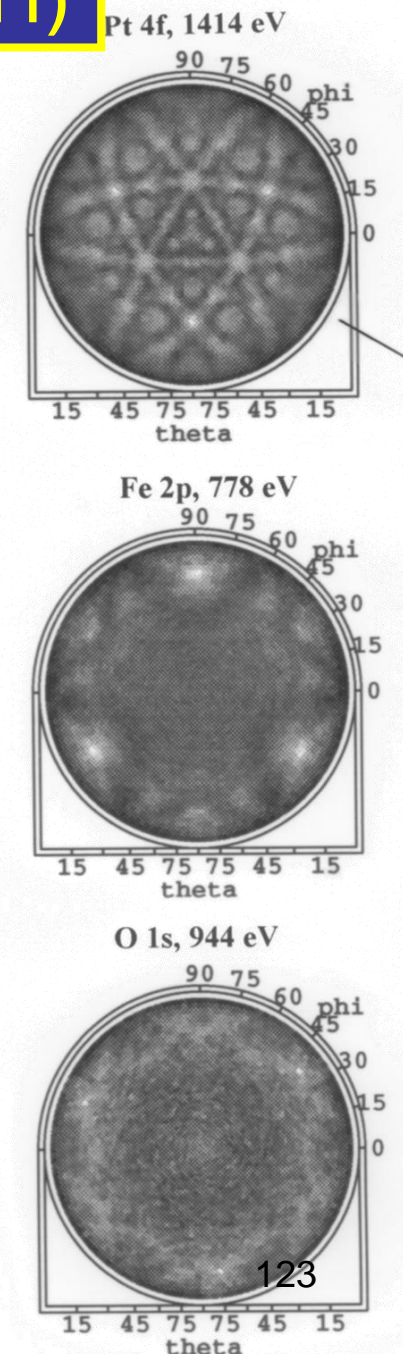
Photoelectron Diffraction

X-ray Photoelectron Diffraction: 1ML FeO on Pt(111)

(a)



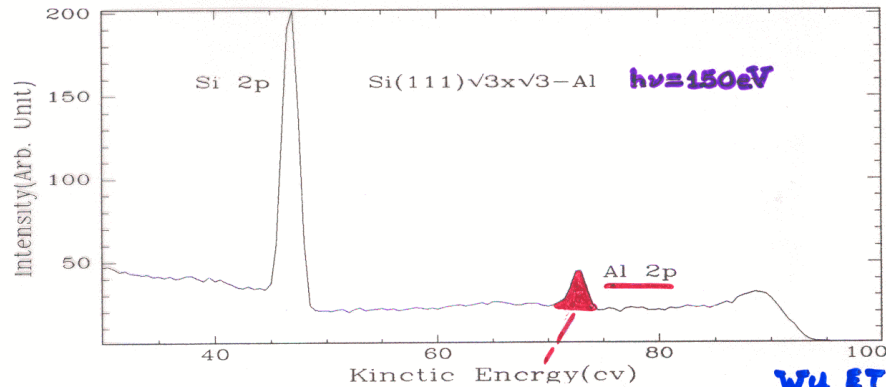
(b)



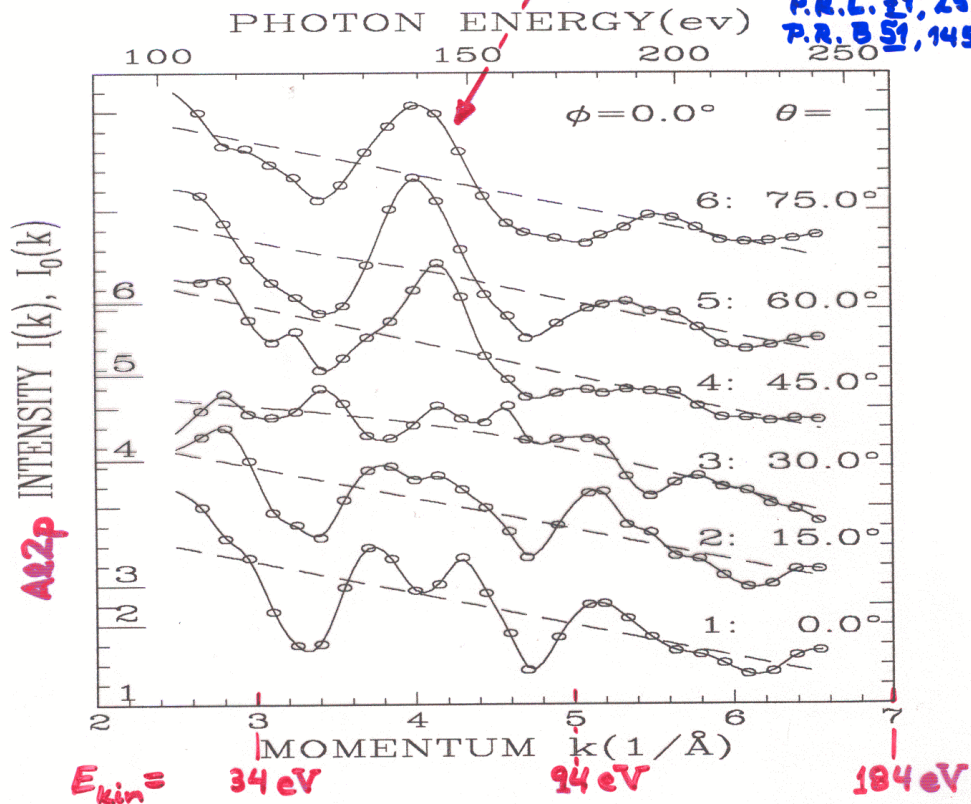
Scanned-energy photoelectron diffraction—an alternative approach (Shirley, Woodruff/Bradshaw, Lapeyre, Chiang et al.)

SCANNED-ENERGY PHOTOELECTRON DIFF.
 $(\sqrt{3} \times \sqrt{3})$ AL ON Si(111)

* 41 diffraction curves χ taken from Al 2p } ~1100 DATA POINTS
 * $\theta = 0 \sim 70^\circ$, $\phi = 0 \sim 60^\circ$

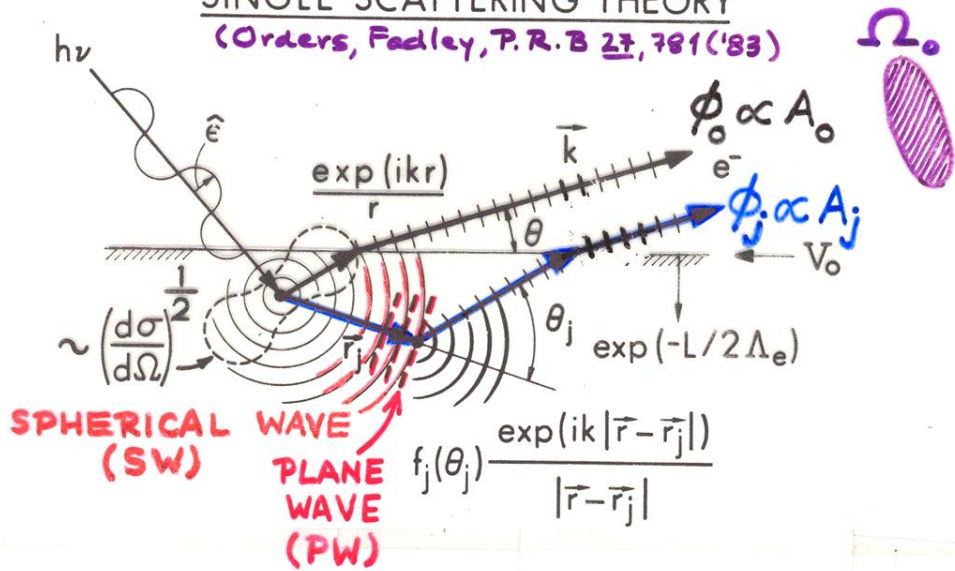


WU ET AL.,
 P.R.L. 31, 251 ('93)
 P.R. B 51, 14549 ('95)



SINGLE SCATTERING THEORY

(Orders, Fadley, P.R.B 27, 781 ('83))



**Photoelectron diffraction:
Simple single-scattering theory for s-subshell emission**

$$\chi(E \text{ or } \vec{k}) \propto \sum_j \frac{F_j(k)}{F_0} \cos \left[\underbrace{kr_j(1 - \cos \theta_j)}_{\text{PATH LENGTH DIFFERENCE (P.L.D.)}} + \underbrace{\psi_j(\theta_j, k)}_{\text{SCATTERING PHASE SHIFT}} \right]$$

(CLUSTER)

$$F_j(k) = (\hat{E} \cdot \hat{r}_j) \frac{|f_j(\theta_j, k)|}{r_j} \underbrace{W_j(\theta_j, k)}_{\text{DEBYE-WALLER}} \exp(-L_j/2\Lambda_e)$$

ELASTIC e⁻-ATOM SCATTERING INELASTIC e⁻-e⁻ SCATTERING

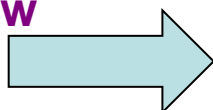
= amplitude of scattered wave

$$F_0 = (\hat{E} \cdot \hat{k}) \exp(-L_0/2\Lambda_e)$$

= amplitude of direct wave

∴ FOURIER TRANSFORM OF $\chi(k) \Rightarrow$
PEAKS AT $\sim \text{P.L.D.} = r_j(1 - \cos \theta_j)$

Various papers by Shirley et al., Woodruff, Bradshaw et. al.



COMPARISON OF SCANNED-ENERGY PD TO EXTENDED X-RAY ABSORPTION FINE STRUCTURE

"NEAR-EDGE" = THEORY OF EXAFS

XAS, XANES,

NEXAFS

"EXTENDED" = EXAFS

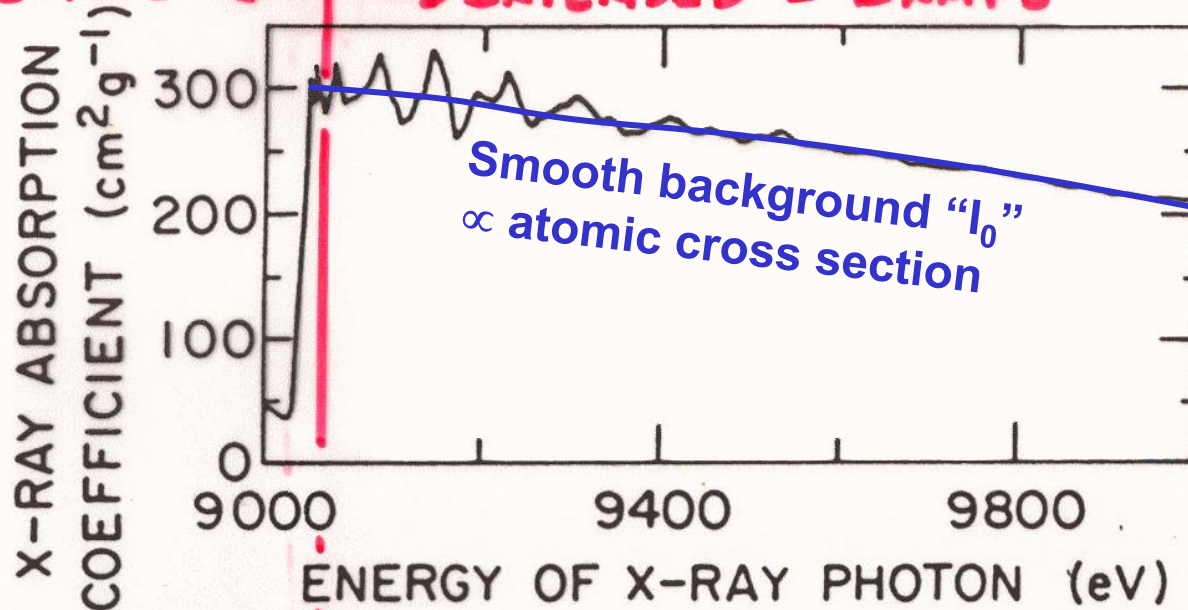
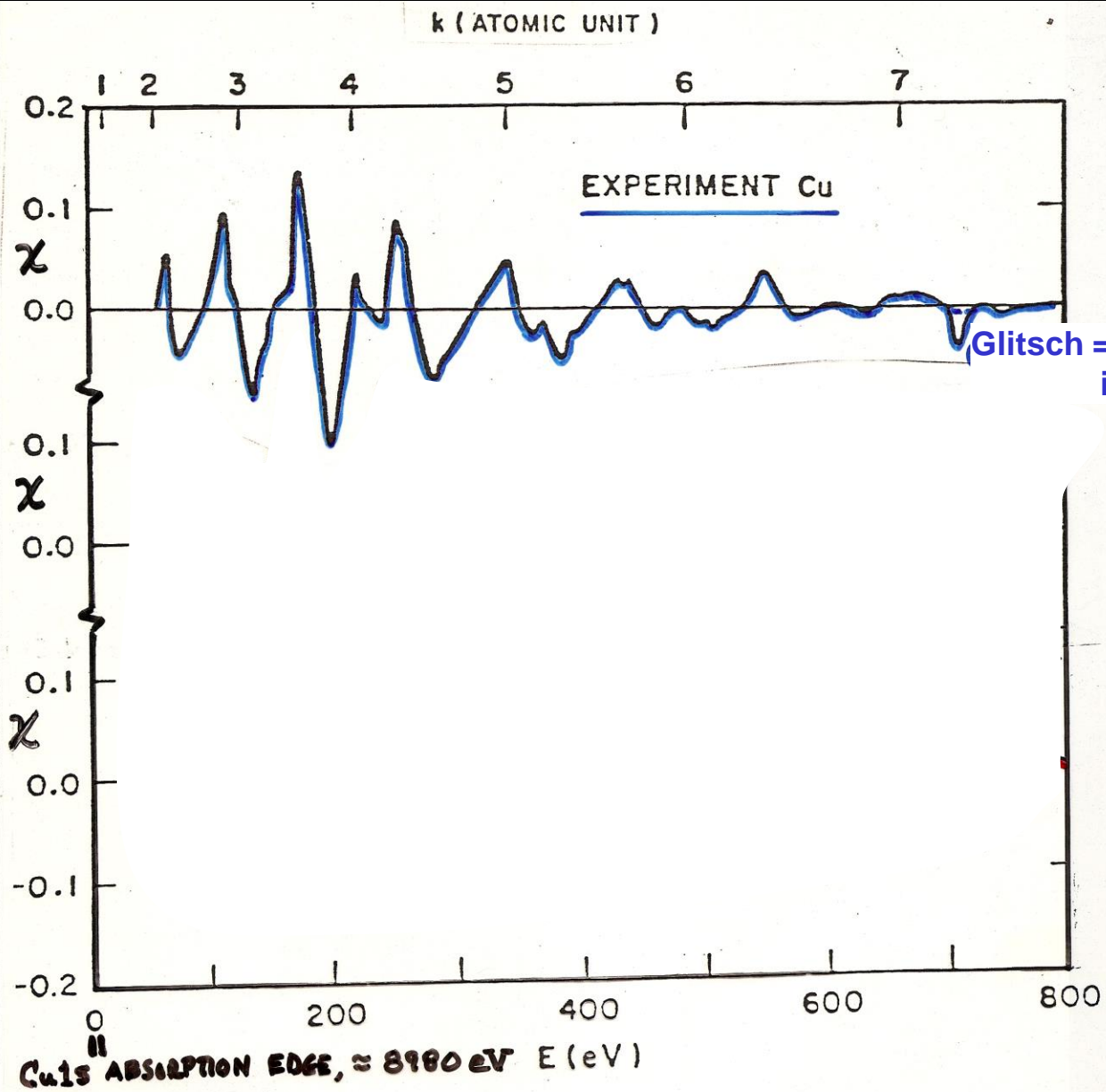


Figure 1.1. The x-ray absorption coefficient for the *K*-edge of copper metal.

~ COPPER
1S BINDING
ENERGY

**Also scanned-energy,
but integrates over all
electron emission
directions**



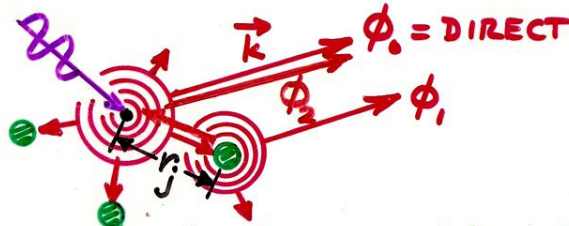
Cu 1s ABSORPTION EDGE, ≈ 8980 eV E (eV)

EXAFS OF THE 1s SHELL OF COPPER

LEE + PENDRY, PHYS. REV. B 11, 2795
(1975)

Theory of Extended X-Ray Absorption Fine Structure

SINGLE SCATTERING PLUS DOUBLE SCATTERING BACK TO EMITTER FROM A CLUSTER OF ~20-100 ATOMS ABOUT EMITTER -



SUM OVER ALL $\phi_1, \phi_2, \dots \propto |\phi_0 + \sum \phi_1 + \sum \phi_2|^2$
 THEN OVER ALL (UNOBSERVED) \vec{k} DIRECTIONS
 →

$$\chi(k) = \frac{\Delta\mu}{\mu_0} = - \sum_j \frac{N_j}{kr_j^2} |f_j(k, \pi)| S_0^2$$

∴ FOURIER TRANSFORM OF $\chi(k)$
 → PEAKS AT $\approx 2r_j$
 → BOND DISTANCES

$$\times \sin[2kr_j + \phi_j(k, \pi)] e^{-2\bar{u}_j^2 k^2 - 2r_j / \Lambda_e(k)}$$

PHASES DUE TO: PATH LENGTH DIFF. ELASTIC SCATT. DEBYE-WALLER FACTOR INELASTIC SCATT.

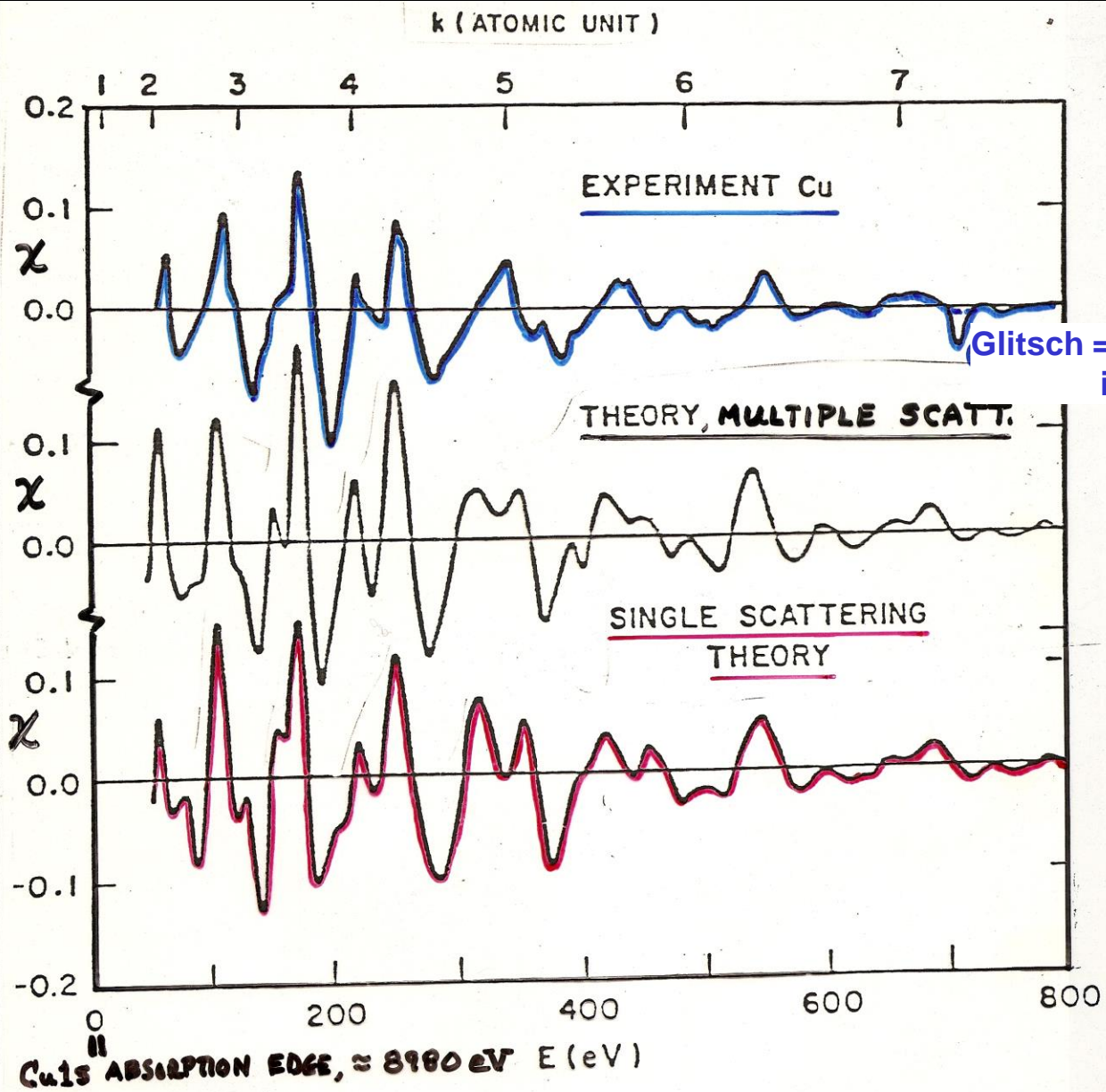
WITH: N_j = NO. SCATTERERS AT DISTANCE r_j .

k = e^- WAVE VECTOR = $\sqrt{2mE}/\hbar$

$|f_j(k, \pi)|$ = BACKSCATTERING AMPLITUDE

$\phi_j(k, \pi) = \psi_j(k, \pi) + 2\delta_j$ = OVERALL BACKSCATT. PHASE SHIFT

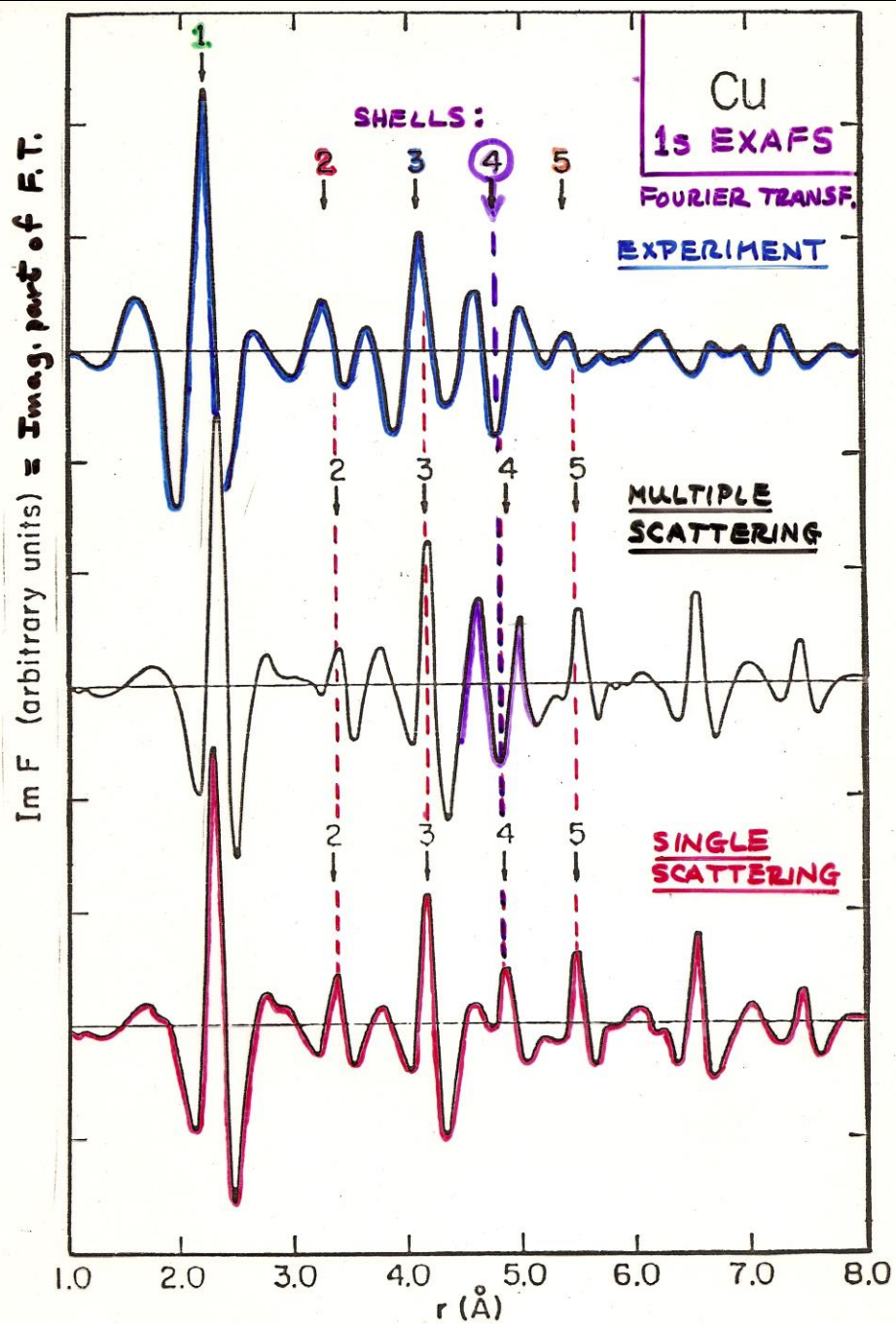
S_0^2 = FRACTION FREE OF "SHAKE" \bar{u}_j^2 = MEAN-SQUARED VIBRATIONAL MOTION
 $= \langle |\Psi_e | \Psi_n \rangle|^2$ $\Lambda_e(k)$ = INELASTIC MEAN FREE PATH



Cu_{1s} ABSORPTION EDGE, ≈ 8980 eV

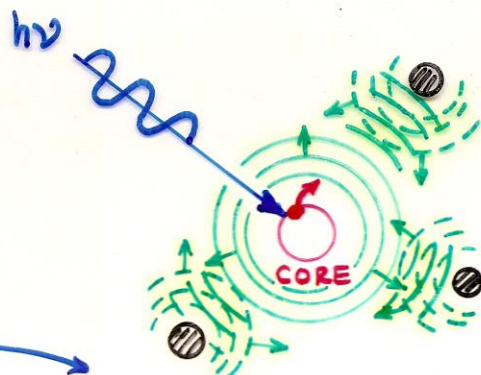
EXAFS OF THE $1s$ SHELL OF COPPER

LEE + PENDRY, PHYS. REV. B 11, 2795
(1975)



LEE & PENDRY, PHYS. REV. B 11, 2795 (1975)

SURFACE EXTENDED X-RAY ABSORPTION FINE STRUCTURE (SEXAFS)



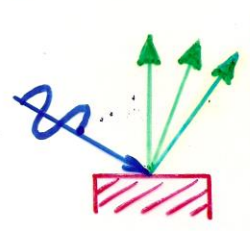
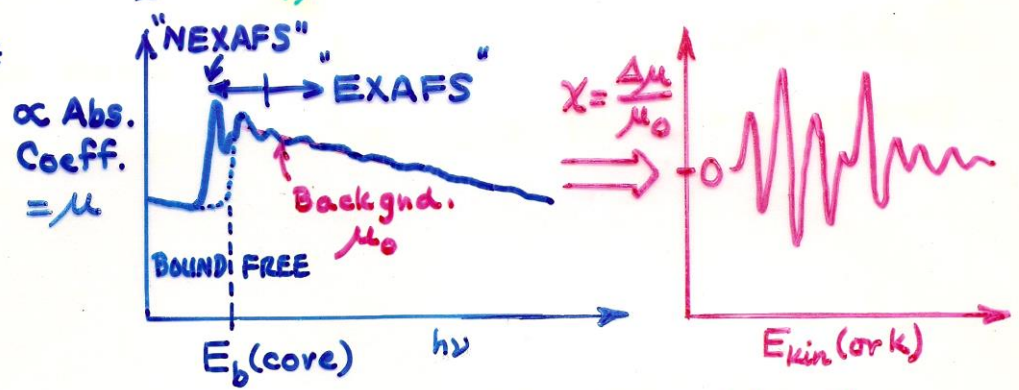
FOR PHOTOELECTRON:

$$E_{kin} = h\nu - E_b(\text{core})$$

$$k = \frac{\sqrt{2mE}}{\hbar}$$

$$\lambda_{e^-} = \frac{2\pi}{k}$$

NEAR EDGE X-RAY ABSORPTION FINE STRUCTURE



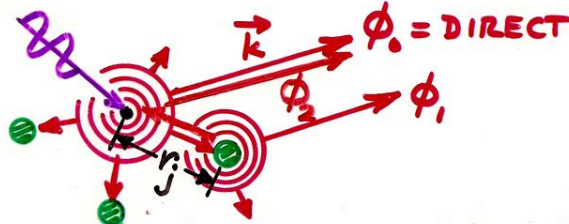
SEXAFS detection by: Auger yield (CMA), $2^{\circ} e^-$ yield, or Ions due to Photon stimulated desorption, or

(P.A. Lee et al., Rev. Mod. Phys. 53, 769 (1981))

X-ray fluorescence (for adsorbates)

Theory of Extended X-Ray Absorption Fine Structure

SINGLE SCATTERING PLUS DOUBLE SCATTERING BACK TO EMITTER FROM A CLUSTER OF ~20-100 ATOMS ABOUT EMITTER -



SUM OVER ALL $\phi_1, \phi_2, \dots \propto |\phi_0 + \sum \phi_1 + \sum \phi_2|^2$
 THEN OVER ALL (UNOBSERVED) \vec{k} DIRECTIONS
 →

$$\chi(k) = \frac{\Delta\mu}{\mu_0} = - \sum_j \frac{N_j}{kr_j^2} |f_j(k, \pi)| S_0^2$$

∴ FOURIER TRANSFORM OF $\chi(k)$
 → PEAKS AT $\approx 2r_j$
 → BOND DISTANCES

$$\times \sin[2kr_j + \phi_j(k, \pi)] e^{-2u_j^2 k^2 - 2r_j/\Lambda_e(k)}$$

PHASES DUE TO: PATH LENGTH DIFF. ELASTIC SCATT. DEBYE-WALLER FACTOR INELASTIC SCATT.

WITH: N_j = NO. SCATTERERS AT DISTANCE r_j .

k = e^- WAVE VECTOR = $\sqrt{2mE}/\hbar$

$|f_j(k, \pi)|$ = BACKSCATTERING AMPLITUDE

$\phi_j(k, \pi) = \psi_j(k, \pi) + 2\delta_j$ = OVERALL BACKSCATT. PHASE SHIFT

S_0^2 = FRACTION FREE OF "SHAKE" || u_j^2 = MEAN-SQUARED VIBRATIONAL MOTION
 $= \langle |\Psi_e | \Psi_g \rangle|^2$ || $\Lambda_e(k)$ = INELASTIC MEAN FREE PATH

COMPARISON OF SCANNED-ENERGY PD TO EXTENDED X-RAY ABSORPTION FINE STRUCTURE

"NEAR-EDGE" =
XAS, XANES,
NEXAFS

"EXTENDED" = EXAFS

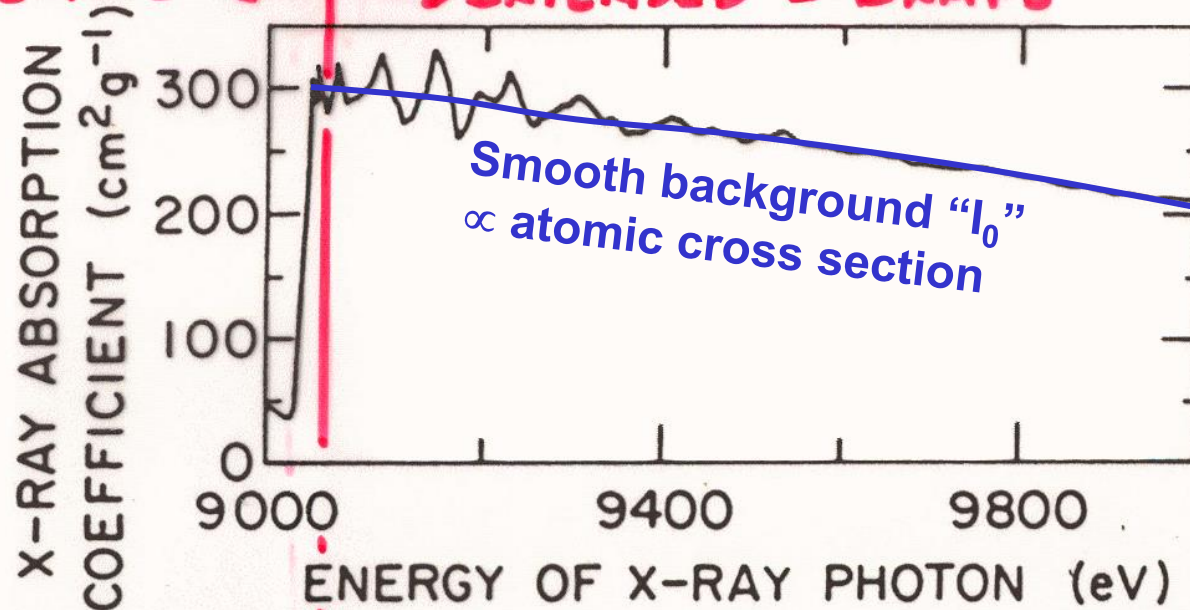
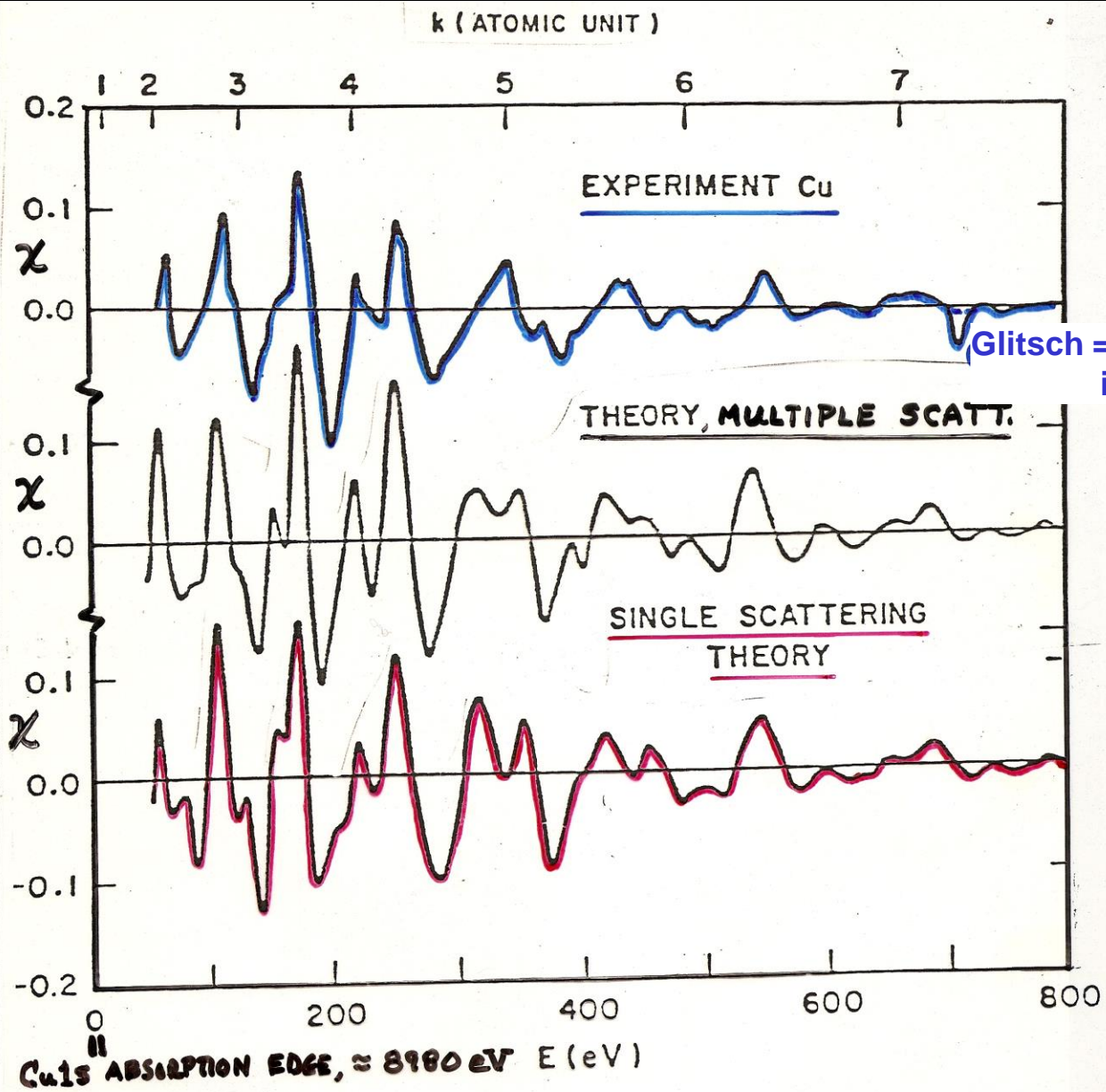


Figure 1.1. The x-ray absorption coefficient for the *K*-edge of copper metal.

~ COPPER
1S BINDING
ENERGY

**Also scanned-energy,
but integrates over all
electron emission
directions**



Glitsch = Bragg reflection in crystal

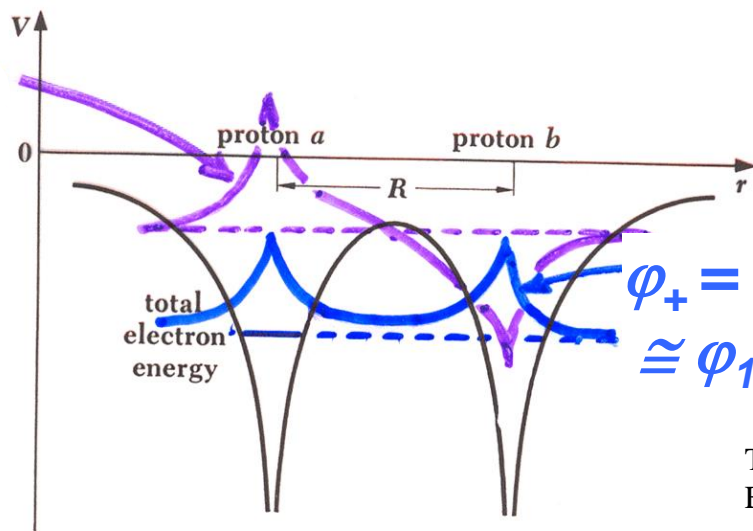
Cu's ABSORPTION EDGE, ≈ 8980 eV E (eV)

EXAFS OF THE 1s SHELL OF COPPER

LEE + PENDRY, PHYS. REV. B 11, 2795 (1975)

The quantum mechanics of covalent bonding in molecules: H₂⁺ with one electron

$$\varphi_- = \varphi_{\text{antibonding}} \cong \varphi_{1sa} - \varphi_{1sb}$$



$$\varphi_+ = \varphi_{\text{bonding}} \cong \varphi_{1sa} + \varphi_{1sb}$$

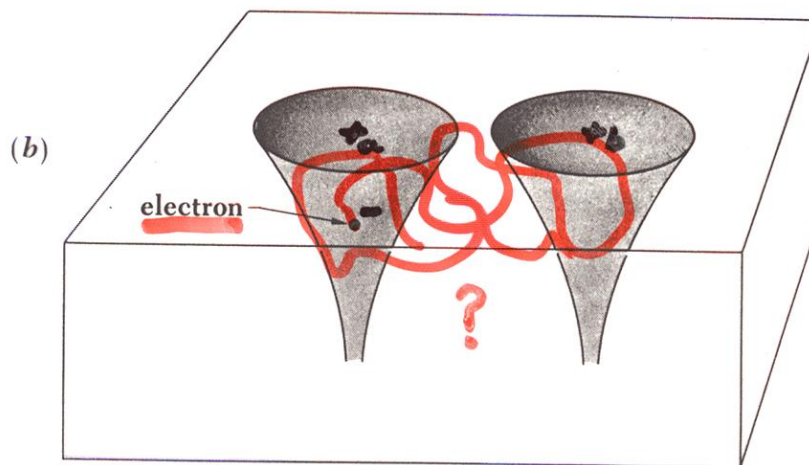


FIGURE 8.4 (a) Potential energy of an electron in the electric field of two nearby protons. The total energy of a ground-state electron in the hydrogen atom is indicated. (b) Two nearby protons correspond quantum-mechanically to a pair of boxes separated by a barrier.

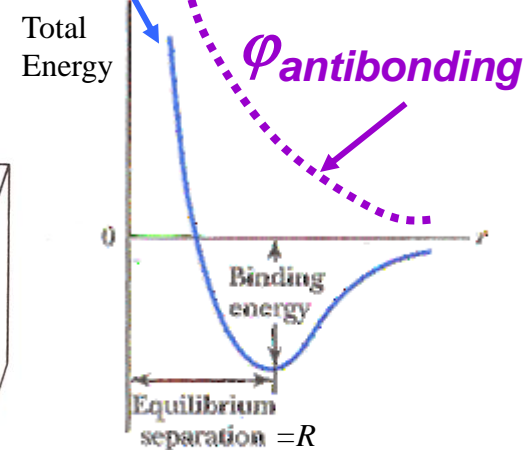
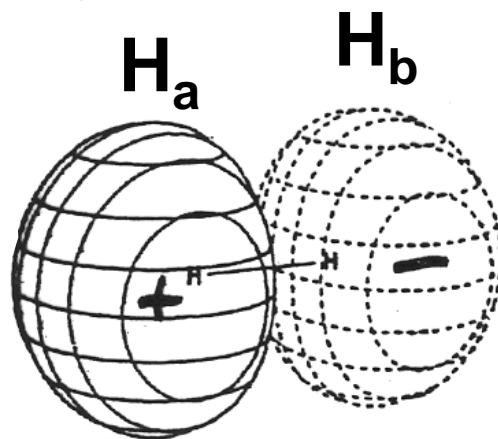


FIGURE 10.2 The net potential energy curve, showing the equilibrium separation and binding energy.

1. Hydrogen

Symmetry: $D_{\infty h}$

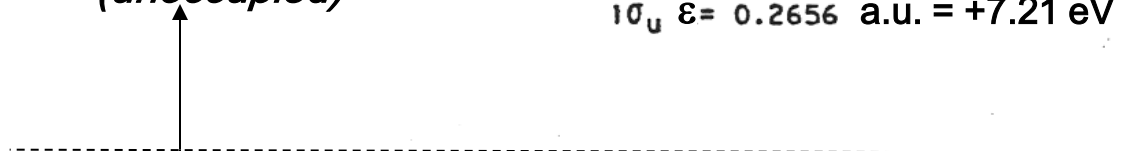


Anti-Bonding

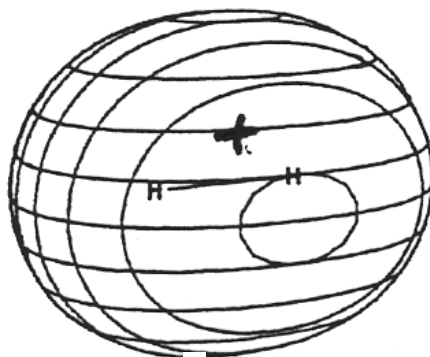
$$\varphi_{anti}^{MO} \cong \varphi_{1sa} - \varphi_{1sa}$$

$$1\sigma_u \quad \epsilon = 0.2656 \text{ a.u.} = +7.21 \text{ eV}$$

ϵ positive
(unoccupied)



ϵ negative
(occupied)



Bonding

$$\varphi_{bonding}^{MO} \cong \varphi_{1sa} + \varphi_{1sa}$$

$$1\sigma_g \quad \epsilon = -0.5944 \text{ a.u.} = -16.16 \text{ eV}$$

(Compare - 13.61 for H atom 1s)

The LCAO or tight-binding picture for CO:

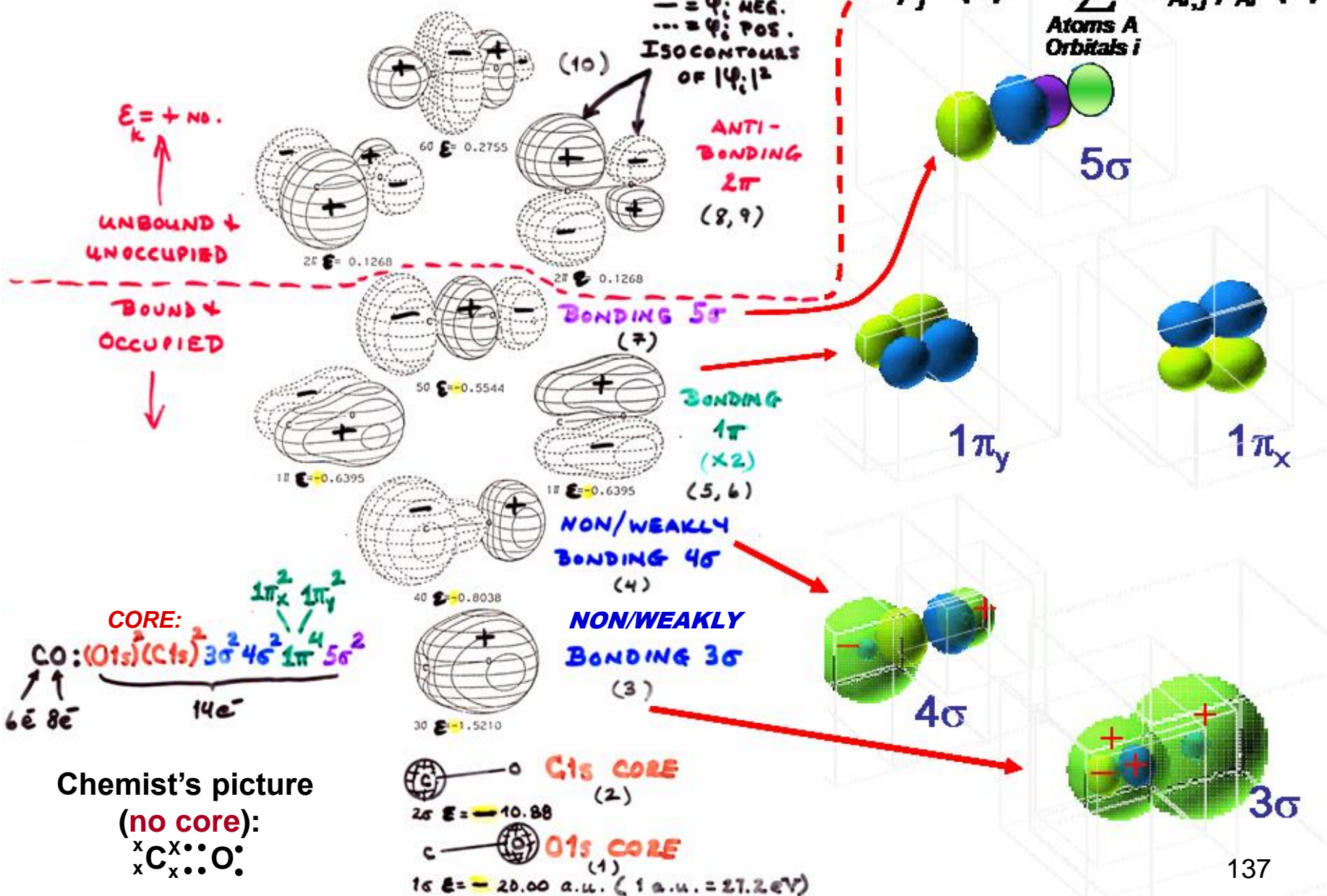
Atomic orbital makeup

15. Carbon Monoxide

Symmetry: $C_{\infty v}$

— = ψ : NEG.
 ... = ψ : POS.
ISOCONTOURS OF $|\psi_i|^2$

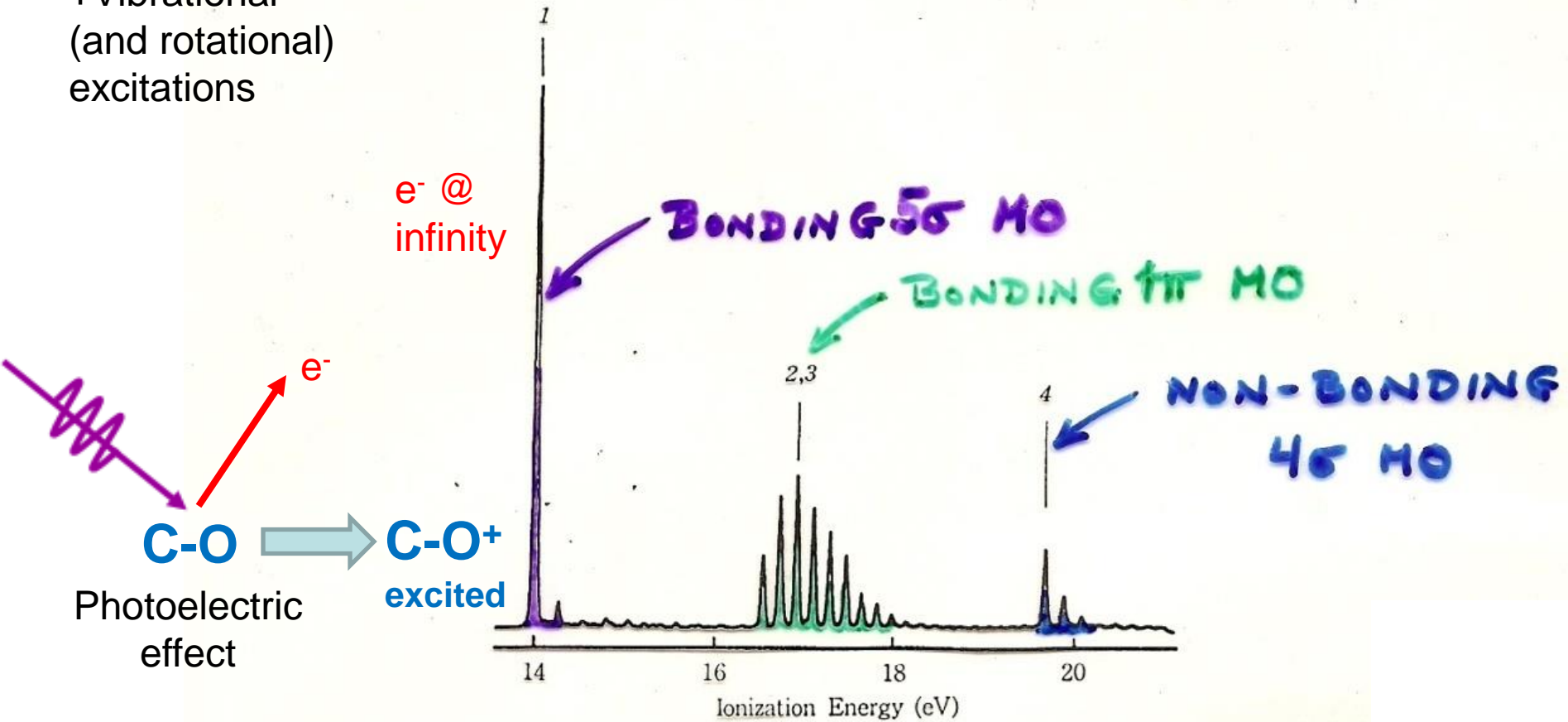
$$\varphi_j^{MO}(\vec{r}) = \sum_{\text{Atoms } A} c_{Aij} \varphi_{Ai}^{AO}(\vec{r})$$



(9) CO Carbon Monoxide

UV PHOTOELECTRON SPECTRUM OF CO

+Vibrational
(and rotational)
excitations



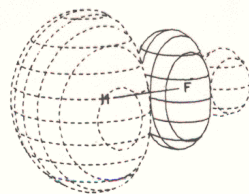
THE ELECTRONS IN HF (OR HCl): ionic molecules

10. Hydrogen Fluoride = HF

Symmetry: $C_{\infty v}$

MO's LIKE HCl

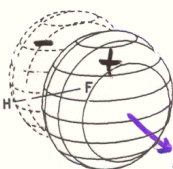
2s, 2p →
3s, 3p



40 E = 0.2906

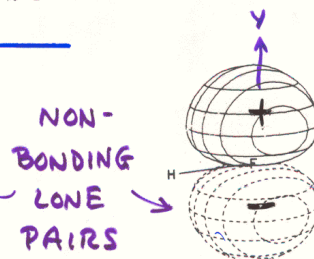
UNOCC.
OCC.

$\approx \psi_{2p_x}$



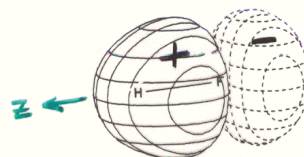
1π E = -0.6505

→ 2π OF HCl (9)



1π E = -0.6505

→ 2π OF HCl (8)



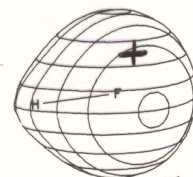
3σ E = -0.7685

→ 5σ OF HCl (7)

BONDING $\approx \psi_{H1s} + \psi_{F2p_z}$

WEAKLY OR NON-BONDING

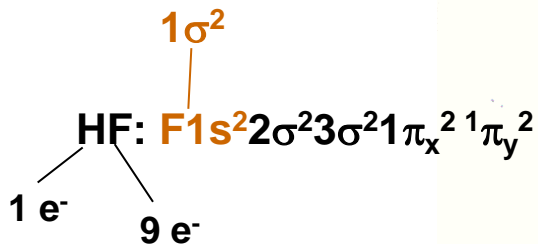
BONDING $\approx \psi_{H1s} + \psi_{F2s}$



20 E = -1.6013

(IN ATOMIC UNITS:
1 a.u. = 27.21 eV)

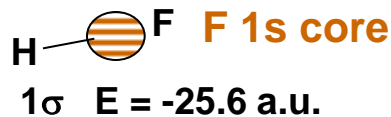
HF EIGENVALUE
= ϵ_k



Chemist's picture (no core):



Three "lone pairs"



But kind of the third "lone pair"

PHOTOELECTRON EMISSION -

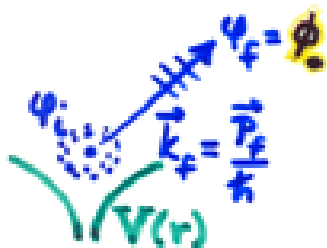
BASIC MATRIX ELEMENTS + SELECTION RULES:

● ATOMIC-LIKE (LOCALIZED) STATES \Rightarrow CORE:

$$\psi_i(\vec{r}) = \psi_{n_i, l_i, m_i}(r, \theta, \phi) = R_{n_i, l_i}(r) Y_{l_i, m_i}(\theta, \phi)$$

PLUS SPIN:

$$\begin{cases} \alpha(\sigma) = m_{s_i} = +\frac{1}{2} = \uparrow \\ \beta(\sigma) = m_{s_i} = -\frac{1}{2} = \downarrow \end{cases}$$



$$\psi_f(\vec{r}, \vec{k}_f) = \psi_{E_f}(\vec{r}, \vec{k}_f) \begin{cases} \alpha(\sigma) \\ \beta(\sigma) \end{cases}$$

$$= 4\pi \sum_{l_f, m_f} i^{l_f} e^{-i\delta_{l_f}^*} Y_{l_f, m_f}^*(\theta_{k_f}, \phi_{k_f}) Y_{l_f, m_f}(\theta, \phi) R_{E_f, l_f}(r) \begin{cases} \alpha(\sigma) \\ \beta(\sigma) \end{cases}$$

PHASE SHIFT OF l_f WAVE IN $V(r)$

DIPOLE APPROX.: INT. $\propto \langle \psi_f | \hat{E} \cdot \vec{r} | \psi_i \rangle^2 = \left| \langle \psi_f | \vec{r} | \psi_i \rangle \right|^2$

EQUIVALENT WITHIN CONSTANT FACTOR



- $\langle \Delta l = l_f - l_i = \pm 1$
TWO CHANNELS
- $\langle \Delta m = m_f - m_i = 0, \pm 1$
LINEAR POLARIZ.
- $\langle \Delta m = \pm 1$, CIRCULAR POLARIZATION

$\Delta m_s = m_{s_f} - m_{s_i} = 0!$
+ with spin-orbit:
 $\Delta j = 0, \pm 1$

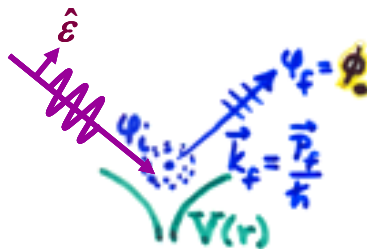
PHOTOELECTRON EMISSION -

BASIC MATRIX ELEMENTS + SELECTION RULES:

• ATOMIC-LIKE (LOCALIZED) STATES \Rightarrow CORE:

PLUS SPIN:

$$\psi_i(\vec{r}) = \psi_{n_i, l_i, m_i}(\vec{r}, \theta, \phi) = R_{n_i, l_i}(r) Y_{l_i, m_i}(\theta, \phi) \begin{cases} \alpha(\sigma) = m_{s_i} = +1/2 = \uparrow \\ \beta(\sigma) = m_{s_i} = -1/2 = \downarrow \end{cases}$$



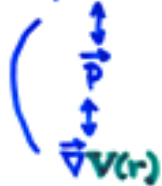
$$\psi_f(\vec{r}, \vec{k}_f) = \psi_{E_f}(\vec{r}, \vec{k}_f) \begin{cases} \alpha(\sigma) \\ \beta(\sigma) \end{cases}$$

$$= 4\pi \sum_{l_f, m_f} i^{l_f} e^{-i\delta_{l_f}} Y_{l_f, m_f}^*(\theta_i, \phi_i) Y_{l_f, m_f}(\theta_f, \phi_f) R_{E_f, l_f}(r) \begin{cases} \alpha(\sigma) \\ \beta(\sigma) \end{cases}$$

PHASE SHIFT OF l_f WAVE IN $V(r)$

DIPOLE APPROX.: INT. $\propto |\langle \psi_f | \hat{\epsilon} \cdot \vec{r} | \psi_i \rangle|^2 = |\hat{\epsilon} \cdot \langle \psi_f | \vec{r} | \psi_i \rangle|^2 \Rightarrow$

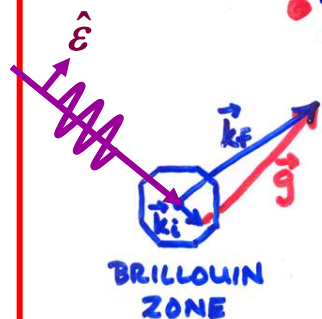
EQUIVALENT WITHIN CONSTANT FACTOR



- $\Delta l = l_f - l_i = \pm 1$
TWO CHANNELS
- $\Delta m = m_f - m_i = 0, \pm 1$
LINEAR POLARIZ.
- $\Delta m = \pm 1$, CIRCULAR POLARIZATION

$\Delta m_s = m_{s_f} - m_{s_i} = 0!$ + with spin-orbit:
 $\Delta j = 0, \pm 1$

• BLOCH-FUNCTION (DELOCALIZED) STATES \Rightarrow VALENCE:



$$\psi_i(\vec{r}) = u_{\vec{k}_i}(\vec{r}) e^{i\vec{k}_i \cdot \vec{r}}$$

$$\psi_f(\vec{r}) = u_{\vec{k}_f}(\vec{r}) e^{i\vec{k}_f \cdot \vec{r}}; E_f = \frac{p_f^2}{2m} = \frac{\hbar^2 k_f^2}{2m}$$

USUALLY NEGLIG.

$$|\langle \psi_f | \hat{\epsilon} \cdot \vec{p} | \psi_i \rangle|^2 = |\hat{\epsilon} \cdot \langle \psi_f | \vec{p} | \psi_i \rangle|^2 \Rightarrow \Delta \vec{k} = \vec{k}_f - \vec{k}_i = -\vec{k}_{ph} + \vec{k}_{PHONON}$$

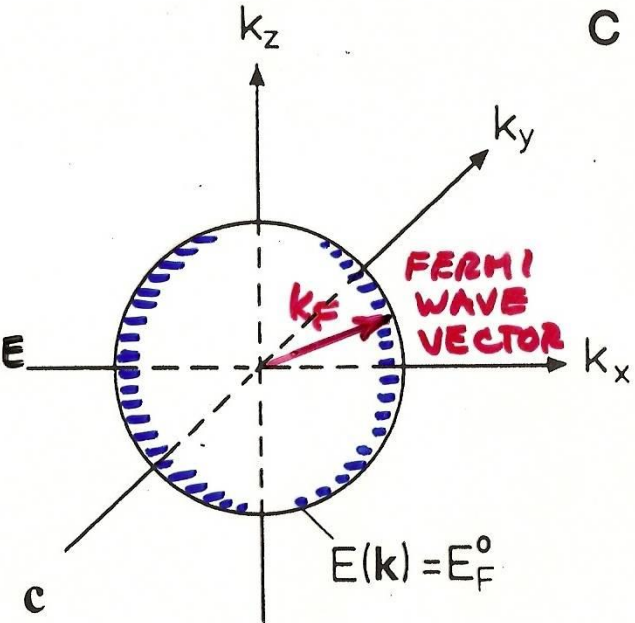
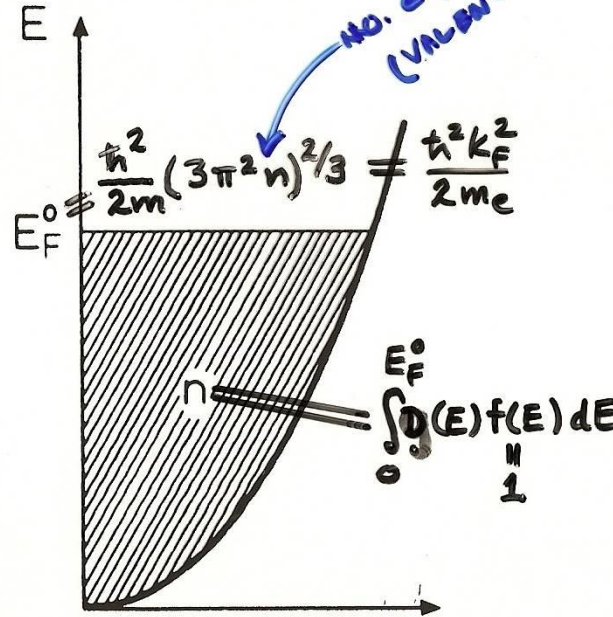
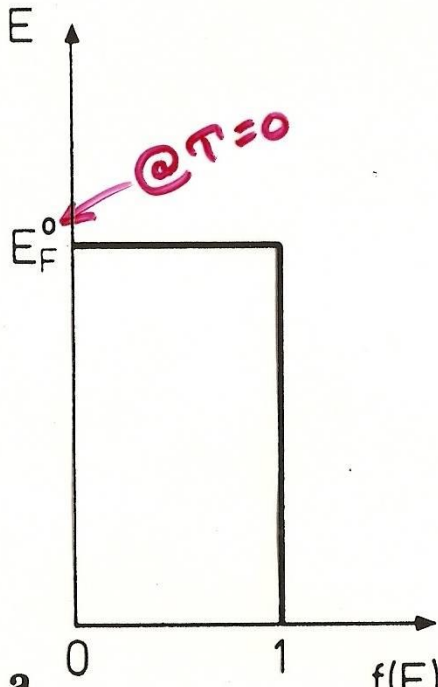
$$= \vec{g}_{BULK} \text{ (or } \vec{g}_{SURF})$$

"DIRECT" TRANSITIONS

BUT LATTICE VIBRATIONS \Rightarrow SUM OVER \vec{k}_{PHONON}
 \Rightarrow FRACTION DIRECT \approx DEBYE-WALLER FACTOR
 $= \exp[-g^2 \bar{u}^2]$

The free-electron solid at absolute zero

$$E(\vec{k}) = \frac{\hbar^2 k^2}{2m_e} = 3.81(k(\text{in } \text{\AA}^{-1}))^2 \text{ (in eV)}$$



FERMI-DIRAC

$$f(E, T) = \frac{1}{e^{(E-E_F^0)/k_B T} + 1}$$

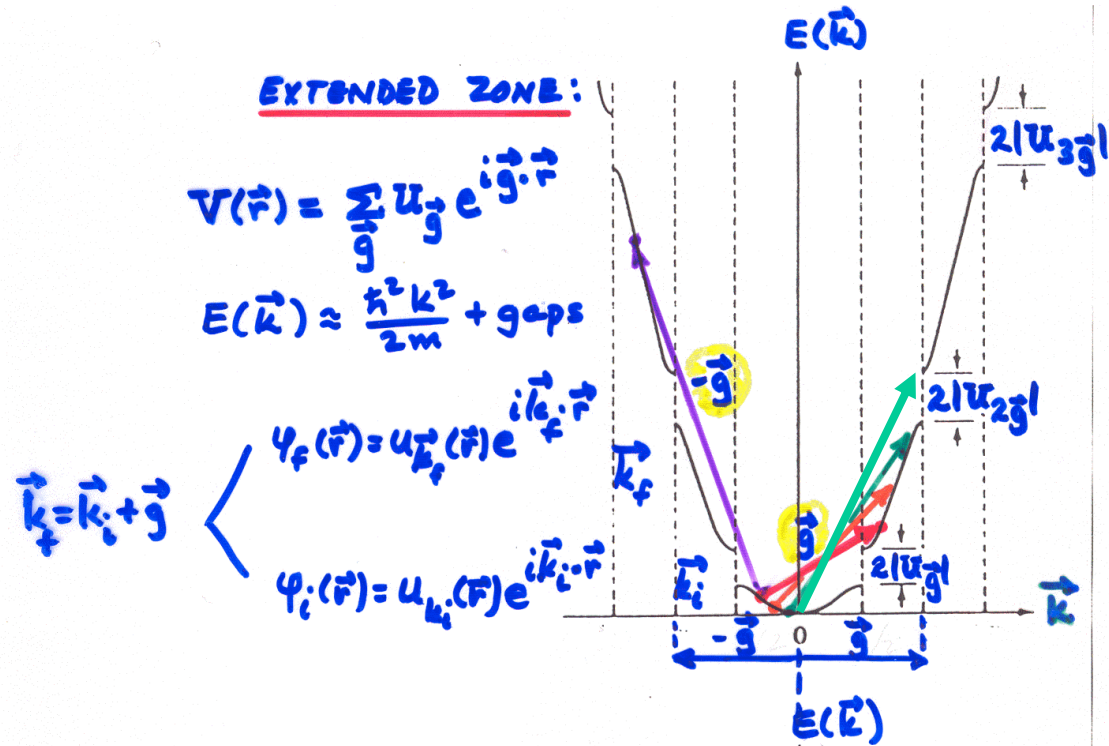
$$g(E) \cdot f(E) \approx \frac{(2m)^{3/2}}{2\pi^2 \hbar^3} E^{1/2}$$

= the density of states

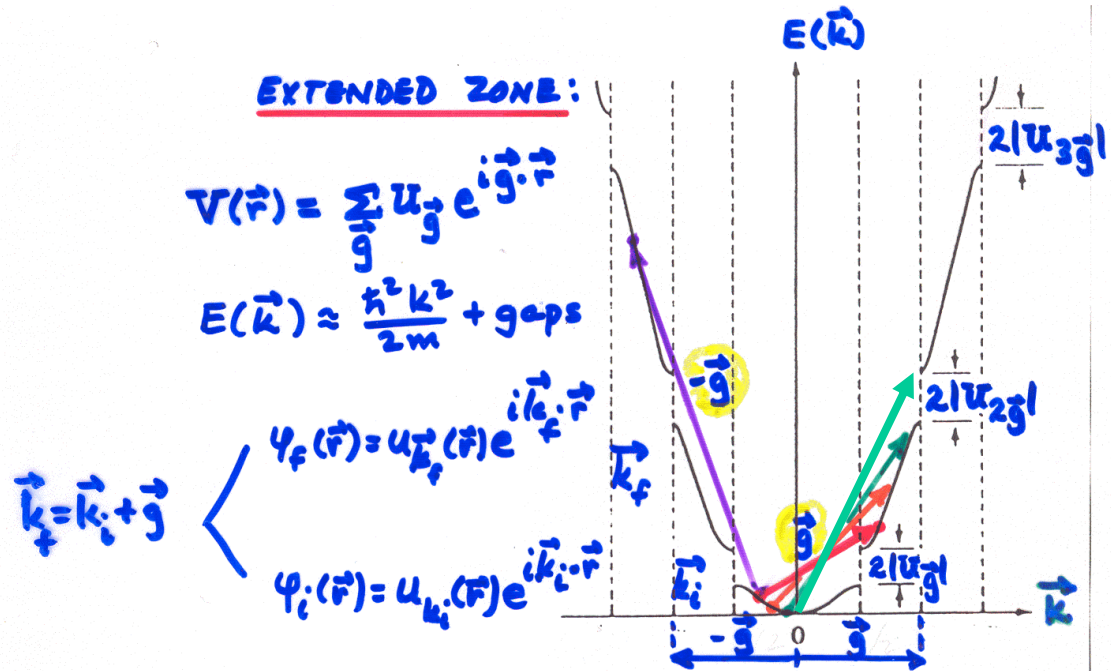
$$k_F = (3\pi^2 n)^{1/3}$$

$$v_f = \hbar k_F / m_e$$

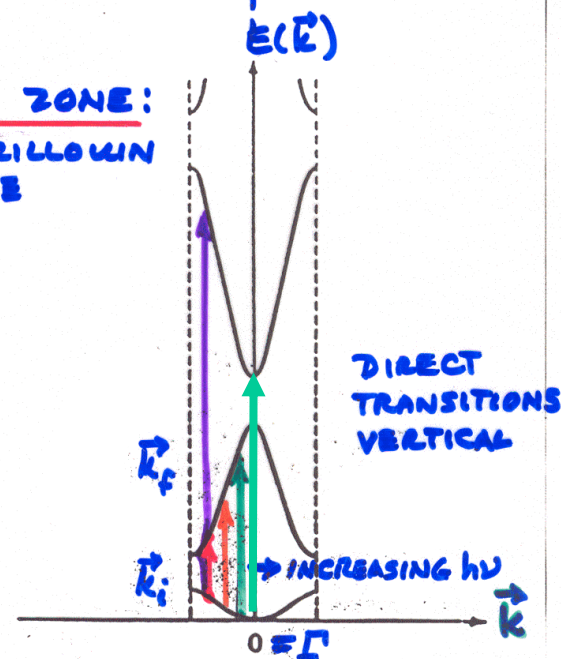
NEARLY-FREE ELECTRONS IN A WEAK PERIODIC POTENTIAL—1 DIM.



NEARLY-FREE ELECTRONS IN A WEAK PERIODIC POTENTIAL—1 DIM.



REDUCED ZONE:
= FIRST BRILLOUIN ZONE



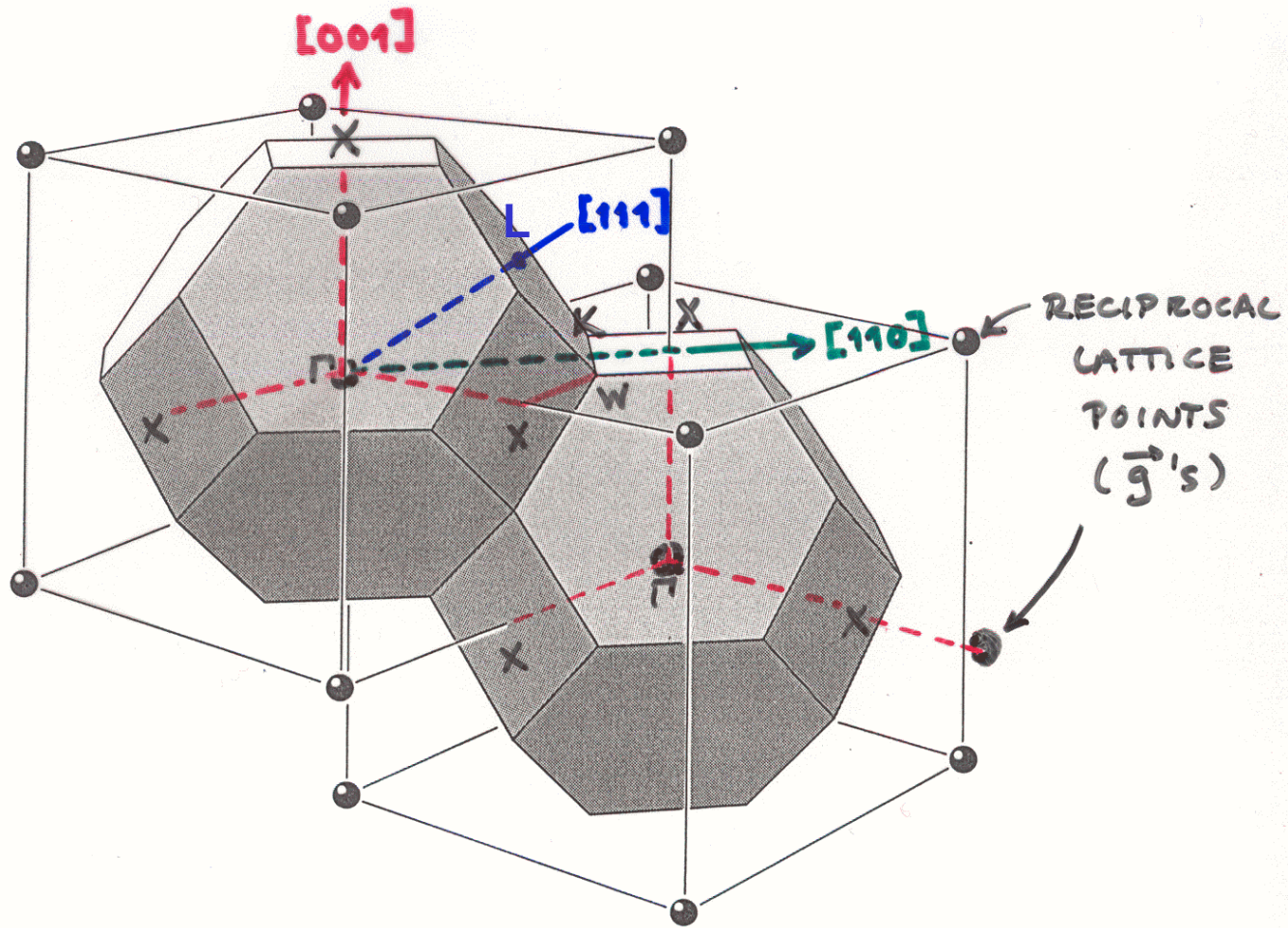


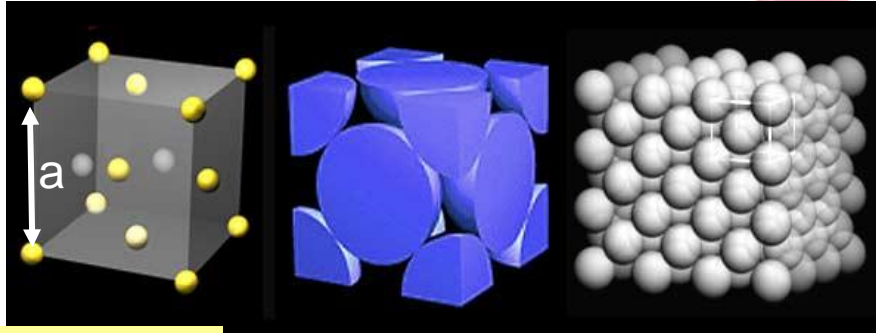
Figure 28 Brillouin zones of the face-centered cubic lattice. The cells are in reciprocal space, and the reciprocal lattice is body-centered, as drawn.

— STACKING OF FCC BRILLOUIN ZONES —

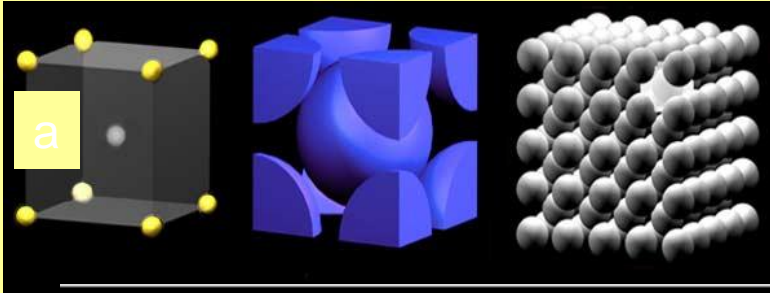
Electronic bands and density of states for "free-electron" metals -

Rydberg = 13.605 eV

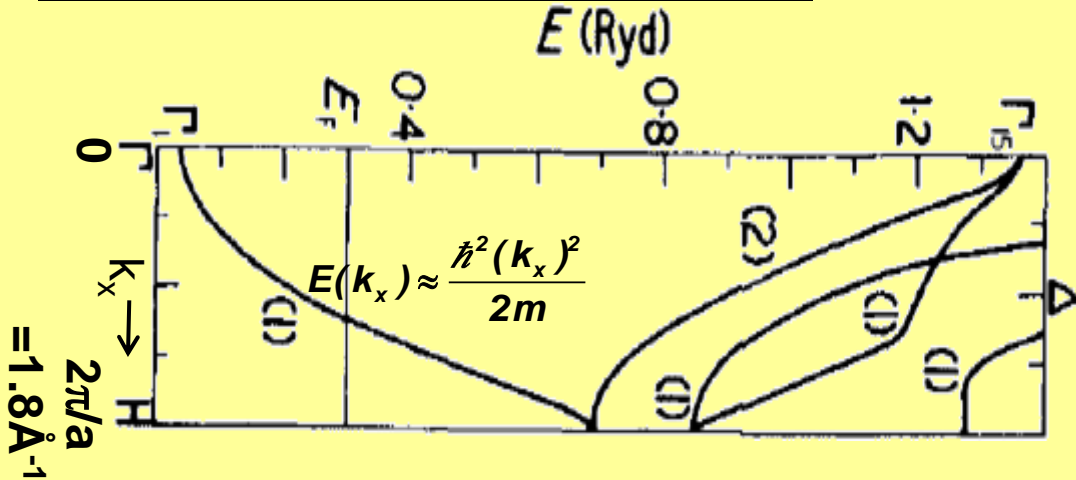
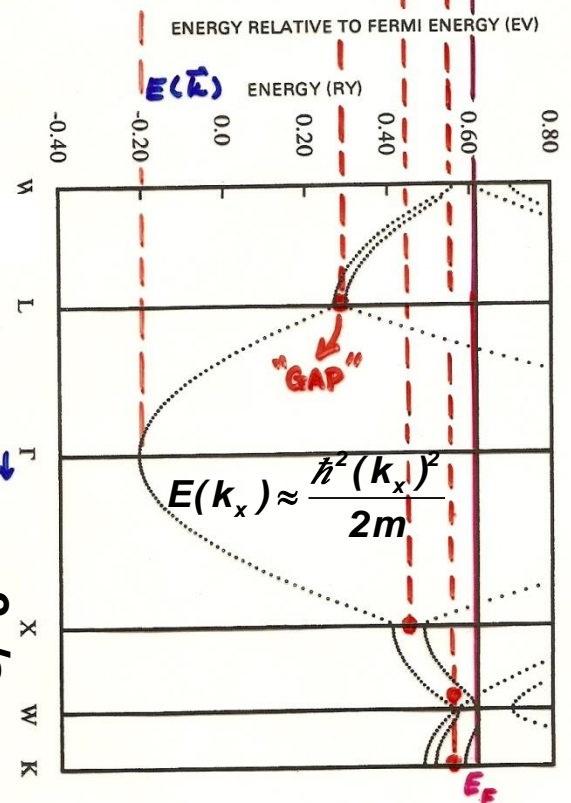
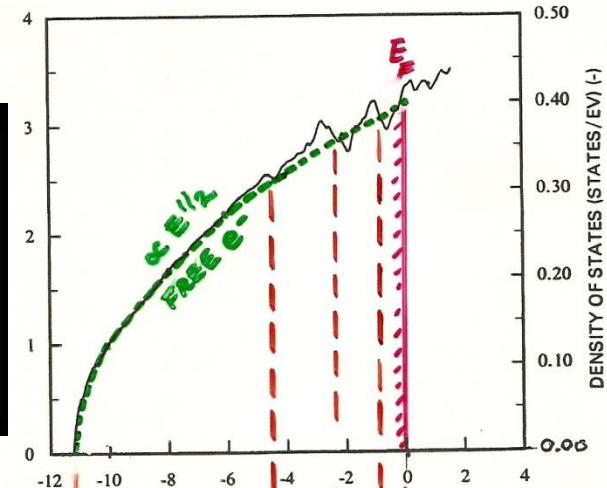
Aluminum—fcc,
 $a = 4.05 \text{ \AA}$
 $1s^2 2s^2 2p^6 3s^2 3p^1$



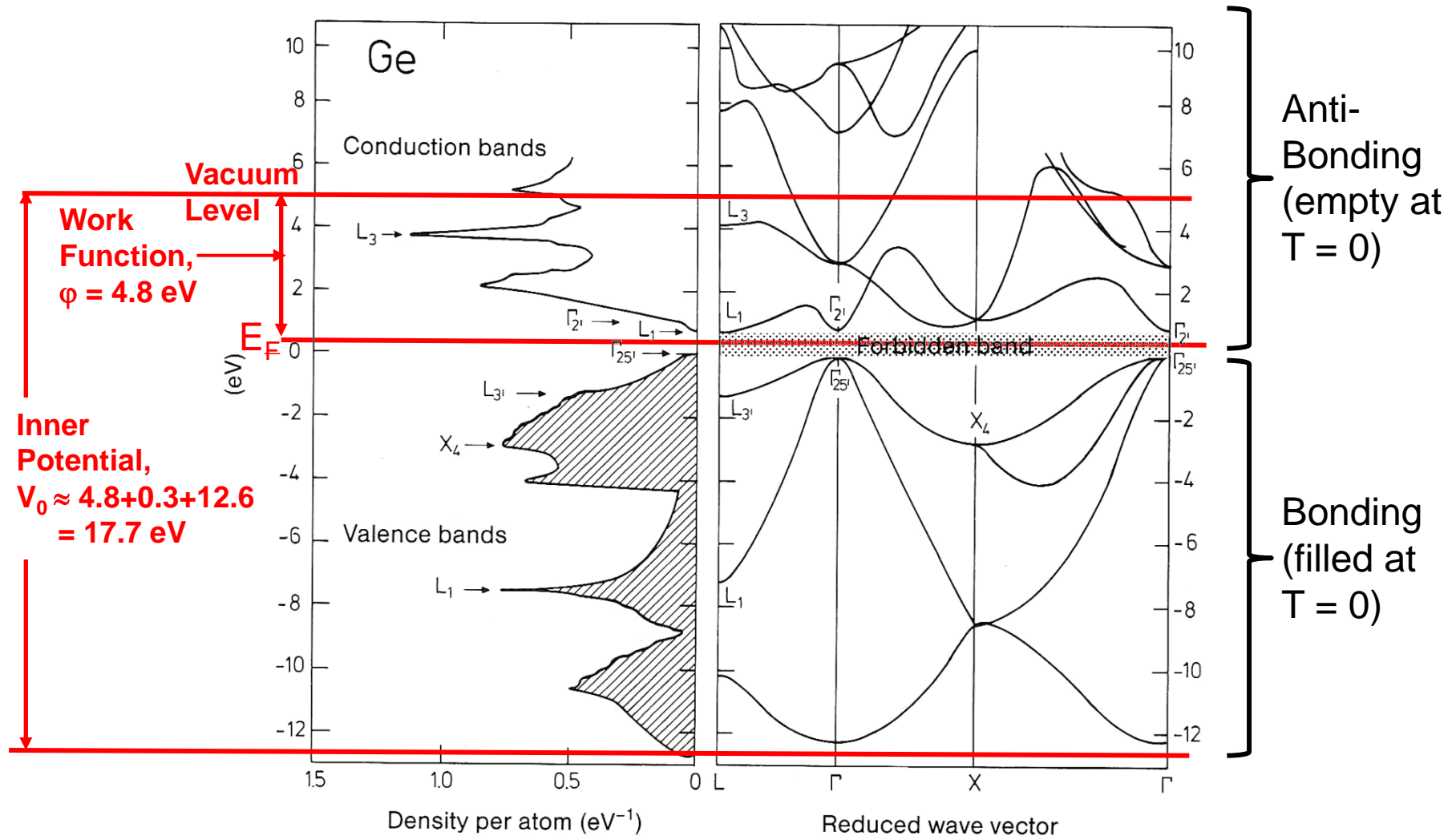
Lithium—bcc, $a = 3.49 \text{ \AA}$
 $1s^2 2s^1$



D.O.S.



Electronic bands and density of states for a semiconductor-Germanium—
 $1s^2 2s^2 2p^6 3s^2 3p^6 3d^{10} 4s^2 4p^2$

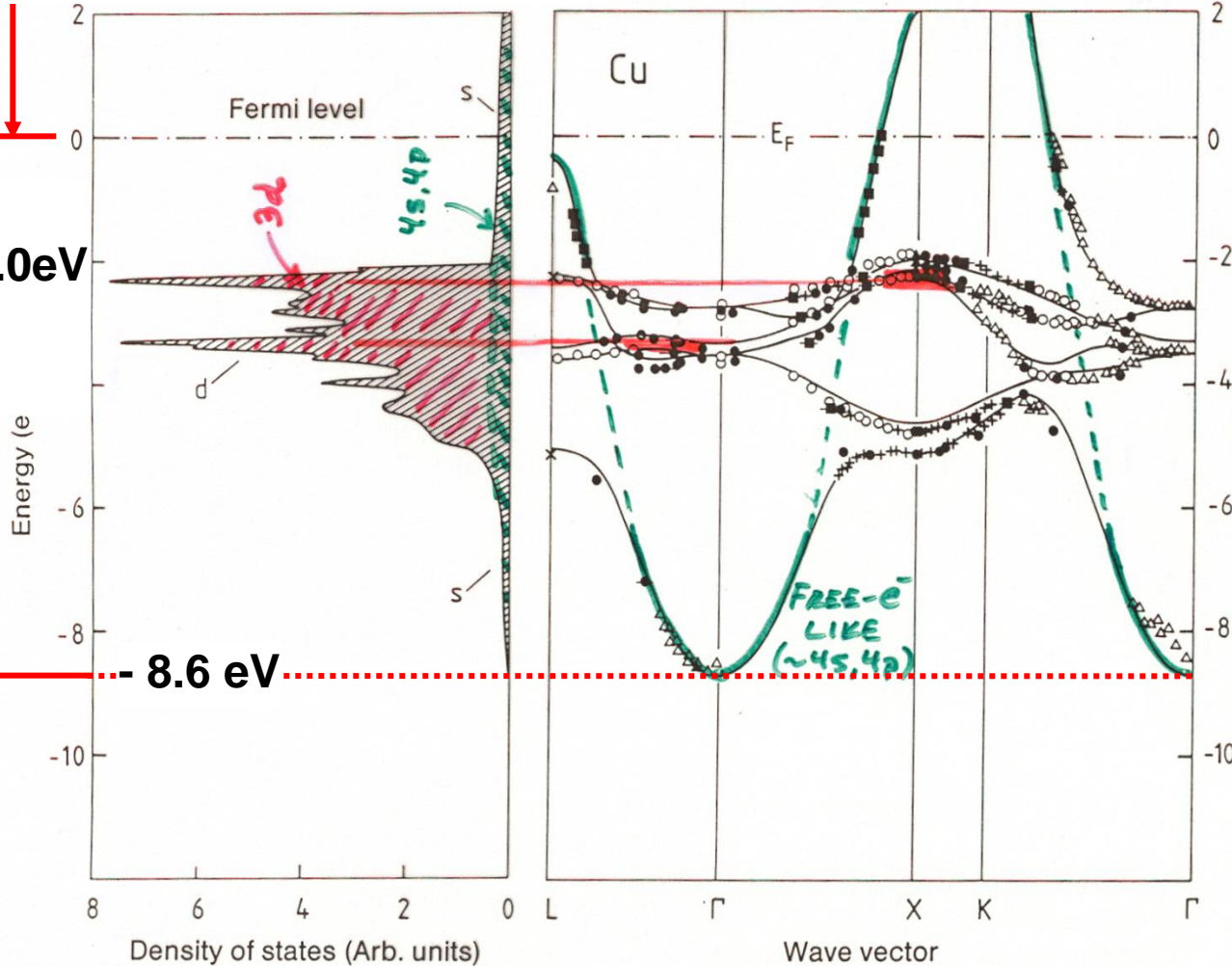


Vacuum level

The electronic structure of a transition metal — fcc Cu

$\phi_{Cu} = 4.4 \text{ eV} = \text{work function}$

$V_{0,Cu} = 13.0 \text{ eV}$



Cu 1s²...3d¹⁰4s¹
ELECTRONIC BANDS
+ DENSITY OF STATE

} MIXING
} 3d LIKE
} MIXING

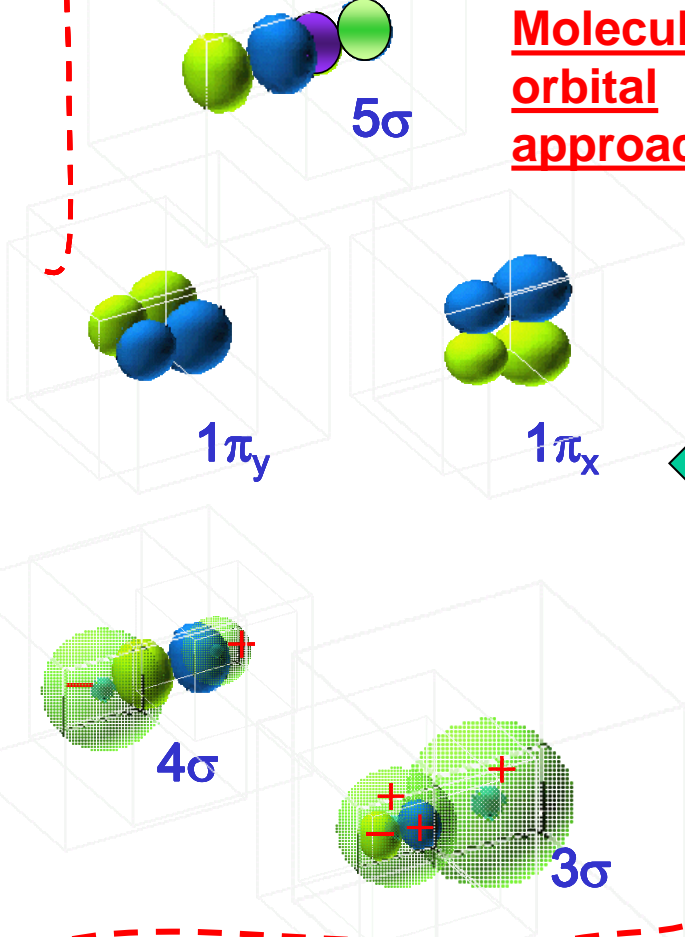
Experimental points from angle-resolved photoelectron spectroscopy (more later)

Fig. 7.12. Bandstructure $E(k)$ for copper along directions of high crystal symmetry (right). The experimental data were measured by various authors and were presented collectively by Courths and Hüfner [7.4]. The full lines showing the calculated energy bands and the density of states (left) are from [7.5]. The experimental data agree very well, not only among themselves, but also with the calculation

Atomic orbital makeup

$$\varphi_j^{MO}(\vec{r}) = \sum_{\text{Atoms } A} \sum_{\text{Orbitals } i} c_{Ai,j} \varphi_{Ai}^{AO}(\vec{r})$$

Molecular orbital approach



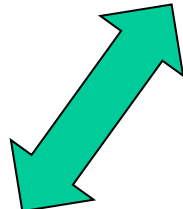
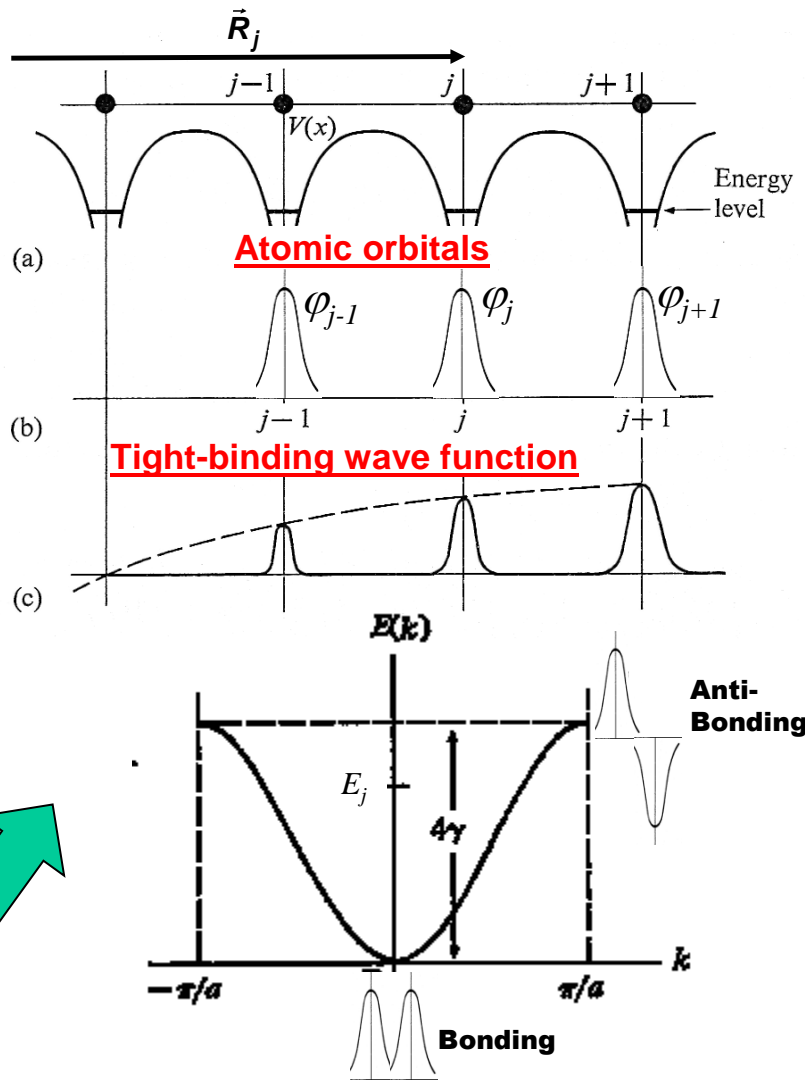
$$\varphi_{\vec{k}}^{BF}(\vec{r}) = \text{a Bloch function}$$

$$\propto \frac{1}{N^{1/2}} \sum_{j=1 \dots N \text{ unit cells at } \vec{R}_j} e^{i\vec{k} \cdot \vec{R}_j} \sum_{Ai} c_{Ai,\vec{k}} \varphi_{Ai}^{AO}(\vec{r} - \vec{R}_j)$$

Ai = basis set of AOs in unit cell

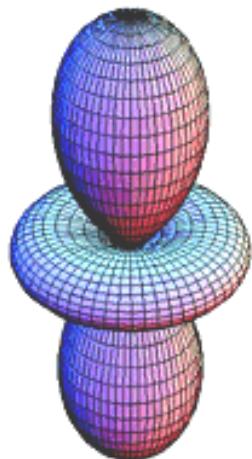
Solid state tight-binding approach

Crystal potential-1D

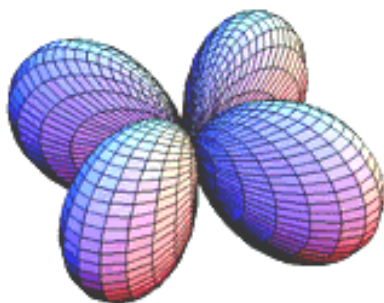


And for the real d orbitals in fcc:

e_g

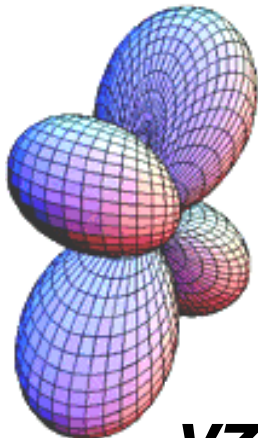


$3z^2-r^2$

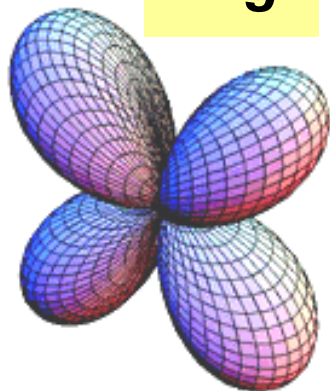


x^2-y^2

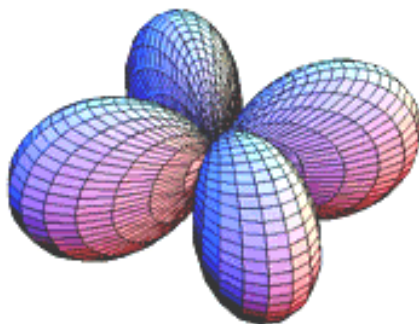
t_{2g}



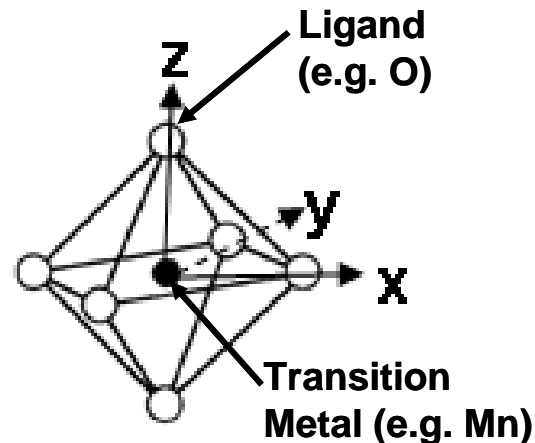
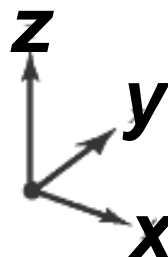
yz



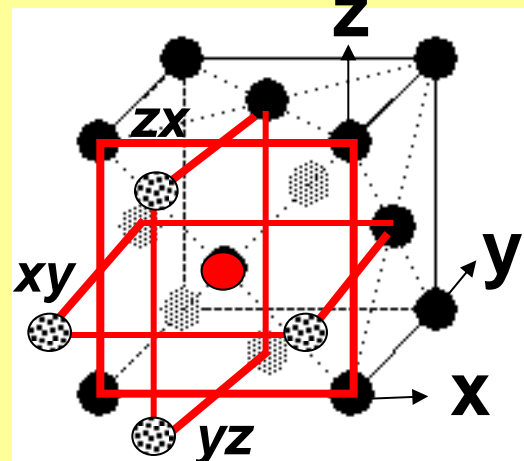
zx



xy

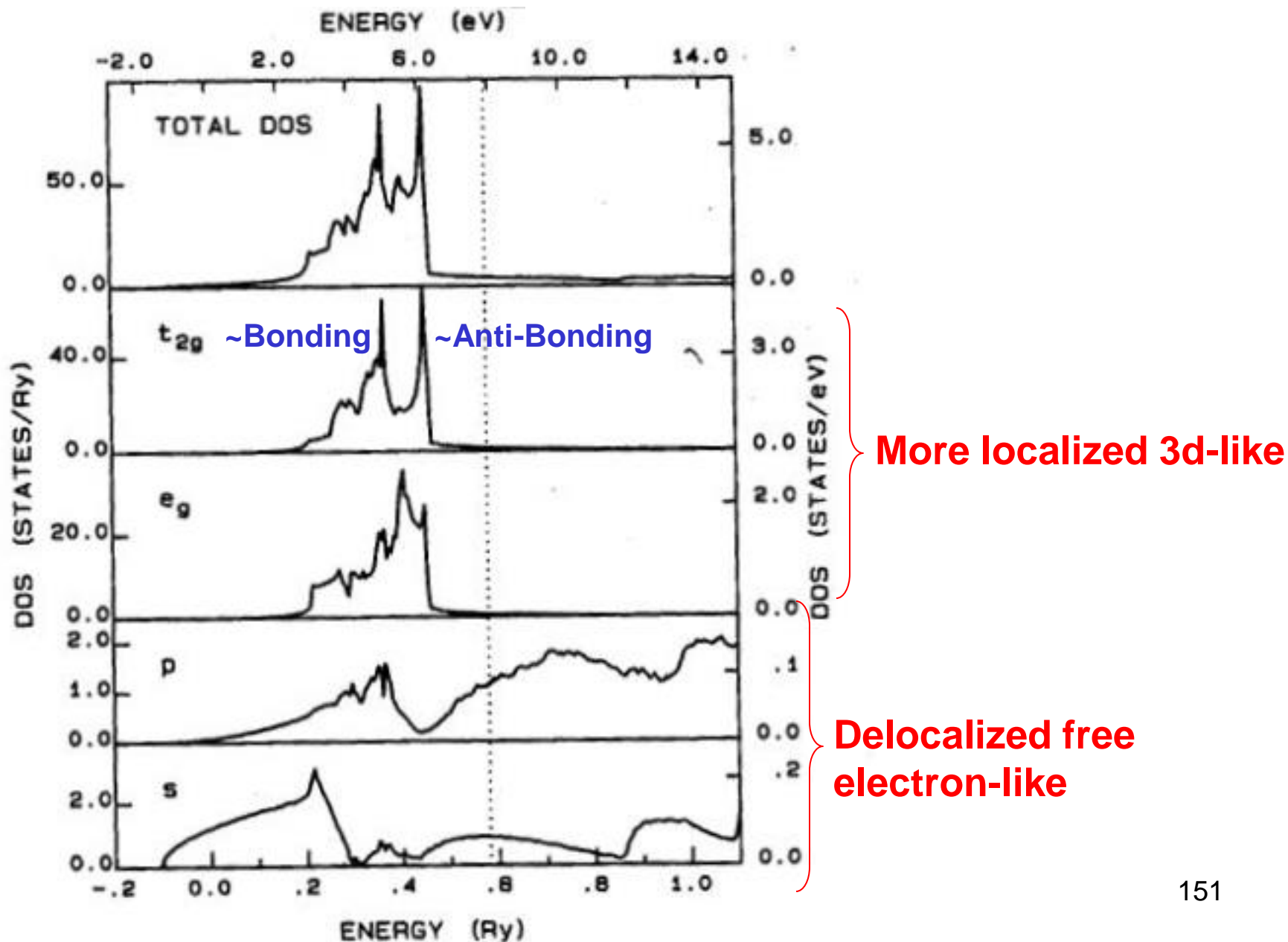


e_g and t_{2g} not equivalent in octahedral (cubic) environment



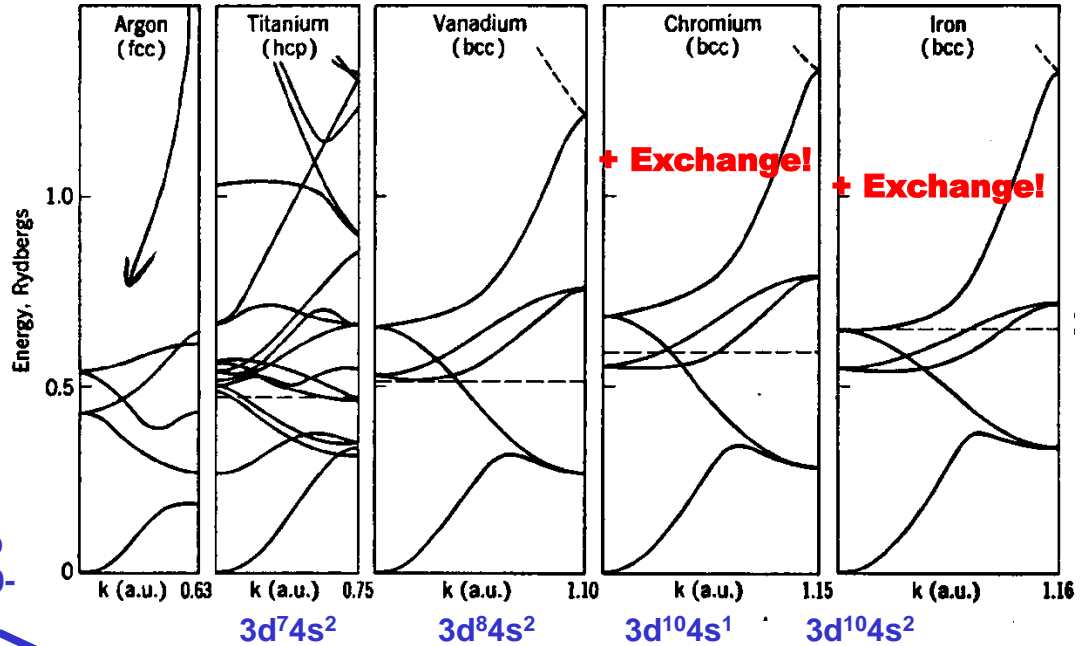
Face-centered cubic— t_{2g} pointing at 12 nearest neighbors

Copper densities of states-total and by orbital type:



The electronic structures of the 3d transition metals—
 ≈ “rigid-band model”

3s²3p⁶ filled + 3d,4s CB 3d²4s² 3d³4s² 3d⁵4s¹ 3d⁶4s²



+ Flat “core-like” Ar 3s, 3p bands at ~1.0-1.5 Rydbergs

Ti ²²	V ²³	Cr ²⁴	Mn ²⁵	Fe ²⁶	Co ²⁷	Ni ²⁸	Cu ²⁹	Zn ³⁰
3d ²	3d ³	3d ⁵	3d ⁵	3d ⁶	3d ⁷	3d ⁸	3d ¹⁰	3d ¹⁰
4s ²	4s ²	4s	4s ²	4s ²	4s ²	4s ²	4s	4s ²

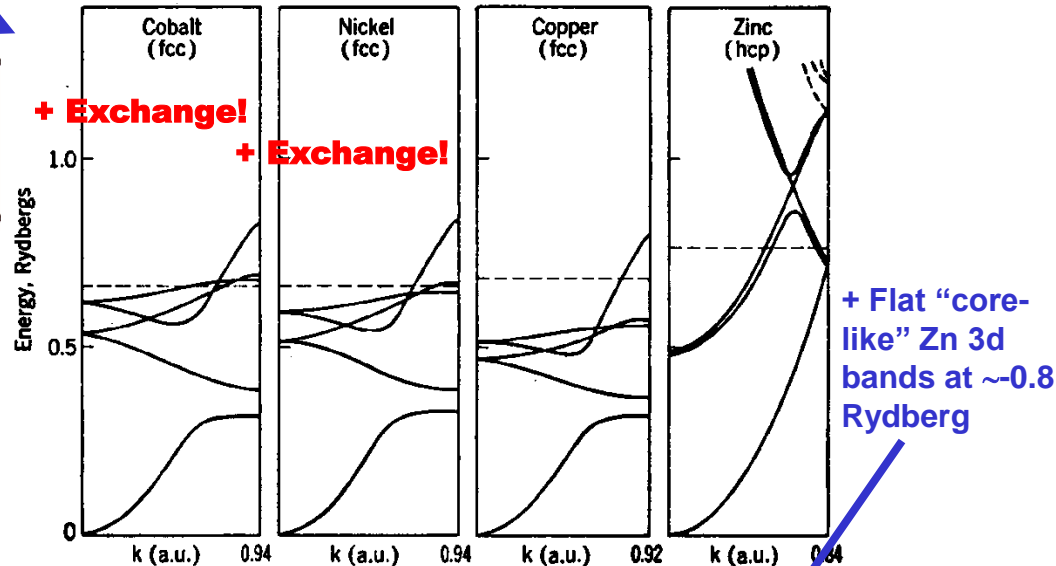
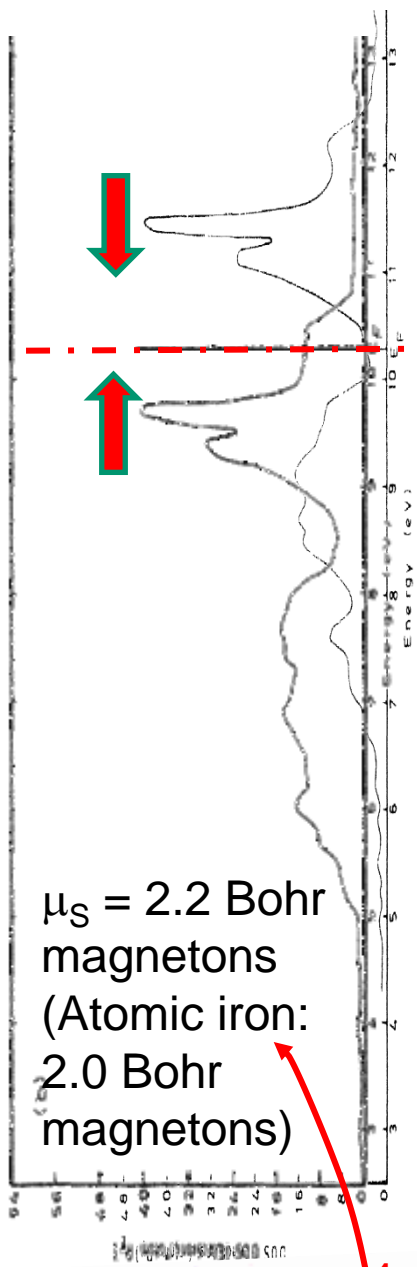


FIG. 10-20. Energy bands of 3d transition elements, along a single direction, from Mattheiss.

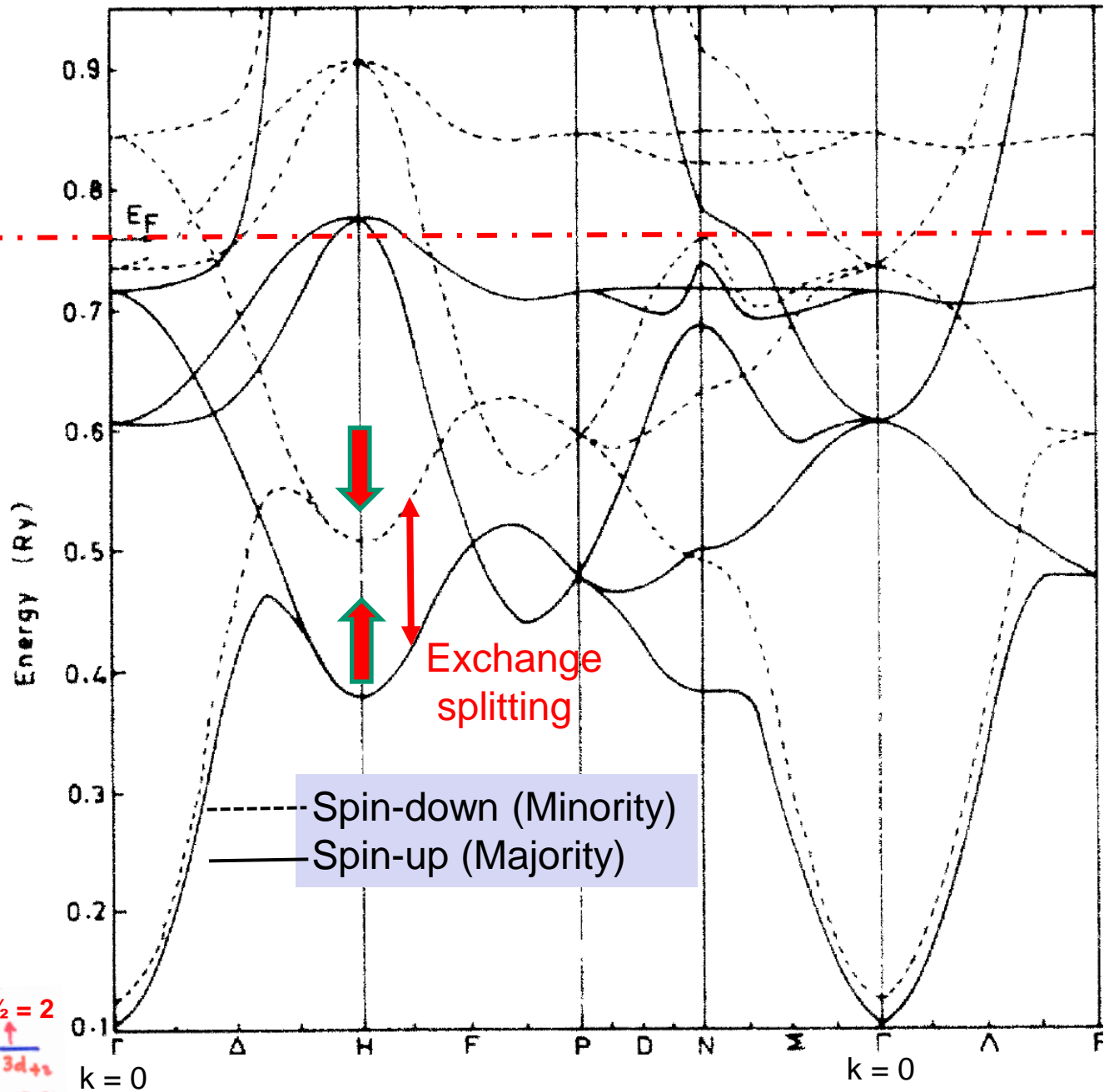
The electronic bands and densities of states of ferromagnetic iron



$\mu_S = 2.2$ Bohr magnetons
 (Atomic iron: 2.0 Bohr magnetons)

$4 \times \frac{1}{2} = 2$

$Fe \ 1s^2 2s^2 2p^6 3s^2 3p^4$
 $3d^6 4s^2$
 $\uparrow\downarrow \ \uparrow \ \uparrow \ \uparrow \ \uparrow$
 $3d_{z^2} \ 3d_{x^2-y^2} \ 3d_{xy} \ 3d_{yz} \ 3d_{zx}$
 \Rightarrow LARGE μ_{3d} + MAGNETISM



Exchange splitting

Spin-down (Minority)
 Spin-up (Majority)

$k=0$

$k=0$

Fe (001)

SPIN-RESOLVED BAND STRUCTURE OF A FERROMAGNET

THEORY:

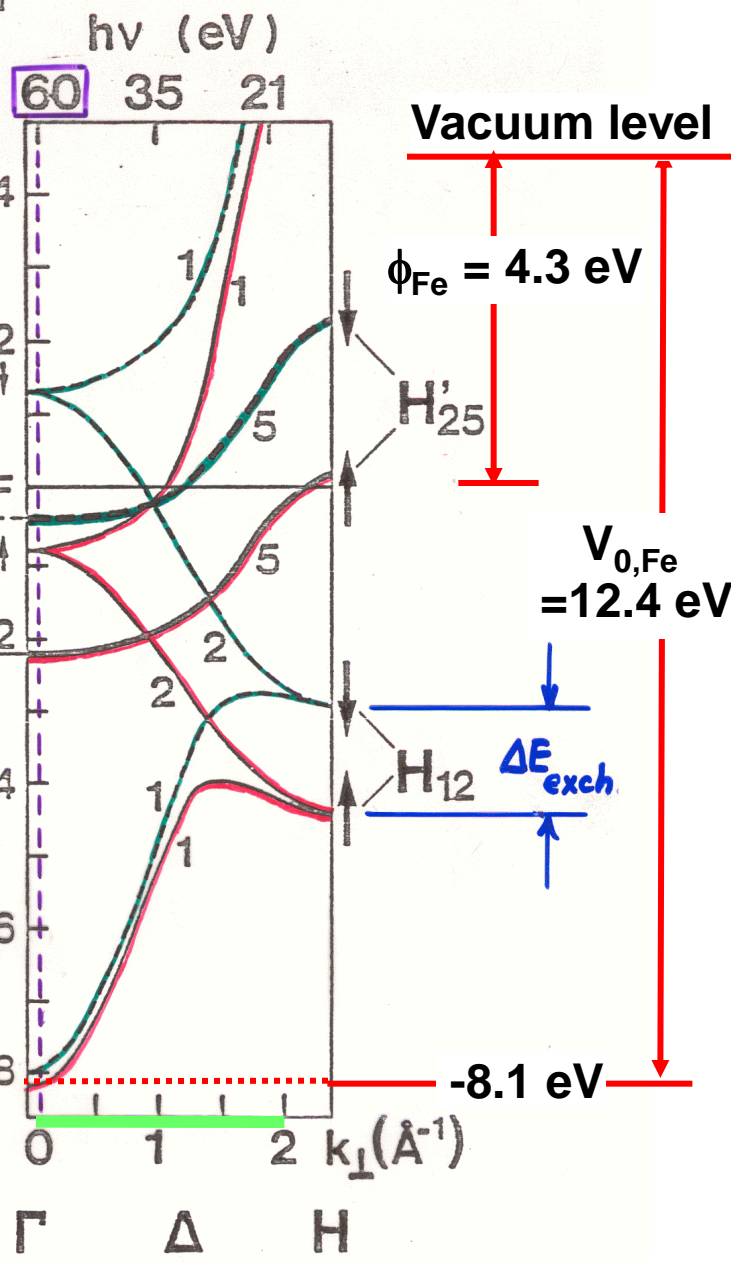
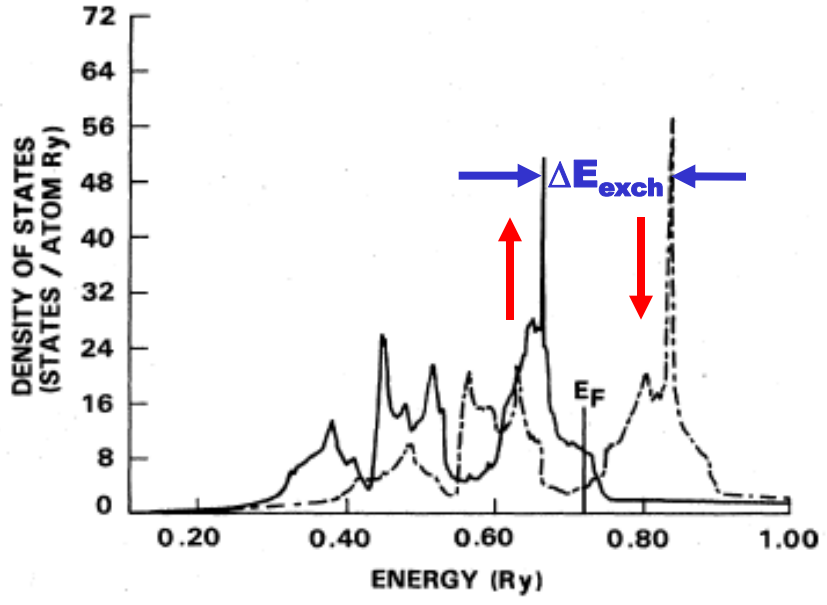
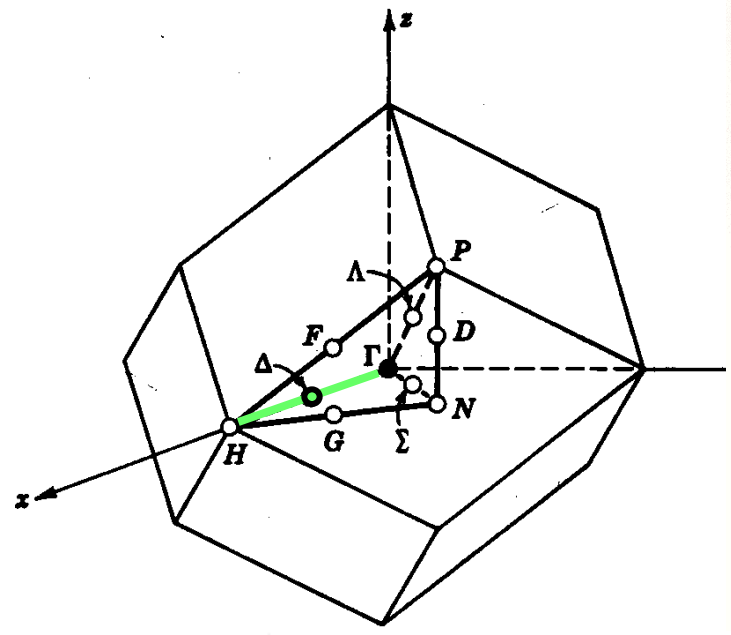


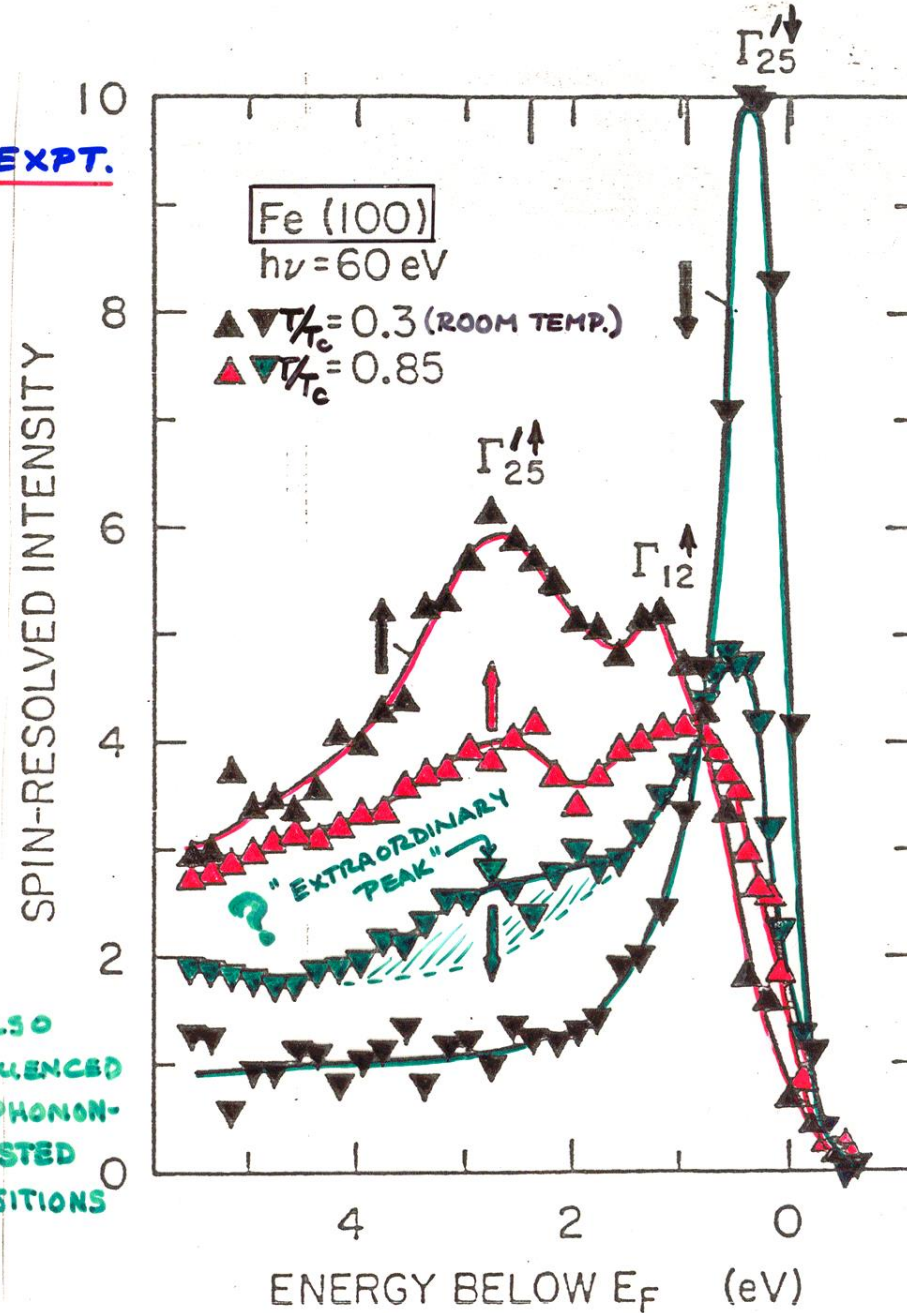
FIG. 4. Density of states at the equilibrium lattice constant of Fe for majority- (solid line) and minority- (broken line) spin states.

Hathaway et al., Phys. Rev. B 31, 7603 ('85)

E. KISKER ET AL., PHYS. REV. B 31, 329 (1985)

Fe: ANGLE AND SPIN-RESOLVED SPECTRA AT Γ POINT

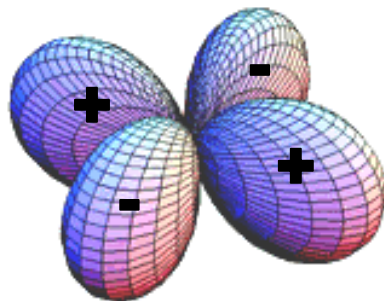
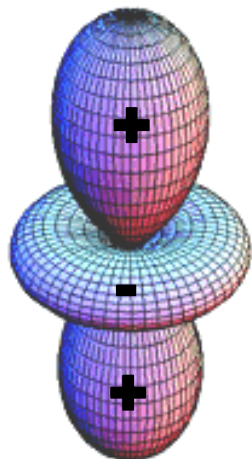
EXPT.



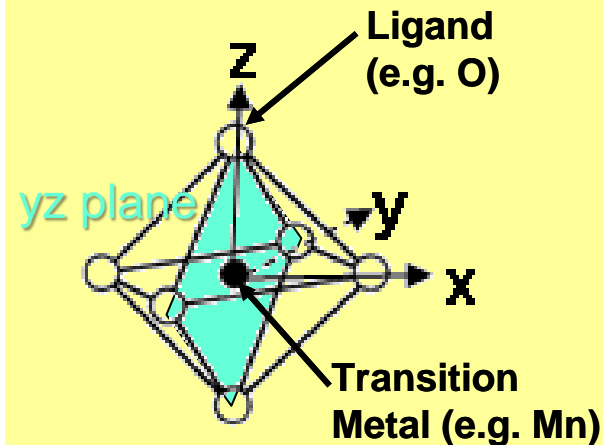
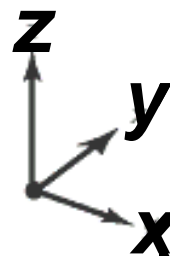
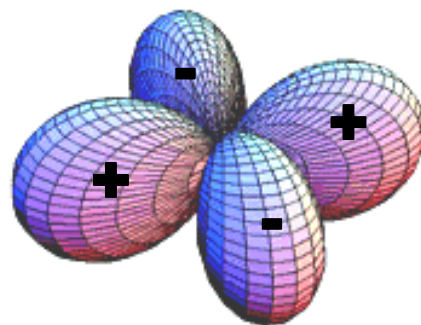
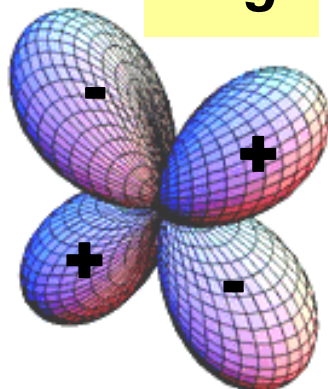
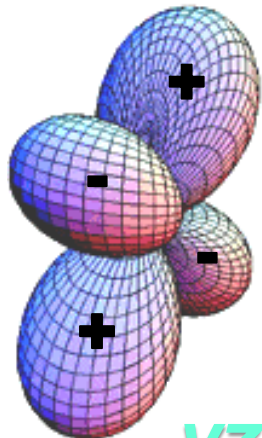
? ALSO INFLUENCED BY PHONON-ASSISTED TRANSITIONS

And for the real d orbitals in octahedral:

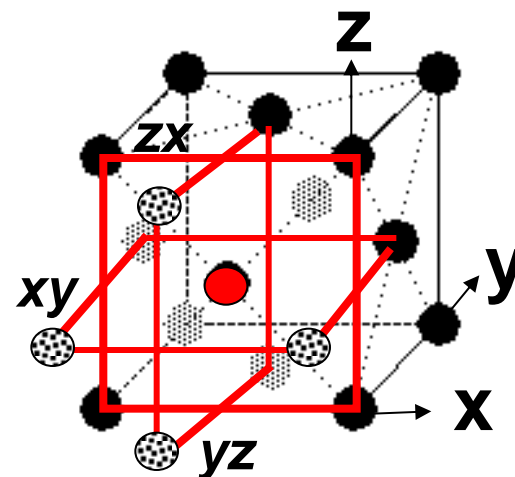
e_g



t_{2g}

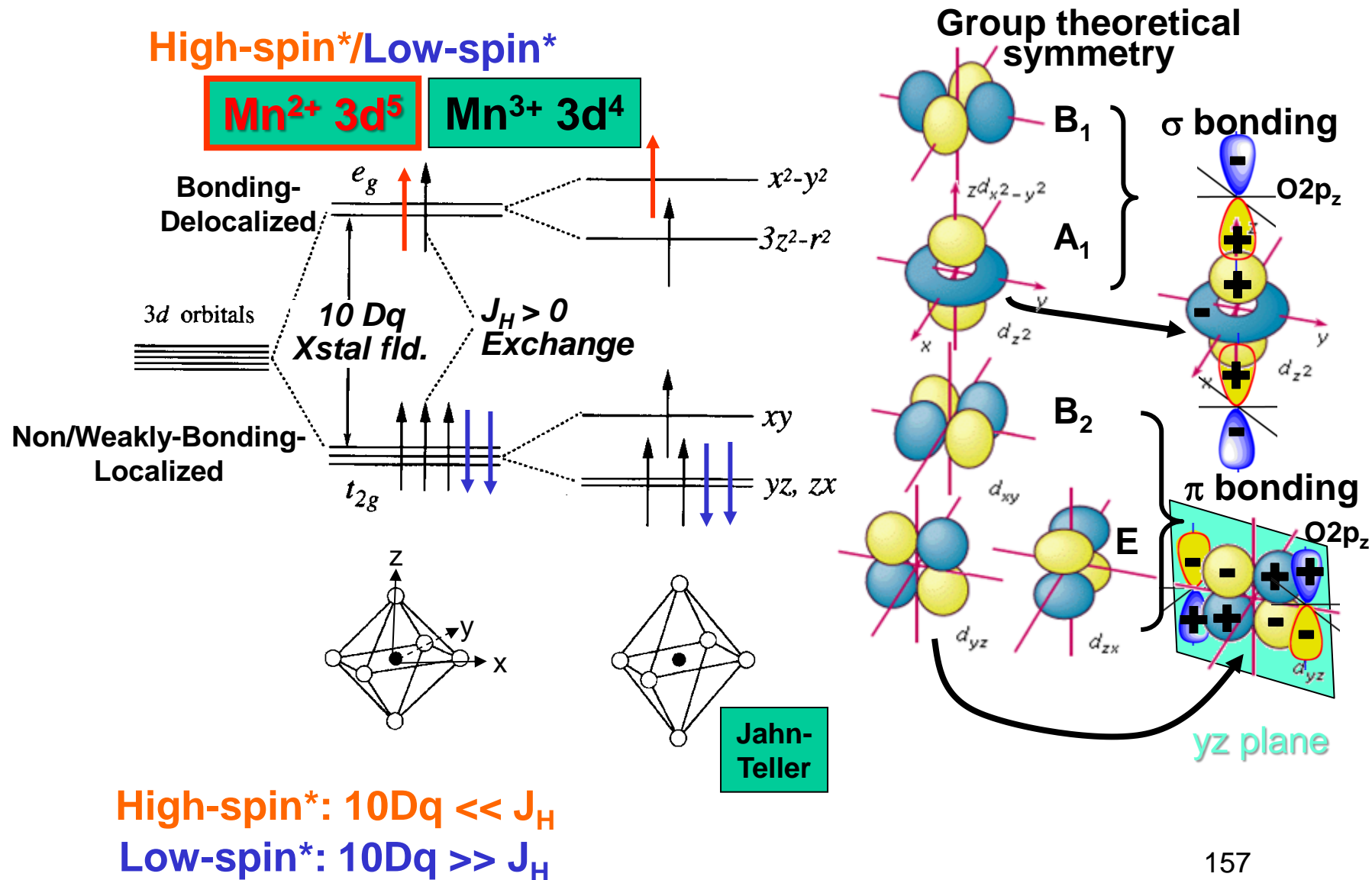


e_g and t_{2g} not equivalent in octahedral (cubic) environment



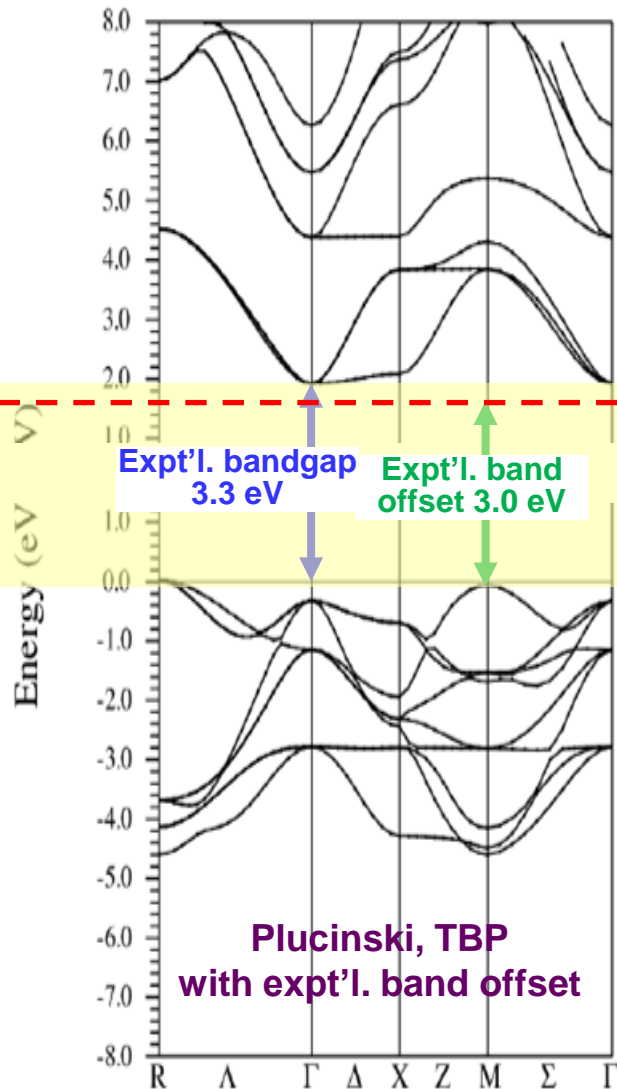
Face-centered cubic—
12 nearest neighbors

E.g.—Crystal field in Mn^{3+} & Mn^{2+} with negative octahedral ligands

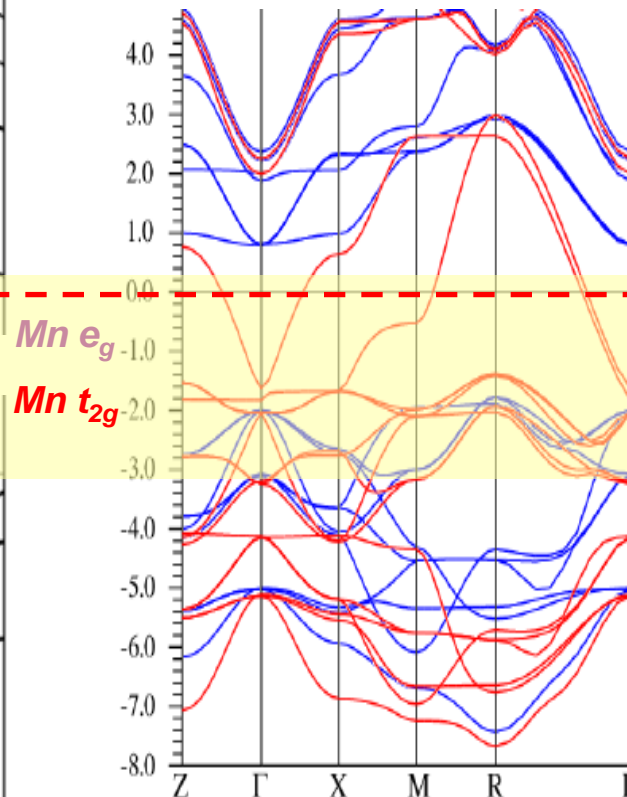


SrTiO₃ and La_{0.67}Sr_{0.33}MnO₃ band structures and DOS

SrTiO₃-band insulator



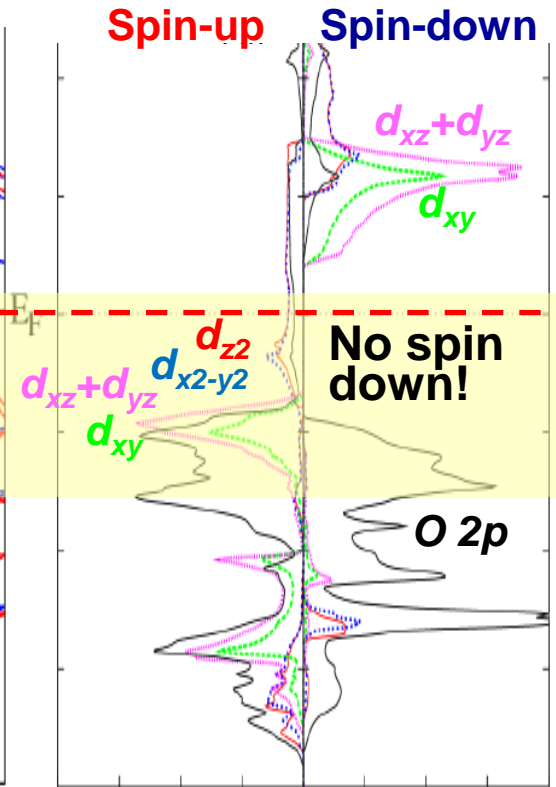
La_{0.67}Sr_{0.33}MnO₃- Half-Metallic Ferromagnet



— Spin-up
— Spin-down

Chikamatsu et al.,
PRB **73**, 195105 (2006);
Plucinski, TBP

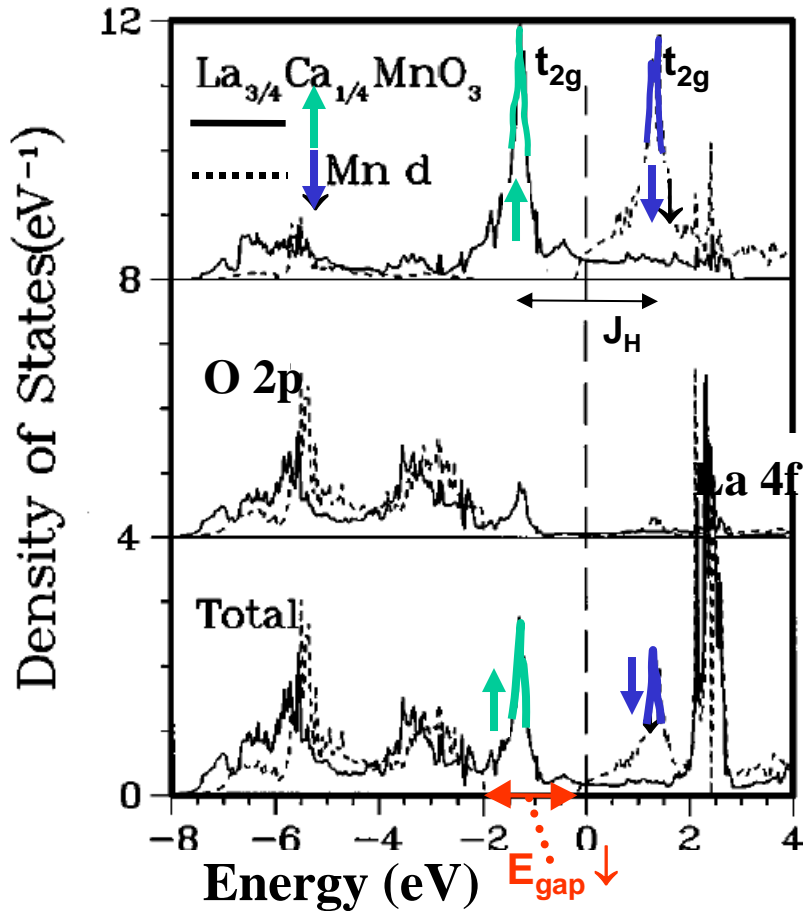
Projected DOSs



Zheng, Binggeli, J. Phys.
Cond. Matt. **21**, 115602 (2009)
Plucinski, TBP

Half-Metallic Ferromagnetism

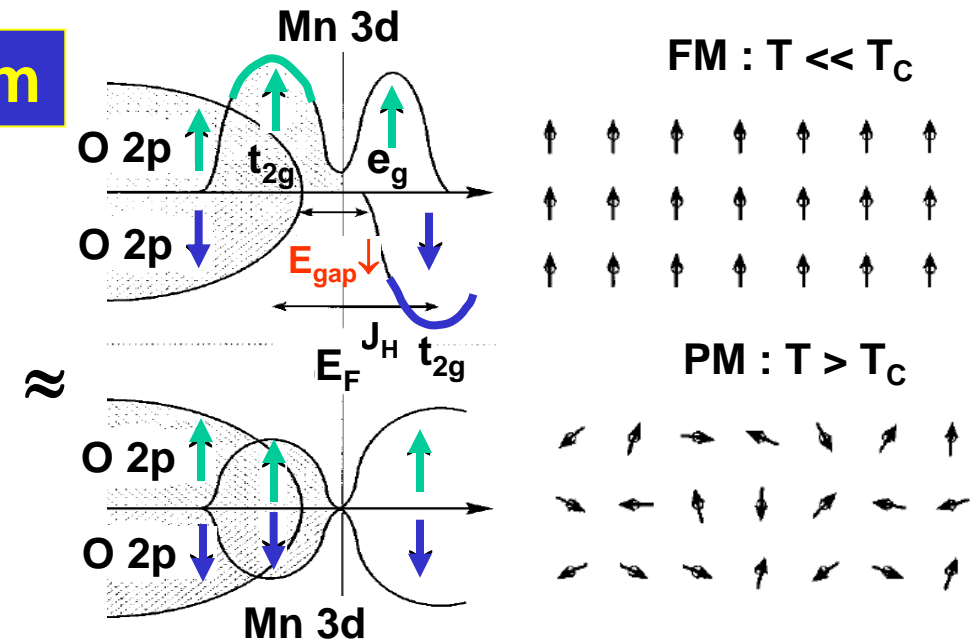
LDA theory- FM $\text{La}_{0.75}\text{Ca}_{0.25}\text{MnO}_3$



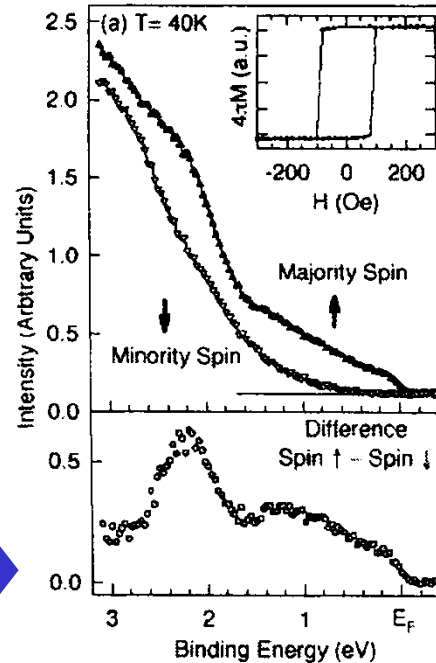
Pickett and Singh, PRB 53, 1146 (1996)

Experiment- spin-resolved PS
 $\text{La}_{0.70}\text{Sr}_{0.30}\text{MnO}_3$ as thin film

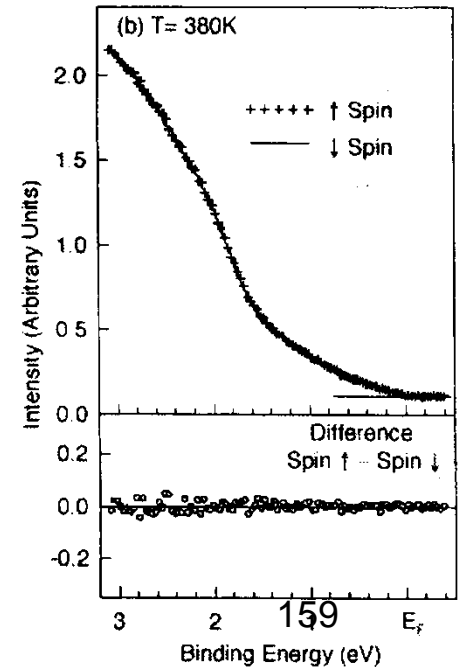
Park et al., Nature, PRB 392, 794 (1998)



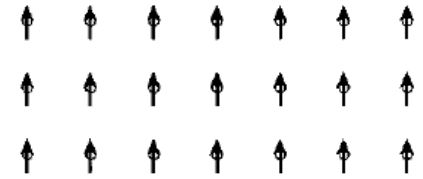
$T < T_C$



$T > T_C$



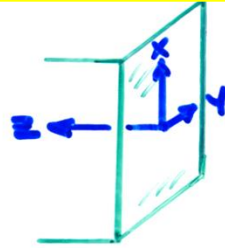
FM : $T \ll T_C$



PM : $T > T_C$



SURFACE ELECTRONIC STATES



$$k_x, k_y \Rightarrow \vec{k}_{||}$$

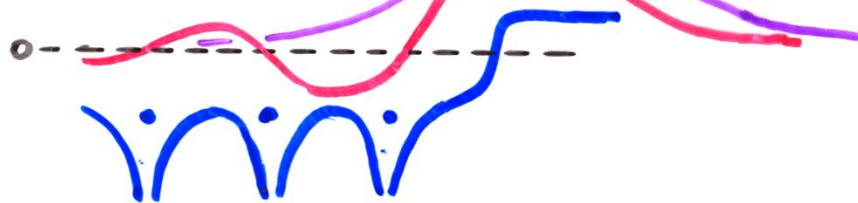
$$k_z \Rightarrow \vec{k}_{\perp}$$

- STRONGLY LOCALIZED NEAR SURFACE
- BLOCH FUNCTION IN $x+y$, BUT DECAYING IN z :

$$\psi_{\vec{k}_{||}}(\vec{r}) \approx u_{\vec{k}_{||}}(\vec{r}) e^{i\vec{k}_{||} \cdot \vec{r}} e^{-\kappa_z z}$$

DECAY CONSTANT

- TWO LIMITING TYPES: TAMM STATE ($\sim d$ character, localized)
- SHOCKLEY STATE ($\sim s, p$ character, delocalized)
(OSCILLATES INTO BULK A LITTLE)



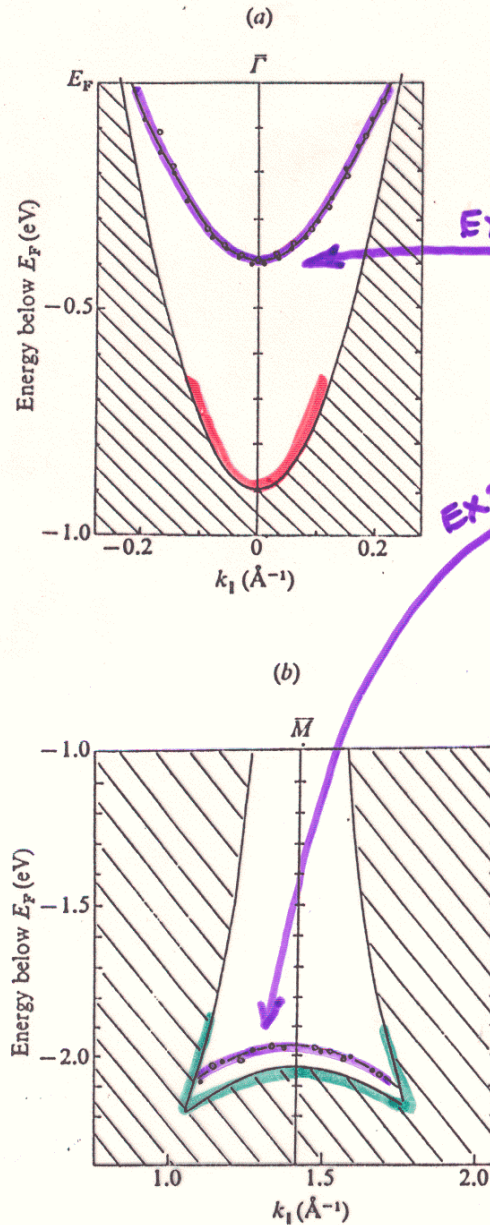
- ONLY EXIST WHEN NO BULK STATE EXISTS AT SAME $\vec{k}_{||} = k_x \hat{i} + k_y \hat{j}$; OTHERWISE MIXING OCCURS + NOT SURFACE-LOCALIZED

Surface states on Cu(111)

Shockley surface state:
s,p makeup

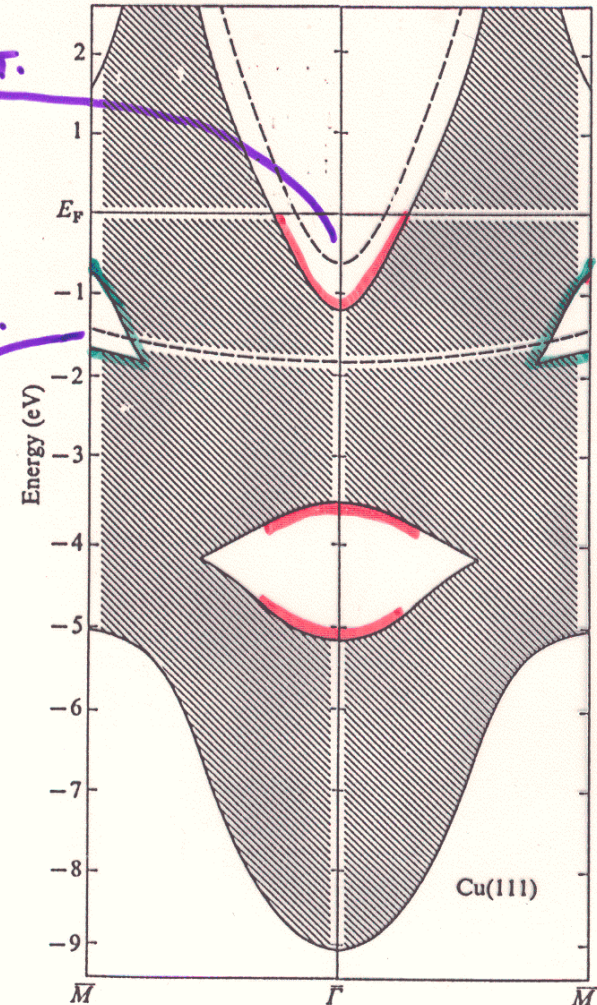
Tamm surface state:
3d makeup

Fig. 4.21. Experimental dispersion of Cu(111) surface states plotted with a projection of the bulk bands: (a) Shockley state near the zone center (Γ point, Kevan, 1983); (b) Tamm state near the zone boundary (\bar{M} point, Heimann, Hermanson, Miosga and Neddermeyer, 1979). Compare with Fig. 4.17.

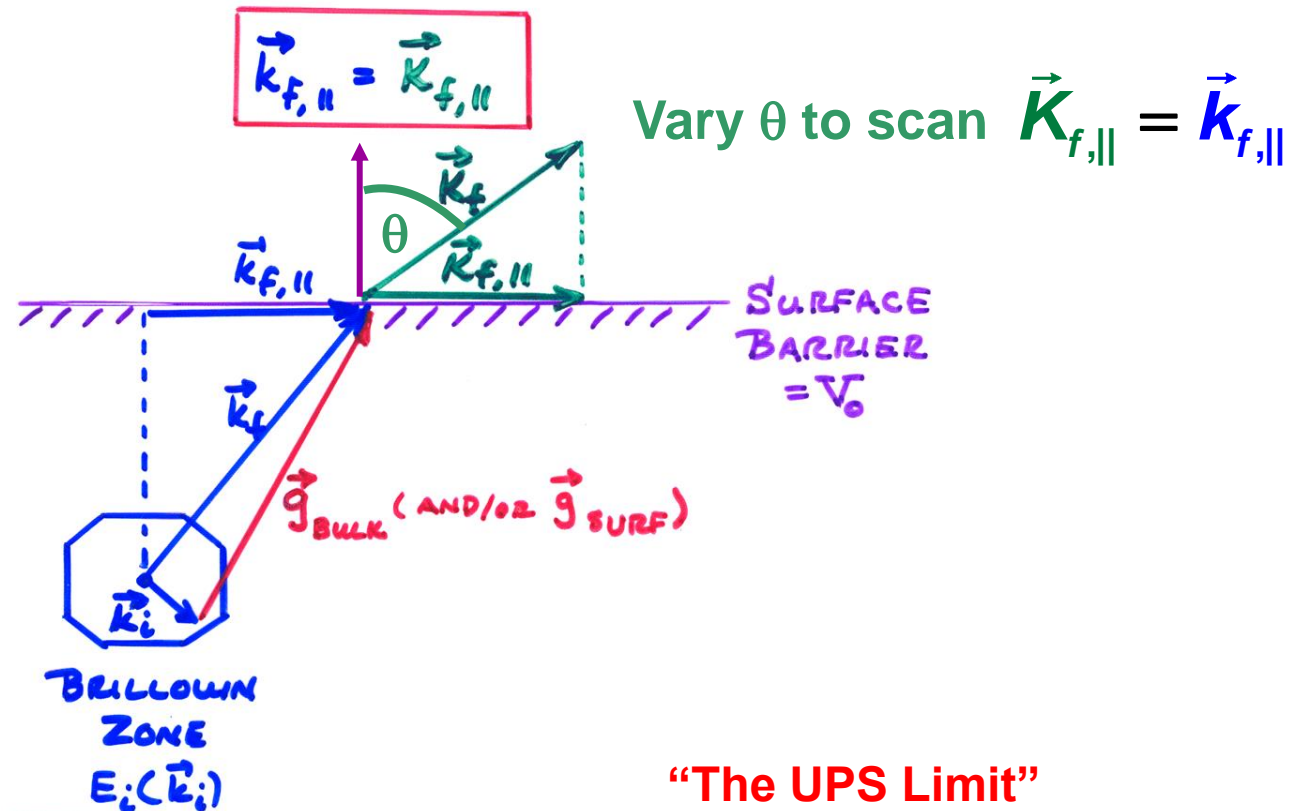


THEORY

Fig. 4.17. Surface states (dashed curves) and bulk projected bands of Cu(111) surface according to a six-layer surface band structure calculation (Euceda, Bylander & Kleinman, 1983).



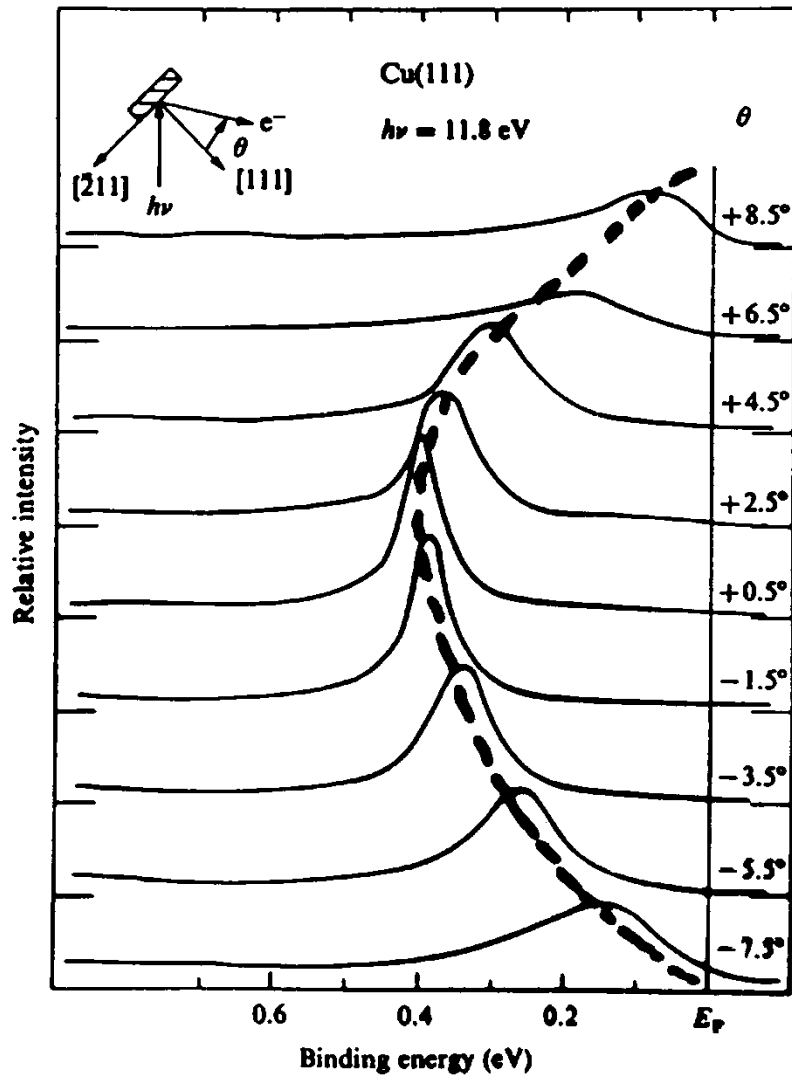
CONSERVATION LAWS IN VALENCE-BAND PHOTOELECTRON SPECTROSCOPY:



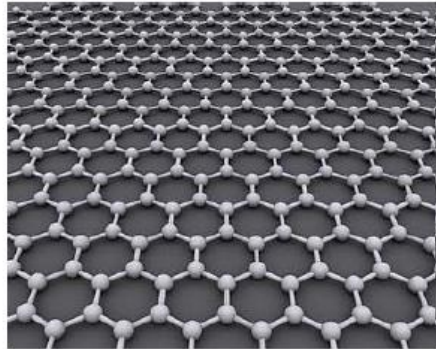
$$\vec{k}_f = \vec{k}_i + \vec{g}_{\text{BULK}} (\vec{g}_{\text{SURFACE}}) + \cancel{\vec{k}_{\text{HY}}} + \cancel{\vec{k}_{\text{PHONON}}}$$

NEGLIGIBLE: $h\nu \lesssim 500$ eV IF $h\nu$ AND/OR T LOW ENOUGH

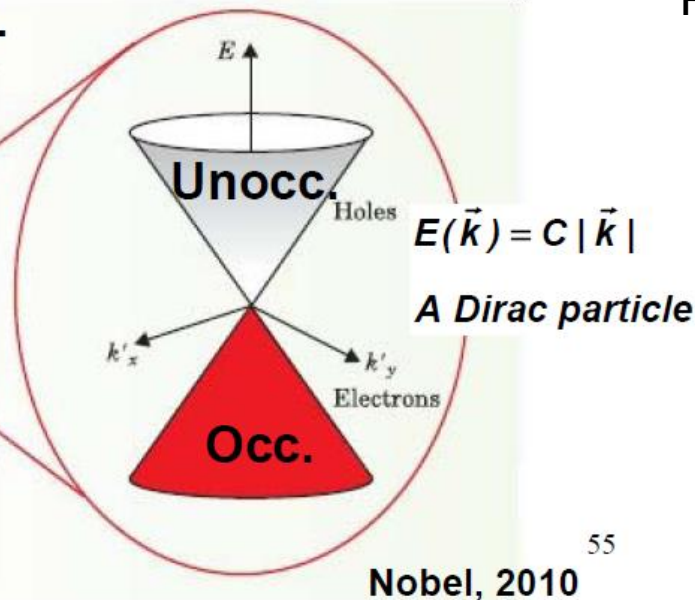
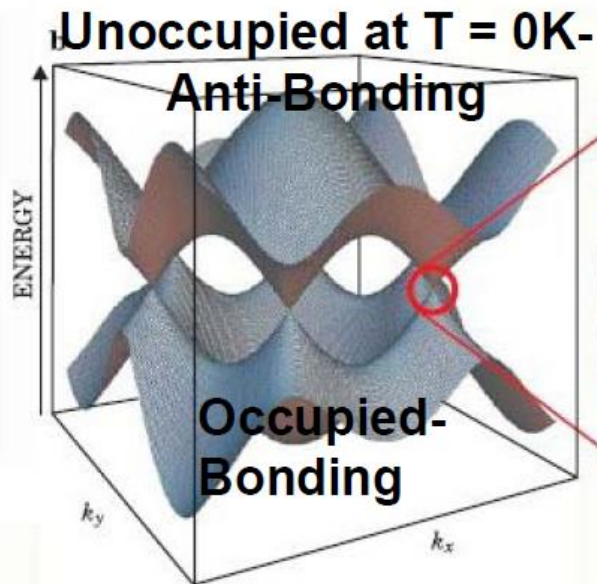
Fig. 4.20. Photoemission energy distribution curves from Cu(111) at different collection angles. Equation (4.32) has been used to express the electron kinetic energy in terms of the binding energy of the electron state (Kevan, 1983).



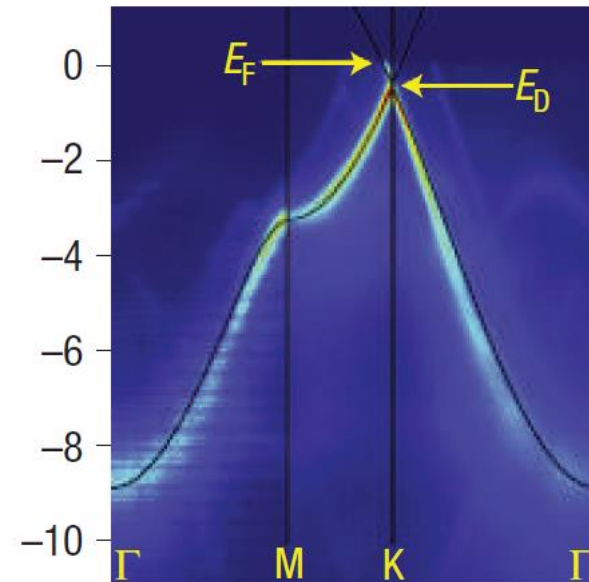
Graphene- A very special 2D case



The Nobel Prize in Physics 2010
 Andre Geim, Konstantin Novoselov
 ... "for groundbreaking experiments
 regarding the two-dimensional
 material graphene"



Photoelectron spectroscopy



Some basic measurements:

